LEAKAGE AND ATMOSPHERIC DISPERSION OF CO_2 ASSOCIATED WITH CARBON CAPTURE AND STORAGE PROJECTS

Alberto Mazzoldi

Thesis submitted to the
University of Nottingham
for the degree of Doctor of
Philosophy

March 2009

Declaration

I hereby declare that the work presented in this thesis has been done by me at the University of Nottingham. It has not been submitted for any other degree. All sources of information have been acknowledged by reference to the authors.

Alberto Mazzoldi

Acknowledgements

I would like to thank Prof. J.J. Colls for his supervision and meticulous examination of this work and of the articles published in scientific journals. His constructive criticism throughout my work has been greatly inspiring; his patience in correcting it very valuable. I would also like to thank E.ON for funding the project.

I warmly thank my uncle Franco and my Aunt Mino for their advices and support during my research.

This thesis is dedicated to my Mum, my Family and my friends.

CONTENTS

CHAPTER 2

CHAPTER 3

CHAPTER 4

LIST OF FIGURES

LIST OF TABLES

Nomenclature

c_a	Specific heat of air (1.005 kJ kg^{-1} K^{-1})
C_H	Bulk transfer coefficient for Sensible Heat ($1.75 \cdot 10^{-3}$)
C_E	Bulk transfer coefficient for Latent Heat ($1.75 \cdot 10^{-3}$)
C_G	Sandy soil heat capacity (dry – saturated) (1.38 – 2.96 MJ m^{-3} K^{-1})
C_1	*k-ε* turbulence model dimensionless constant equal to 1.44
C_2	*k-ε* turbulence model dimensionless constant equal to 1.92
C_s	Dimensionless turbulence production factor equal to 1.5
C_E	*Dimensionless turbulence viscosity constant for the k-ε model, equal to 0.09*
C_D	Dimensionless turbulent energy dissipation constant for the *k-l* model, equal to 0.3
C_μ	Dimensionless turbulence viscosity constant for the *k-l* model, equal to 0.1887
F_s	Rate of momentum gain per unit volume due to pollutant emissions (N m^{-2})
$F_{g/p}$	Force due to: (g) gravitational acceleration, (p) interaction with droplets/particles (N m^{-2})
g	Gravitational acceleration (9.8 m s^{-2})
G	Turbulence production rate by shear = $\sigma \nabla u$ (m^2 s^{-3})
G_h	Heat flux from the ground (W m^{-2})
H	Sensible heat flux (W m^{-2})
h_m	*Specific enthalpy of species m (J kg^{-1})*
I	Specific internal energy (J kg^{-1})
J	Heat flux vector (W m^{-2})
k_c	Thermal conductivity (W m^{-1} K^{-1})
k	Turbulent kinetic energy per unit mass (m^2 s^{-2})
l	Turbulent length scale (m)
LE	Latent heat flux (W m^{-2})
P	Pressure (MPa)
Q_s	Short wave radiation flux (W m^{-2})
Q_l	Long wave radiation flux (W m^{-2})
$Q_{s/p/h}$	*Rate of specific internal energy gain due to: (s) pollutant emissions, (p) interaction with particles, (h) surface energy budget* (J kg^{-1} s^{-1})
R_l	Enthalpy of vaporization of water (2.5 kJ g^{-1})
S	Solar constant (1367 W m^{-2})
T	Temperature (K)
u	Fluid velocity (m s^{-1})
u^*	Friction velocity (m s^{-1})
v	Wind speed (m s^{-1})
W_p	Turbulence production due to interaction with particles (m^2 s^{-3})
V_e	Cloud travel speed (m s^{-1})
z_0	*Ground roughness parameter (m)*
k_w	Water thermal conductivity (4°C) (0.57 W m^{-1} K^{-1})
C_w	Water volumetric heat capacity ($4.19 \cdot 10^{-6}$ J m^{-3} K^{-1})
k_{ice}	Ice thermal conductivity (0°C) (2.24 W m^{-1} K^{-1})
C_{ice}	Ice volumetric heat capacity (1.9 J m^{-3} K^{-1})
LH_s	Latent heat of sublimation (CO_2, T=190 K) (576.5 J g^{-1})

Greek letters

ρ	Density of CO_2 at gaseous (T = 20°C and -78°C), solid and supercritical state, respectively (1.8, 2.8, 1562, ~960 kg m^{-3})
ρ_m	*Mass density of species m (kg m^{-3})*
ρ_{amb}	Density of air (1.2 kg m^{-3})
ρ_b	Sandy soil dry density (1,600 kg m^{-1})
K_G	Sandy soil thermal conductivity (dry-saturated) (0.3 – 2.20 W m^{-1} K^{-1})
Φ_G	Sandy soil thermal diffusivity (dry – saturated) (0.24 – 0.74 m^2 s^{-1})

$\delta_{s/p}$	Source term for species due to (s) pollutant emission, (p) droplet evaporation/condensation (kg s^{-1})
μ	Primary (shear) viscosity of fluid (kg m^{-1} s^{-1})
λ	Secondary (bulk) viscosity of fluid (kg m^{-1} s^{-1})
σ_d	Stefan-Boltzmann constant (5.67×10^{-8} W m^{-2} K^{-4})
σ	Newtonian viscous stress tensor (N m^{-2})
φ	Joule-Thomson coefficient for CO_2 (1.3 K MPa^{-1})
ε	Dissipation of turbulent kinetic energy (m^2 s^{-3})
ζ	Monin-Obukhov similarity variable = z/L, dimensionless
κ	Von Karman constant = 0.41, dimensionless
k	Ratio of specific heats (cp/cv) for gaseous CO2 (1.29, dimensionless)
θ	Potential temperature (K)
θ_v	Soil water content (0 – 1)
Φ	Latitude (Nottinghamshire, 52°N)
σ_h	Turbulent Prandtl number, dimensionless
σ_k	Dimensionless turbulence model constant for the k equation equal to 1.0
σ_ε	Dimensionless turbulence model constant for the ε equation equal to 1.2
$\Psi_{(\zeta}$	Similarity profile
ν_t	Turbulent viscosity (kg m^{-1} s^{-1})
χ	Ground roughness conversion factor (3)

ABSTRACT

Climate change is affecting planet Earth. The main cause is anthropogenic emissions of greenhouse gases, the principal one being carbon dioxide, released in the atmosphere as a by-product of the combustion of hydrocarbons for the generation of energy. Carbon capture and storage (CCS) is a technology that would prevent carbon dioxide from being emitted into the atmosphere by safely sequestering it underground. For so doing, CO_2 must be captured at large emission points and transported at high pressure to underground reservoirs, where the gas can be injected and stored for thousands of years to come. During surface transportation, leakages from high pressure facilities would pose a risk to the general public, for carbon dioxide is toxic at high concentrations.

In this study, atmospheric dispersion of carbon dioxide is studied by the usage of software that solves mathematical equations and algorithms simulating the pollutant dispersion. Dispersion models are used to estimate or predict downwind distances covered by toxic concentrations of the pollutant, emitted from sources such as high-pressure transportation facilities within CCS projects. Two modelling tools from two different classes (Gaussian ALOHA 5.4 and Computational Fluid Dynamics PANACHE 3.4.1) have been evaluated against release field experiments using the statistical model evaluation method proposed by Hanna et al. (1993, 2004) and Hanna and Chang (2001), and applied for the consideration of the dense gas CO_2, released in large amounts due to leakages

Predictions from the two models have been compared and the limitations of both examined, when dealing with a gas that presents the distinctive physical characteristics of carbon dioxide. The models have been used and compared in simulating representative failure cases within CCS transportation with release parameters taken from the literature. The Computational Fluid Dynamics (CFD) model showed a much higher precision when describing the release of the gas from a HP facility, mainly when dealing with the jet release caused by leakages of any dimensions.

When dealing with the transportation of toxic gases, the magnitude of hazards posed by potential failure events within the transportation system is proportional to the extent of the area covered by toxic concentrations of the gas, when modelling representative leakages. Results of this investigation depict a lowering of the Risk involved in the transportation of CO_2 by up to an order of magnitude, when modelling the same releases with CFD tools, instead of the more common Gaussian models.

The European Union recognizes that deployment of CCS for hydrocarbon power generation, in parallel with the production of renewable energies, is the only way to meet the target for temperature stabilization. For its Impact Assessment on CCS, the EU used results from a risk assessment compiled after the utilization of a Gaussian model. In this thesis, a criticism of this choice is put forward, considering that, when introducing the technology to the general public and regional scale administrators, a Risk Assessment derived using results from Gaussian models can over-estimate the risk in a way not favourable to the purpose.

CHAPTER 1

CLIMATE CHANGE: CAUSES, EFFECTS, SOLUTIONS

Introduction

In the present chapter, the research carried out during three years at the University of Nottingham will be introduced. Starting with a description of the causes and effects of climate change, the technology of carbon dioxide underground sequestration (Carbon Capture and Storage, CCS) will be described as one of the most prominent solutions to the problem, particularly for those countries intending to rely heavily on fossil fuels (mainly coal) in their future energy mix.

The transportation of CO_2 via pipeline is the most convenient way of carrying the waste gas on land: from a capture power plant – i.e. an industry provided with the means for separating and compressing CO_2 – to the surface projection of the prescribed underground reservoir. The expertise in transporting gases at high pressure will be described, introducing the importance of risk assessment when evaluating the overall safety of this kind of processes, both for deciding the routes for transportation systems and during operation. A review of European projects for the next decade dealing with Climate Change and CCS is outlined.

In the last part of this chapter a short introduction to atmospheric modelling is pursued with an initial description of the two models utilized throughout this thesis. The chapter concludes with a short thesis overview.

1.1 Climate Change: an introduction

During the last several billion years, infrared-absorbing gases, such as carbon dioxide (CO_2) and water vapour, have caused the earth to be warmer than it would have been otherwise (Keeling et al., 1996, Mintzer, 1990, Schwartz and Randall, 2003), allowing life to develop in its most diverse forms.

There is almost global consensus among the scientific community that there exists a causal relationship between human activities and climate change, with compelling evidence that climatic changes result from the combination of natural variability and human influences, in particular greenhouse gases emitted from the use of fossil fuels and land-use changes (Houghton et al., 2001, Leggett, 2000, Steffen, 2006).

An increasing body of observations gives a collective picture of a warming world and other changes in the climate system, Figure 1.1 depicts this trend. The global average surface temperature increased over the 20^{th} century by about 0.6°C (Karl et al., 2002, NASA, 2002). New analyses of proxy data for the Northern Hemisphere indicate that the increase in temperature in the 20th century is likely to have been the largest of any century during the past 1,000 years (Crowley, 2000). It is also likely that, in the Northern Hemisphere, the 1990s was the warmest decade and 1998 the warmest year (IPCC, 2001).

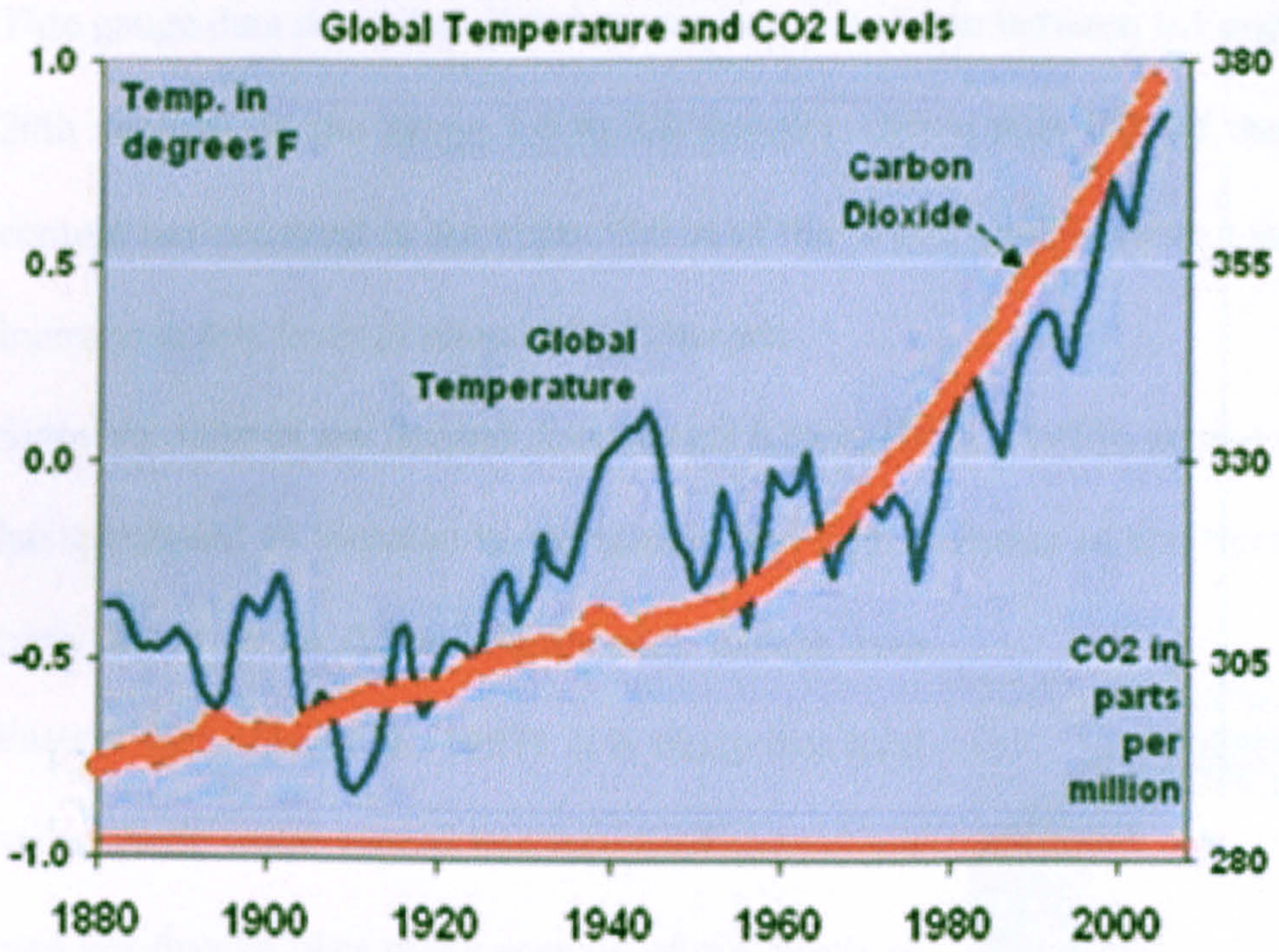

Figure 1.1 - Temperature variations in the last century (Kelly and Goulden, 2008). In the y axis, variations from the last 1,000 year average.

On average, minimum temperatures are increasing at about twice the rate of maximum temperatures (0.2 versus 0.1°C/decade).

1.1.1 Evidence

Snow cover and ice extent have decreased (Cavalieri et al., 2003, Steffen, 2006). Northern Hemisphere spring and summer sea-ice extent has decreased by 10 to 15% since the 1950s. It is likely that there has been about a 40% decline in Arctic sea-ice thickness during late summer to early autumn in recent decades and a considerably slower decline in winter sea-ice thickness (Rothrock et al., 1999) – Figure 1.2. Global average sea level has risen and ocean heat content has increased (Lambeck and Chappell, 2001).

Tide gauge data show that global average sea level rose between 0.1 and 0.2 m during the 20th century (in the range 1.0 to 2.0 mm/yr). More than half of the increase in heat content has occurred in the upper 300 m of the ocean, equivalent to a rate of temperature increase in this layer of about 0.04°C/decade.

Since the time of the Second Assessment Report (IPCC, 1995), annual land precipitation has continued to increase in the middle and high latitudes of the Northern Hemisphere (very likely to be 0.5 to 1%/decade), except over Eastern Asia (Dai et al., 1997). It is likely that total atmospheric water vapour has increased several per cent per decade over many regions of the Northern Hemisphere, due to increased evaporation rate. Changes in total cloud amounts over Northern Hemisphere mid- and high latitude continental regions indicate a likely increase in cloud cover of about 2% since the beginning of the 20th century, which has now been shown to be positively correlated with decreases in the diurnal temperature range.

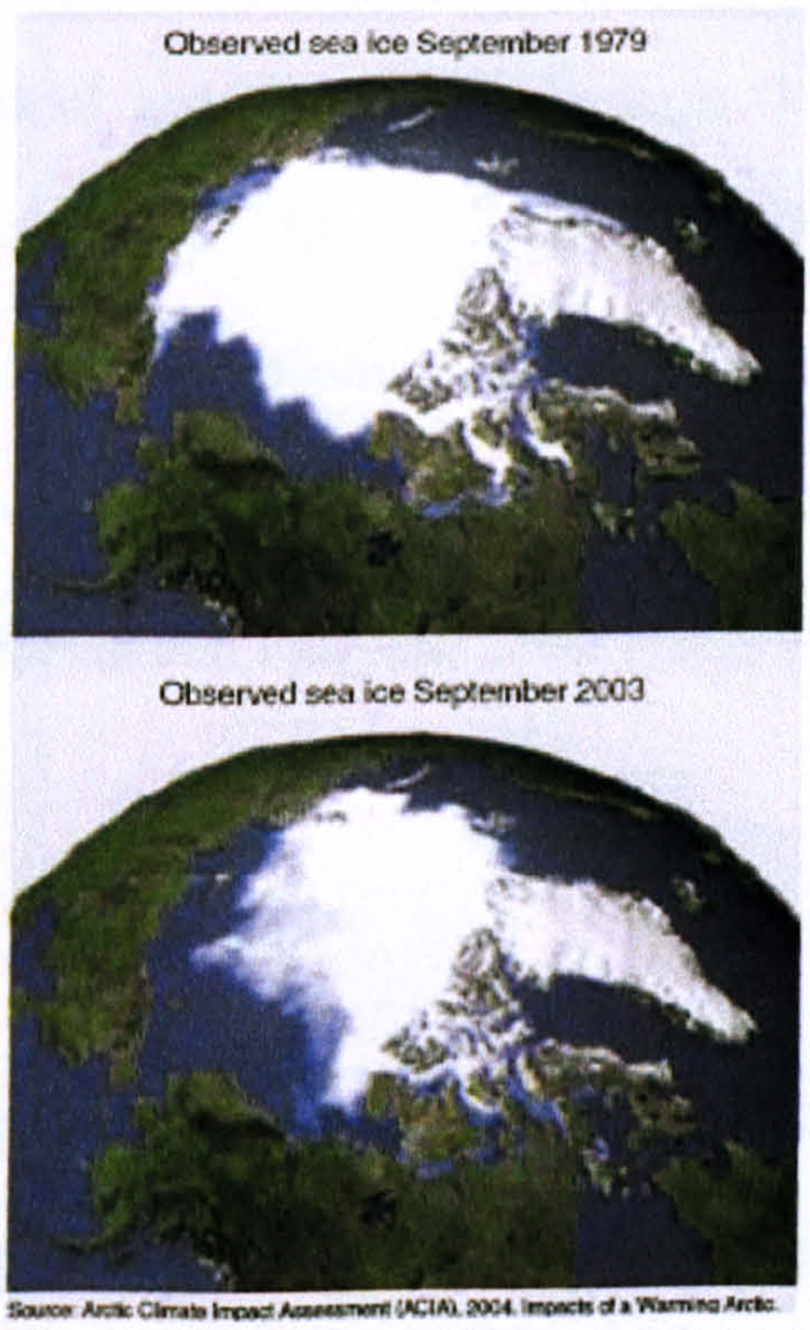

Figure 1.2 - Artic sea ice cover extent (Steffen, 2006).

1.1.2 Causes

The Earth absorbs radiation from the Sun, mainly at the surface. This energy is then redistributed by the atmospheric and oceanic circulations and radiated back to space at longer (infrared) wavelengths. For the annual mean and for the Earth as a whole, the

incoming solar radiation energy is balanced approximately by the outgoing terrestrial radiation. Any factor that alters the radiation received from the Sun or lost to space, or that alters the redistribution of energy within the atmosphere and between the atmosphere, land and ocean, can affect climate (IPCC, 2001). A change in the net radiative energy available to the global Earth-atmosphere system is termed here a radiative forcing. Positive radiative forcing tends to warm the Earth's surface and lower atmosphere. Negative radiative forcing tends to cool them.

As it is well known, increases in the concentrations of greenhouse gases reduce the efficiency with which the Earth's surface radiates to space. More of the outgoing terrestrial radiation from the surface is absorbed by the atmosphere and re-emitted at higher altitudes and lower temperatures. This results in a positive radiative forcing that tends to warm the lower atmosphere and surface (Lorenzoni and Pidgeon, 2006, Quaas et al., 2004, WWF, 2005).

1.1.2.1 Anthropogenic carbon dioxide emissions

Carbon dioxide (CO_2) is the greenhouse gas responsible for the greater part of the changes in the climate system (WWF, 2005). Current anthropogenic emissions of CO_2 are primarily the result of the consumption of energy from fossil fuels.

Global average atmospheric CO_2 concentration increased from 280 ppm at the start of the industrial revolution (~1750) to 381 ppm in 2006. Figure 1.3 shows the CO_2 emission trend through recent history. The present concentration is the highest during the last 650,000 years (Canadell et al., 2007, Siegenthaler et al., 2005) and probably during the last 20 million years (Pearson and Palmer, 2000). The growth rate of global average atmospheric CO_2 for the period 2000–2006 was 1.93 ppm yr^{-1} (or 4.1 petagrams of

carbon (PgC, 1 petagram = 10^{15} g) yr^{-1}. This rate is the highest since the beginning of continuous monitoring in 1959 and is a significant increase over growth rates in earlier decades: the average growth rates for the 1980s and the 1990s were 1.58 and 1.49 ppm yr^{-1}, respectively (Scripps, 2009).

About 10 to 30 % of the current total anthropogenic emissions of CO_2 are estimated to be caused by land-use conversion. The analysis of Houghton (2001) indicated that the net flux due to land-use change was 2.0 ± 0.8 PgC yr^{-1} during the 1980s, almost entirely due to deforestation of tropical regions.

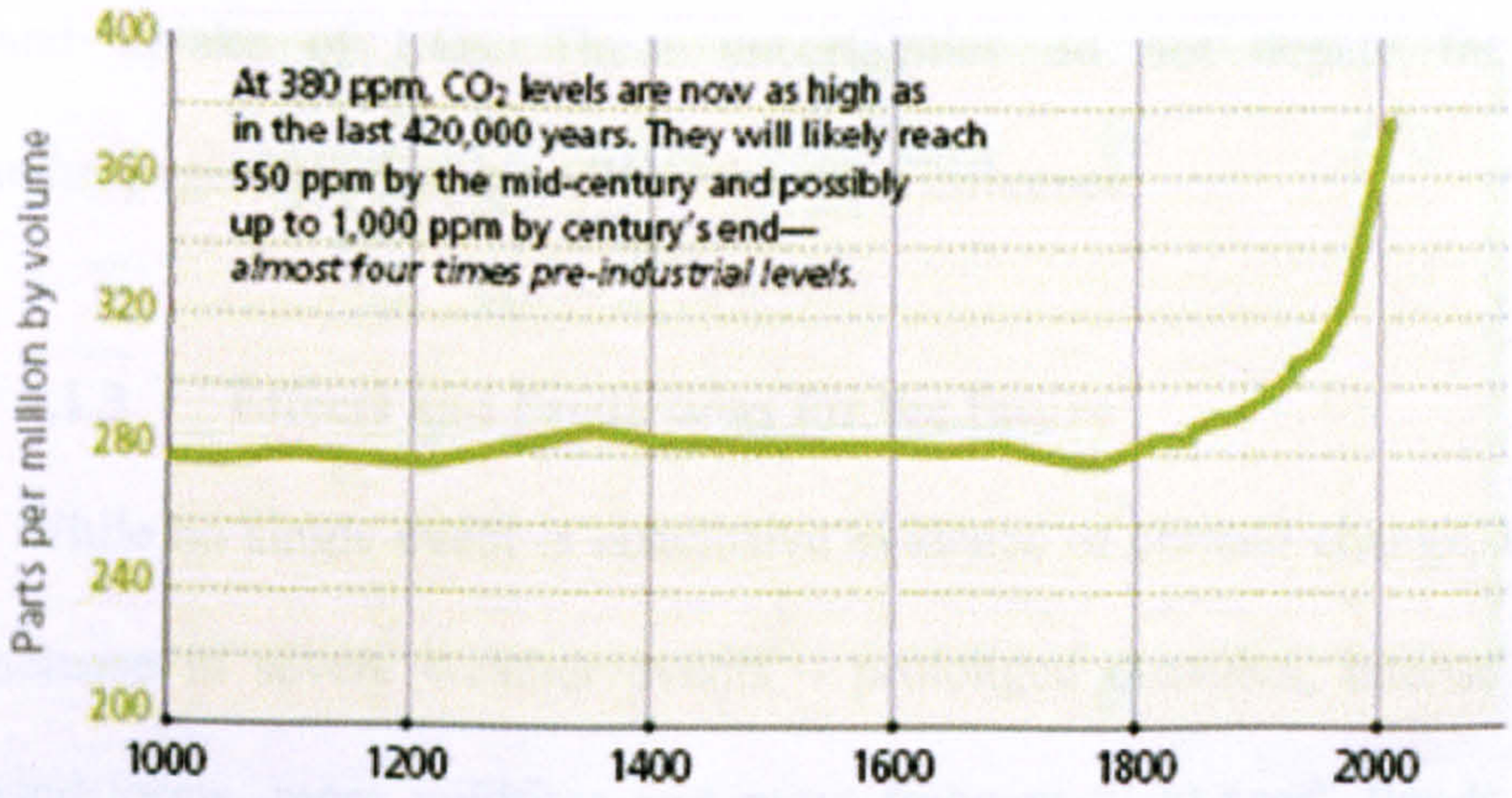

Figure 1.3 - Atmospheric concentration of CO_2 through the last millennium (Leggett, 2000).

In conclusion, anthropogenic CO_2 emissions are virtually certain to be the dominant factor determining CO_2 concentrations throughout the 21st century. The importance of anthropogenic emissions is underlined by the expectation that the proportion of emissions taken up by both ocean and land will decline at high atmospheric CO_2 concentrations (even if absolute uptake by the ocean continues to rise).

Recent studies (Raupach et al., 2007) indicate that the world is not simply consuming more energy, but is also generating it in a less climate-compatible way. While in the 1990s worldwide emissions had been growing by 1.1% a year, between 2000 and 2004 global emissions grew by more than 3% a year – faster than the most pessimistic projections of the UN Intergovernmental Panel on Climate Cange (IPCC) and also faster than economic growth, implying constant or slightly increasing trends in the carbon intensity of energy worldwide (EU, 2008b).

There is considerable uncertainty in projections of future CO_2 concentration, because of uncertainty about the effects of climate change on the processes determining ocean and land uptake of CO_2. These uncertainties do not negate the main finding that anthropogenic emissions will be the main influence.

1.1.3 Effects and Predictions for the future

While no single event is conclusive evidence of climate change, the relentless pace of increase in severe weather events – prolonged droughts, intense heat waves, violent windstorms, more wildfires and more frequent "100-year" floods – is indicative of a changing climate. Polar ice is melting at rates unforeseen in the 1990s. As melt water seeps down to lubricate their base, some Greenland outlet glaciers are moving 14 kilometres per year (Epstein and Mills, 2005), twice as fast as in 2001, making linear projections for sea level rise this century no longer applicable. North Atlantic freshening – from melting ice and Arctic rainfall – is shifting the circulation pattern (i.e. the Gulf Stream) that has helped stabilize climates for millennia. Indeed, the slowing of the Ocean

Conveyor Belt and the degree of storm destructiveness are occurring at rates and intensities that previous models had projected would occur much later this century.

If humans don't curb use of fossil fuels, the planet will warm 8°C by the year 2300. The polar ice caps will disappear and oceans will rise 7 m (Oppenheimer and Todorov, 2006). At the poles, the average temperature would rise more than 20° C, models predict.

1.1.3.1 The 2 degrees Celsius target

On December 2007, the UN Climate Change Conference in Bali, Indonesia, was hailed as a defining moment in the global response to climate change. It saw the agreement of a roadmap for negotiations on the next Kyoto commitment period starting in 2012.

The Bali conference followed the latest report of the IPCC. The IPCC gave its strongest indication yet that climate change is occurring as a result of greenhouse gas emissions resulting from human activity and found that current action was failing to reduce these emissions. It concluded that climate change would lead to mostly adverse impacts on humans and the environment, including some that could be abrupt and irreversible (IPCC, 2007b). The IPCC report indicates that if we are to have a good chance of avoiding dangerous climate change (dangerous climate change is thought to occur at temperature increases greater than 2° C above pre-industrial levels) global emissions would have to have peaked by 2015, reducing globally by 50-85% by 2050 (from 2000 levels). Annex 1 countries (developed countries as defined in the UN Framework Convention on Climate Change), would have to reduce emissions by 25-40% by 2020 and 80-95% by 2050 (IPCC, 2007a). Non-Annex 1, or developing, countries would in many cases still be permitted to increase their emissions, but at a slower rate. Overall, the aim of the process is to stabilize CO_2 concentration in the atmosphere at 450 ppm (MPs, 2008). However,

reducing emissions by these amounts might still only give a 50% chance of avoiding dangerous climate change. Increasing these odds would require more stringent targets and earlier emissions reductions.

1.1.4 Solution to climate change: Bio- and Renewable Energy

Climate change caused by emissions of greenhouse gases (GHGs) from human activities is one of the greatest threats to people, economies and ecosystems in the 21st century. As stated above, the goal of EU climate policy is to keep global mean temperature rise to less than 2 °C above pre-industrial levels in order to avoid dramatic damage to ecosystems and disruption to the climate system (Ackerman and Stanton, 2006). To meet these targets, the world needs to fundamentally change the way it generates and uses energy in the coming decades.

Renewable energy sources are those whose stock is rapidly replenished by natural processes, and which aren't expected to be depleted within the lifetime of the human species (Heavner et al., 2001). Renewable energy sources – solar, wind, biomass, geothermal, hydro and tidal – could make important contributions to sustainable development. Over the next twenty years, economically recoverable renewable resources will increase as a result of cost reductions from technological improvement and expanding markets (IEA, 2001).

Environmental impacts of renewable energy are site specific, but generalizations are still possible. Renewable energy is usually more environmentally friendly than alternative energy sources, especially with regard to air emissions. On the negative side, renewable energy can make large tracts of land unusable for competing uses, affect marine life, bird

life and onshore flora/fauna, and produce visual and noise pollution. Table 1.1 lists the costs associated with the use of different sources of renewable energy and below, each of these is briefly described.

Table 1.1 - Renewable Energy Cost Assessment (IEA 2001).

	Current Cost	**Cost reduction by 2020**
Bio-energy	High. Cost-effective in applications with low fuel cost. Co-firing is a *relatively low-cost retrofit* option.	10-15%
Wind onshore	Relatively low; lowest compared to other renewables	Up to 15-25%
Wind offshore	High	20-30%
Solar Photovoltaic	Very high. Cost-effective only in niche markets	30-50%
Solar Thermal	Very high	30% +
Geothermal	High	10%
Hydro	Low for large projects	10%

1.1.4.1 Bio-energy

Bio-energy is a term used to describe energy derived from organic materials (living plants) and plant components. Crops grown for bio-energy include traditional crops such as wheat and oilseed rape, but also dedicated energy crops, such as short-rotation willow-coppice, unusual grasses and forestry products. The great appeal of bio-energy is that it is theoretically a renewable source of energy: crops can be converted to energy either by being processed into liquid fuel for the transport sector (bio-fuels) or by being burnt in power plants (biomass). With combustion, carbon dioxide is released. Bio-energy production is never a neutral process when it comes to greenhouse gases (Bird Life

International, 2006). During production, processing and transportation of the crops there are many other inputs to consider: fossil fuels are used to power tractors for working the land; fertilizers and pesticides are needed to grow the energy crops; N_2O, which is one of the most potent greenhouse gases, is released from fields that are intensively fertilized; converting the crop into fuel is energy-intensive. Moreover, large scale production of biomass crops would entail large deforestation and conversion of heterogeneous cyclic cultures to steady, persistent biomass growth, with potential soil impoverishment and farmers' malnutrition (Aldhous, 2004, Ernsting, 2007).

1.1.4.2 Renewable energy sources

Natural processes can be exploited for producing energy. This way, air pollutants from energy production are minimized.

Hydro-energy is used in generating electricity from falling water. The cost of implementing the hydro-technology is predicted to be huge for current energy needs. Large-scale hydro-energy projects may disturb local ecosystems, reduce biological diversity or modify water quality (WWF, 2005) and, moreover, the sites where it could be developed in large-scale in different countries, are usually already used for other applications.

Tidal energy relies on tides and tidal currents as a possible source of vast amounts of electrical energy. Specially designed machines submerged in the water may be able to capture large amounts of energy from the rising and falling tide and from ocean currents. Tidal power has great potential for future power and electricity generation because of the massive size of the oceans, and might provide a big percentage of e.g. England's electrical needs (Mueller and Wallace, 2008).

Geothermal energy has great potential as source of alternative energy, harnessing the energy being naturally produced by the Earth. Huge amounts of geothermal energy are present below the surface of the planet. Geothermal energy would take humanity a long way in the direction of independence from oil and coal (Lund and Freeston, 2000), and is relatively inexpensive.

Wind energy uses turbines put in motion by the wind to make mechanical energy and convert it to electrical energy. Since no combustion occurs in wind power generation, there are no direct emissions of greenhouse gases or other pollutants. Every megawatt-hour (1,000 kilowatt-hours) of electricity generated by a wind turbine offsets the equivalent of 500 to 1,000 kg of carbon dioxide, depending on the type of fuel used to generate the electricity (Tegen, 2006). Given this advantage plus the steadily declining costs of this kind of energy, wind may be one of the most significant renewable energy sources for the next few decades.

Each day more *Solar energy* hits the Earth than the total energy that the 6.7 billion inhabitants of the planet would consume in 25 years (Stoddard et al., 2006). Clean energy from the sun can replace power sources that pollute the environment. The few emissions of greenhouse gases or air pollutants generated by solar energy technologies occur mostly during the manufacturing process. A 100 MW solar power plant, over its 20-years life, will avoid more than 3 million tons of carbon dioxide emissions when compared with the cleanest conventional fossil fuel-powered electric plants available today. Solar power generation can be a profitable business, researchers have found out

Renewable energy will be a highly dynamic part of the clean technology spectrum for several decades to come, beyond just climate change. Energy security too is a key plank

of policy, especially in countries like the UK and the US whose domestic oil and gas supplies are a dwindling part of the energy mix. Climate change mitigation and energy security are not in themselves stimulants in free markets, as their associated price signals are relatively weak. In order to achieve a level playing field, these factors need to be monetised through carbon pricing or taxes, incentives for renewable energy production or a combination of both (Wolfe, 2008). Germany, Spain, Japan, several States of the US and those other governments that have recognised this, have achieved significant market growth and an early mover advantage for their industry.

The wider European Union is now expected to follow thanks to an ambitious sustainable energy package of policies recently negotiated. The Renewable Energy Directive part of this package will give all EU states a target for the penetration of renewable energies into the total energy mix by 2020. The average will be 20% of overall energy – electricity plus heat plus transport. The UK (as a late adopter) will have a target of 15% - a ten-fold increase on the 2005 level. This requires a huge acceleration in the rate of deployment even from the higher levels achieved since the introduction of the Renewables Obligation (Wolfe, 2008).

1.2 Solution to climate change: CO_2 underground sequestration

Carbon capture and storage (CCS) is an approach to mitigating climate change by capturing carbon dioxide from large point sources such as power plants and subsequently storing it away (i.e. underground) safely instead of releasing it into the atmosphere

(Gronkvist et al., 2006, Holloway, 2001, IPCC, 2005). Technology for capturing CO_2 is already commercially available for large CO_2 emitters, such as power plants.

1.2.1 Prospective geological formations for storage

The Earth's crust has prevented liquid and gaseous hydrocarbons from reaching the surface environment for up to millions of years. On these bases, scientists believe it can be the safest place for CO_2 to be stored indefinitely. The compressed gas would be injected under impermeable cap rocks, in permeable reservoirs of different geological history.

There are three priority types of geologic formations in which CO_2 can be stored, and each presents different opportunities and challenges (Figure 1.4):

- *Depleted oil and gas reservoirs.* These are formations that held crude oil and natural gas over geologic time periods. In general they involve a layer of porous rock with a layer of impermeable rock above, forming a dome. It is the dome shape that traps hydrocarbons. This same dome offers great potential to trap CO_2 and makes these formations excellent sequestration opportunities. As a commercial benefit, CO_2 injected into a depleting oil reservoir can enable incremental oil to be recovered (Li et al., 2006).

- *Unmineable coal seams* are too deep or too shallow to be mined economically. All coals have varying amounts of methane adsorbed onto pore surfaces, and wells can be drilled into unmineable coal beds to recover this coal bed methane (CBM). CO_2 is preferentially adsorbed onto the surface of the coal, releasing the methane, which is then exploited. Two or three molecules of CO_2 are adsorbed for each molecule of

methane released, thereby providing an excellent storage sink for CO_2 (Amorino et al., 2005).

- *Saline aquifers* are layers of porous rock that are saturated with brine. They are much more common than coal seams or oil and gas bearing rock, and represent an enormous potential for CO_2 storage capacity (IPCC, 2005). However, much less is known about saline formations than is known about crude oil reservoirs and coal seams and there is greater uncertainty associated with their amenability to CO_2 storage.

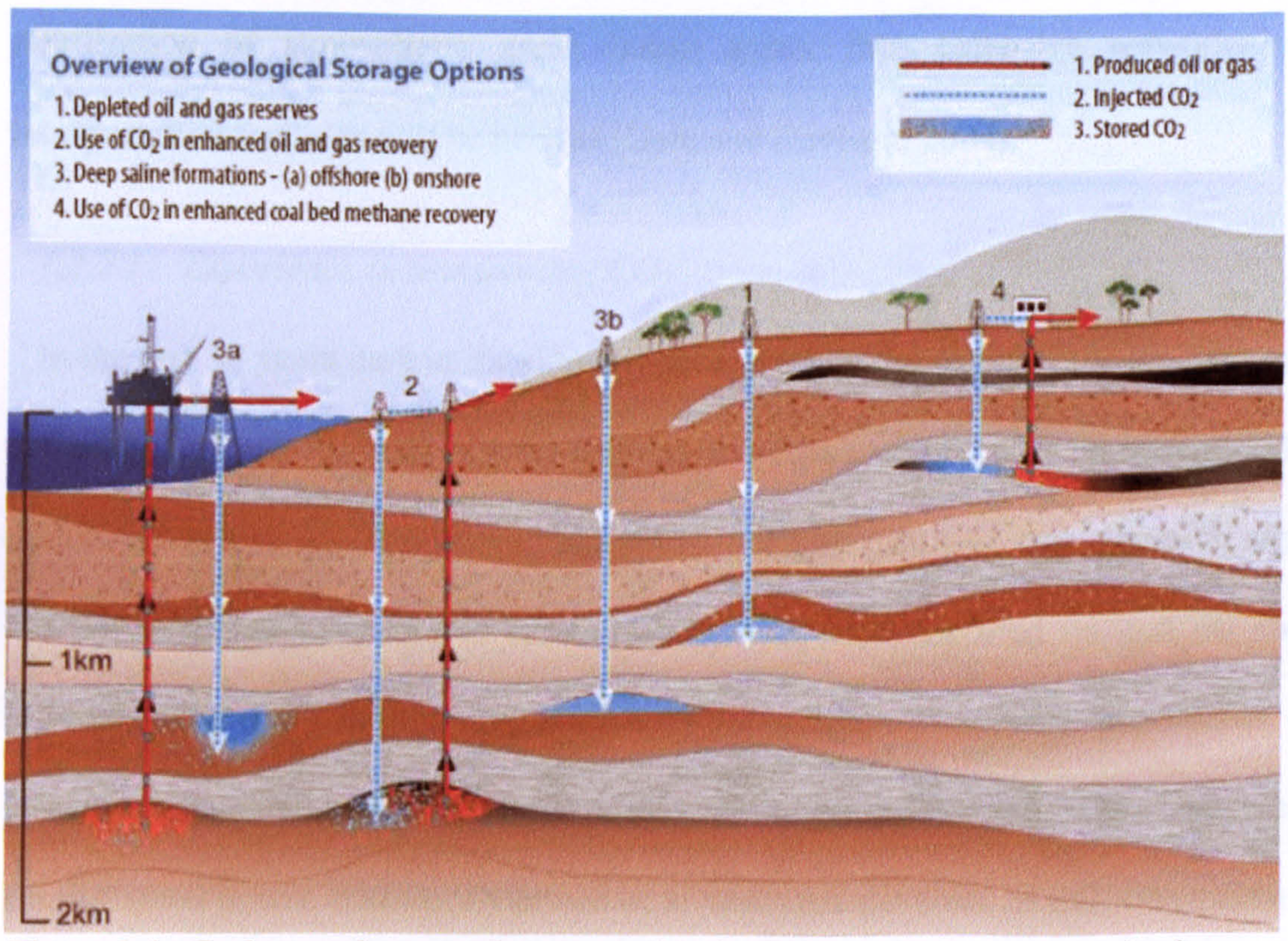

Figure 1.4 - Carbon underground sequestration in different geological repositories.

The Norwegian oil firm Statoil is currently injecting 1 Mt CO_2 yr^{-1} under the seabed in the North Sea (Sleipner project). Operations begun as early as 1996 and the foreseen available reservoir volume would accommodate up 600 Mt of captured CO_2.

1.2.2 Transportation of CO_2 in CCS projects

Although capture and storage of CO_2 is studied intensively worldwide, the biggest efforts are in the processes of CO_2 capture in industrial plants (with the aim of reducing the costs of separating and pressurizing CO_2) and monitoring of CO_2 after underground injection, studying the best target reservoirs with the possibility of enhancing hydrocarbon production.

The critical linking process, between the separation of CO_2 and its subsequent storage, is its transportation. If CCS technology is to gain public acceptance and be introduced widely, achieving the magnitude of CO_2 reductions needed for the UNFCC goal of stabilization of atmospheric green house gases, then extensive networks of CO_2 transportation facilities will be needed (Gale and Davison, 2004).

1.2.2.1 Experience in transporting CO_2

In the last 30 years carbon dioxide has been used by the oil industry for enhancing the production of hydrocarbons, via the restoration of the pressure gradient in semi-exhausted oil and gas reservoirs (Amorino et al., 2005). A significant CO_2 transportation capability has developed to meet this need. Currently, CO_2 is transported on and off shore by different means: road, railway, marine and pipelines. All these alternatives can in principle be applied in a future large scale transportation system for CO_2 recovered from fossil-fuelled power stations. Svensson et al. analysed the costs of CO_2 transportation for different scenarios, concluding that, for on-shore transportation, only the pipeline alternative remains. Pipeline costs depend strongly on the volumes being transported and, to a lesser extent, on the distances involved, averaging some 1-5 USD/t CO_2 per 100 km

for the on-shore pipeline case, the cost falling to 0.3-0.5 USD/t CO_2 for the off-shore shipping mean (Svensson et al., 2004).

The experience gained in moving hazardous liquids can be applied to the transportation of CO_2, taking into account the particular behaviour of this fluid when a leakage from a superficial/shallow facility occurs. CO_2 properties, transportation, pipeline design and control considerations are discussed further in Chapter 4.

1.2.2.2 Risk in CO_2 transportation

Risk analysis is a tool for quantifying risk and is normally based on the product of frequency and consequence of a hazard (Engebø et al., 2007). Hence, in order to determine the risk there are several discrete sets of information that need to be developed. These are listed below:

- ✓ Identification of hazards;
- ✓ Frequency of occurrence of hazards;
- ✓ Consequences of hazard occurring.

Risk analysis of geological sequestration is made more complex by the absence or scarcity of data for frequencies and consequences (Vendrig et al., 2003). On the other hand, there is already CO_2 transportation expertise in some developed countries, and the issues in this concern are reasonably understood and can be quantified.

1.2.2.3 Effects of CO_2 intake by humans

CO_2 is a cerebral vasodilator. Its main mode of action is as an asphyxiant although it also exerts toxic effects at cellular level. While, at low concentrations, gaseous carbon dioxide appears to have limited toxicological effect, at higher concentrations it leads to an

increased respiratory rate, tachycardia, cardiac arrhythmias and impaired consciousness. Concentrations above 10% by volume may cause convulsions, coma and death (Langford, 2005). Exposure can cause acidosis with symptoms of headache, nausea, visual disturbances and respiratory problems, typically occurring only after concentrations reach 15,000 ppm. People including skiers in topographical hollows and workers in confined spaces have died as a result of CO_2 asphyxiation around a volcano that was emitting CO_2 in the USA (Rogie et al., 2001). Some 1700 people are reported to have died from CO_2 asphyxiation as a result of CO_2 release from Lake Nyos, Cameroon (Plasynski and Beckert, 2008).

Chapter 4 deals in more depth with the analysis of risk in CO_2 transportation for CCS projects, analyzing failure cases and frequencies, consequences, human and environmental risk for engineered modular transportation systems. There is naturally a possibility of leakage from this infrastructure through component failure or third-party intrusion. The failure probability of some parts of the high-pressure transportation system has been well documented in the oil industry literature (Burgherr and Hirschberg, 2005, Hirschberg et al., 2004, Townes et al., 2004), and the principal causes of natural gas/CO_2 pipeline incidents have been classified: relief valve failure, weld/gasket/valve packing failure, corrosion and outside forces. In their study, Vendrig et al. (2003) reported an overall failure probability from a CCS transportation facility of about 0.32 yr^{-1}[†], irrespective of its location (underground or above the surface) but with much higher

[†] This result is valid for a modular pipeline system comprehensive of CO_2 recovery at source, Converging pipelines, one Booster station, 10km pipeline and one injection plant. Singular modules have lower probability but one integral transportation system would have a higher failure probability (it would comprehend more than 10 km of pipeline and maybe more than one booster station).

likelihood for surface compartments (i.e. CO_2 Recovery at source, Booster stations and Injection facilities).

Depending on the size of a potential leak, the pressure at which the CO_2 is transported (in this study assumed to be 10 MPa) and whether or not the facility involved in the spill is buried, a different amount of carbon dioxide will be released in the atmosphere, posing a hazard to people and the environment in the proximity of the release. Shape and size of the formed cloud and the velocity of CO_2 in dispersing to safe concentration will be dependent on atmospheric conditions (stability, wind speed and direction, turbulence, pressure and temperature) and site topography (CO_2 is denser than air and tends to stay near the surface).

1.2.3 CCS, current European status

In order to limit climate change to a manageable level, the European Council recognised that urgent action is needed. The EU is committed to adopt the necessary domestic actions and take the lead internationally to ensure that global average temperatures do not exceed pre-industrial levels by 2° C (EU, 2007). In order to meet the 2° C target, it has been proposed that the EU pursues in the context of international negotiations the objective of a 30% reduction in GHG emissions by developed countries by 2020 (compared to 1990 levels). With this aim in mind, carbon capture and storage is considered as one of the temporary technological solution to control CO_2 emissions from large point sources.

1.2.3.1 Costs of CCS and barriers to overcome

Investment of the order of billions of euros is required to bring CCS to market. Moreover, CCS-equipped coal-fired power plants face some 25-75% increase in operating costs, compared with non-CCS plants – mostly due to efficiency losses and costs of capture and CO_2 transport. However, experts estimate that with a focused R&D and demonstration effort, this increase in CCS costs can be brought down by 50% between now and 2020 (EU, 2008b).

Public policy is essential to ensure CCS deployment because it is a technology that is almost exclusively driven by political concerns and diversification of energy supply: it has no separate short-term commercial rationale. In the long term, however, there are positive impacts to consider which can be summarized: the positive economic revenue from learning-by-doing (decreasing the overall CCS costs), the benefits of technology exports (European industry would become leading players in a potentially burgeoning global market for CCS technology), the creation of high-skilled jobs, the potential positive feedback of achieving global climate objectives from deployment in the EU and any associated benefits coming from air pollution reductions.

If commercial barriers to CCS deployment represent the main obstacle, the environment, health and safety risks are also to be considered. In doing this, all the components of CCS must be accounted for, namely capture, transport, injection and storage. Although it is likely that CO_2 storage sites will present the greatest regulatory challenge, because of the novel nature of the activity, CO_2 transportation also presents hazard issues, as it will be seen throughout this thesis.

1.2.3.2 European perspective for the coming decade

Analysis of the different options has shown that without CCS the costs of meeting the required GHG emission reductions (around 30% by 2030) could be up to 40% higher than with CCS (IPCC, 2007a).

CCS technology is already used in industry but will need to be adapted for use in large-scale power plants and improved through advanced R&D. European industry is clearly involved and strategic research needs are well defined. Over 20 potential demonstration projects have been signaled by European industry in the past two years (ZEP, 2008). Bringing a sufficient number of them to realization in the required time (i.e. to be fully operative by 2015) necessitates a concerted action by European industry, Member States and the European Community.

For post-2020, the European Commission is scrutinizing four main options concerning the inevitability of CCS application (EU, 2008a): (a) Making CCS mandatory for new coal-fired power plants from 2020 onwards; (b) Making CCS mandatory for new coal- and gas-fired power plants from 2020 onwards; (c) Making CCS mandatory for new coal-fired power plants from 2020 onwards, together with retrofit of existing plants (built between 2015 and 2020) from 2020; (d) Making CCS mandatory for new coal- and gas-fired power plants from 2020 onwards, together with retrofit of existing plants (built between 2015 and 2020) from 2020.

The European energy businesses involved in power generation from fossil fuels will gain in CCS an important instrument enabling them to remain major players in the European energy landscape and providing also new business opportunities. They can therefore rightly be expected to make significant commitments of their own resources in the

interest of early demonstration. Public funds may also be needed for some projects, albeit for a limited part of the demonstration period and at levels depending on future carbon prices (EU, 2008b).

At this stage it is hard to say with any certainty what the impacts of delaying widespread European deployment to a later date would be. Intuitively, later deployment in Europe will delay the commercial availability of the technology, which in turn may mean either that the mid-century climate goals are missed (with the attendant consequences) or that the required abatement will have to be done at higher costs due to the more limited learning and hence limited cost reduction.

1.3 Leakages from CCS transportation facilities

Carbon dioxide is denser than air and tends to remain close to the surface, posing a major health hazard. Its dispersion would be influenced by the specific topography of the area (Mazzoldi et al., 2007). Modelling of CO_2 atmospheric dispersion is a *conditio-sine-qua-non* before the start of any transportation program for CCS and during its working life, mainly if the facility affected by potential leakages is located in the proximity of an inhabitated area, a place of historic interest and/or a social amenity such as roads.

1.3.1 Atmospheric dispersion modelling

A model is a simplified picture of reality. Its purpose is the simulation of physical, chemical or biological processes through the utilization of mathematical algorithms that take into account a number of variables of importance in the development of the process. An ideal model is one that can account for all these variables. Due to the complexity of

many processes and the large number of variables governing the evolution of these, real models do not usually contain all the features of the real systems but represent the features of interest for the management issue or scientific problem it is wished to solve by their use. Models are widely used in science to make predictions and are often used to identify the best solutions for the management of specific environmental problems.

Air quality models are used to predict the transport and the turbulent dispersion of dangerous gases released in the atmosphere. Several studies regarding potential atmospheric dispersion of CO_2 leaked from CCS transportation facilities have been drawn up in the last decade (IEA, 2003, Kruse and Tekiela, 1996, Turner et al., 2003, Vendrig et al., 2003), examining as a first objective the maximum extent of the plume created by a specified leak for particular atmospheric conditions. These investigations were carried out utilizing Gaussian puff models to simulate the dispersion of the toxic gas in the atmosphere, in the vicinity of the leak. In this thesis, a Gaussian model will be used in its own right and the results compared with those of an alternative computational fluid dynamics (CFD) model. The latter will also be used to investigate dispersion situations for which the Gaussian model is not appropriate.

1.3.1.1 Gaussian models

Gaussian-plume models are widely used, well understood, easy to apply, and until more recently have received international approval (MacDonald et al., 2004). Even today, from a regulatory point of view, ease of application and consistency between applications is important. Also, the assumptions, errors and uncertainties of these models are generally well understood.

The Gaussian-plume formula is derived assuming 'steady-state' conditions. That is, the Gaussian-plume dispersion formulae do not depend on time, although they do represent ensemble time averages. The meteorological conditions are assumed to remain constant during the dispersion from source to receptor, which is effectively instantaneous. Emissions and meteorological conditions can vary from hour to hour and within hours but the model calculations in each hour are independent of those in other hours.

Gaussian-plume models are generally applicable when:

a) Pollutants are chemically inert, a simple first-order mechanism is appropriate, or the chemistry may be carried out as a post-processing step;

b) Terrain is not steep or complex;

c) Meteorology may be considered spatially uniform;

d) There are no complex obstacles on the terrain;

e) There are few periods of calm or light winds.

Gaussian atmospheric dispersion models give conservative results for dispersion over relatively short distances or low-level sources. Validations show these models are more likely to over- rather than under-predict ground-level concentrations, which offers some degree of safety in the regulatory environment when assessing discharges from short or low-level sources (Bluett et al., 2004).

1.3.1.2 Computational Fluid Dynamics models

Computational Fluid Dynamics (CFD) is a branch of fluid mechanics that uses numerical methods and algorithms to solve and analyze problems that involve fluid

flows. Computers are used to perform the large number of calculations required to simulate the interaction of fluids with the complex surfaces used in engineering.

The most fundamental consideration in CFD is how to treat a continuous fluid in a discretized fashion. One method is to discretize the spatial domain into small cells to form a volume mesh or grid, and then apply a suitable algorithm to solve the equations of motion (Euler equations for inviscid, and Navier-Stokes equations for viscid flow) in each of the volume elements. CFD codes solve conservation equations for mass, momentum and energy (i.e. Navier-Stokes equations), accounting for the mixing and transport of a chemical species by solving conservation equations describing convection and diffusion for the species. For turbulent flows, the Reynolds-averaged approach is employed to solve the Navier-Stokes equations.

CFD techniques are increasingly being used to model short-range atmospheric dispersion, especially the flow and dispersion around buildings and other geometrically complex structures. The proper application and accuracy of such CFD techniques have been assessed by many studies (Burman, 1998, Dharmavaram et al., 2005, Koutsourakis et al., 2003, Pullena et al., 2005, Riddle et al., 2004, Scargiali et al., 2005, Tang et al., 2006), that demonstrated CFD simulation to be a proven and applicable tool in support of environmental assessment studies.

1.4 Thesis overview

The main issue debated in this work is the atmospheric dispersion of carbon dioxide after leakages from CCS transportation facilities and the risk for humans associated with

this process. This thesis is arranged in seven chapters. In this first chapter an introduction to the problem and a brief overall discussion has been given. In the subsequent chapters, specific topics dealing with different aspects of the problem will be addressed.

The second chapter introduces the two atmospheric dispersion models used for simulating the dispersal of the highly concentrated waste gas (i.e., the Gaussian ALOHA 5.4 and the CFD PANACHE 3.4.1), listing the assumptions made and the equations used in both.

The third chapter presents an evaluation exercise in which results from the two models in simulating field releases trials are compared between and against field observations. The two sets of trials used for evaluating the models are the Prairie Grass and Kit Fox field experiments.

The fourth chapter begins introducing the reader to carbon dioxide's chemical properties and its huge temperature decrease consequent to a pressure drop (Joule-Thomson effect). Afterwards, a more detailed view of a hypothetical CO_2 transportation modular system is given, describing the leakage event probabilities for the different leak sizes considered. Data for modular engineered system, failure occurrence frequencies, representative leak sizes and amounts of released gas have been taken from the report of Det Norske Veritas (DNV) (Vendrig et al., 2003). In the second part of the chapter, consequences of leak occurrence were considered, modelling release dispersion with the Gaussian and CFD models. Risk analyses for the generic CO_2 transportation system have been drawn up and results from the two models compared.

In chapter five, the formation of a dry ice bank after a downward leakage from a CO_2 transportation facility is discussed. The sublimation rate of solid carbon dioxide was

calculated, assuming an energy balance at the surface of the bank representing characteristic atmospheric conditions in the UK. The dispersion of the resultant gas (the risk engendered) was simulated using the atmospheric dispersion models described.

Computational Fluid Dynamics models can account for high-speed gas release into the atmosphere. In the sixth chapter, the potential of the CFD tool is explored in simulating the dispersion of the dense gas after the jet-release occurring as a consequence of a leakage, due to the high pressure within the transportation system. In the same chapter CFD is used to simulate the dispersion of CO_2 within the complex built environment of an industrial site.

Chapter seven presents the conclusions of the study and suggestions for future research directions.

CHAPTER 2

ATMOSPHERIC DISPERSION MODELLING

Introduction

Atmospheric dispersion modelling is the mathematical simulation of how air pollutants disperse in the ambient atmosphere. It is performed with computer programs that solve the mathematical equations and algorithms which simulate the pollutant dispersion. The dispersion models are used to estimate or to predict the downwind concentration of air pollutants emitted from sources such as industrial plants and vehicular traffic. Such models are important to governmental agencies tasked with protecting and managing the ambient air quality.

A dispersing vapour cloud will generally move (advect) in a downwind direction and spread (diffuse) in the lateral and vertical directions. A cloud of gas that is denser than air also spreads under gravity as it sinks, and can hence move upwind to a small extent.

'Transport and Diffusion Code' is the software engine that computes advection and diffusion. The principal mechanism of diffusion is turbulence, which has traditionally been represented as a stochastic process (e.g. Gaussian modelling). A stochastic process evolves in time according to probabilistic equations – that is, the behaviour of the system is determined by one or more time-dependent random variables. On the other hand, a

deterministic process is governed and predictable in terms of definitive laws, such as dynamics equations (i.e. CFD modelling).

2.1 ALOHA 5.4

ALOHA (Areal Location of Hazardous Atmospheres) is a computer program designed for use on site at accidental chemical spills when evacuation information is needed rapidly (Reynolds, 1992). It can be used to model the dispersion of a cloud of pollutant gas in the atmosphere and display a diagram that shows an overhead view of the regions, or threat zones, in which it predicts that key hazard levels (LOCs, Levels Of Concern) will be exceeded. For each LOC chosen, ALOHA estimates a threat zone where the hazard is predicted to exceed that LOC at some time after a release begins. Figure 2.1 gives an example of the information provided by ALOHA.

ALOHA is a tool that can be used during emergency situations and, as such, meets certain criteria, such as:

- ✓ *Operates on common computers*. The model must run quickly on small computers (PC or Macintosh) which are transportable and affordable for most users. Algorithms and physics represent a compromise between accuracy and speed so that good results are available quickly enough to be of immediate use;
- ✓ *User friendly*. The program must be clear and easy to use so less experienced responders can use it during high-pressure situations with minimal chance of error;
- ✓ *Reliable*. The user interface is designed to minimize operator error, the program checks and cross-checks all entries before proceeding to solutions.

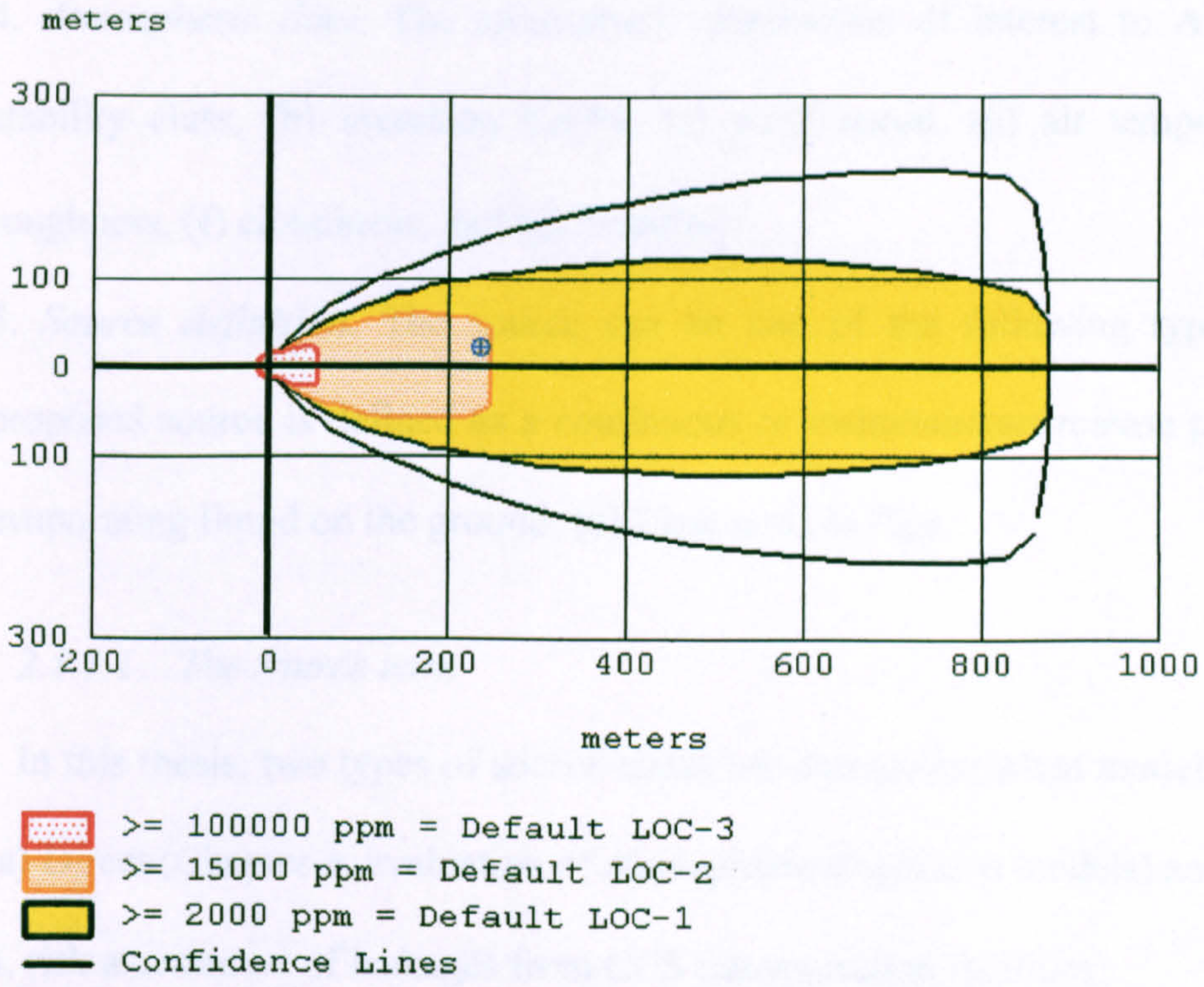

Figure 2.1 - ALOHA's diagram. Threat zones for the three Levels of Concern chosen. The point highlighted in the figure is for later consideration (paragraph 2.1.4).

2.1.1 ALOHA inputs

To be of maximum use, ALOHA requires a minimal amount of information which the user can enter easily with the help of an extensive graphical interface.

1. *Geographic location and time.* Location is used to calculate incoming solar radiation and elevation is used to calculate ambient air pressure;

2. *Site definition.* Ground roughness is needed to calculate dispersion. Information about a particular building of interest is used to predict indoor concentrations and doses;

3. *Chemical definition.* Chemical selection determines all physical and chemical properties of the material under study. In this study, carbon dioxide (CO_2) is considered;

4. *Atmospheric data.* The atmospheric parameters of interest to ALOHA 5.4 are (a) stability class, (b) inversion height, (c) wind speed, (d) air temperature, (e) ground roughness, (f) cloudiness, and (g) humidity;

5. *Source definition.* The source can be one of the following types: (a) Direct, the proposed source is defined as a continuous or instantaneous release point; (b) Puddle of evaporating liquid on the ground; (c) Tank and (d) Pipe.

2.1.1.1 The source term

In this thesis, two types of source terms are considered when modelling with ALOHA: (a) Direct (Chapter 3, evaluation of atmospheric dispersion models) and (b) Pipe (Chapter 4, risk assessment of leakages from CCS transportation facilities).

Direct injection of a gas in the atmosphere is the simplest of all algorithms and the most hypothetical (i.e. less likely to happen in reality). The direct source is a point release and can be either a continuous emission of rate Q (kg s^{-1}) or an instantaneous release of total mass, M (kg).

The gas pipe release calculations are based on modifications made by Wilson (Wilson, 1979) to the model developed by Bell (Bell, 1978). A key assumption in the theory is that the process is almost entirely isothermal at temperature T, defined by the user. Adiabatic decompression of the gas within a distance of 200 pipe diameters from the leak is assumed. Beyond that distance, the flow is approximately isothermal with frictional heating and adiabatic cooling in near balance. Wilson showed that an exponential was the correct solution of an isothermal, quasi-steady state pipe-flow, and that the release of gases from a finite length of pipe can be approximated by a double exponential of the form:

$$Q_{(t)} = Q_0 (1 + \alpha)^{-1} [\exp(-t/\alpha^2\beta) + \alpha \exp(-t/\beta)], \qquad (2.1)$$

where $Q_{(t)}$ is the rate of mass discharge per unit time, Q_0 is the initial mass flow at the time of the rupture, α is a non-dimensional mass conservation factor and β is the release rate time constant, dependent on the gas exit temperature and specified in Wilson (1979).

The pressure in most pipelines will be much greater than ambient pressure, therefore, Q_0 is calculated assuming a choked flow condition.

2.1.2 Dispersion model, neutral gas

Neutral gases do not alter the density of the ambient air, and thus have no effect on air flow. Known as passive contaminants, field studies have shown that neutral gases disperse such that their concentration distributions fit well to Gaussian (bell-shaped) curves. Models that use this distribution are called Gaussian plume models.

The classical Gaussian plume is a steady-state model that requires a continuous release of contaminant. The ensemble average (i.e. probabilistic) plume shape is approximated by time averages sufficient to smooth the effects of plume meandering, see Figure 2.2.

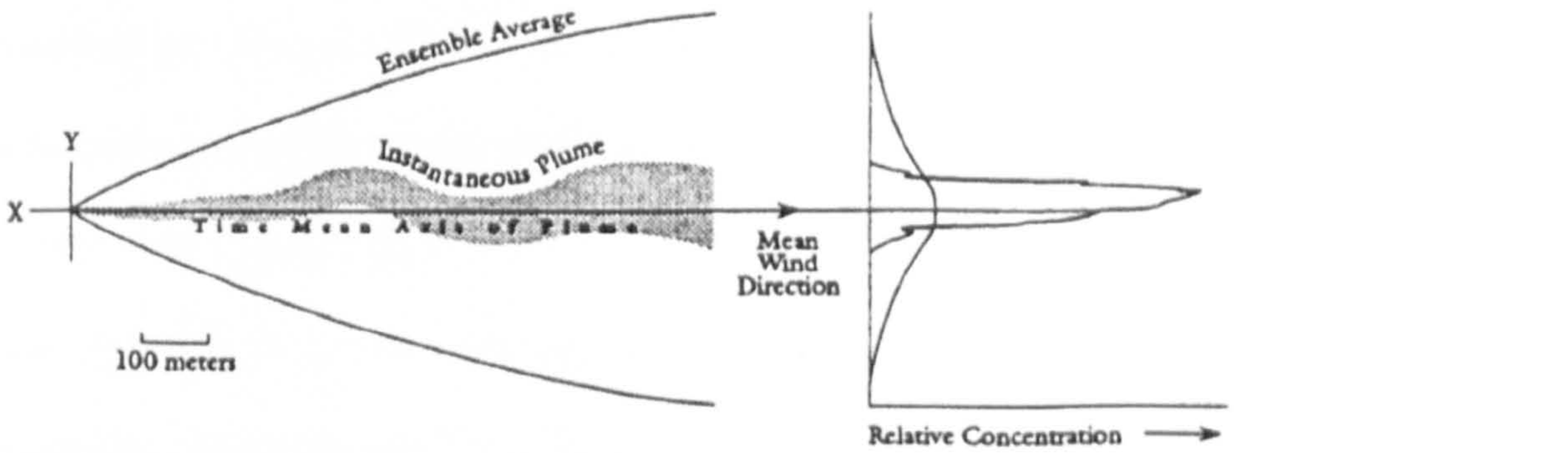

Figure 2.2 - Plan view of a continuous Gaussian plume. The ensemble concentration average is predicted by dispersion theory (Reynolds, 1992).

The equation for the Gaussian plume is a function only of the mean wind speed (assumed constant) and the crosswind and vertical standard deviations [$\sigma_y(x)$ and $\sigma_z(x)$ in equation 2.2, below]. The source strength, Q, is the mass of material released per unit time. The time averaged wind speed, U, is uniform everywhere. For a continuous point source release, the contaminant concentration, $C(x,y,z)$, is given by:

$$C(x,y,z)=\frac{Q}{2\pi\sigma_y\sigma_z U}\exp\left[-\frac{1}{2}\left(\frac{y}{\sigma_y}\right)^2\right]\left\{\exp\left[-\frac{1}{2}\left(\frac{z-h_s}{\sigma_z}\right)^2\right]+\exp\left[-\frac{1}{2}\left(\frac{z+h_s}{\sigma_z}\right)^2\right]\right\} \quad (2.2)$$

where σ_y and σ_z are the standard deviation of gas concentration in the cross-wind and vertical directions; both are functions only of the downwind distance, x. The z-dependent terms model the trapping effect of the ground by proposing a mirror source at distance h_s beneath the ground. The standard deviations are referred to as the dispersion parameters. ALOHA estimates these parameters from the values of time, wind speed and direction, ground roughness, stability class and cloud index input by the user (Hanna et al., 1982).

2.1.3 Dense gas dispersion

When a gas that is denser than air is released, it initially behaves very differently from a neutrally buoyant gas. The dense gas will first "slump" or sink. As the gas cloud moves downwind and spreads, some of the vapour can travel upwind of its release point (Britter, 1989). Farther downwind, as the cloud becomes more diluted and its density approaches that of air, its behaviour approaches that of a neutrally buoyant gas. This takes place when the concentration of the dense gas in the surrounding air drops below about 1 % (10,000 ppm). For small releases, this will occur in the first few meters. For large releases, this may happen much further downwind.

ALOHA assumes the ground below a leaking pipeline facility/tank or puddle to be flat, so that the fluid spreads out evenly in all directions. It does not account for pooling within depressions, for liquid/gas flow across sloping ground, or for the effect of topography on the surface concentration levels of a leaked heavy gas (e.g. CO_2).

The dense gas dispersion model in ALOHA is almost identical to the similarity model proposed by Colenbrander (Colenbrander, 1980), see Figure 2.3.

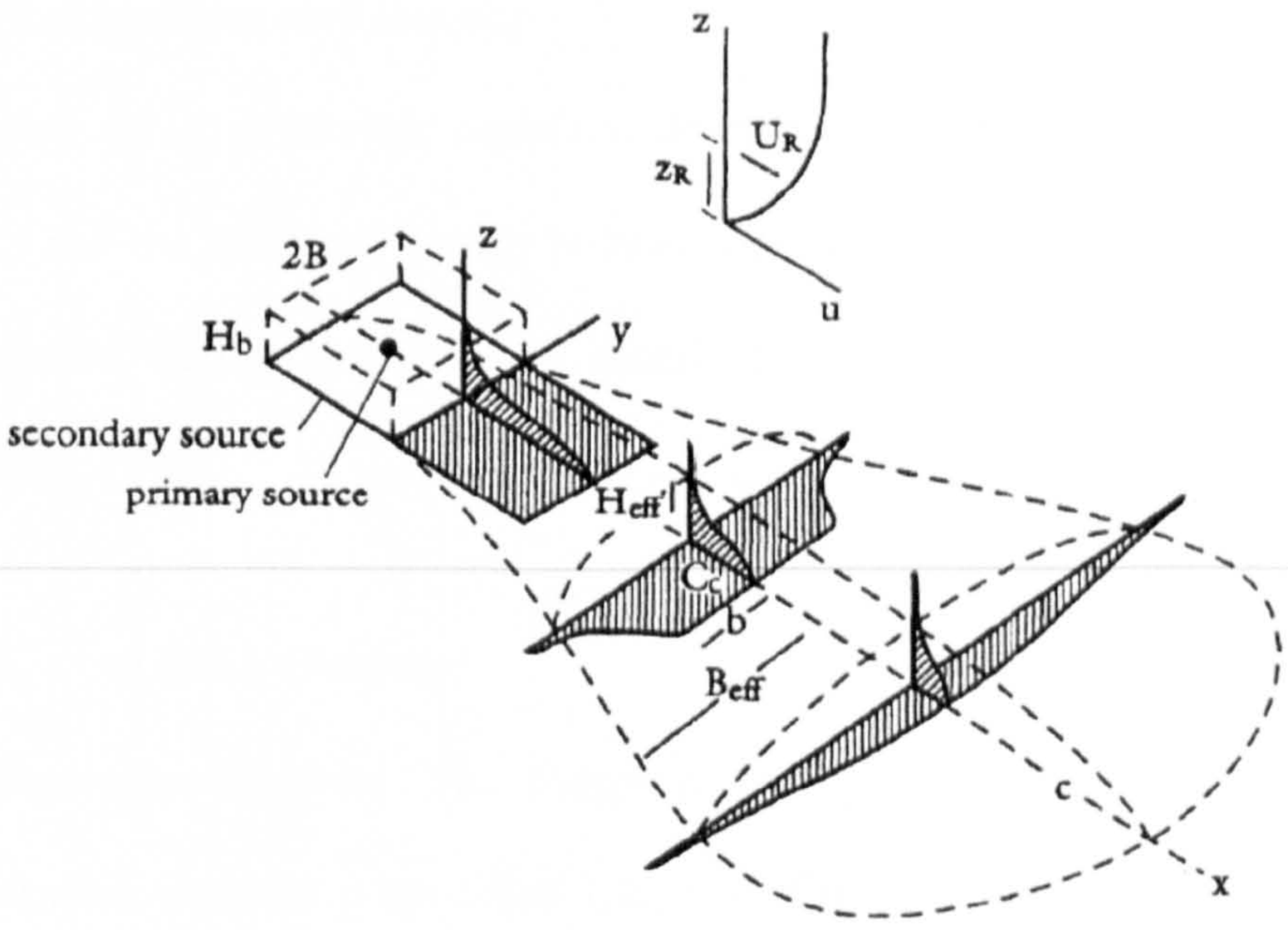

Figure 2.3 - Plume model proposed by Colenbrander (1980) and used in ALOHA.

The plume is assumed to be composed of (i) a horizontally homogeneous core of width 2b which has vertical dispersion, and (ii) Gaussian-shaped edges. The concentration is calculated as:

$$C(x,y,z)=\begin{cases} C_c(x)\exp\left[-\left(\dfrac{|y|-b(x)}{S_y(x)}\right)^2-\left(\dfrac{z}{S_z}\right)^{1+n}\right] & |y|>b(x) \\ C_c(x)\exp\left[-\left(\dfrac{z}{S_z}\right)^{1+n}\right] & |y|\le b(x) \end{cases} \tag{2.3}$$

Four variables in the above equation are functions of x and must be computed for each downwind step: $C_c(x)$ is the centreline ground-level concentration; $S_y(x)$ is the lateral dispersion parameter; $S_z(x)$ is the vertical dispersion parameter and $b(x)$ is the half-width of the homogeneous core section;

A coupled set of parametric equations describing the effective cloud width, height and velocity and the mass and energy balance, approximating the mean density of the cloud gas mixture during the time, is described in the ALOHA theoretical description (Reynolds, 1992).

2.1.4 ALOHA Outputs

1. *Dispersion footprint.* The footprint is a plan view of the area in which the concentration exceeds a specified Level of Concern. Often called the "dead canary footprint" after the practice of using a canary in a cage as an indicator of poisonous gases in mines, the footprint covers the area on which the concentration exceeds the prescribed concentration level at any time within the hour following initiation of a release. A dashed line which surrounds the footprint defines the possible error in footprint direction due to inability to adjust for changes in wind direction. The area within the dashed line will vary depending on the selected atmospheric stability. An example of the dispersion footprint window is given in Figure 2.1.

2. *Concentration vs time.* This plot tells the user the amount of chemical present at a specific location. Two curves are drawn in this plot, one for the pollutant concentration in the open air, and another for its concentration inside a hypothetical building. The latter feature of the Gaussian model is not used in this thesis.

3. *Source strength vs time.* This plot tells how rapidly the chemical is being released into the atmosphere.

4. *Concentration at point.* ALOHA is able to calculate the concentration of the released chemical released at any position in the dispersion area considered (Figure 2.1), during the time for which the dispersion is calculated. Figure 2.4 shows how ALOHA calculated CO_2 concentration indoors and outdoors at a distance from the source.

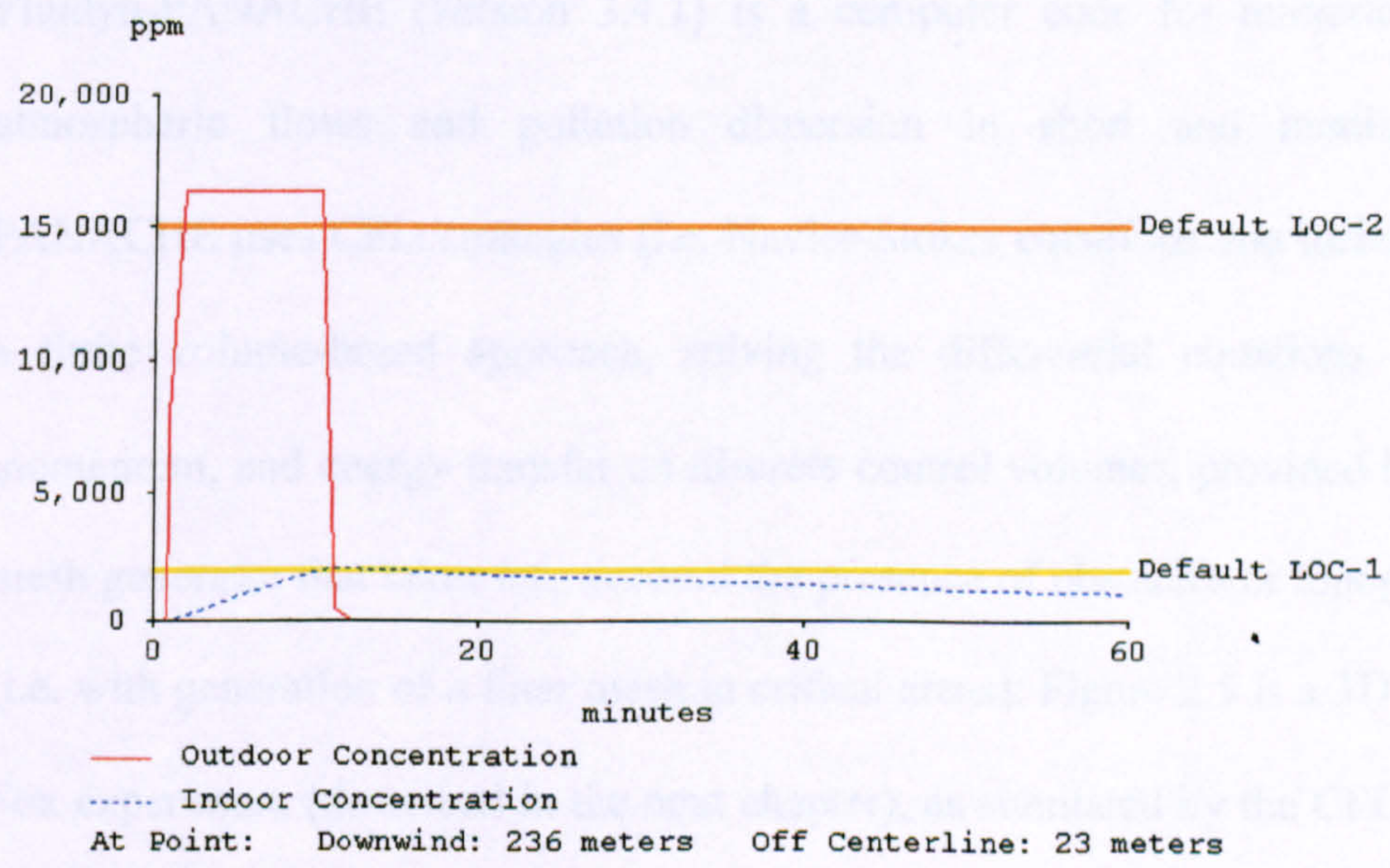

Figure 2.4 - Concentration at a point away from the source. The exact position of the point in relation to the source is displayed in Figure 2.1.

2.2 Computational Fluid Dynamics: PANACHE

Within Gaussian models for atmospheric dispersion of dense gases, a correction is made for the presence of buildings and other complex features by using a surface roughness parameter, which is only a crude approximation (Hanna et al., 2004). A need exists to obtain realistic estimates of dense gas plume dispersion in complex environments, particularly accounting for the presence of buildings or other plant obstructions, the turbulence developed around them, and the effects of complex topography. With the advance of computational technology and computing power, Computational Fluid Dynamics (CFD) tools are becoming more available for solving a wide range of problems.

Fluidyn-PANACHE (version 3.4.1) is a computer code for numerical simulation of atmospheric flows and pollution dispersion in short and medium-range scales. PANACHE uses CFD strategies (i.e. Navier-Stokes equations and turbulence models) in a finite volume-based approach, solving the differential equations governing mass, momentum, and energy transfer on discrete control volumes, provided by a non-uniform mesh generator that takes into account the presence of obstacles or topographical features (i.e. with generation of a finer mesh in critical areas). Figure 2.5 is a 3D image of the Kit Fox experiment (described in the next chapter), as simulated by the CFD model, together with the ground projection of the grid/control volumes.

In Figure 2.5 it can be clearly seen how PANACHE deals with obstacles and features of interest (e.g. the source term, which in the Kit Fox experiment is a square area ground source – the green square in the figure), generating a finer mesh in their surroundings.

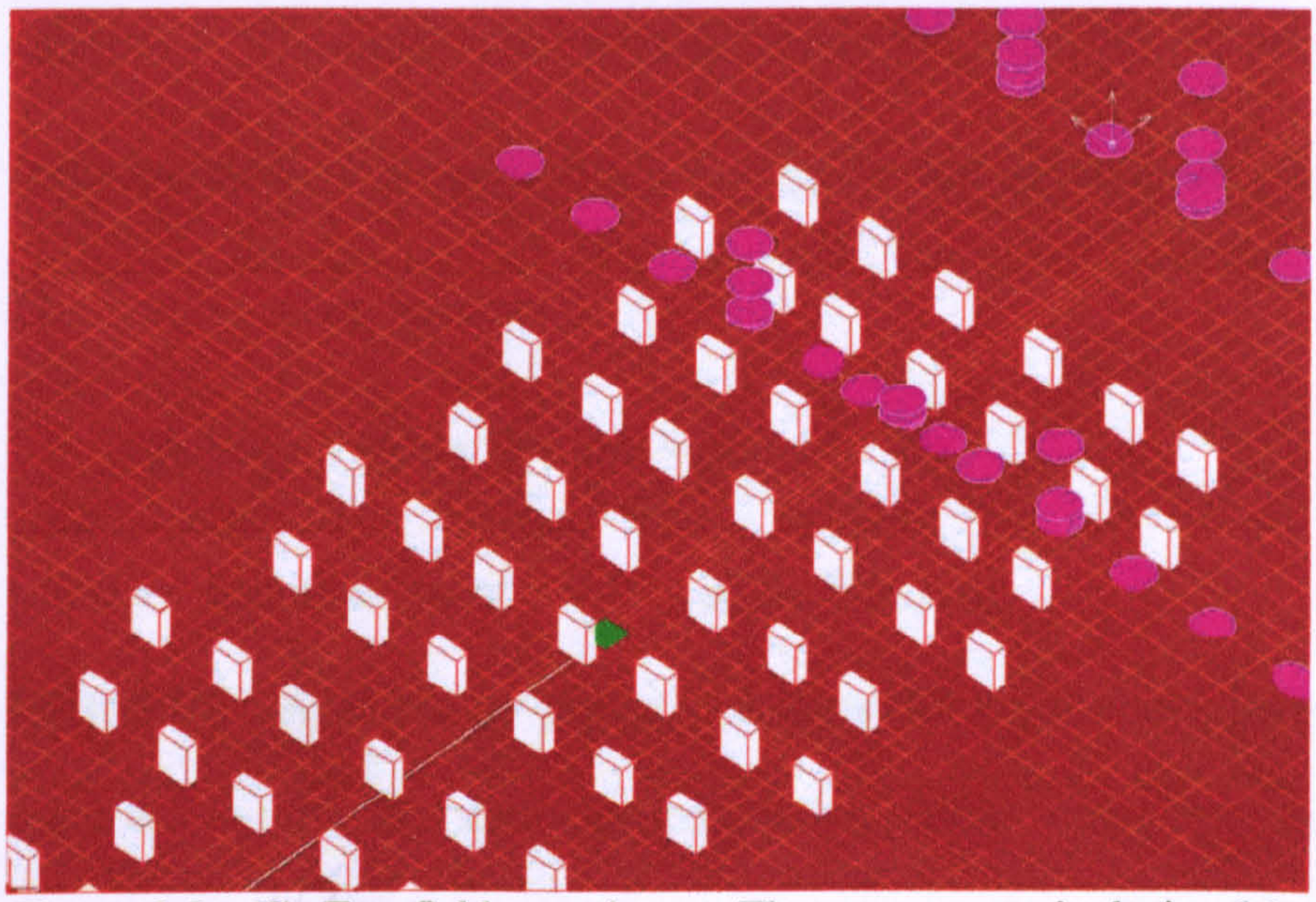

Figure 2.5 - Kit Fox field experiment. The area source is depicted in green; in violet are the different Monitor Points for recording gas concentrations and the grid on the ground is PANACHE mesh' projection.

2.2.1 Numerical scheme

As every CFD tool, PANACHE resolves the Navier-Stokes equations, accounting for the conservation of mass, momentum and energy. The continuity equation for total fluid density is:

$$\partial\rho/\partial t + \nabla\bullet[\rho u] = \delta_s + \delta_p \qquad (2.4)$$

where ∇ denotes the gradient of the considered quantity on the three dimensions; other symbols are as described in the Nomenclature. The appropriate SI units are implicitly assumed for all quantities.

The momentum equation for the fluid mixture is:

$$\partial\rho u/\partial t + \nabla\bullet[\rho uu\ \sigma] = \nabla P + F_s + F_g + F_p \qquad (2.5)$$

where σ = Newtonian viscous stress tensor (= $\mu[\nabla u+(\nabla u)^T]+\lambda(\nabla \bullet u)i$), μ,λ = first and second coefficients of viscosity, $\lambda = -2/3\mu$, T = transpose, i = unit dyadic;

The internal energy equation is:

$$\partial \rho I/\partial t + \nabla \bullet [\rho u\, I\, J] = \nabla \bullet u + \rho\varepsilon + Q_s + Q_p + Q_h \qquad (2.6)$$

where J = heat flux vector = $k\nabla T + \rho\Sigma[h_m \nabla(\rho_m/\rho)]$.

PANACHE solves the governing equations described above both in three-dimensional space and in time. The spatial differentiation is done over a three dimensional mesh made up of arbitrary hexahedrons. A control-volume or integral-balance approach is used to construct the finite difference approximations for each of these control-volumes to preserve local conservation of differenced quantities. The time differentiation enables a unified approach towards both transient and steady state phenomena and is carried out over a sequence of time steps. An implicit procedure enables the use of unlimited time steps.

Two different approaches to compute the gravitational force in the momentum equation have been used for the trials in this study:

- Buoyancy model, in which buoyancy terms due to density differences drive momentum:

$$F_g = (\rho - \rho_{amb})\, g \qquad (2.7)$$

where ρ_{amb} = ambient air density; g = gravitational acceleration vector.

- Full Gravity Model:

$$F_g = \rho\, g \qquad (2.8)$$

2.2.2 Boundary conditions

Boundary conditions are specifications of properties on the surfaces of the domains and are required to fully define the flow simulation. Ambient mean wind speed and air temperature profiles are boundary conditions (supposing they are constant over the domain area), represented by logarithmic functions for all the trials in this study. Such that:

$$v(z) = u^*/\kappa \, [\ln(z/z_o) \, \Psi_1(\varsigma)] \tag{2.9}$$

$$\theta(z) = \sigma_h \theta^*/\kappa \, [\ln(z/z_o) \, \Psi_2(\varsigma)] \tag{2.10}$$

where θ^* = temperature scale; $\Psi_1(\varsigma)$ and $\Psi_2(\varsigma)$ = similarity profile. The surface friction velocity, u^*, the temperature scale θ^*, and the Monin-Obukhov length, L are related by: $L = u^{*2}T / (g \kappa \theta^*)$ and $\theta^* = Q_h / (\rho C_p u^*)$.

The micrometeorological parameters, u^*, θ^*, and L are evaluated for different atmospheric stability classes. For unstable and neutral conditions $u^* = U^* [1+a \ln(1+bQ_0/Q_1)]$, where $U^* = \kappa v/\ln(z_m/z_0)$ is the friction velocity for neutral conditions, $z_m = 4h_{an} z_0$, h_{an} = anemometer height, $Q_0 = Q_h/\rho C_p \; Q_1 \; \theta U^{*3}/(\kappa g \; z_m)$, θ = potential temperature, a and b are constants dependent on z_o and z_m (Transoft, 2006). For stable conditions, Equations (2.9) and (2.10) are solved in L and the other parameters are found via their relations. Figure 2.6 displays the growth of wind speed with height by a logarithmic law, as accounted for by PANACHE (and ALOHA).

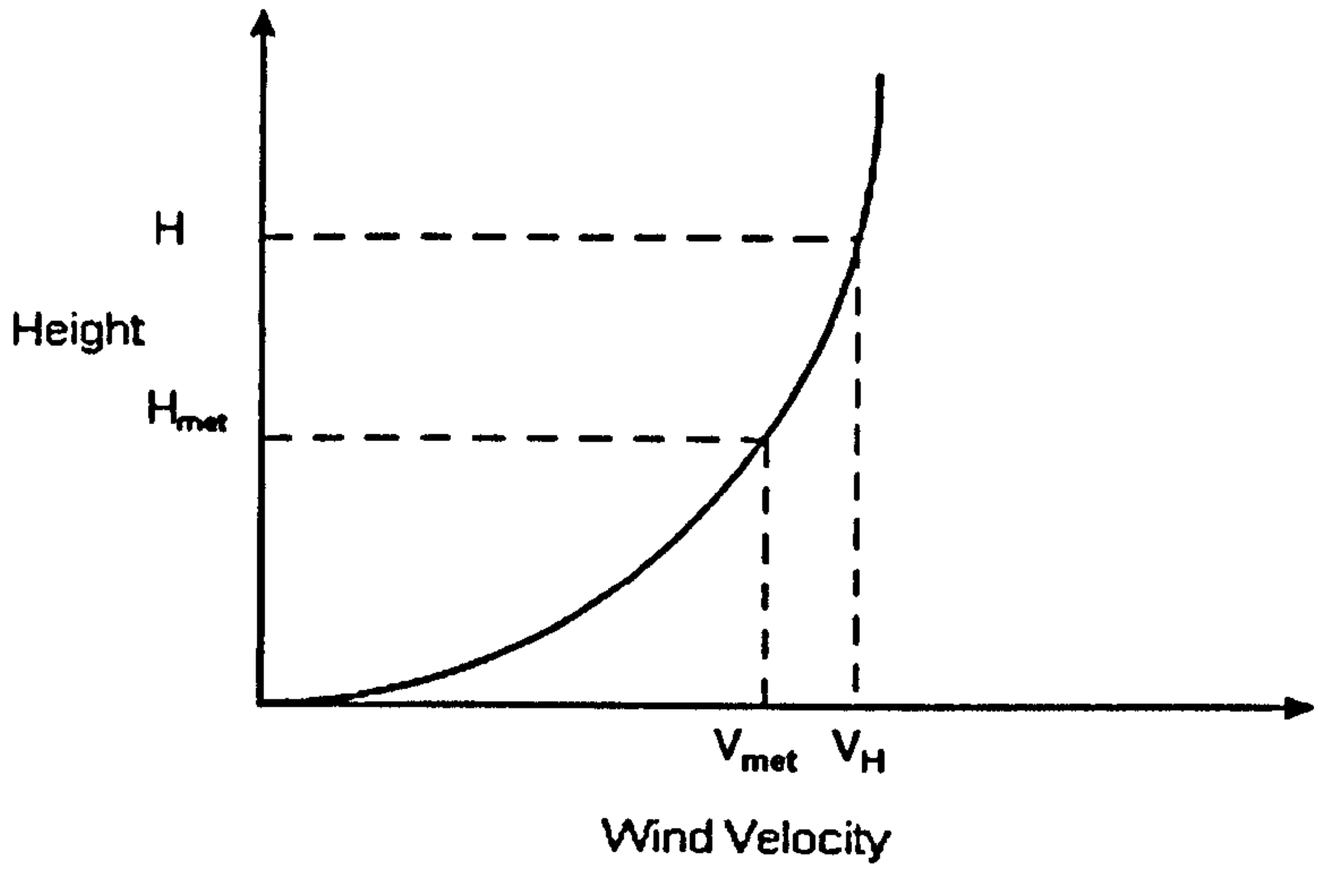

Figure 2.6 - Wind velocity v increases with height following a logarithmic law.

The ground roughness is another boundary condition which can vary greatly with the nature of the area considered (presence of fields, forest, water bodies, etc.) and the presence of small artefacts (small buildings are not considered individually but only in terms of increased ground roughness).

PANACHE can deal with walls with three types of velocity boundary conditions (Transoft, 2006); in the Kit Fox trials (see next chapter about PANACHE evaluation) walls were dealt with using the Log-Law condition (within which the wall shear stress and heat transfer in the boundary layer are computed from the standard logarithmic law of the wall), and introduced into momentum and energy equations. It is assumed that neutral conditions prevail near ground. This assumption is not far from truth as near the ground z is very low leading to low values of v and θ – eq. (2.9) and (2.10) – which means that neutral conditions apply in that region.

It would be desirable to account for the fact that wind speed and direction vary with time and space over a continuous spectrum but, as long as small scale wind variations cannot

be predicted and for the purpose of keeping the computational time tractable, mean values are used.

2.2.3 Turbulence models

Turbulent flow can be defined as the viscous flow in which fluid particles move in a random and chaotic way within the flow field (Sklavounos and Rigas, 2004). The designation of viscous flow refers to the flow of a real fluid regardless of its viscosity value. Velocity and all other fluid properties vary continuously, with strong concurrent molecular mixing between adjacent fluid layers. In atmospheric flows, turbulence is among the dominant mechanisms in the mixing and dilution of gaseous releases (Devaull et al., 1995). Table 2.1 displays how atmospheric stability classes can be (roughly and empirically) related to the driving forces of wind speed, solar radiation and cloud cover (Smith, 1999). Atmospheric stability levels are subdivided into 6 classes, from A (extremely unstable) to F (very stable) (Pasquill, 1961).

Table 2.1 – Pasquill-Gifford atmospheric stability classes related to wind speed and solar radiation (smith, 1999)

Wind speed (m/s)	DAY Incoming solar radiation			NIGHT	
	Strong	Moderate	Slight	> 4/8 cloud	< 3/8 cloud
< 2	A	A - B	B		
2 - 3	A - B	B	C	E	F
3 - 5	B	B - C	C	D	E
5 - 6	C	C - D	D	D	D
> 6	C	D	D	D	D

Lower values of gas dilution – that sometime can even be negative (i.e. increases in gas concentration) – are also associated with the presence of natural obstacles (i.e. trees),

human structures (i.e. buildings) and ground surface roughness. This is particularly true for a dense gas such as carbon dioxide. In the evaluation exercise (described in the next chapter) and in other simulations in this study, both of the turbulence models described below were used within PANACHE.

2.2.3.1 k-ε model

The standard *k-ε* model (Sklavounos and Rigas, 2004) is modified to include the effects of buoyancy and the stability of the atmosphere by means of the Richardson number (the non-dimensional parameter characterizing the stability of the atmosphere in terms of temperature), defined as:

$$Ri = g/T \cdot (\partial\theta/\partial z) \cdot \rho/G \qquad (2.11)$$

Ri is negative for unstable conditions and positive for stable conditions.

The equations for *k* (turbulence generation) and *ε* (turbulence dissipation) are given below:

$$\partial\rho k/\partial t + \nabla [\rho u\, k - (\mu/\sigma_k)\nabla k] = 2/3\rho k \nabla \cdot u + G\,(l\, Ri/\sigma_h)\,\rho\varepsilon + W_p \qquad (2.12)$$

$$\partial\rho\varepsilon/\partial t + \nabla [\rho u\, \varepsilon - (\mu/\sigma_\varepsilon)\,\nabla\varepsilon] = \varepsilon/\kappa\, [C_1\, G\,(l\, Ri/\sigma_h) - C_2\,\rho\varepsilon + C_s W_p] \qquad (2.13)$$

where σ_h is the Prandtl number which for the *k-ε* model = 1.11.

The turbulent viscosity is given by:

$$\nu_t = C_E\, k^2/\varepsilon \qquad (2.14)$$

2.2.3.2 k-l model

This is a one-equation model where the Equation (2.12) for k is solved while the turbulent length scale is specified algebraically. σ_h in Equation (2.12) for the present model is not constant but is a function of Ri. Equation (2.13) is not solved and ε in equation (2.12) is defined as:

$$\varepsilon = C_D k^{3/2}/l \qquad (2.15)$$

The length scale, l, is prescribed algebraically for different atmospheric stability conditions: stable (E, F) unstable (A, B) and neutral (C, D).

The turbulent viscosity is given as

$$\nu_t = C_\mu \; k^{1/2} \, l \qquad (2.16).$$

As for all numerical models, the run times for PANACHE depend directly on the product of number of grid cells, number of seconds simulated and number of time steps per second.

In the next chapter PANACHE's capabilities have been evaluated against two well-known atmospheric dispersion field experiments, Prairie Grass and Kit Fox. For these trials the CFD model was run on a single laptop provided with two 2.00 GHz Pentium 5 processors: within four weeks about 100 tracer release trials of the two field experiments described could be simulated. Representative computational times for the two experiments were: for Prairie Grass, with a grid consisting of 74,640 CVs and with 900 s of simulated time, it took between 1 and 3 hours per simulation, with longer simulation times for unstable atmospheric conditions (classes A and B). For Kit Fox, with about

228,000 CVs and 300-1100 s simulated time, the elapsed time on the PC for one run varied from 3 to 10 hours.

CHAPTER 3

EVALUATION OF ATMOSPHERIC DISPERSION MODELS

Introduction

Under normal circumstances, the theory of atmospheric dispersion is a tool for studying the movement of waste products in the atmosphere. Because this branch of atmospheric science is concerned with the effects of atmospheric motion on suspended pollutants, it is applicable to a variety of release conditions, including unintentional releases of materials that are not necessarily waste products, but are potentially harmful for humans and biota (Pine et al., 1998).

Pollutants released into the atmosphere consist of particles and gases with atmospheric residence times that span from a few minutes to many years. The movement of these pollutants is governed by the motion of the atmosphere, which determines both the path that the airborne contamination will follow and its dilution.

CFD models solve the basic time dependent Navier–Stokes equations, using a small grid size (of the order of 1m or less) that depends on the complexity of the site. CFD models are especially useful when the plume is dispersing within arrays of obstacles such as buildings in urban or industrial areas or other types of obstruction such as pipe racks and tanks (Hanna et al., 2004).

In this chapter, performances of the CFD model Fluidyn-PANACHE are evaluated against field trials of the Prairie Grass experimental campaign (Barad, 1958) and compared with results from the Gaussian model NOAA-ALOHA 5.4. Furthermore, because the PANACHE CFD model is intended for use at industrial sites and urban sites with numerous obstacles, the focus has been on field experiments involving obstacles. For this reason, the Kit Fox (Hanna and Chang, 2001) set of trials was also chosen for in-depth evaluation of the two models.

3.1 Field experiments

In the following sections the Prairie Grass and Kit Fox atmospheric dispersion field experiments will be described, along with the methodology for evaluating atmospheric dispersion models [Hanna et al. (1993, 2004), Hanna and Chang (2001)].

3.1.1 The Prairie Grass field campaign

The Prairie Grass field experiments (Barad, 1958) were conducted at O'Neill, Nebraska, during July and August 1956. The tracer used was SO_2, released at an elevation of 0.45 m from a point source, with the duration of each release being about 10 minutes. Maximum concentration were measured by samplers installed at a height of 1.5 m along five concentric arcs, located 50, 100, 200, 400 and 800 m downwind of the source (Figure 3.1). The test site, a relatively flat hayfield, was mown prior to the experiment. The wind measurements were taken by an anemometer 2 m above the ground, recording a wind speed ranging from 2 to 10 m s^{-1} over the entire set of trials; atmospheric stability covered the entire spectrum from A (unstable) to F (stable).

Although the Prairie Grass field study was conducted about 50 years ago, it remains a valid dataset on medium range diffusion from a near-surface release (Chang, 1998), owing to its high quality. Forty-three simulations were conducted with PANACHE and ALOHA representing each experimental condition for which the data were available. Examples of previous studies include Briggs (Briggs, 1982, Briggs, 1988), Van Ulden (Van Ulden, 1978), and Horst (Horst, 1979). The classic "Pasquill-Gifford" dispersion curves (Gifford, 1976) used in many dispersion models were partly developed based on the Prairie Grass data.

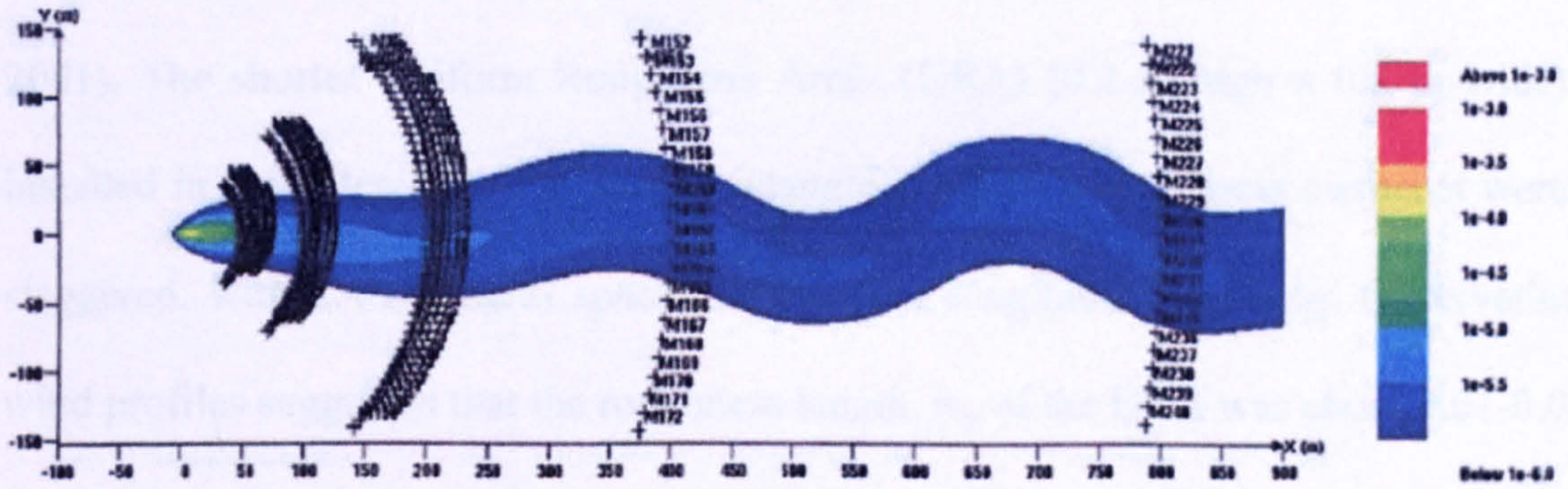

Figure 3.1 - Locations of five arcs (x=50, 100, 200, 400, and 800 m) in the Prairie Grass experiment (Barad, 1958).

3.1.2 The Kit Fox field campaign

The Kit Fox experiment was carried out in summer 1995 at the US-DOE Nevada test site. It was intended to demonstrate the effects on dense gas clouds of relatively large roughness typical of industrial process plants. A desert surface was artificially roughened using a combination of flat billboard obstacles in order to simulate the roughness of an industrial site and its surroundings at about 1/10 scale. It was impractical to carry out the experiment at an actual oil refinery or chemical plant, and it would have been prohibitively expensive to construct an artificial full-scale refinery at the test site. Pure

gaseous CO_2 was released at ground level from a 1.5 m x 1.5 m square source placed near the middle of the obstacle array, with a nearly constant emission rate of about 4 kg s^{-1} for 2-5 min periods (continuous "plumes") or for 20 s periods (transient "puffs"), including both neutral and stable atmospheric conditions.

Combinations of two types of flat "bill-board" shaped plywood obstacle arrays were used. The taller Equivalent Roughness Pattern (ERP) array (2.4 m square billboards) was installed in the inner 39 m x 85 m rectangle, with staggered roughness elements – 6.1 m lateral spacing and 8.1 m along-wind spacing. Observations of wind profile suggested that the roughness length, z_0, of the ERP was about 0.12-0.24 m (Hanna and Chang, 2001). The shorter Uniform Roughness Array (URA) (0.2 m high x 0.8 m wide) was installed in the outer 120 m x 314 m rectangle. The URA roughness elements were also staggered, with 2.4 m lateral spacing and 2.4 m longitudinal spacing. Observations of wind profiles suggested that the roughness length, z_0, of the URA was about 0.01-0.02 m.

Eighty-four fast-response (one reading per second) concentration monitors were installed on the four downwind arcs (25, 50, 100 and 225 m; Figure 3.2), together with five meteorological towers recording wind speed and direction data every second[‡] (WRI, 1998).

[‡] Within PANACHE simulations, only 77 monitor points have been used, the ones installed on MET towers in the real scenario were not present during computer simulations, as MET towers themselves.

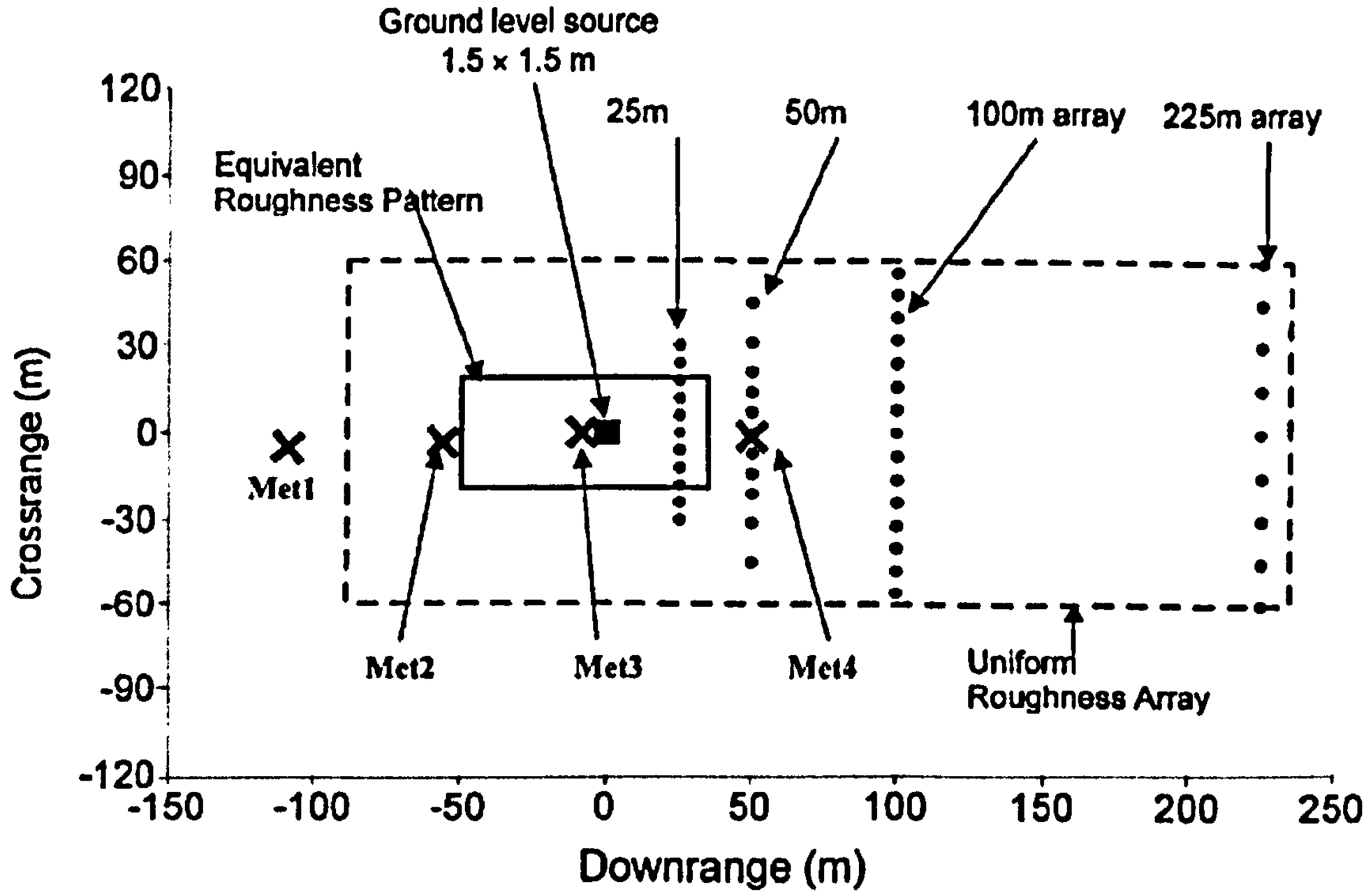

Figure 3.2 - Plot plan of the Kit Fox site showing the locations of the meteorological towers, the concentration monitoring arcs, the source, the ERP array, and the URA array.

There was a total of 52 release experiments, split into four sets for the statistical analysis: 6 ERP trials (with ERP and URA arrays present) with "plume" release (duration of 120 s or greater), 13 ERP trials with "puff" releases (duration 20 or 25 s), 12 URA trials (with only URA array installed) with "plume" releases and 21 URA trials with "puff" releases. When the ERP was removed (leaving the URA), the CO_2 release rate was decreased to about 1.6 kg s^{-1}.

3.2 Statistical model performance evaluation method

The PANACHE model has been evaluated following the directives for atmospheric dispersion model performance measures suggested by Weil (Weil et al., 1992), Hanna et al. (1993) and the American Society for Testing and Materials (ASTM, 2000). The

statistics applied herein are based on a methodology suggested by Hanna (Hanna et al., 1993) and summarized by Chang and Hanna (2004).

The Prairie Grass (PG) and Kit Fox (KF) field experiments both involved the release of a certain amount of pollutant from a specific source (point for PG and area for KF) and the capture of maximum concentration data by tracer samplers installed on arcs at specific downwind distances. The evaluation focussed on the maximum concentration observed and predicted on a given arc during a given experimental trial. Although the location of the monitor with the observed maximum is not necessarily the same as the location of the monitor with the predicted maximum, the use of maximum concentrations on arcs for the model evaluation exercise is standard for evaluating dispersion models against field experiments in open terrain (Hanna et al., 2004).

The following equations define the statistical performance measures, which include the fractional bias (FB), the geometric mean bias (MG), the normalized mean square error (NMSE), the geometric variance (VG) and the fraction of predictions within a factor of two of the observations (FAC2) (Hanna and Chang, 2001):

$$FB = \frac{(\overline{C}_o - \overline{C}_p)}{0.5(\overline{C}_o + \overline{C}_p)}, \tag{3.1}$$

$$MG = \exp(\overline{\ln C_o} - \overline{\ln C_p}), \tag{3.2}$$

$$NMSE = \frac{\overline{(C_o - C_p)^2}}{\overline{C}_o \overline{C}_p}, \tag{3.3}$$

$$VG = \exp\left[\overline{(\ln C_o - \ln C_p)^2}\right] \tag{3.4}$$

$$FAC2 = \text{fraction of data that satisfy } 0.5 \leq \frac{C_p}{C_o} \leq 2.0 \qquad (3.5)$$

where: C_o = observations of concentration (highest value recorded); C_p = model predictions of concentration (highest value predicted); overbar ($\overline{C}$) = average over the data set.

A perfect model would have MG, VG and FAC2 = 1; FB and NMSE = 0. Because of the influence of random atmospheric processes these values are not attainable, and the minimum performance measures for a model to be defined as "acceptable" [summarized by Chang and Hanna (2004), based on extensive experience with model evaluations] are as follows (Hanna, 2003):

- The fraction of predictions within a factor of two from observations is about 50% (i.e., FAC2 > 0.5);
- the mean bias is within ±30% of the mean (-0.3 < FB < 0.3 or 0.7 < MG < 1.3);
- the random scatter is within a factor of about two of the mean (NMSE < 4 or VG < 1.6).

The linear measures FB and NMSE can be overly influenced by infrequent extreme observed and/or predicted concentrations, whereas the logarithmic measures MG and VG may provide a more balanced treatment of extreme high values; it is necessary to consider all the performance measures taken together to make a decision concerning model acceptance (Chang and Hanna, 2004).

3.3 Results and discussion

3.3.1 Prairie Grass

Equations (3.1)-(3.5) were applied to the dataset of observed maximum concentrations against predictions made by PANACHE and ALOHA. Table 3.1 (next page) shows concentration results for PANACHE and ALOHA for the trials under different meteorological conditions.

Results were divided into categories, each category referring to concentrations recorded at different arcs. Figure 3.3 represents observed values against predictions by the CFD model, the diagonal lines being the boundaries for model acceptability.

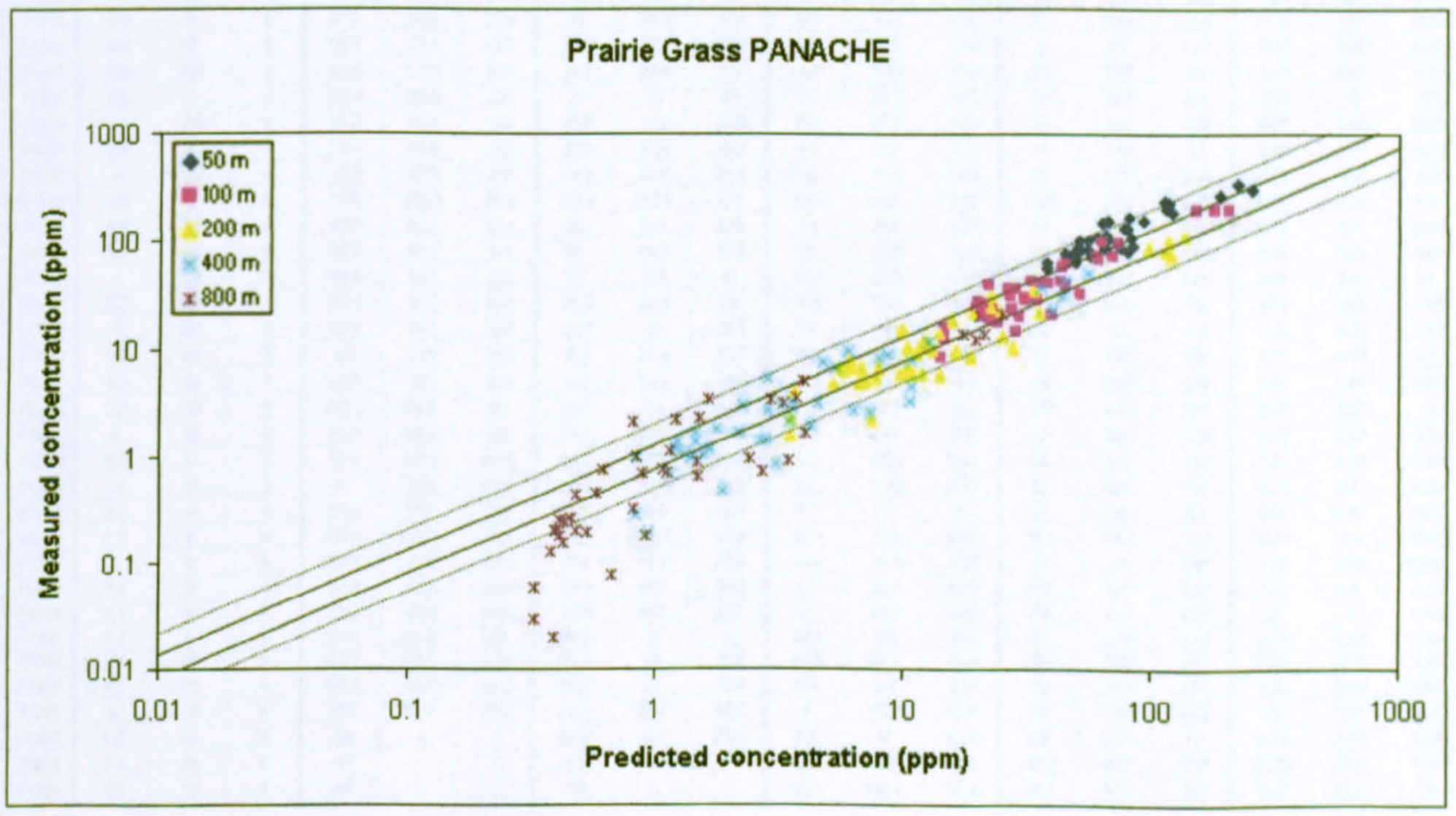

Figure 3.3 - Observed concentrations against PANACHE' predictions for Prairie Grass. Diagonal lines are boundaries for prediction acceptability, where dotted lines are limits for 0.5 ≤ Cp/Co ≤ 2.0.

PANACHE' predictions at arc 1 underestimate the concentration values by a factor of about 1.5. In order to ensure acceptable simulation times, the small point source (about 1

cm diameter) and the relatively large domain (~1000 m) led to the choice of a coarser grid than normally used. Consequently, the model will over-estimate the gas dilution in the CVs near the source, and this may account for the under-predictions at the nearest arc. Other modellers adopted the same strategy to deal with the same issue (Hanna et al., 2004).

				50 m			100 m			200 m			400 m			800 m		
Trial no	u (m/s)	CC (x)	PG	Co MAX	PAN	ALOHA	Co MAX	PAN	ALOHA	Co MAX	PAN	ALOHA	Co MAX	PAN	ALOHA	Co MAX	PAN	ALOHA
PG07	4.2	0	2	36.3	44.8	51.6	9.5	14.3	13	1.8	3.5	3.26	0.3	0.83	0.82	0.03	0.33	0.21
PG08	4.9	0	3	154.9	92.8	97.1	41.8	43.6	24.6	9.3	11.2	6.24	1.5	2.65	1.61	0.26	0.43	0.42
PG09	6.9	30	3	71.7	49.3	68.7	20.3	21.46	17.4	5	6.8	4.42	1	1.4	1.14	0.19	0.41	0.3
PG10	4.6	30	2	66.2	44.4	48.1	15.8	14.67	12.1	4.1	3.64	3.04	1	0.85	0.77	0.06	0.33	0.19
PG15	3.4	0	1	147	83.4	28.8	38.8	22.3	7.21	7.8	6.1	1.81	1.7	1.46	0.46	0.2	0.53	0.12
PG16	3.2	0	1	67.4	48.2	30.4	12.7	14.8	7.62	2.3	3.51	1.91	0.2	0.94	0.48	0.02	0.38	0.12
PG17	3.3	70	4	235.4	113.2	164	98.2	63.4	42.9	30.8	22.5	11.5	9.5	8	3.22	3.48	1.65	0.96
PG18	3.5	10	5	231.1	117.2	396	94.8	73.4	102	35.1	33.5	26.5	11.7	12.7	7.1	5.17	3.93	2
PG19	5.8	30	3	78.4	80.2	90.8	19.7	22.1	23	4.7	5.25	5.83	0.7	1.15	1.5	0.13	0.38	0.4
PG20	8.6	20	4	61.9	49.2	115	19.1	23.1	30.1	5.6	7.68	8.06	1.2	1.68	2.26	0.29	0.46	0.67
PG21	6.1	100	4	104.2	65.5	80.3	36.2	26.7	21	10.8	11.9	5.62	3.3	3.5	1.58	1.17	1.16	0.471
PG22	6.4	60	4	85.2	64.2	72.3	30.8	27.1	18.9	10.1	13	5.06	3.2	4.55	1.42	0.91	1.48	0.42
PG23	5.9	0	4	63.4	38.2	65.4	22	22.9	17.1	6.9	10.4	4.58	2.2	3.46	1.28	0.74	1.12	0.38
PG24	6.2	0	4	56.1	38.1	62.5	18.2	23.9	16.3	6	11.9	4.38	2	4.2	1.23	0.69	1.48	0.37
PG25	2.8	100	1	109.4	82.9	37.5	14.7	28.4	9.4	2.3	7.44	2.36	0.5	1.87	0.6	0.06	0.67	0.15
PG28	2.6	0	5	183.8	120.5	376	73	70	99	22	35.7	25.9	7.9	10.7	6.9	3.19	3.3	1.95
PG29	3.5	-99	4	86.6	75.4	113	32.8	52.2	29.5	10.2	27.8	7.89	3.4	10.6	2.21	0.96	3.48	0.68
PG33	6.5	-99	4	75.3	44.5	107	23.1	20.6	28.1	6.9	6.71	7.51	1.4	1.46	2.1	0.27	0.41	0.63
PG34	9	20	4	72.8	47.1	105	24.9	22.9	27.4	6.9	7.94	7.34	1.9	1.79	2.06	0.46	0.48	0.61
PG36	1.9	0	6	299	256.1	48.8	194.5	205.4	12.2	72.4	118.9	3.08	22.9	39.9	0.78	13.91	21.26	0.2
PG37	4.6	30	4	83.5	52.4	82.1	29.1	34.6	21.5	8.4	18.4	5.75	2.7	7.28	1.61	0.77	2.7	0.48
PG38	4.1	80	4	132.8	80.1	104	57	44.2	27.1	19	15.6	7.27	5.9	5.37	2.04	2.38	1.52	0.61
PG41	4	-99	5	164.4	81.9	232	69	61.8	61	24.6	22.5	15.9	8.9	8.62	4.26	3.58	3.71	1.2
PG42	5.9	-99	4	100.4	50.7	91.8	36.8	28.8	24	11.5	12.4	6.42	2.9	3.58	1.8	0.79	1.09	0.54
PG43	5	100	3	89.4	84.1	104	20.7	40	26.3	5.8	14	6.7	0.9	3.1	1.72	0.19	0.91	0.45
PG44	5.7	80	3	69	60.4	93.8	18.2	24.4	23.7	5.2	7.01	6.03	1.1	1.55	1.55	0.21	0.48	0.41
PG45	6.1	90	4	131.8	77	163	41.5	38.6	42.5	14.4	14	11.4	3.1	3.25	3.19	1.02	0.84	0.96
PG46	5.2	90	4	203.3	114.5	187	72.2	60	48.9	21.9	19.2	13.1	7.5	4.72	3.67	2.29	1.22	1.1
PG48	9	10	4	80.7	55.9	122	23.6	27.6	31.8	6.1	9.67	8.51	1.7	2.19	2.38	0.47	0.58	0.71
PG49	6.3	10	3	77.1	50.2	82.3	24.1	19.9	20.8	6.7	5.65	5.29	1.2	1.22	1.36	0.21	0.39	0.36
PG50	6.6	10	3	87	50.5	81.8	27.9	20.3	20.5	6.6	5.79	5.21	1.4	1.24	1.34	0.21	0.4	0.35
PG51	6.1	10	4	100.1	55.7	163	26.3	21.6	42.7	6.7	6.12	11.4	1.1	1.32	3.2	0.16	0.43	0.96
PG53	2.6	0	6	339.4	223.4	1010	192.4	179.7	289	83.1	113.1	76.9	30.4	43.4	20.7	12.19	19.6	5.85
PG54	4	0	4	154.7	66.3	101	61.4	45.7	26.4	22.3	24.6	7.07	8.1	7.9	1.98	3.45	2.83	0.592
PG55	5.4	0	4	77.3	48.7	77.6	30.3	31.5	20.3	9.7	16.3	5.43	2.8	6.3	1.52	1.01	2.4	0.48
PG56	4.3	0	4	112.9	66.1	98.3	39.9	45.2	25.7	13.2	25.2	6.89	4.6	10.7	1.93	1.7	4	0.58
PG57	8.7	0	4	101.6	65.2	149	29.2	31	39	10.4	10.4	10.4	3.1	2.25	2.83	0.79	0.62	0.87
PG59	2.6	50	6	266.9	191.4	880	193.3	164	263	84.5	96.9	67.4	35.7	36.9	18.1	13.79	17.4	5.12
PG60	4.9	70	4	109.9	60.4	74.9	42.5	33	19.6	15.5	9.9	5.24	5.3	2.82	1.47	2.16	0.82	0.44
PG61	8	30	4	70.3	57.7	125	20.1	29.3	32.7	6	10.9	8.75	1.5	2.77	2.46	0.34	0.82	0.73
PG62	5.2	60	3	-99	-	-	40.9	35.7	25.9	11.5	12	6.59	2.8	2.84	1.7	0.72	0.69	0.45
PG32	2.2	10	6	-99	-	-	-99	-	-	100.1	118.6	81.5	42.1	44.7	21.9	20.53	20.3	6.18
PG58	1.9	30	6	-99	-	-	-99	-	-	110.9	136.4	93.5	49.9	55.1	26.1	20.7	24.9	7.11

Table 3.1 - Listing of emission rate (g s^{-1}), temperature (K), wind speed (m s^{-1}) at 2 m height, cloud cover (%) and Pasquill-Gifford stability category for the Prairie Grass experiment trials. Maximum observed (Co) and predicted concentrations (ppm) by PANACHE and ALOHA are also listed. Data for Prairie Grass are from Hanna et al. (1993). "-99" means missing

Statistical values for PANACHE (Table 3.2) are all well within the limits for acceptable models. In particular, the fractional bias suggests that the mean value of model

predictions agree with observations, while the proportions of the entities measuring the extent of the typical error (NMSE and VG) demonstrate an average scatter of less than half the mean of observations.

Table 3.2 - Comparison between the CFD tool PANACHE and the Gaussian plume model ALOHA 5.4, using the statistical method suggested by Hanna and Chang (2001) for the Prairie Grass experiment predictions.

	FB	NMSE	MG	VG	FAC2
ALOHA	0.34	1.98	1.24	2.08	0.76
PANACHE	-0.03	0.23	0.93	1.49	0.86

For the two largest arcs (400 and 800 m), while the average values are acceptable, a proportionately larger deviation from observed values can be seen (Figure 3.3). The results dataset (Table 3.1) shows a large over-prediction of concentrations at this arc for the trials with unstable atmosphere (classes A and B), with errors up to one order of magnitude. This may be due to the over-prediction of turbulence dissipation by the k-ε model and consequent over-prediction of gas concentration far from the source. Other modellers have reported this disagreement under unstable atmospheric conditions for the k-ε model (Sklavounos and Rigas, 2004).

For the trials with very stable atmospheric conditions (class F), on the other hand, the k-ε model under-predicted the concentration of SO_2 by up to a factor of five for each arc. For this reason the k-l turbulence model was used within the trials with very stable atmosphere (i.e. trials PG32, PG36, PG53, PG58 and PG59), and proved to perform much better for class F conditions.

For purpose of comparison, the Prairie Grass field trials were also simulated using the Gaussian model ALOHA 5.4. The Gaussian model also gave good results, although it

showed an average under-prediction at short distances and over-prediction at long distances for unstable atmospheric conditions (classes A and B), and an average over-prediction at short distances and under-prediction at long distances for stable conditions (classes E and F – Table 3.1). For neutral stability, the fit varies with wind speed, the model slightly over-predicting for high values of ambient wind speed ($v > 6$ m s^{-1}) and significantly under-predicting for low values ($v < 3$ m s^{-1}). These limitations are characteristic of Gaussian dispersion models that calculate the plume size and 2D concentration limits using algebraic equations. A graphical presentation of the Gaussian model performance is given in Figure 3.4.

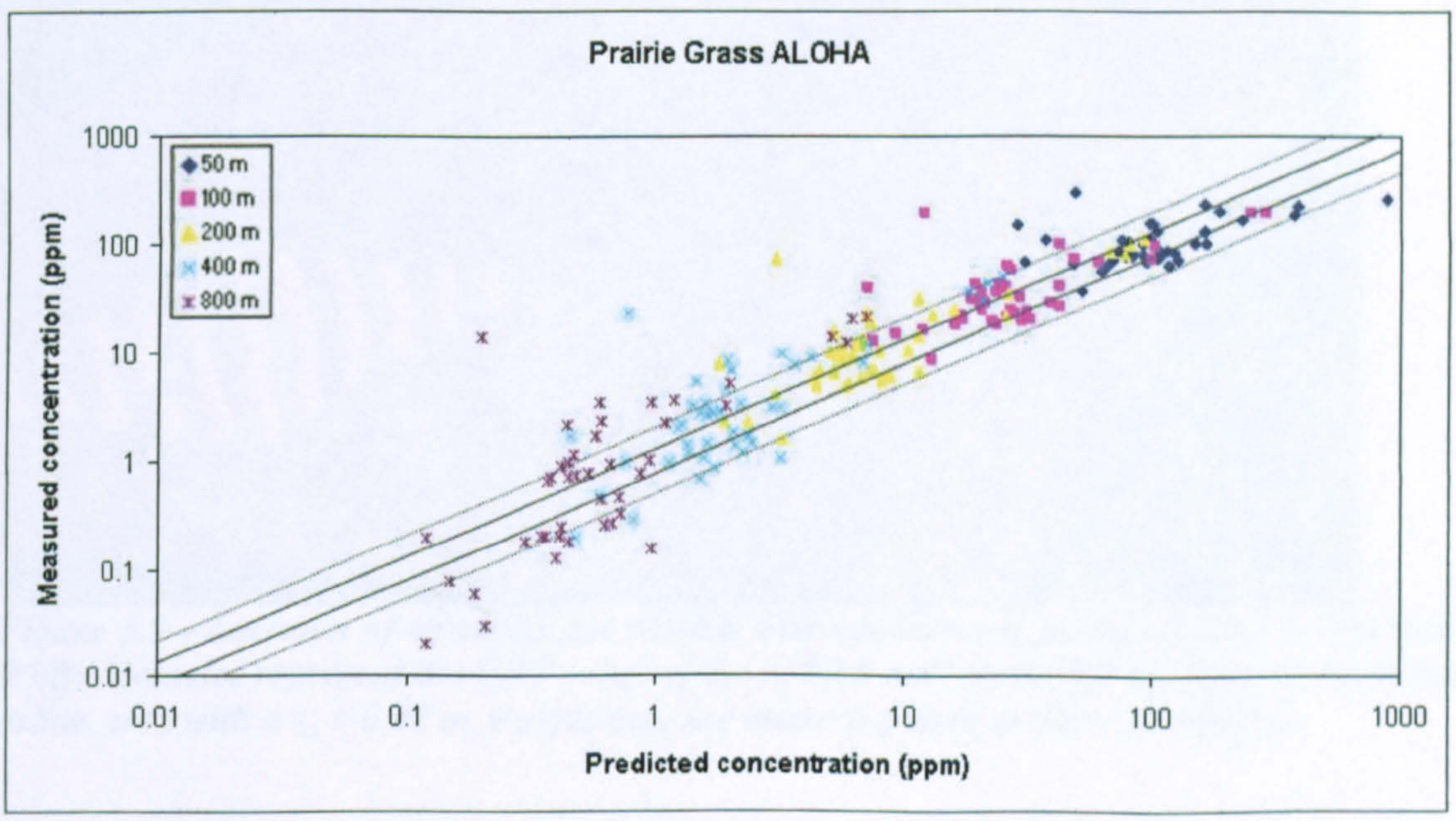

Figure 3.4 - ALOHA' predictions against observations for the Prairie Grass trials.

A summary of results and comparison between PANACHE and ALOHA can be seen in Table 3.2. For ALOHA, linear measures (FB and NMSE) are on the border of acceptability criteria, due to large errors within some trials, particularly for very stable and unstable atmospheric conditions and in cases of very low wind speed. On the other

hand, logarithmic measures compensate for this characteristic behaviour of Gaussian models, weighting extremely high errors.

3.3.2 Kit Fox

Figure 3.5 shows the arrangement of the test field as simulated by PANACHE. The URA obstacles array was substituted by a homogeneous urban area with average building height of 0.2 m, in order to have a surface roughness length z_o between 0.01 and 0.02 m, as prescribed by Hanna and Chang (2001).

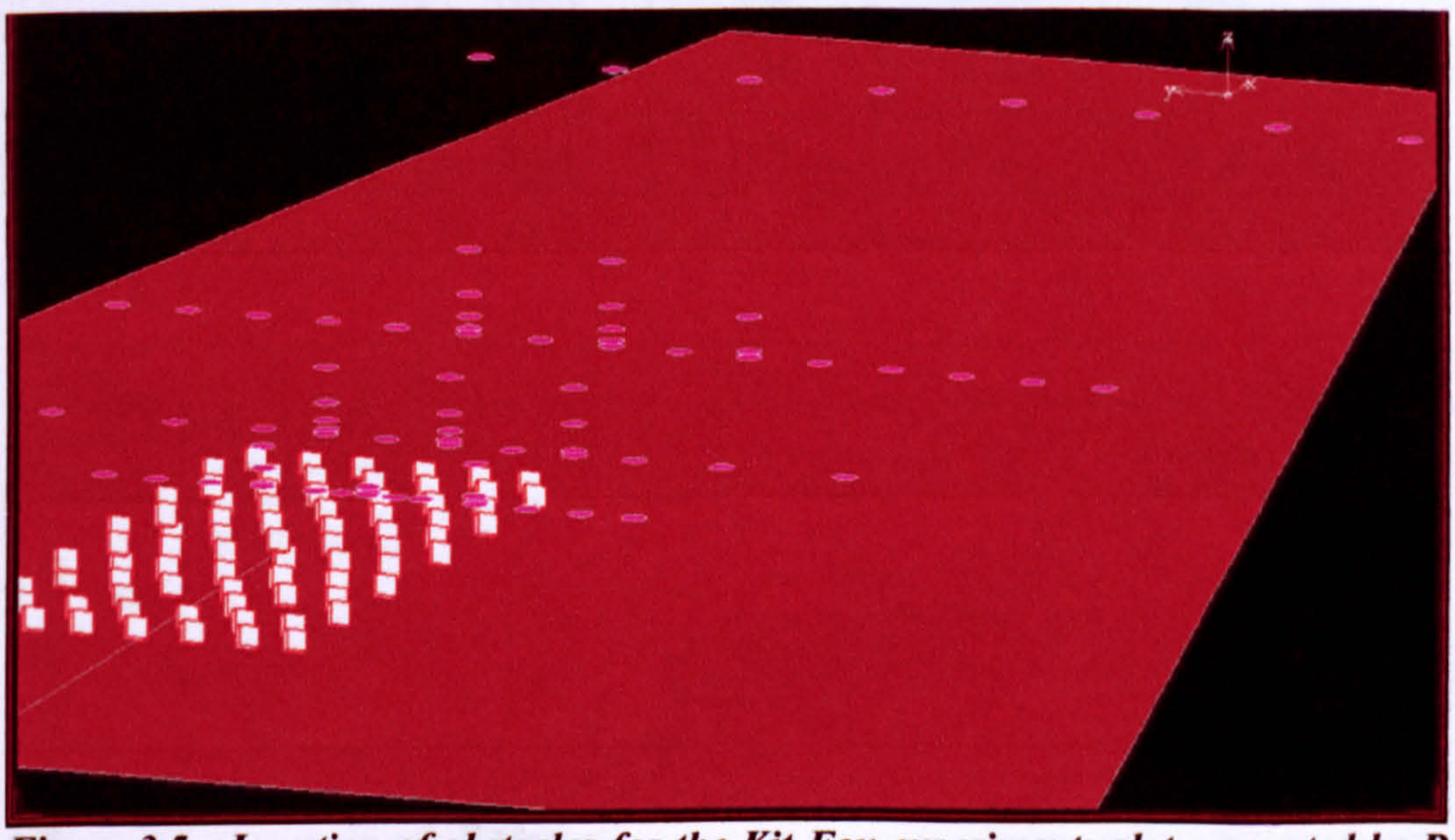

Figure 3.5 - Location of obstacles for the Kit Fox experiment: plot generated by PANACHE. White obstacles represent the URP array of 2.4 m high billboards, the red ground represents an urban area with a z_o = 0.02 m. Purple dots are monitor points at different heights.

Within PANACHE, the *k-l* model was used exclusively for evaluation of turbulence generation and dissipation for the Kit Fox trials. It performed slightly better than the *k-ε* model, the latter tending to under-estimate gas concentration more at each arc. Predicted values from PANACHE were compared with observations using equations (3.1)-(3.5), as for the Prairie Grass trials. Table 3.3 shows the performance measures for the four sets of

trials of the Kit Fox experiment, and Figure 3.6 is a graphical display of results. In terms of parameter ranges the overall model results show an average under-prediction which is particularly evident for continuous release trials. This tendency is justifiable bearing in mind that simulations were carried out using constant values for wind speed and direction, taking the average value of data recorded each second at the test field (Hanna and Chang, 2001).

Table 3.3 - Comparison between PANACHE' and ALOHA' predictions within the Kit Fox field experiment. Simulations from ALOHA only for continuous release trials.

	N	FAC2	FB	NMSE	MG	VG
ALOHA	18	0.72	0.16	0.76	1.26	2.91
PANACHE	52	0.94	0.3	0.32	1.3	1.29

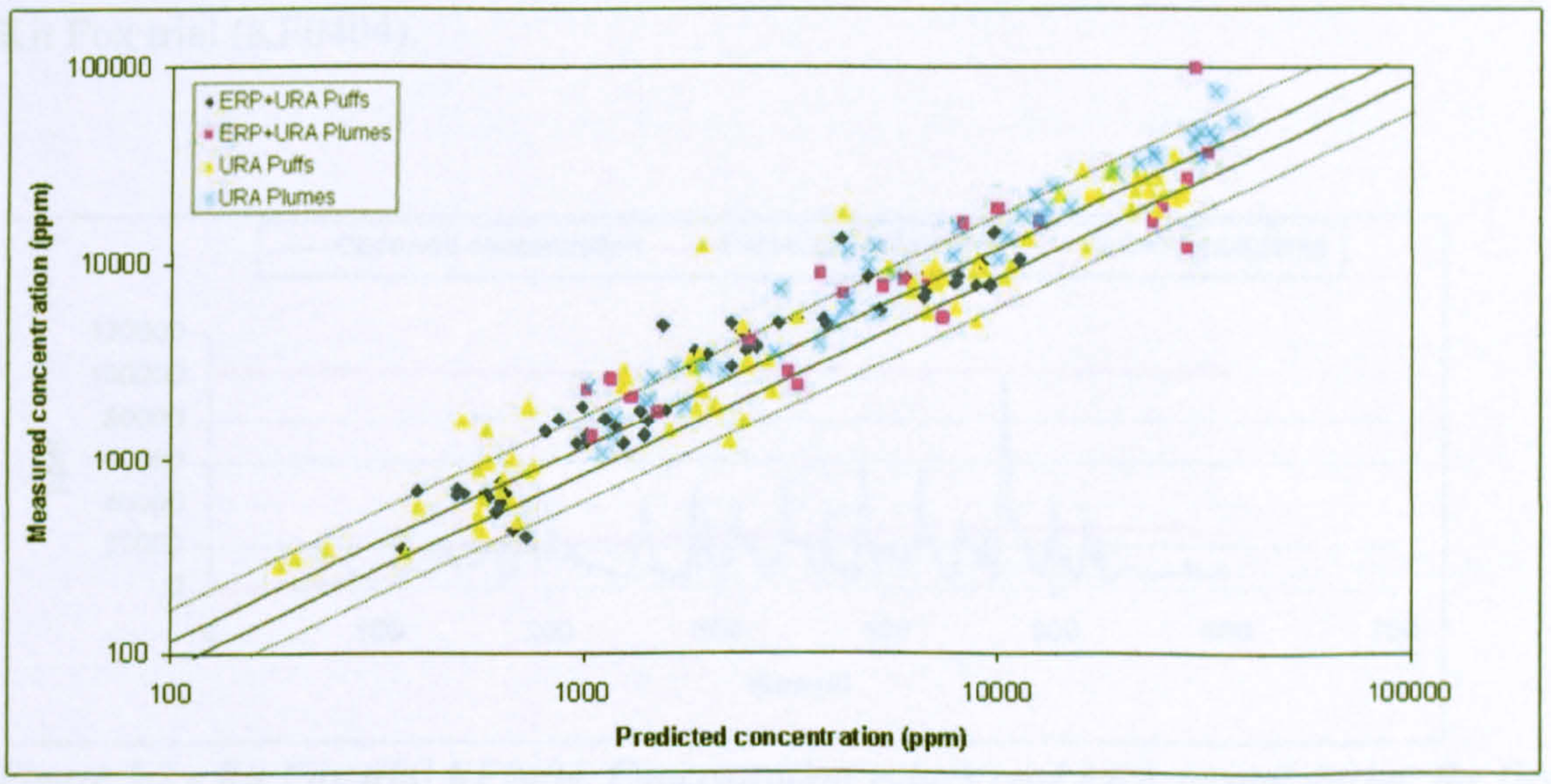

Figure 3.6 - PANACHE predictions against observation for the Kit Fox trials.

CO_2 is about 1.5 times denser than air (ρ_{CO2} = 1.8 kg m^{-3} at STP) and some 30% less viscous (Oldenburg and Unger, 2004); these differences reduce the mixing with ambient air compared to that of a more buoyant pollutant. Thus, the effect of a non-homogeneous

wind on the gas dispersion could be seen as a differentiated impulse on diverse parts of the moving puff/plume, leading to an irregular concentration pattern within the cloud – the gas accumulating randomly inside the plume. Over the Kit Fox experiment, this is particularly evident for the trials with ERP obstacles present, the latter acting as preferential accumulation sites for the gas.

The master data set (WRI, 1998) reports that wind speed and direction values varied significantly during each experiment, by up to 5 m s^{-1} and 20° respectively, within a few seconds. It also reports cloud concentration values varying by up to 30,000 ppm in just one second (this is mainly true for the continuous release trials). Figure 3.7 is a comparison of concentration values recorded by the monitor point that read the highest concentration (P1911) with values calculated by PANACHE and by ALOHA, during a Kit Fox trial (KF0404).

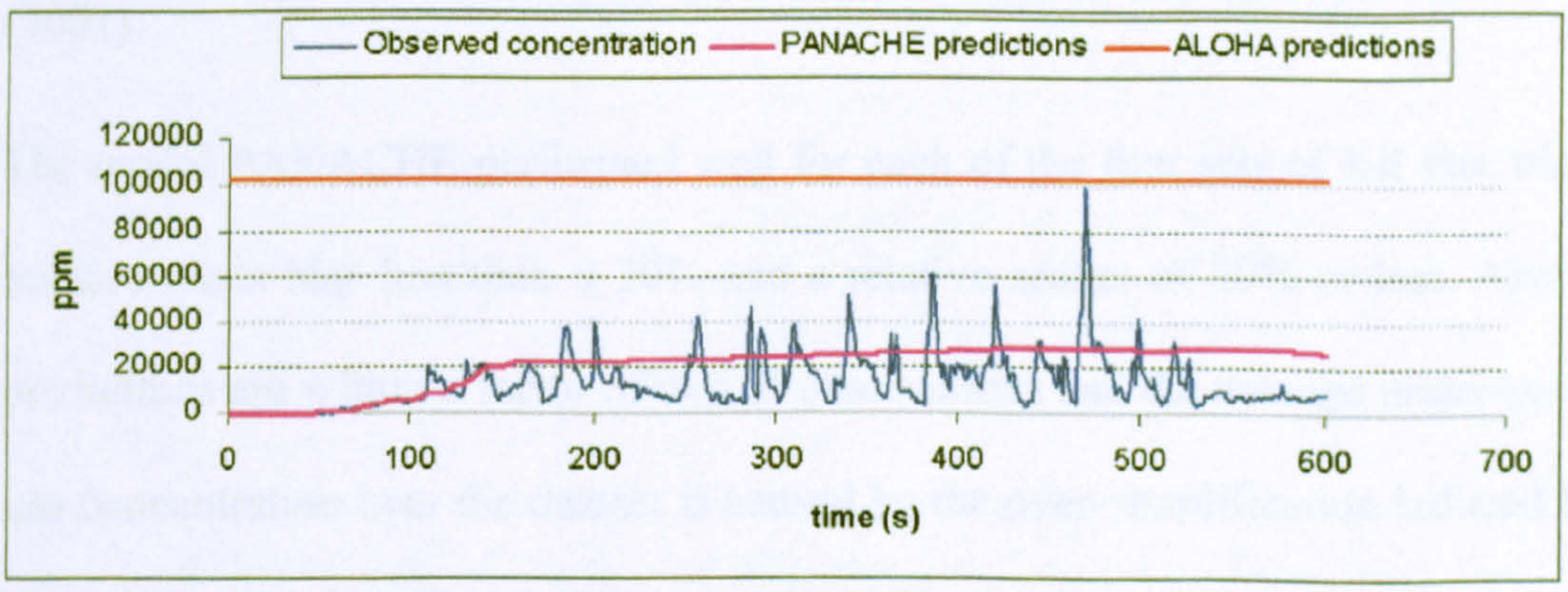

Figure 3.7 - Kit Fox trial KF0404. Concentration values read each second during the first 10 minutes of the trials at monitor point P1911 (x = 25 m) against values calculated by PANACHE and ALOHA(Mazzoldi et al., 2008).

Although the CFD performance for this trial reveals a strong under-prediction while Gaussian prediction is nearly perfect with respect to Figure 3.7 (and then also when

appreciated within the performance evaluation method by Hanna et al., considering only MAX values), from a risk analysis point of view, predicted concentration values give a measure of the hazard (i.e. dose of potentially inhaled gas over a certain time span) affecting a person, if present. The peak of MAX observed concentration in Figure 3.7 should be interpreted as an outstanding value that can be used as a parameter for model performance evaluation but only as an upper limit. Models using constant wind parameters (i.e. giving fairly constant concentration predictions) should in many cases not be acceptable if forecasting values higher than MAX as they would overestimate the overall hazard when used for Risk Assessments – see the case of ALOHA' prediction in Figure 3.7.

It is suggested that the minimum ranges for acceptable model performance be adjusted to (e.g.): $0 < FB < 0.5$ and $1 < MG < 2$. The ranges of the other two measures (NMSE and VG) are consistent as defined by Hanna et al (1993 and 2004) and Hanna and Chang (2001).

The model PANACHE performed well for each of the four sets of Kit Fox trials, with a relative mean bias less than $\pm 30\%$ and a relative scatter of 60% or less. About 90% of predictions are within a factor of two of observations and the average under-prediction of gas concentration over the dataset is caused by the over-simplification induced by the use of an average value for wind speed and direction. There is little trend with atmospheric stability or downwind distance, while data suggest the best predictions to be at higher average values of wind speed. WRI (1998) reports less wind speed variation within trials with higher average values.

The CFD model has been compared with predictions from the dense gas algorithm of ALOHA 5.4. As can be seen from Table 3.3, the Gaussian model also performed well over the Kit Fox trials, although with some limitations within simulations set-up, described below. The minimum release duration computed by ALOHA is 1 minute, so that puff releases (20 seconds duration) could not be modelled. ALOHA can account for only one surface roughness over one scenario, so that for the ERP+URA continuous releases the simulations have been worked out with the ERP value for z_0 taken as constant over the domain. Moreover, ALOHA can account for continuous releases only from point sources, thus, the 1.5 m square ground source effect could not be evaluated within the trials. Nevertheless, its results are well within the range for model acceptability.

3.3.3 Cloud travel speed, V_e

In an attempt to test the fitness-for-purpose of the software PANACHE in a time-related issue (i.e. how closely it can anticipate the movements and dispersion of airborne pollutants with time), it has been used to calculate the speed of the moving cloud along the 225 m length of the Kit Fox test field. Observed values were taken from the WRI file. Cloud travel speeds V_e were estimated for all Kit Fox trials, at all the arcs. Speeds were assumed to equal monitoring arc distance divided by time of travel, from the source to the monitor points that recorded maximum concentrations at each of the four distances. The values reported in Table 3.4 are ratios of predicted against observed speeds (m s^{-1}).

Speed was calculated using the arc distance from the source divided by the first arrival time of the 50% MAX concentration of the cloud, at the monitor point where the

maximum concentration was recorded for the particular arc, both for observed and predicted concentrations.

Table 3.4 - Ratios between predicted against observed cloud speed values (m s^{-1}) for the different trials, recorded at each of the four arcs within PANACHE.

	25 m	50 m	100 m	225 m
ERP puff	0.71	0.86	1.15	0.84
ERP cont.	0.91	0.82	1.25	0.94
URA puff	1.1	0.85	1.57	1.06
URA cont.	0.7	0.53	1.13	0.74

As described in the previous paragraph, the maximum concentration values of the cloud are the product of random accumulation of the dense gas. Using the first arrival of the 50% MAX concentration for speed estimation makes clear that what is calculated is the velocity of the arriving, thickening cloud, regardless of the short-term concentration fluctuations. This technique is suggested by Hanna and Chang (2001).

As observed during the experiment (Hanna and Chang, 2001), the puffs/plumes were seen to accelerate by a factor of up to three or four due to the vertical dispersion of the cloud as it moved downwind from the 25 m arc to the 225 m arc. This is due to the cloud being brought under the influence of higher wind speeds at greater heights.

As it can be seen from Table 3.4, PANACHE gave estimates of cloud speed with an average error of about 20%, accounting for its acceleration further downwind (i.e. there is no evident discrepancy of speed ratios among the four arcs, for any of the subset). From the values reported in the table, no particular trend for the predicted velocity can be seen – accounting for presence/absence of obstacles and puff/plume releases.

3.3.4 Evaluation exercise results

PANACHE has been evaluated against the Prairie Grass and Kit Fox field experiments, involving a total of about 100 trials. The statistical model performance evaluation method suggested by Hanna and Chang (2001) for the evaluation of atmospheric modelling software has been applied to the results: outcomes put the model performances well within the limits of acceptability for atmospheric dispersion software. The average under-prediction of results within Kit Fox trials is due to the extreme short-term variation in wind speed and direction during the field experiment.

It is suggested that the boundary values of performance ranges be lowered for two of the statistical measures (FB and MG) as defined by Hanna et al. (1993, 2001, 2003 and 2004) for model acceptability measures within the gas dispersion risk assessment context. In fact, from the above, it is evident that CFD models may only under-predict results: not accounting for processes leading to the generation of highly differentiated gas concentration in clouds over time and space, CFD tools give an accurate description of average gas concentrations omitting the naturally occurring short-term concentration peaks.

CHAPTER 4

TRANSPORTATION OF CO_2 IN CCS PROJECTS – A RISK ANALYSIS

Introduction

Although capture and storage of CO_2 is being studied intensively worldwide, the biggest efforts are concentrated in two main areas: firstly, the processes of CO_2 capture in industrial plants, with the aim of reducing the costs of separating and pressurising CO_2; secondly, CO_2 monitoring after underground injection, studying the best target reservoirs with sometimes the possibility of enhancing hydrocarbon production.

The critical linking process, between the separation of CO_2 and its subsequent storage, is its transportation. If CCS technology is to gain public acceptance and be introduced widely, achieving the magnitude of CO_2 reductions needed for the UNFCC goal of stabilization of atmospheric green house gases, then extensive networks of CO_2 transportation facilities will be needed (Gale and Davison, 2004).

The main objective of this chapter is the consideration of leakage consequences as modelled by the two atmospheric dispersion models evaluated and compared in the previous chapter. Data for the transportation modular system, failure occurrence frequency, leak sizes and CO_2 inventories for each module were taken from the report of DNV (Vendrig et al., 2003).

For non-engineered system components (i.e. the geological storage site excluding injection facilities), no risk assessment has been possible because of the lack of empirical evidence on which to base the probability of release of CO_2 from this part of the system (EU, 2008b, Vendrig et al., 2003).

4.1 Experience in transporting CO_2

In the last 30 years carbon dioxide has been used by the oil industry for enhancing hydrocarbon production, via the restoration of pressure gradient in semi-exhausted oil and gas reservoirs (Amorino et al., 2005), mainly in South and North America with an overall oil production of up to 196,000 barrels per day (data for 1998, Gale and Davison, 2004).

Currently, CO_2 transportation is performed on- and off-shore by various means: road, railway, ship and pipeline. All these alternatives can in principle be applied in a future large scale transportation system for CO_2 recovered from fossil fuelled power stations. Svensson analyzed the costs of CO_2 transportation for different scenarios, concluding that, when evaluating the economics, only three alternatives remain: pipelines (on- and off-shore), waterborne carriers (off-shore) and combinations of these (Svensson et al., 2004). However, pipeline costs depend strongly on the volumes being transported and, to a lesser extent, on the distances involved. These costs average 1-5 USD t^{-1} CO_2 per 100 km for the on-shore pipeline case, falling to 0.3-0.5 USD t^{-1} CO_2 for off-shore shipping (IPCC, 2005).

Altogether, 6,000 km of CO_2 pipelines are being operated in the USA primarily for Enhanced Oil Recovery (EOR), transporting a total of more than 80 Mt y^{-1} of CO_2 (Koornneef et al., 2008). To make a comparison, in the USA there are over 2 Mkm of natural gas transportation pipelines and more than 250,000 km of hazardous liquid pipelines (anhydrous ammonia, crude oil, fuel oil, diesel fuel, condensate, gasoline and others) (Gale and Davison, 2004). The experience gained in moving these liquids can be applied to the transportation of CO_2, taking into account the particular behaviour of this fluid when a leakage from a superficial/shallow facility occurs (see later paragraphs).

4.1.1 Design and control considerations

The design implications for transporting CO_2 compared to other gases appear to be well understood (Barrie et al., 2004, Gale and Davison, 2004, Zhang et al., 2006). CO_2 pipeline operators have designed minimum specifications for composition. The mechanical requirements for CO_2 pipeline design are subject to standards, the major one being the USA Code of Federal Regulations, Parts 190-195 (USA, 2004).

CO_2 is a commonly used industrial material. However, it is an acid gas and will react with water to form carbonic acid, in conditions of low H_2S concentration; carbonic acid corrosion of carbon steel has been recognized for years as a major source of damage in oilfield equipment and gas pipelines, and is commonly referred to as "sour corrosion" (Barrie et al., 2004, CAPP, 2002). Internal pipeline corrosion is an important cause of gas loss in gas transportation: it can pose serious problems in systems transporting pure CO_2. Dry carbon dioxide does not corrode the carbon-manganese steel generally used for pipelines (the absence of water reacting with carbon dioxide preventing the formation of

carbonic acid), due to the CO_2 stream being "dry" – i.e. <0.5 gH_2O $(Nm^3CO_2)^{-1}$ (Rogers and Mayhew, 1980). Seiersten calculated that over a 12 year period, the corrosion rate in an operating pipeline amounts to 0.25-2.5 μm yr^{-1} (Seiersten, 2001).

Because of the Joule-Thomson effect (see paragraph 4.2.1), CO_2 cools dramatically during decompression, so pressure and temperature must be controlled continuously. To be transported in a pipeline CO_2 must be compressed to ensure that single-phase flow is achieved: the most widely used operating pressure is between 7.4 and 21 MPa. Above 7.4 MPa, CO_2 exists as a single dense phase (i.e. super-critical phase) over a wide range of temperature; clearly, a transmission pipeline can experience a wide range of ambient temperatures, so maintaining stability of this single phase is important in order to avoid considerations of two-phase flow that could result in pressure surges and flow blockages (Barrie et al., 2004). In practice, carbon dioxide is likely to be transported on-shore below 105 atm, which is the maximum allowed for permitting over land (Kaarstad and Hustad, 2003). Therefore, in this study a transportation pressure of 100 atm (10 MPa) will be assumed.

It is necessary to estimate the pressure drop along the pipeline so that recompression stations can be placed at appropriate intervals and prevent the choking point being reached when two-phase flow occurs in the pipeline. The pressure drop is dependent on the temperature, flow rate and geometric characteristics of the pipeline such as diameter, length and elevation changes (Zhang et al., 2006). Following the work of DNV, the average length of pipeline between two consecutive boost pumps has been set at 50 km. Usually, oil industry practice in control methodology is to use an automatic control system to monitor volumetric flow rates and pressure fluctuations in the pipeline, coupled

with block valves (Emergency Shut Down valves, ESD) at set distances that can be shut off in the event of pipeline failure (Gale and Davison, 2004, Robye et al., 2002). One issue in the design of the pipeline is the number of block valves for a chosen distance (i.e., the frequency of the valves). The distance between the block valves has three impacts, which are:

- ✓ The shorter the distance, the higher the cost of the pipeline;
- ✓ The shorter the distance, the greater the risk of leakage from the valves themselves;
- ✓ The greater the distance, the greater the volume contained between the block valves; this will increase the volume of CO_2 released to atmosphere in the event of a leak and hence present a greater risk.

The optimum compromise between cost and safety must be derived and is likely to be site specific, depending on a number of factors such as local topography, meteorological conditions and population density. Kruse and Tekiela (1996) compared the distance between valves (either 5 or 30 km), for a pipeline operating at 60 bar (6 MPa). The study showed that, with valves at 5 km intervals, a safety distance from the pipeline of 150 m was required but, at 30 km intervals, safety distance increased to 600 m. The study concluded that the larger safety distance would be difficult to achieve in densely populated areas, so shorter valve separations are required.

In this thesis, a modular engineered transportation system has been considered for evaluating the hazard in transporting CO_2. In the pipeline modules (2 and 4) an ESD valve spacing of 50 km was assumed, irrespective of location.

4.2 CO_2 properties

There are four different phases for carbon dioxide, i.e. solid, gas, liquid and supercritical/dense phase. The phase diagram in Figure 4.1 shows the boundaries between these. Solid, liquid and gaseous CO_2 coexist at the triple point of -56° C and 0.52 MPa. If either the pressure or the temperature is below these values, CO_2 can only exist in either gaseous or solid form (this last is also known as "dry ice"). The other interesting position is the critical point, which occurs at a temperature of 31.1° C and a pressure of 7.28 MPa. Above this critical pressure and at higher temperatures than -60° C, only one condition exists, i.e. the supercritical/dense phase. In this phase CO_2 has a liquid-like density but it behaves as a gas, i.e. it occupies the volume of its container (Pasquetto and Patrone, 1994).

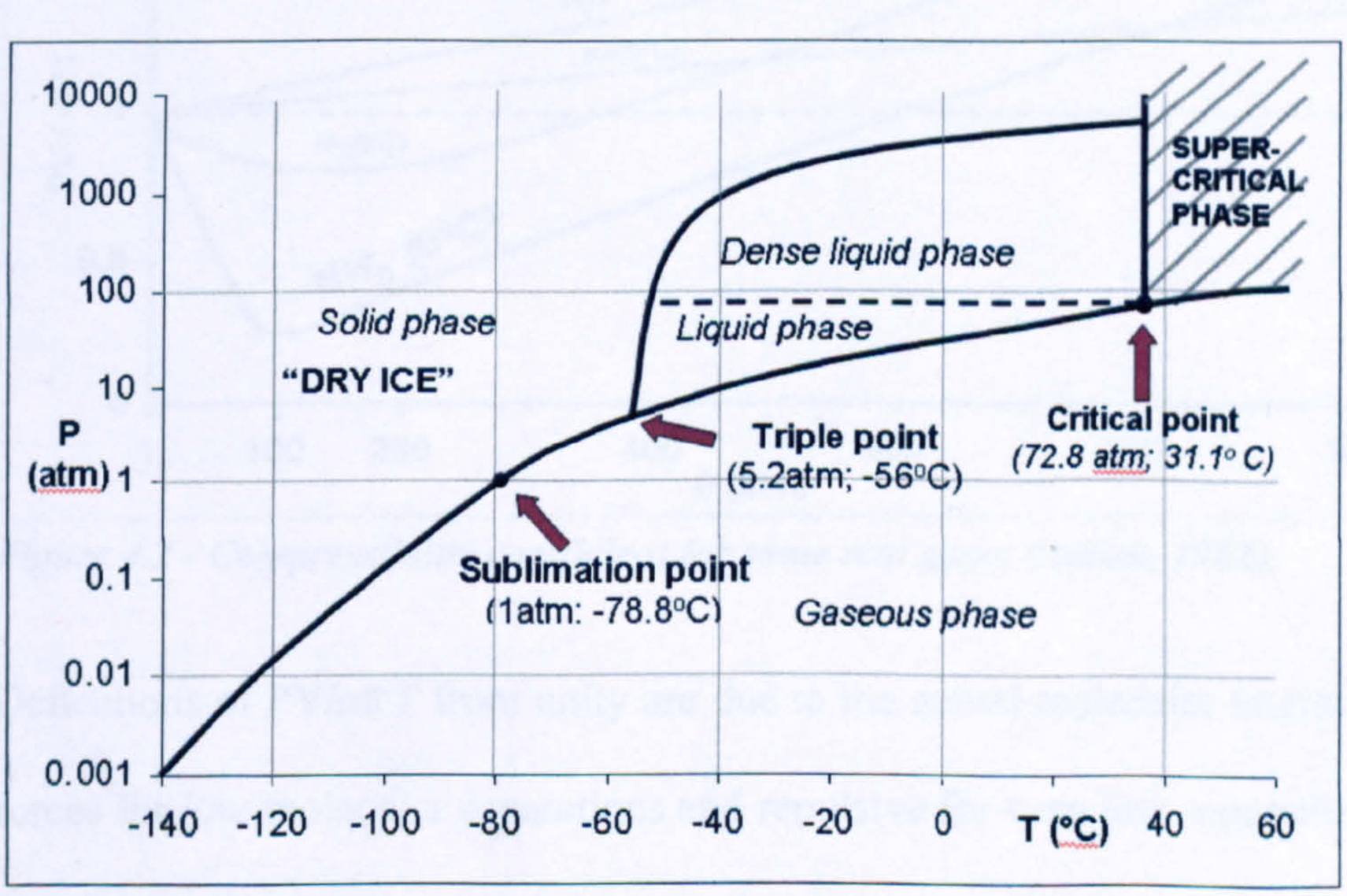

Figure 4.1 - CO_2 phase diagram (Pasquetto and Patrone, 1994).

4.2.1 The Joule-Thomson effect

An ideal gas is a hypothetical gas whose molecules have negligible size, bounce off each other with perfect elasticity, and for which the intermolecular forces are negligible when they are not in contact. The equation of state of an ideal gas is: $PV = nRT$ (or $PV/nRT = 1$), where P is the pressure of the gas, V its volume, n is the number of moles of gas, R is the universal gas constant (0.08205784 L atm K^{-1} mol^{-1}) and T is the temperature. This equation suggests that the ratio PV_m/RT (where $V_m = V/n$, molar volume) is the same for all gases that present an ideal behaviour. In practice, PV_m/RT for real gases varies with pressure, as illustrated in Figure 4.2.

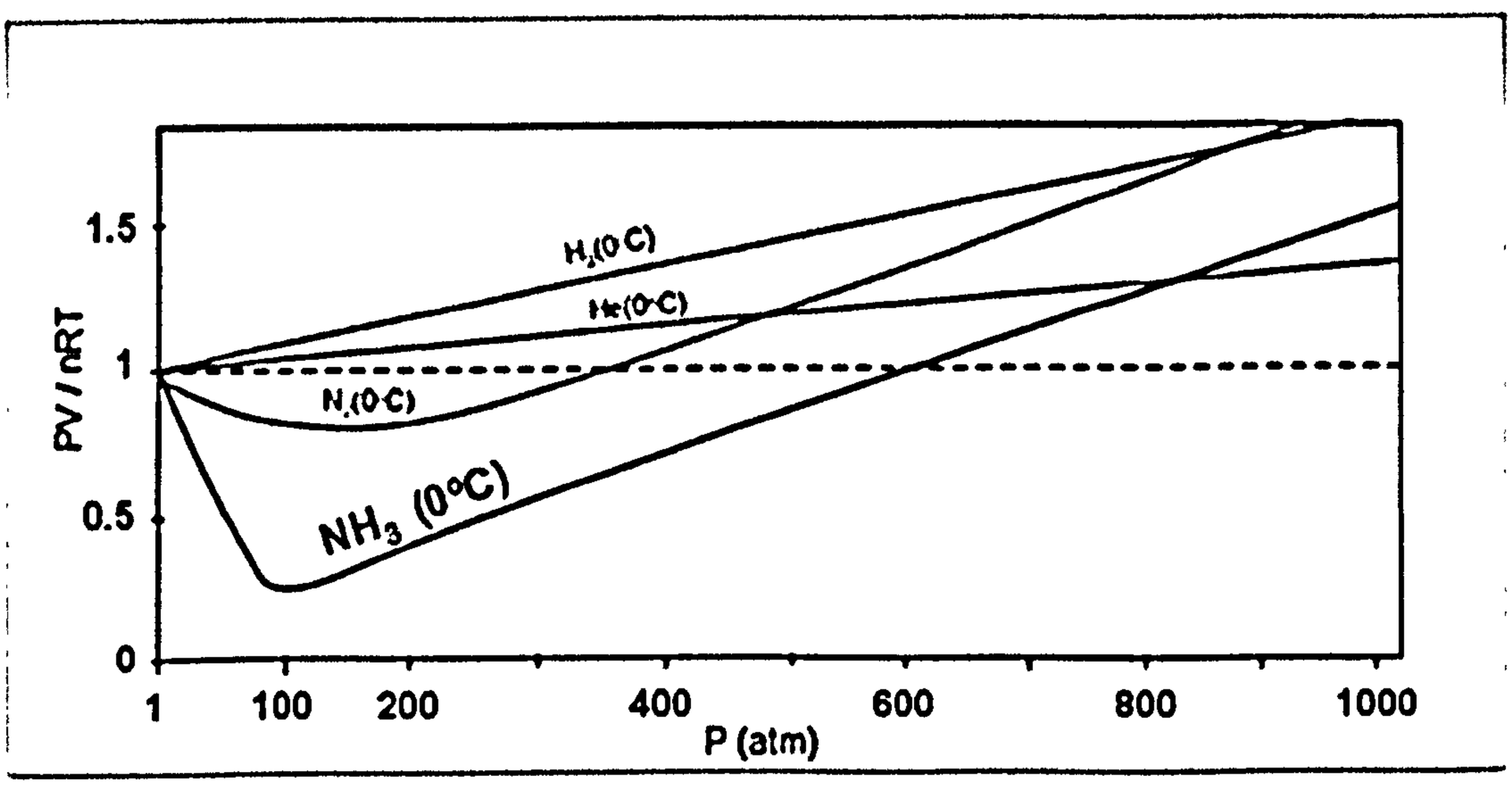

Figure 4.2 - Compressibility coefficient for some real gases (Atkins, 1981).

Deflections of PV/nRT from unity are due to the actual molecular interactions (attractive forces for low molecular separations and repulsive for very low separations). Some gases like ammonia, nitrogen and carbon dioxide present, for moderately high pressure, values of this ratio lower than 1. This implies that, for particular P-T conditions, the molar volume of the gas is lower than that for an ideal gas. In Figure 4.2, the compressibility

coefficient is an index of the resistance of the gas to compression: values lower than 1 imply a reduction of the molar volume due to attractive interactions between the molecules. Thus, while the effective dimensions of molecules reduce the free volume that can be occupied by the molecules themselves (and this can be seen as an effect of repulsive forces at very low molecular separation – very high pressure), attractive forces reduce the pressure exerted by the gas toward the walls of the container (at relatively lower pressure). The experimental interpretation of this was given by Van der Waals with his equation, which is a modification of the ideal gas equation: $[P + a (n/V)^2] (V - n b) = n R T$, where a and b are the Van der Waals parameters, accounting respectively for the pressure reduction (a) and for molecular volume (b). Table 4.1 displays these parameters – characteristic of each gas – for the gases in Figure 4.2 and for carbon dioxide.

Table 4.1 - Values of Van der Waals parameters for some gases (Atkins, 1981).

Gas	a (L^2 atm mol^{-2})	b (L mol^{-1})
Hydrogen (H_2)	0.244	0.027
Helium (He_2)	0.034	0.024
Nitrogen (N_2)	1.39	0.039
Ammonia (NH_3)	4.17	0.037
Carbon dioxide	3.59	0.043

From Table 4.1, the parameter a (which accounts for attractive forces) for carbon dioxide is more similar to that of ammonia than to those of the other gases. When ammonia (or carbon dioxide) experiences a pressure drop (e.g. from 100 atm to 1 atm), their molecules do work against the above mentioned attractive forces. The energy for this work is taken directly from their kinetic energy, decreasing the gas temperature.

The Joule-Thomson equation relates the temperature change to the pressure change for real gases:

$$\Delta T = \varphi \cdot \Delta P \qquad (4.1)$$

where φ is the J-T coefficient. For carbon dioxide the value of the J-T coefficient was found experimentally: $\varphi_{CO2} = 1.3$ K atm^{-1} (Atkins, 1981). The temperature drop caused by the above pressure change would be around 130 K – Equation (4.1).

As will be seen later on (Chapter 6) the high efflux speed characterizing a leak-flow from a high pressure transportation facility is expected to provide the necessary heat for carbon dioxide to re-convert entirely (or at least for the biggest part) to its gaseous state, from whatever percentage of dry-ice formed after the Joule Thomson cooling. On the other hand, it is paramount to account for the density of the gas after its second phase change (from solid to gas). In fact, near the sublimation temperature, CO_2 has a density of 2.8 kg m^{-3}, much higher than in STP conditions (1.8 kg m^{-3}, at 20° C). In this chapter it will be seen how the CFD tool can account for this and how the heavy gas behaves differently for the two atmospheric conditions considered (in terms of plume downwind lengths), compared to buoyant gases and to results from Gaussian simulations, involving the same CO_2 dispersion scenarios.

4.3 Risk Analysis

As stated in Chapter 1, the analysis of risk is based on the product of frequency and consequence of hazards. Release frequency data were derived from the oil and gas

industry and the consequences of potential releases of CO_2 were then modelled using the CFD and Gaussian software for atmospheric dispersion, previously described.

For the purposes of this study a generic modular pipeline system was used for the risk analysis, covering CO_2 capture operations through the various on-shore injection points. This work does not cover the off-shore transportation and injection facilities (i.e. ship carriers and platforms); also, being based on a generic modular transportation system which can be applied to all transportation projects, it does not attempt to present Risk Assessments, which require knowledge of specific systems, their surroundings (i.e. presence of complex topography, urban details and specifically sensitive areas) and potential impacts.

4.3.1 Consequences of CO_2 intake by humans

In paragraph 1.2.2.3, the general effects of CO_2 inhalation were described. Table 4.2 provides a more detailed list of typical human responses to CO_2 at different concentrations, during different exposure times.

In this thesis, key concentration limits, determined and used for the risk analysis, are as follows. The tolerable concentration without negative environmental impacts is identified at 2,000 ppm or 0.2 % (Vendrig et al., 2003). For humans, the STEL (Short-Term Exposure Limit) level of 1.5 % or 15,000 ppm is used as a guide for maximum exposure. This is the concentration below which no negative impacts will be observed on people after an exposure of 15 minutes (HSE, 2005).

Table 4.2 - Effects of different CO_2 different exposure times (Vendrig et al., 2003).

CO_2 concentration		Time	Effects
Percent	ppm		
17-30	170,000-300,000	Within 1 minute	Loss of controlled and purposeful activity, unconsciousness, convulsions, coma, death
> 10-15	100,000-150,000	1 minute to several minutes	Dizziness, drowsiness, severe muscle twitching, unconsciousness
7-10	70,000-100,000	Few minutes-1.5 minutes to 1 hour	Unconsciousness, near unconsciousness, Headache, increased hearth rate, shortness of breath, dizziness, sweating, rapid breathing
6	60,000	1-2 minutes-<16 minutes-Several hours	Hearing and visual disturbance Headahce. dyspnoea Tremors
4-5	40,000-50,000	Within a few minutes	Headache, dizziness, increased blood pressure, uncomfortable dyspnoea
3	30,000	1 hour	Mild headache, sweating, dyspnoea at rest
2	20,000	Several hours	Headache, dysopnea upon mild exertion

The concentration range of 7-10% will probably be fatal. In particular, 100,000 ppm (10%) has been used to delineate the downwind boundary of potentially fatal modelled plume concentration after leakage from transportation facilities.

4.3.2 The Engineered System

Specific details of CO_2 transportation systems and capture/sequestration plants are not available and so, in order to undertake a risk analysis, it is necessary to identify generic sections of plant and piping that, combined appropriately, can account for the majority of potential projects.

CO_2 will be recovered from potential sources, such as power stations, possibly by means of an amine solution scrubber (Vendrig et al., 2003). It will be transported on-shore by surface/shallow pipeline systems at a pressure of about 100 atm (10 MPa, well into its supercritical state) and eventually injected underground with or without an "end-of-pipe" compressor to maintain the stability of the high density waste gas.

4.3.2.1 Modular system

There are eight modules in the generic delivery system. Some will appear once in a system (e.g. recovery at source) while others can be repeated tens of times (e.g. specified lengths of piping). A description of each module is provided in Table 4.3, with indications of the length of piping each one is assumed to include. In the present study, of the eight modules listed in Table 4.3, only five have been considered, specifically the onshore modules 1 to 5. For these modules, the bulk of the data has been derived from the databases of offshore incident frequencies and the American Gas Association (Gale, 2001, Skovholt, 1993, Smith and Warwick, 1981, Vendrig et al., 2003).

Table 4.3 - Descriptions of Modules in the generic engineered system (Vendrig et al., 2003).

Module no.	Module description	Module pipe length
1	CO_2 recovery at source	500 m
2	Converging pipelines	100 m
3	Booster station	100 m
4	Pipelines	10 km
5	Injection plant.	500 m
6	CO_2 riser to offshore platform from submerged pipelines	N.A.
7	Line down to containment region	N.A.
8	Tanker transport	N.A.

Each module is illustrated in Figure 4.3 through Figure 4.7. The modules themselves, which have been kept simple for this study, are described below together with relevant assumptions. More assumptions for each module, mainly in terms of operating parameters, are described later, together with failure consequence analysis.

Module 1 covers that part of the system from after the scrubber at the source through the storage and compression of the gas and the associated pipelines for this part of the process. The module is assumed to comprise 500 m of generic plant piping, a storage vessel and compressor, as shown in Figure 4.3, together with an appropriate number of flanges, valves (including emergency shut down - ESD - valves) and fittings.

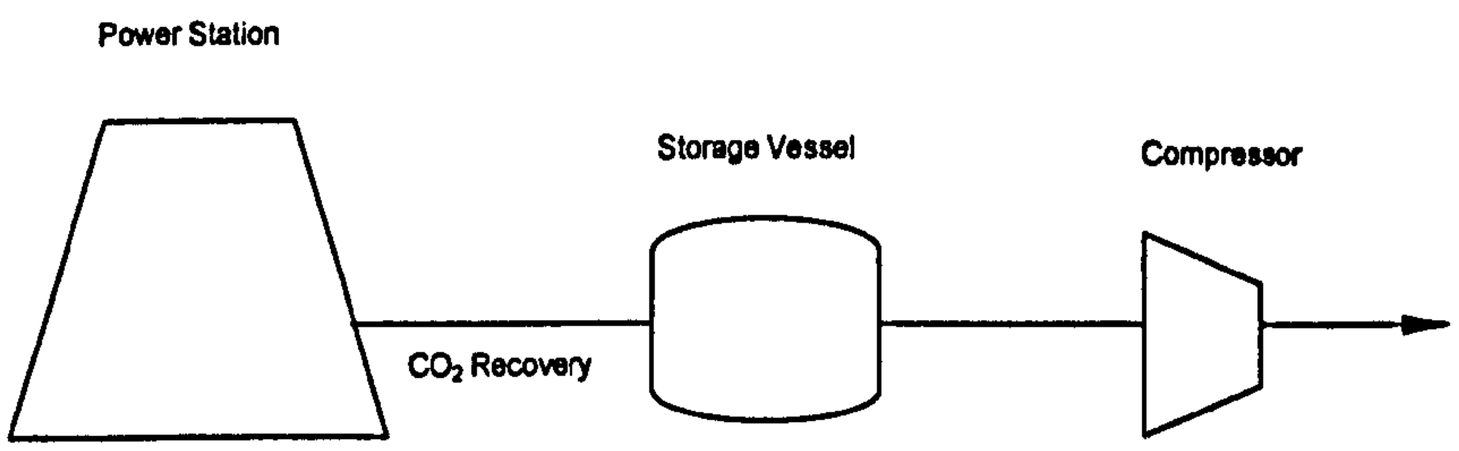

Figure 4.3 - Module 1: CO_2 recovery at source.

Module 2 accounts for sections of pipeline from two CO_2 sources – i.e. two power plants or from two CO_2 scrubbers at one plant. It is assumed that pipelines onshore are buried and the length of pipe work in this module is 100 m, see Figure 4.4.

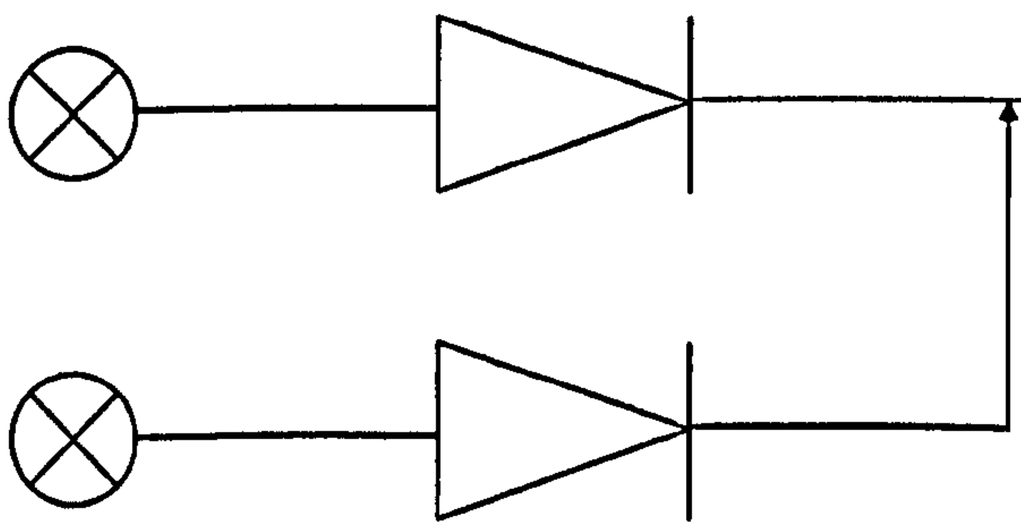

Figure 4.4 - Module 2: Converging Pipelines.

Module 3. Every 50 to 100 miles an onshore pipeline will feature an ESD valve, a relief valve and a booster pump, collectively referred to as a booster station (Figure 4.5). By following a conservative approach it will be assumed that such fittings are featured every 50 km, with the length of pipeline required for each booster station being around 100 m. All such fittings will be isolatable by means of block valves upstream and downstream and all valves will have associated flanges.

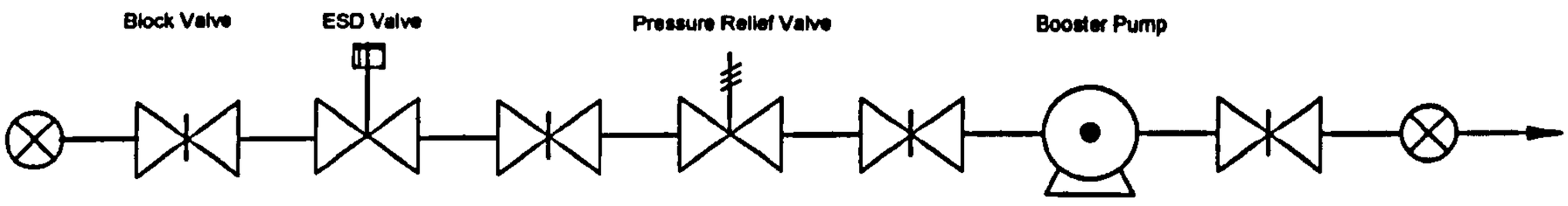

Figure 4.5 - Module 3: Booster Station.

Module 4 comprises a 10 km section of pipeline with a diameter of 30" (0.762 m). Following current USA and UK practice for waste gas transportation pipelines, high pressure CO_2 transportation pipelines in CCS projects will be buried at a depth of 1 m. In this leakage risk study, it is assumed that all releases will reach the surface and result in direct CO_2 emission to the atmosphere.

Module 5, the Injection plant, comprises 500 m of generic plant piping, a pressure vessel and two pumps (as for Module 3, considered to be centrifugal), as shown in Figure 4.6. As with Module 1, the generic plant piping is considered to account for all fitting requirements.

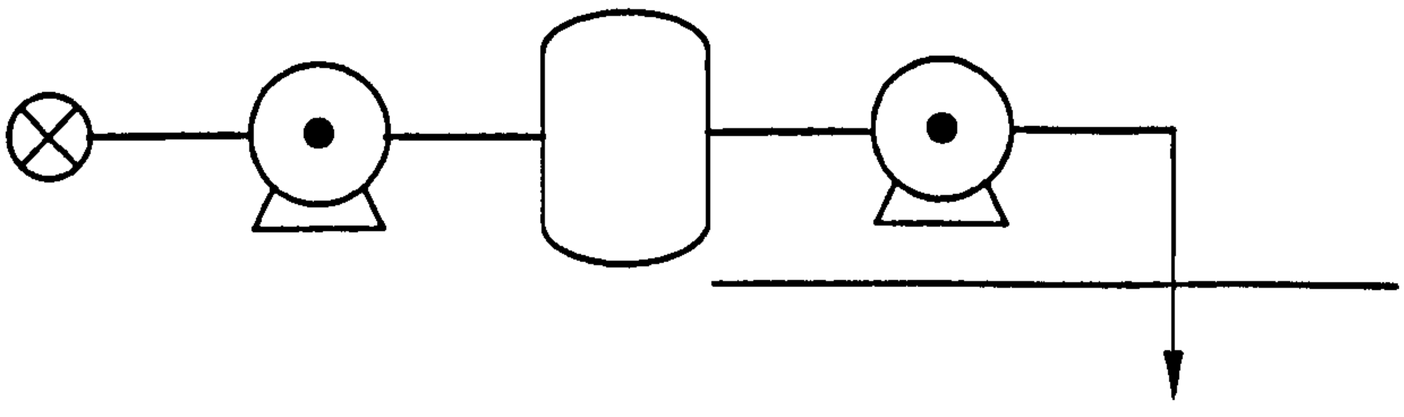

Figure 4.6 - Module 5: Injection Plant.

4.3.3 Failure cases of the Engineered System

The first stage in any risk analysis is to identify the potential accidents that could result in the release of a hazardous material, carbon dioxide in this case, from its normal containment. The modular approach to the engineered system is based on components such as pipe-work, equipment and vessels. Process failure data is well-established and data is available to define representative accident scenarios for all of the generic items included in the modular system. These hazards of the engineered system include failures caused by mechanisms such as corrosion, vibration or external impacts and apply to components including the following: pipelines (buried and surface), flanges, valves, fittings, pressure vessels, pumps and compressors.

The range of possible releases for a given component covers a broad spectrum, from a pinhole leak up to a catastrophic pipe or vessel rupture. It is not practicable, particularly in a generic study such as this, to consider every part of the range and, instead, representative failure cases are generated. Therefore, for each module and each component, four different leak frequency scenarios have been considered:

- Full-bore pipe rupture (applied to all leaks of equivalent diameter > 150 mm)
- Large leaks, 100 mm equivalent diameter (covering leaks from 50 to 150 mm)
- Medium leaks, 30 mm equivalent diameter (10 to 50 mm), and
- Small leaks, 7 mm equivalent diameter (3 to 10 mm)

4.3.4 Failure frequency analysis

The data of failure frequency are taken from the work of Vendrig et al. (2003). They have been derived from DNV's library and are based primarily on hydrocarbon failure data. These are considered to be the best available data and to be equally applicable to

pipes and equipment carrying carbon dioxide, particularly for generic systems. Table 4.4 gives a summary of failure rates per year, for each module.

Table 4.4 - Failure rate summary per Module year (Vendrig et al., 2003).

Module		Failure rate (per module year)	Leak every *x* years
1	CO_2 recovery at source	$1.5 \cdot 10^{-1}$	7
2	Converging pipelines	$4.6 \cdot 10^{-3}$	217
3	Booster station	$4.0 \cdot 10^{-2}$	25
4	Pipelines	$3.4 \cdot 10^{-4}$	2941
5	Injection plant.	$1.8 \cdot 10^{-1}$	6

It should be noted however, that modifications are often applied to generic failure data when used for specific applications for which local conditions are known (e.g. manufacturing quality, staff training, extreme weather or seismology). New installations may also be expected to have greater reliability than suggested by the failure data, which are necessarily based on (albeit the most recent) historical records. This effect cannot be quantified and is typically considered as a necessary conservatism in the data. The databases from which DNV extracted the failure data utilised in this work span the last forty years of oil, gas and waste product transportation.

Table 4.5 gives the breakdown of failure rates associated with each module by the representative leak size given in the previous paragraph. The leak frequency broadly decreases with the leak size (while the consequence associated with a release will increase with the leak size).

Table 4.5 - Failure rate distribution, per year, for Modules 1 to 5 (Vendrig et al., 2003).

Module	Small (3-10 mm)	Medium (10-50 mm)	Large (50-150) mm)	Full-bore (>150 mm)
1	$9.6 * 10^{-2}$	$5.1 * 10^{-2}$	$2.0 * 10^{-3}$	$5.6 * 10^{-3}$
2	$3.5 * 10^{-3}$	$8.8 * 10^{-4}$	$1.0 * 10^{-4}$	$1.5 * 10^{-4}$
3	$3.5 * 10^{-2}$	$3.8 * 10^{-3}$	$3.0 * 10^{-4}$	$8.8 * 10^{-4}$
4	$1.4 * 10^{-4}$	$9.5 * 10^{-5}$	$2.0 * 10^{-5}$	$8.5 * 10^{-5}$
5	$1.2 * 10^{-1}$	$5.3 * 10^{-2}$	$2.1 * 10^{-3}$	$5.8 * 10^{-3}$

4.3.5 Consequence assessment of the Engineered System

The cases for which consequence analysis is required have been derived from the frequency analysis summarized above, i.e. each of the leak sizes defined for each module. Once the leak and release parameters have been defined, dispersion modelling is conducted to determine a plume footprint for the 2,000, 15,000 and 100,000 ppm ranges.

The CFD model PANACHE 3.4.1 is used to simulate the atmospheric dispersion of the leaked gas. The results are used to derive transects of risk to individuals exposed to the concentrations of interest, for each module. For the purpose of comparison, these results are also compared with those from the Gaussian model ALOHA 5.4. A short discussion on the comparison is given at the end of this chapter and in the final chapter.

4.3.5.1 Consequence assessment methodology

For each module, potential releases are split into representative leak sizes and the release rate is used to determine a representative probability of detection and isolation (by either 'automatic' or 'manual' means), which is proportional to the leak size. These different event outcomes determine the duration of release which, combined with the release rate and the inventory of each section, control the total amount of carbon dioxide

that is released. Further classification arises from sub-dividing each release event into two representative weather categories for subsequent dispersion modelling.

Process conditions assumed for simulations are based on the default system characteristics given in Table 4.6. A time varying release is modelled by using a constant release rate corresponding to the time at which 25% of the inventory has been released (Vendrig et al., 2003).

In general, the quantity of carbon dioxide released is based on the amount within the isolatable section plus the amount that leaks before isolation occurs. The latter depends on the size of the leak and on the time delay before the section is isolated. The duration is taken as the time to isolate the section plus the time taken for the inventory remaining in the section after isolation to be released.

Table 4.6 - System characteristics - data from Vendrig et al. (2003).

Parameter	Value	
Atmospheric stability class	F2	D5
Ambient temperature (°C)	5	10
Ambient pressure (mbar)	1003	997
CO_2 temperature during transportation (°C)	Mod 1	Mod 2/3/4/5
	20	30
CO_2 pressure during transportation (MPa)	Mod 1	Mod 2/3/4/5
	2	10
Pipeline diameter (inches)	Mod 1/2/3/4	Mod 5
	30	10
Flow rate (Mt/year)	Mod 1/5	Mod 2/3/4
	3	20

As it can be seen from Table 4.6, two combinations of wind speed and atmospheric stability classes have been utilized, which are D5 (neutral stability, D, and 5 m s^{-1} wind

speed) and F2 (high stability, F, and 2 m s^{-1} wind speed). The prevailing atmospheric conditions within the UK were approximated by 80% D5 and 20% F2, broadly representing the critical dispersion conditions of high wind speed for short-duration releases and low wind speed with stable stratification for long duration releases (Vendrig et al., 2003). These combinations are widely used by the UK HSE (Health and Safety Executive) for generic assessments, where site specific wind information is not available (Griffiths, 1991).

4.3.5.2 Model input parameters

For the simulations described in this paragraph both the Gaussian and the CFD models have been used. The former requires specification only of wind speed, atmospheric stability class and release rate; the CFD software requires a more detailed specification in terms of grid sizes, turbulence models used, assumptions made on supercritical carbon dioxide releases after leak events, release flow velocity and direction.

For the purpose of comparing CFD results with Gaussian, plume lengths after leakages from high pressure facilities have been considered with a release flow speed near 0 m s^{-1}. In fact, ALOHA evaluates the jet release after high pressure leakage using its own algorithm which can consider ESD valves distance of up to 10 km and use data such as inlet pressure and pipeline diameter for evaluating the total inventory of CO_2 released. This way, transportation leakage data would be different from DNV's (Vendrig et al., 2003) and comparison with CFD simulations would not be possible. Thus, in this chapter, velocity of the release has not been considered when evaluating the risk involved in the process even with the CFD tool. The near zero release velocity can reflect a worst case scenario, for carbon dioxide is a dense gas and its tendency to stay close to the ground

would be offset by a rapid initial motion of the gas. In any case, risk assessments within gas transportation have always been carried out without considering the high speed (jet) flow originating after a leak from a high-pressure transportation system (Kruse and Tekiela, 1996, Turner et al., 2003, Vendrig et al., 2003, Woodhill, 2003).

As already stated all releases from buried sources are assumed to reach the surface. The CO_2 phase change (from supercritical to solid and then to gaseous state) was not considered, allowing the supercritical flow to reconvert entirely to gas phase thanks to the jet-mixing effect (i.e. the resistance imposed by air to the high speed flow), at a temperature of -60° C. Atmospheric conditions considered were F2 and D5, as prescribed by HSE (2001) and the size of the domain is dependent on the release rate of each trial. The number of Control Volumes on the grid was always between 50,000 and 100,000, using an inhomogeneous grid generator with a finer mesh near the flow source (i.e. the leak). As described in chapter three, the turbulence models used in these trials were the *k-ε* for simulations under D5 conditions and *k-l* for F2 conditions.

4.3.6 Key assumptions and hazard range results for each module

Module 1 – CO_2 Recovery at Source

Release parameters and resulting hazard ranges for the generic CO_2 Recovery at Source module are summarized in Table 4.7. Key assumptions made are:

- Recovered CO_2 is in vapour phase upstream of the compressor (in Chapter 6, simulations within a typical plant environment have been made considering CO_2 in its supercritical state, downstream of the compressor).

- No significant inventory of stored CO_2 has been assumed for this module (about 9 t, based on 500 m of piping. In Chapter 6, a much shorter length of piping has been considered).
- A flow rate of 3 Mt yr^{-1} has been assumed, with a representative pipe diameter of 30" and process conditions of around 20 atm at 20° C.

Table 4.7 - Hazard ranges for representative releases from Module 1, CO_2 Recovery at Source.

Leak case	Release parameters			Maximum downwind distance (m)											
				100,000 ppm				15,000 ppm				2,000 ppm			
	Duration (s)	Rate (kg/s)	Inventory (kg)	D5		F2		D5		F2		D5		F2	
				PAN	ALO	PAN	ALO	PAN	ALO	PAN	ALO	PAN	ALO	PAN	ALO
Full-bore	600	95	57000	47	53	36	102	149	249	127	647	378	879	336	2000
Large	816	43	35329	29	36	21	77	125	166	111	425	322	593	306	1300
Medium	3600	4	14040	7	11	6	25	38	51	33	112	117	188	102	356
Small	3600	2	7560	5	-	4	19	25	36	22	77	73	136	69	245

- Leak events with release rates greater than 10% of normal flow rate are detected automatically, with isolation effective after 10 minutes. Due to residual inventory of the isolatable section, for smaller leaks the duration is at least 1 hour – at which time the cloud formed by the leaked gas will have reached steady state, irrespective of whether detection and isolation occur.

Module 2, 3, 4 – Pipelines and related Modules

Release parameters and resulting hazard ranges for the generic Pipeline, Converging Pipelines and Booster Station Modules (respectively, Module 4, 2 and 3) are summarized in Table 4.8. Key assumptions are:

- There is no specific isolation associated with modules 2 and 3, so the consequences of release are the same as for the Pipeline Module 4.

- Distance between onshore valve stations (i.e. isolation points) has been assumed to be 50 km, with supercritical carbon dioxide in the pipeline at about 30° C and a pressure of 10 MPa.

Table 4.8 - Hazard ranges for representative releases from Module 2, 3 and 4, pipelines and related Modules.

Leak case	Release parameters			Maximum downwind distance (m)											
	Duration (s)	Rate (kg/s)	Inventory (kg)	100,000 ppm				15,000 ppm				2,000 ppm			
				D5		F2		D5		F2		D5		F2	
				PAN	ALO	PAN	ALO	PAN	ALO	PAN	ALO	PAN	ALO	PAN	ALO
Full-bore	600	1800	1080000	152	263	125	363	440	1200	339	2200	627	4000	585	7800
Large	3600	633	2278800	112	157	94	195	340	705	292	600	440	2300	422	6200
Medium	3600	57	205200	35	42	28	84	169	192	148	493	254	681	238	1600
Small	3600	3.1	11160	13	10	9	22	34	44	28	97	90	164	76	310

- The most realistic flow through pipelines has been taken as 20 Mt yr^{-1}, with a representative pipe diameter of 30".
- The inventory of the isolatable section is greater than 10,000 t.
- Leak events with release rates greater than 10% of normal flow rate are detected automatically, with isolation effective after 10 minutes. Due to residual inventory of the isolatable section, for smaller leaks the duration is at least 1 hour – at which time the cloud formed by the leaked gas will have reached steady state, irrespective of whether detection and isolation occur.

Module 5 – Injection Plant

Release parameters and resulting hazard ranges for the generic Injection Plant Module are summarized in Table 4.9. Key assumptions are:

- This module is assumed to be isolatable from the adjacent module – which for on-shore transportation system is presumed to be the Pipeline Module 4.

Table 4.9 - Hazard ranges for representative releases from Module 5, Injection Plant.

Leak case	Release parameters			Maximum downwind distance (m)											
	Duration (s)	Rate (kg/s)	Inventory (kg)	100,000 ppm				15,000 ppm				2,000 ppm			
				D5		F2		D5		F2		D5		F2	
				PAN	ALO	PAN	ALO	PAN	ALO	PAN	ALO	PAN	ALO	PAN	ALO
Full-bore	600	95	57000	47	53	36	102	149	249	127	647	378	879	336	2000
Large	600	95	57000	47	53	36	102	149	249	127	647	378	879	336	2000
Medium	3600	57	205200	35	42	28	84	129	192	108	493	204	681	188	1600
Small	3600	3.1	11160	13	10	9	22	34	44	28	97	90	164	76	310

- The inventory of the isolatable section (i.e. the Module) is assumed to be around 18 t, based on 500 m of 10" diameter pipe, with CO_2 being at 100 atm and 30° C. The representative flow rate through this module is assumed to be 3 Mt yr^{-1}.
- Isolation occurs within 600 s of the release event for large and full-bore rupture leak events, assuming that release rates greater than 10% of the normal flow-rate are detectable.

4.3.6.1 Discussion

From the results tables (4.7, 4.8, 4.9), from paragraph 4.2.1 (Joule-Thomson effect) and from Chapter 2, the CFD tool can account for the predominant differences in important physical characteristics between the two fluids (air and carbon dioxide) in a mixture. The density, viscosity and temperature of CO_2, particularly after the substantial impact of the Joule-Thomson effect, profoundly distinguish the two gases. In the simulations, downwind lengths of concentrated plumes have been found to be higher within the less

stable D5 atmospheric conditions than with F2. Results clearly show how the wind speed is more effective in lengthening the plumes than atmospheric turbulence is in dispersing the concentrated clouds. This dispersing behaviour particularly characterizes plumes of higher concentration, where for the 100,000 ppm plumes (see tabled results) the divergence in length between D5 and F2 results is the highest in terms of percentage. For the two different atmospheric stability classes, downwind extension differences for the 15,000 and 2,000 ppm plumes decreases almost linearly with concentration (see tables). It is fairly easy to visualize how a cold dense gas such as CO_2 would respond to natural atmospheric turbulence impulses in an attenuated way, compared with normally buoyant gases, particularly when in high concentrations. It has been found that simulating CO_2 releases with the gas at ambient temperature causes PANACHE to underestimate downwind plume extent by about 20% (with respect to the results in Tables 4.7, 4.8 and 4.9). In contrast, ALOHA accounts only for gases dispersing at ambient temperature: this is a drawback of the Gaussian software when attempting to model CO_2 dispersion after leakage from a high-pressure facility.

Below, downwind plume lengths delineated by the three criteria concentrations considered, as predicted by the Gaussian and the CFD tools, will be discussed and compared.

4.3.7 Human and environmental risk analysis of the Engineered System

Risk associated with impacts to people and the environment is determined by combining the identified release events and their failure rates (paragraph 4.3.4) with the consequences (paragraph 4.3.6). These risks of impacts to people and the environment

should not be confused with the risk of fatality, which is assessed separately in section 4.3.8.

The dispersion of carbon dioxide is dependent on wind conditions – hence the risk of impacts on personnel or the environment depends on the direction of the wind, which, as discussed extensively in Chapter 3, may be highly variable during the duration of a release. For this generic analysis, the wind is assumed to be constant in speed and direction.

The risk to the population and the environment due to concentrations of 15,000 and 2,000 ppm has been evaluated as the downwind plume length in conjunction with the frequency of leaks that could generate those plumes. In the case of the 100,000 ppm concentration, risk of fatality was calculated using areas covered by the clouds of concentrated gas.

These areas were calculated differently for each of the two models. PANACHE-simulated CO_2 leaks give a well shaped plume whose area could be approximated by an ellipse. Within ALOHA, results show less precision when plotted on a horizontal plane and the area subjected to the risk has been taken as a 30^{o} segment downwind of the release point. Figure 4.7 displays the representation of plume simulations by the two models. From the figure, the greater precision of the CFD model in calculating differences in gas concentration, even between two very close points, is offset by its inability to consider variable wind direction. In its turn, ALOHA accounts for unpredictable variations of the wind direction by extending the potentially endangered area via the widening of the plume (dotted lines in Figure 4.7).

The risk of life lost is examined more extensively in paragraph 4.3.7.

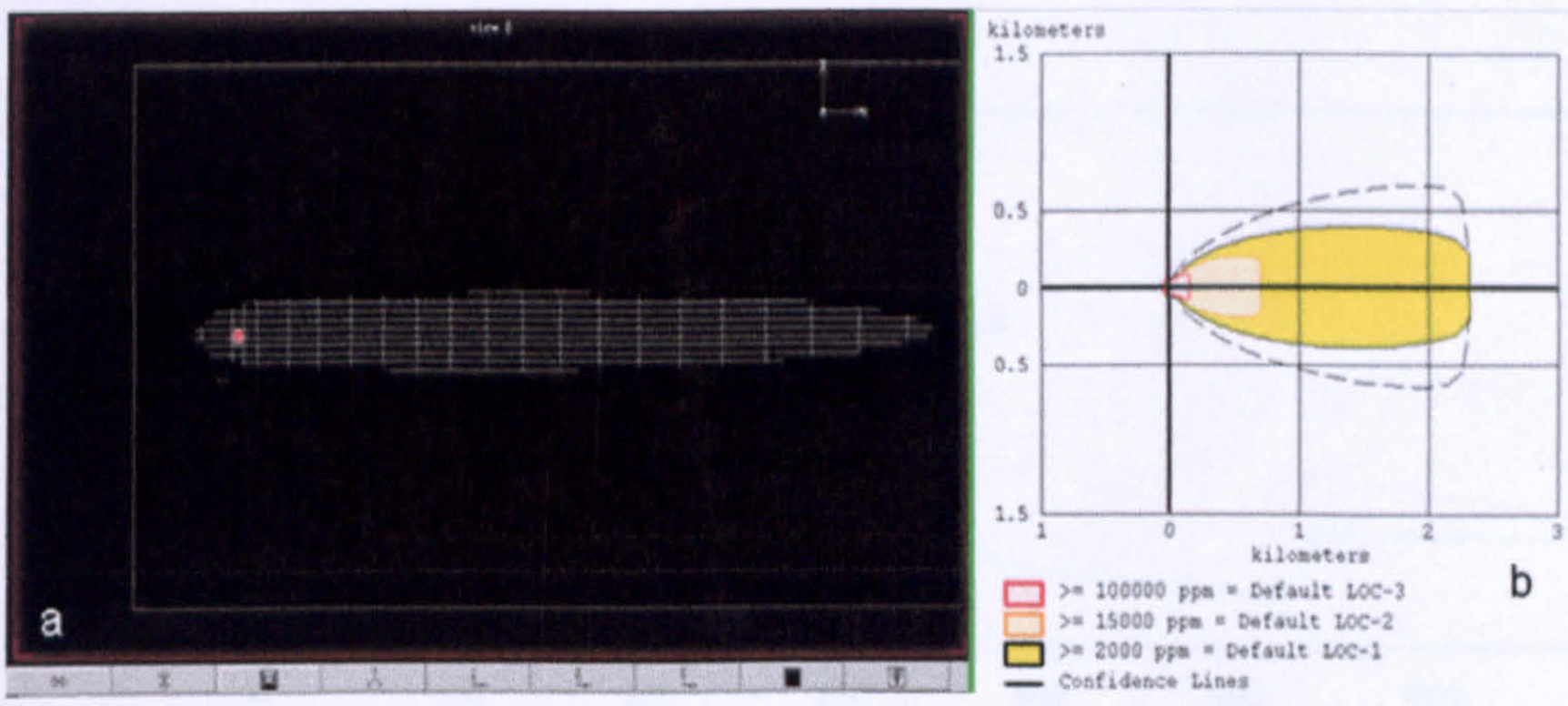

Figure 4.7 - xy views of plumes of concentrations after a 100 mm failure within Module 1 and in D5 conditions, as simulated by a) PANACHE and b) ALOHA.

The frequencies of failure, as reported in Table 4.5, are factored according to the frequency of prevailing atmospheric conditions to give the frequency of consequences occurring (i.e. the concentration of interest), as is detailed below. These last can be plotted against distance to produce an individual risk transect for each module. Risk transects give the risk of the concentration of interest being experienced by a single person (or "target") within the area subtended by a 30° arc downwind from the source.

4.3.7.1 Overview of impact risk results

Combining leak frequency and maximum downwind distances reached by resultant clouds, Figures 4.8 and 4.9 show how the frequency of concentrations of 2,000 and 15,000 ppm, as modelled by PANACHE, vary with distance for each module.

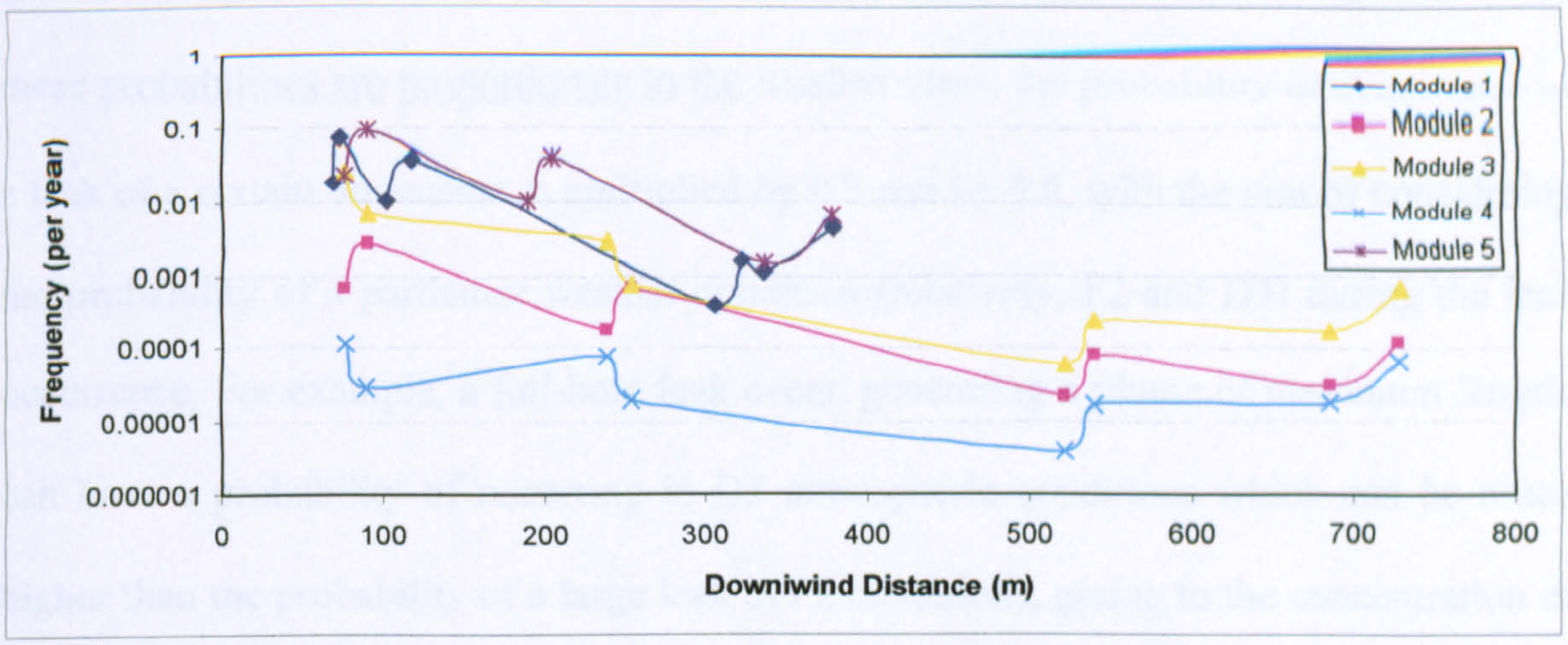

Figure 4.8 - Probability of experiencing a concentration of 2,000 ppm of CO_2 at different distances from the CCS transportation facilities considered (i.e. Modules 1 to 5). Downwind distance values calculated by PANACHE.

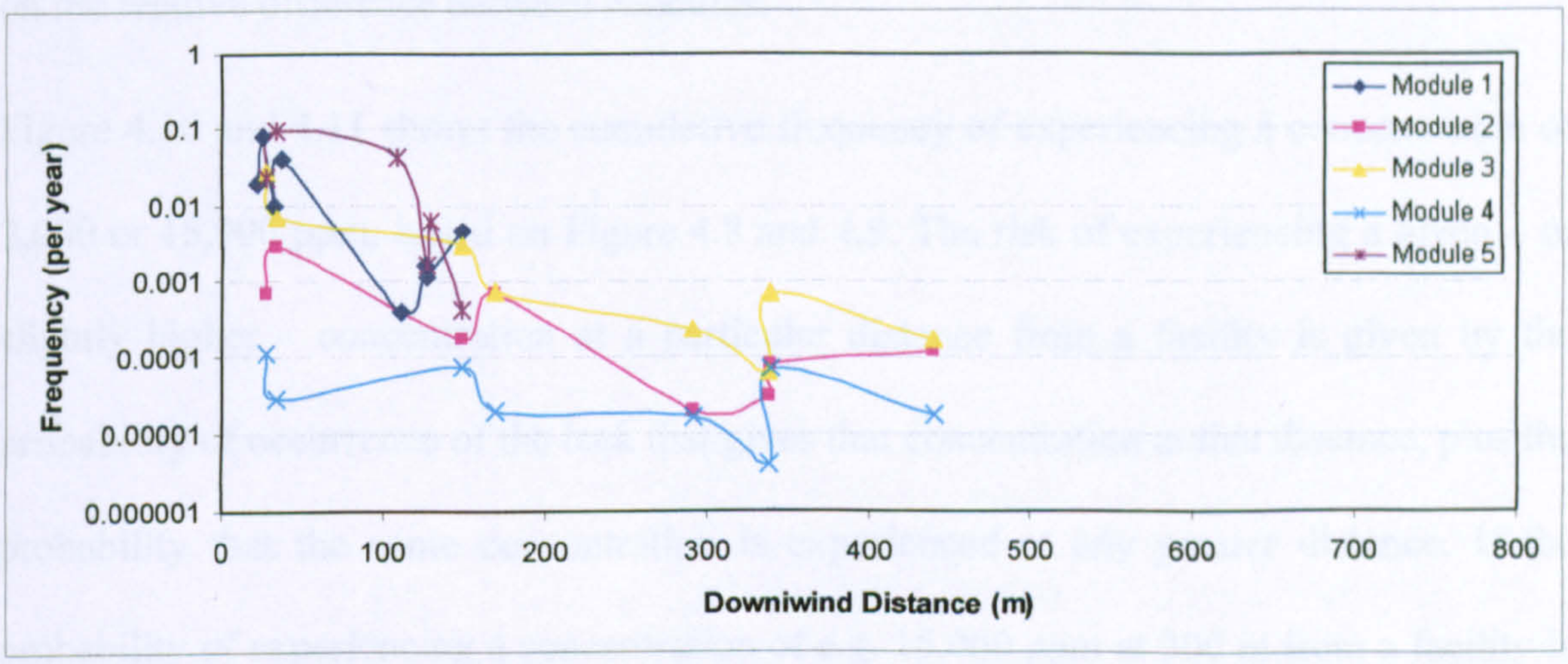

Figure 4.9 - Probability of experiencing a concentration of 15,000 ppm of CO_2 at different distances from the CCS transportation facilities considered (i.e. Modules 1 to 5). Downwind distance values calculated by PANACHE.

From the figures it can be seen that, paradoxically, the risk of experiencing a specific concentration at a particular distance from one module may at times be lower than the risk of experiencing the same concentration at a greater distance. The leakage frequency data used for this work, Table 4.5, give for each of the five modules a higher probability for the occurrence of a full-bore leak (>150 mm) than for the occurrence of a large leak

(50-150 mm), where the first gives concentration hazards further downwind. Moreover, these probabilities are proportionate to the weather class: the probability of occurrence of a leak of a certain dimension is multiplied by 0.2 and by 0.8, with the aim of considering the probability of a particular weather condition (relatively, F2 and D5) during the leak occurrence. For example, a full-bore leak event, generating a plume of maximum length, can have a probability of occurring in D5 atmospheric conditions which can be much higher than the probability of a large leak in F2 conditions, giving to the concentration of interest a higher probability of occurrence at greater distances. The explanation suggests that these two figures give only a measure of the risk and that the main focus should be on the relative difference between Modules.

Figure 4.10 and 4.11 shows the cumulative frequency of experiencing a concentration of 2,000 or 15,000 ppm, based on Figure 4.8 and 4.9. The risk of experiencing a given – or slightly higher – concentration at a particular distance from a facility is given by the probability of occurrence of the leak that gives that concentration at that distance, plus the probability that the same concentration is experienced at any greater distance. If the probability of experiencing a concentration of e.g. 15,000 ppm at 300 m from a facility is 0.003 yr^{-1} and the same probability at 200 m is 0.001 yr^{-1}, assuming that a concentration of 15,000 ppm at 300 m from the source will impose a higher concentration at 200 m, the corrected value for this probability at 200 m will be 0.004 yr^{-1}.

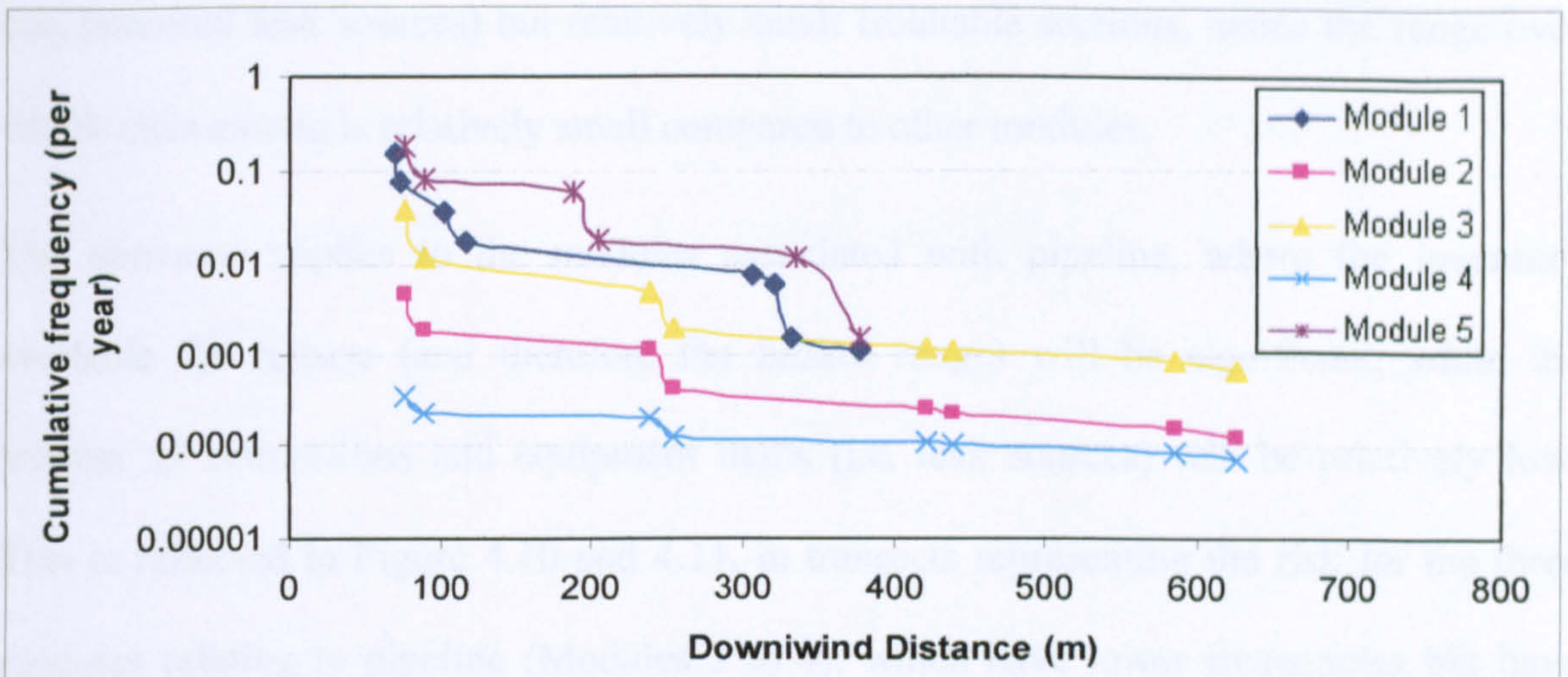

Figure 4.10 - Transects of Risk of individual being exposed to concentration of 2,000 ppm, for each Module. Downwind distance values calculated by PANACHE.

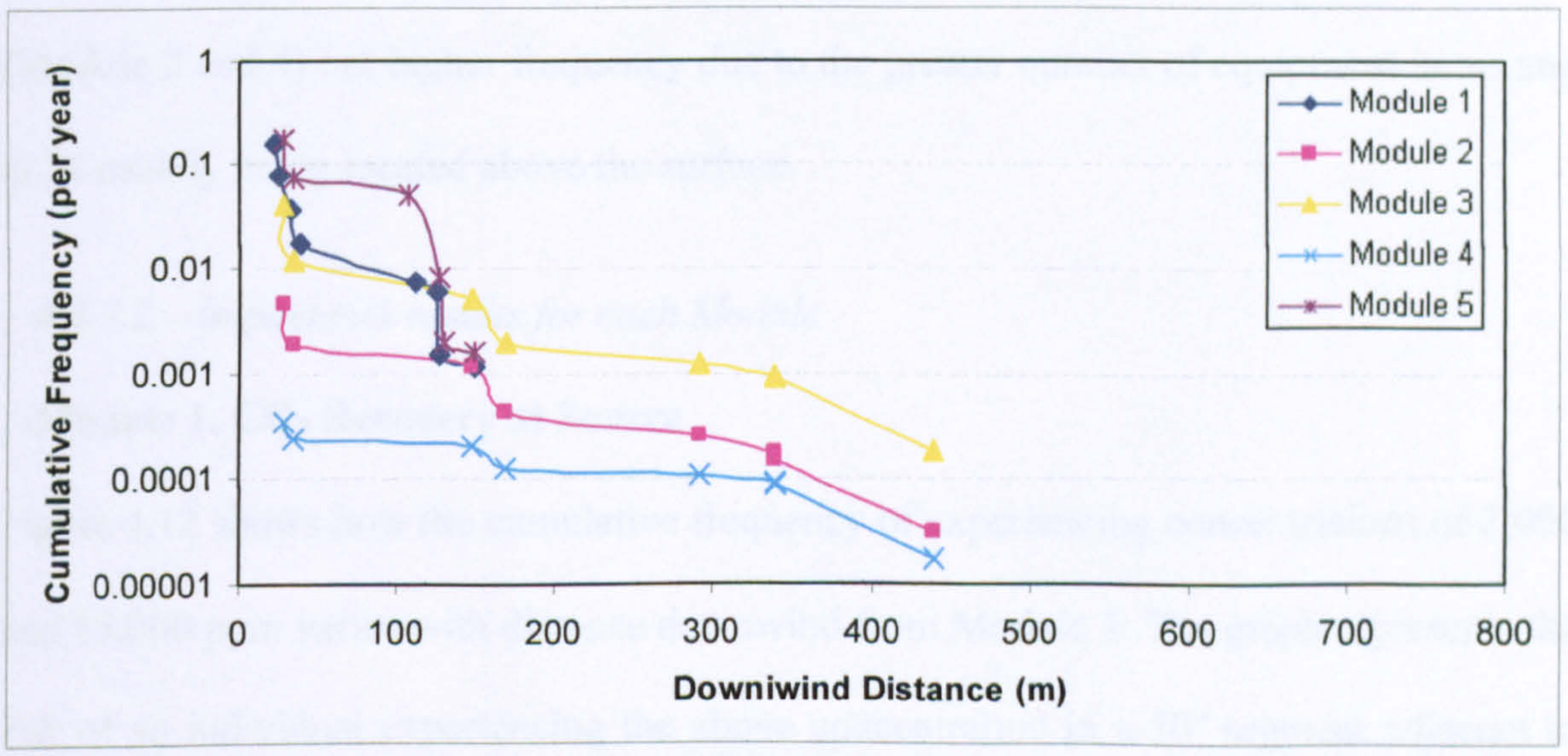

Figure 4.11 - Transects of Risk of individual being exposed to concentration of 15,000 ppm, for each Module. Downwind distance values calculated by PANACHE.

The graphs in Figures 4.10 and 4.11 display the cumulative frequency of experiencing concentrations of 2,000 and 15,000 ppm downwind of each module It is shown how the highest frequencies associated with the potential for impact on people apply to Modules 1 (CO_2 recovery at source) and 5 (Injection Plant). Both of these modules represent "process areas", which are anticipated to have a relatively large quantity of equipment

(i.e. potential leak sources) but relatively small isolatable sections, hence the range over which risks extend is relatively small compared to other modules.

The converse applies to the modules associated with pipeline, where the inventory available for release (and therefore the hazard range) will be significant, while the number of connections and equipment items (i.e. leak sources) will be relatively low. This is reflected in Figure 4.10 and 4.11, in transects representing the risk for the three modules relating to pipeline (Modules 2 to 4), which have lower frequencies but have impacts that reach significantly further than those for the above 'process' area. The Booster Station (Module 3) has the same profile of consequences as pipeline sections (Module 2 and 4) but higher frequency due to the greater number of equipment items and to its usually being located above the surface.

4.3.7.2 Impact risk results for each Module

Module 1, CO_2 Recovery at Source

Figure 4.12 shows how the cumulative frequency of experiencing concentrations of 2,000 and 15,000 ppm varies with distance downwind from Module 1. The graph represents the risk of an individual experiencing the above concentration in a 30° segment adjacent to Module 1. The downwind distance values have been calculated with both the CFD PANACHE and the Gaussian ALOHA atmospheric dispersion software.

The risk of receiving 15,000 ppm locally to the plant is almost 10^{-1} per year. This is true using both models, where actually the same frequency data of 10^{-1} is used to characterize the risk at ~50 m for ALOHA and at ~20 m for PANACHE. The frequency drops significantly for a small increase in distance. Within PANACHE (Figure 4.12a), the risk

reduces gradually with distance from around 0.2 at less than 30 m, to around 10^{-3} at 150 m. Within ALOHA (b), the risk of receiving 15,000 ppm CO_2 concentration drops to 10^{-2} at about 200 m and continues to decrease up to about 600 m.

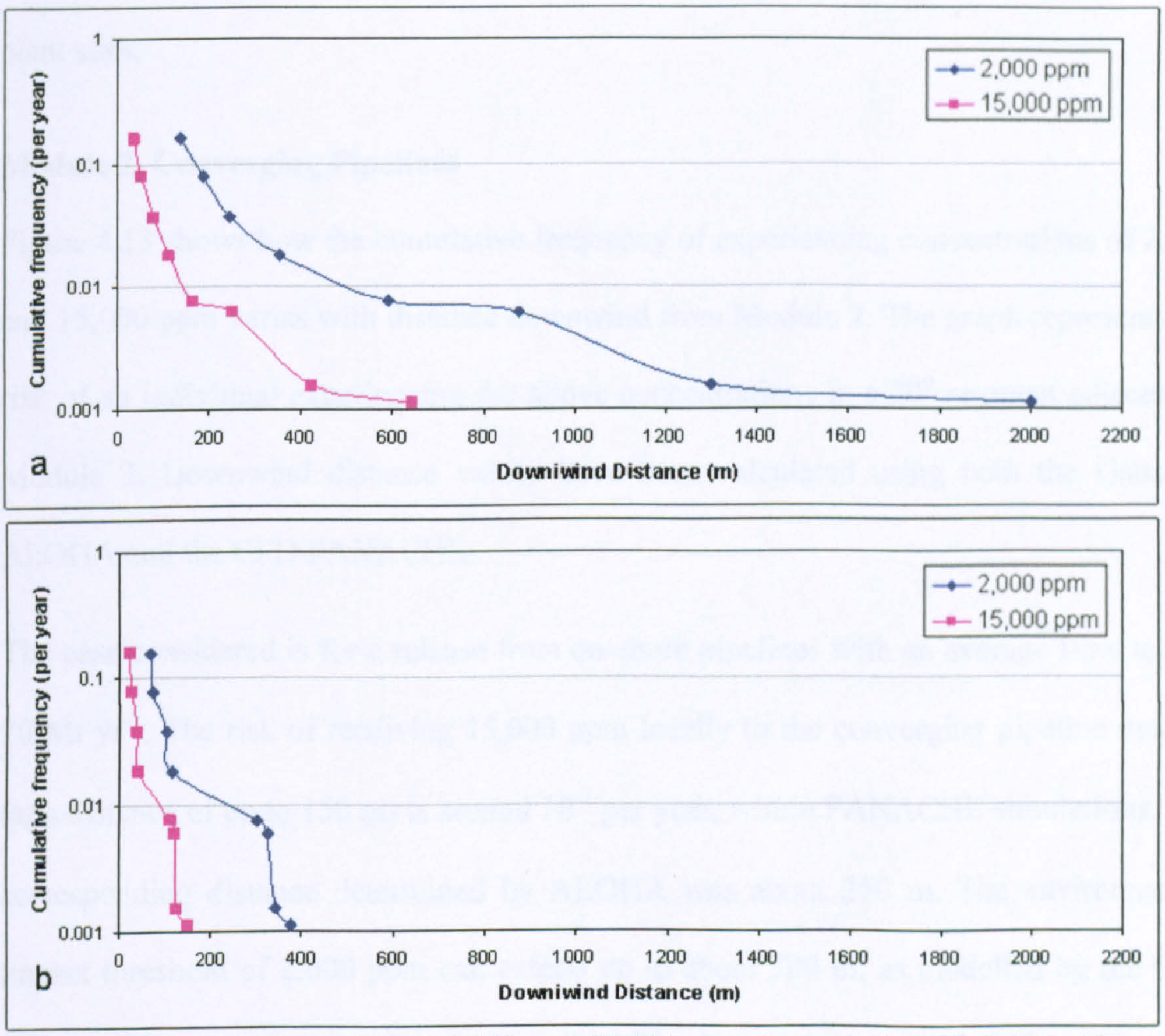

Figure 4.12 - Individual Risk of 2,000 and 15,000 ppm downwind to Module 1. Downwind distances values calculated by a) ALOHA and b) PANACHE.

The probability of people experiencing a concentration of 2,000 ppm follows the same trend as for 15,000 ppm, but involves greater distances. Figure 4.12 shows how PANACHE's predictions reduce the risk area by a factor of up to 5 with respect to the Gaussian model ALOHA.

In this chapter the local obstructions in the plant environment, which is a working place involving pipes, walls, building and other artefacts, was not considered in the simulations, enabling the CFD model to be compared more directly with the Gaussian model. In Chapter 6 simulations are presented that incorporate the built environment at plant sites.

Module 2, Converging Pipelines

Figure 4.13 shows how the cumulative frequency of experiencing concentrations of 2,000 and 15,000 ppm varies with distance downwind from Module 2. The graph represents the risk of an individual experiencing the above concentrations in a 30° segment adjacent to Module 2. Downwind distance values have been calculated using both the Gaussian ALOHA and the CFD PANACHE.

The case considered is for a release from on-shore pipelines with an average flow rate of 20 Mt yr^{-1}. The risk of receiving 15,000 ppm locally to the converging pipeline module (at a distance of up to 150 m) is around 10^{-3} per year, within PANACHE simulations. The corresponding distance determined by ALOHA was about 250 m. The environmental impact threshold of 2,000 ppm can extend up to about 700 m, as modelled by the CFD tool, or 8 km as calculated by the Gaussian. The hazard ranges (probability of leakage occurrence) for this Module are about one order of magnitude lower than those for Module 1. In practice, the smaller number of fittings and equipment items, with respect to the Recovery Plant Module, makes the risk of accidental release much lower

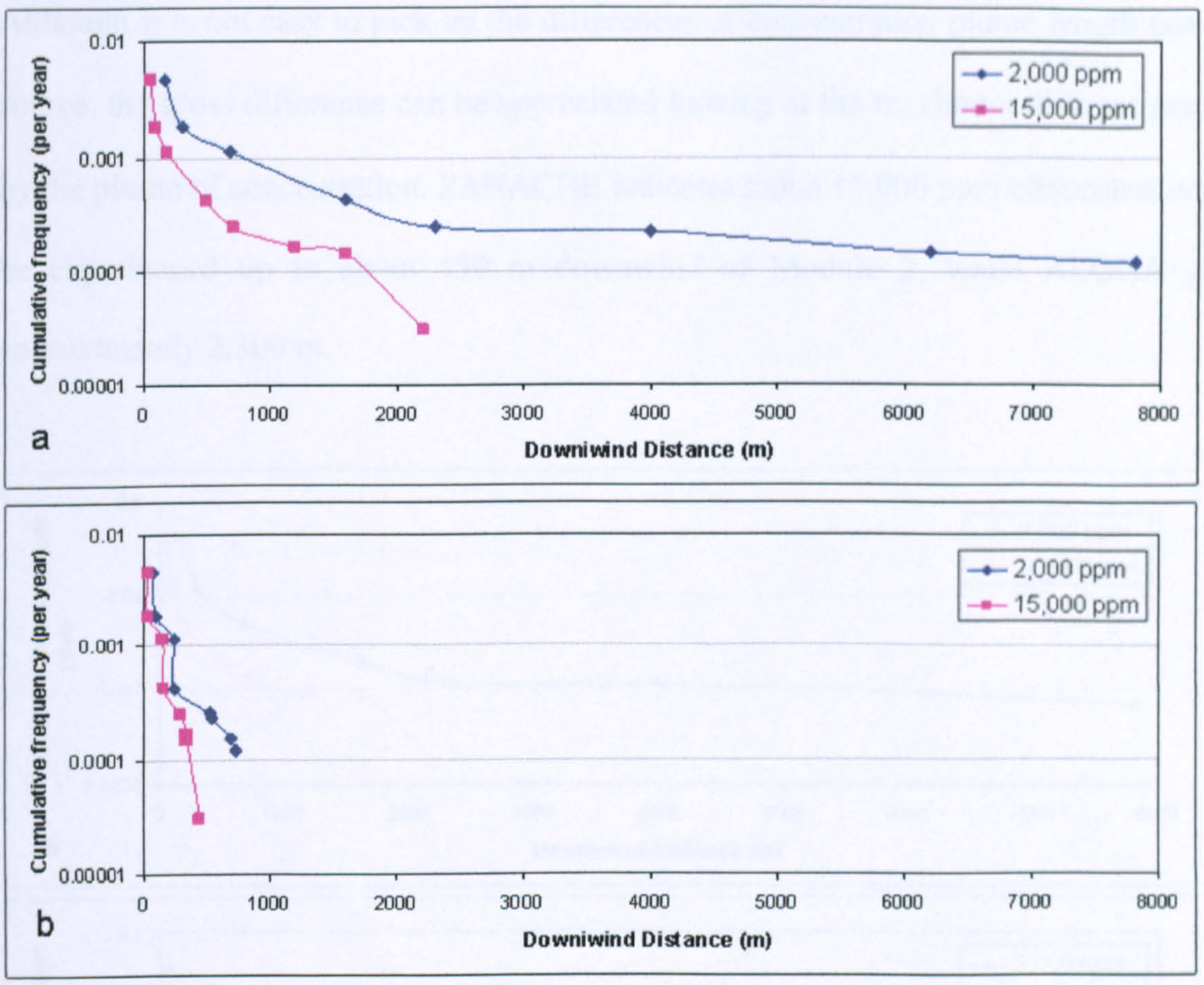

Figure 4.13 - Individual Risk of 2,000 and 15,000 ppm downwind to Module2. Downwind distances values calculated by a) ALOHA and b) PANACHE.

Module 3, Booster Station

The leakage consequences associated with the Booster Station Module are the same as those for Module 2 (and Module 4) and hence failure frequencies are the only changes from the risk results presented for Module 2. Figure 4.14 shows how the cumulative frequency of experiencing a concentration of 2,000 or 15,000 ppm varies with distance downwind of Module 3, as modelled by PANACHE and ALOHA.

The risk of experiencing the concentration of 15,000 ppm is quite high compared to surrounding pipelines, but only in the proximity of the Module – in the order of tens of meters, as modelled by PANACHE, decreasing with distance to the magnitude of 10^{-4}.

Although it is not easy to pick up the differences of concentration plume length near the source, the gross difference can be appreciated looking at the maximum distance reached by the plume of concentration. PANACHE indicates that a 15,000 ppm concentration can be experienced up to about 450 m downwind of Module 2, while ALOHA gives approximately 2,300 m.

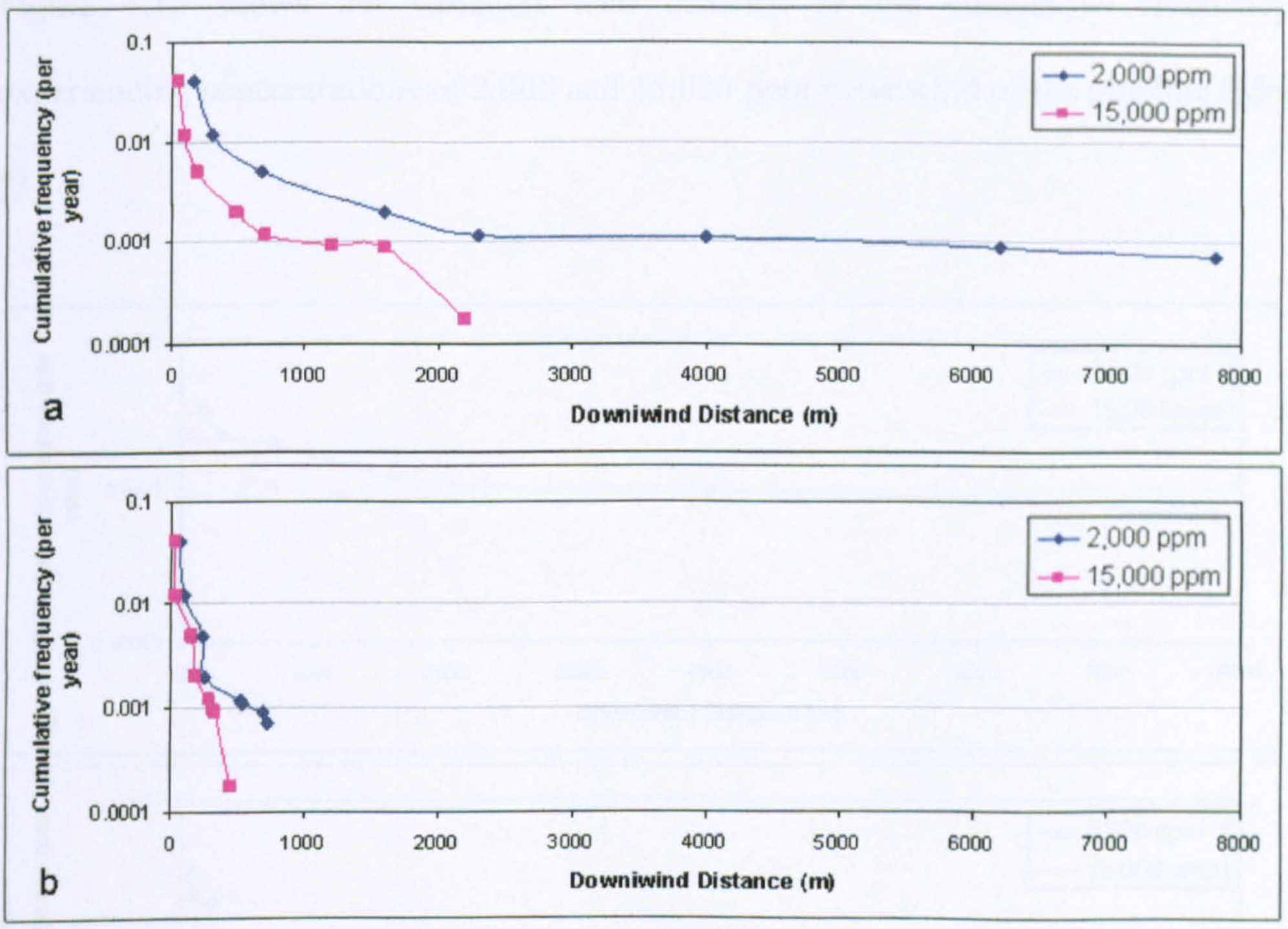

Figure 4.14 - Individual Risk of 2,000 and 15,000 ppm downwind to Module 3. Downwind distances values calculated by a) ALOHA and b) PANACHE.

The greatest difference between the CFD and Gaussian software relates to simulations of CO_2 dispersion after Full-Bore leaks from Modules 2, 3 and 4, when calculating the 2,000 ppm concentration contour. ALOHA predictions give a downwind distance for this plume that is more than ten times the distance calculated by PANACHE.

It must be noted that this module is likely to be placed above the surface, due to e.g. ease of maintenance (Mazzoldi et al., 2007). In Chapter 5, the sublimation rate of frozen CO_2 will be considered, as a downward leakage might occur from surface modules, creating a deposit of solid carbon dioxide ('dry ice').

Module 4, Pipeline

Figure 4.15 shows the variation with distance of the cumulative frequency of experiencing concentrations of 2,000 and 15,000 ppm downwind of the pipeline (Module 4).

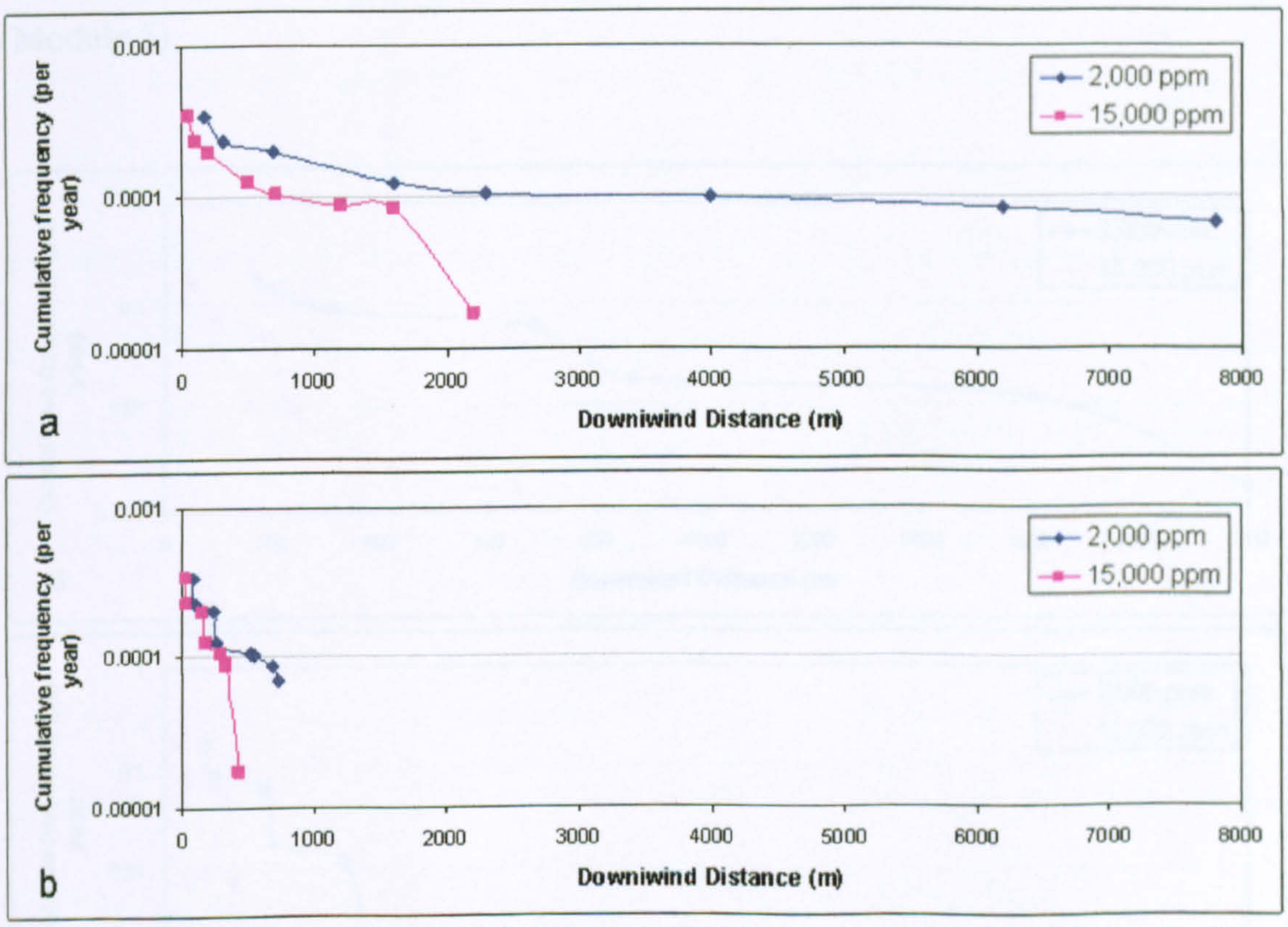

Figure 4.15 - Individual Risk of 2,000 and 15,000 ppm downwind to Module4. Downwind distances values calculated by a) ALOHA and b) PANACHE.

The flow rate considered is 20 Mt yr^{-1}, as for Modules 2 and 3. As detailed above, the same leak data were assumed for this Module as for Pipeline modules 2 and 3 –

specifically, the same Emergency Shut Down valve frequency [(50 km)$^{-1}$]. It should be noted, however, that the number of valves is expected to be increased near inhabited areas and facilities (e.g. roads, railways). The risk of experiencing a concentration of 15,000 ppm at a distance of up to about 350 m is around 10^{-4} per year, as modelled by PANACHE. ALOHA gives a downwind extent of up to more than 1,500 m for the same hazard occurrence.

Module 5, Injection Plant

Figure 4.16 shows how the cumulative frequency of receiving a concentration of 2,000 or 15,000 ppm decreases with distance downwind from the source, around an Injection Plant (Module 5).

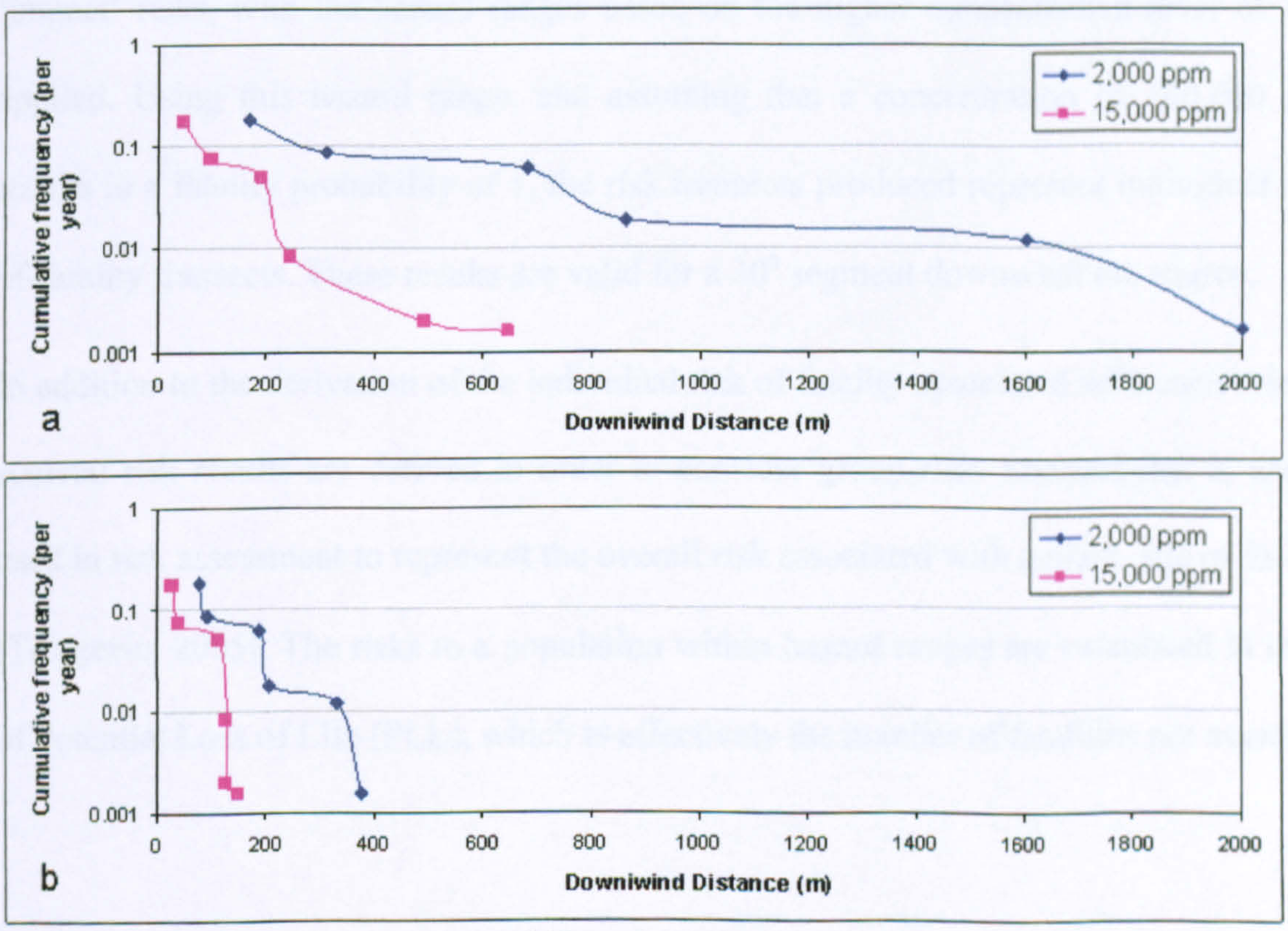

Figure 4.16 - Individual Risk of 2,000 and 15,000 ppm downwind to Module5. Downwind distances values calculated by a) ALOHA and b) PANACHE

A flow rate of 3 Mt yr^{-1} has been considered, through a pipe system with an average diameter of 10 inches. The risk of receiving a concentration of 15,000 ppm is, as mentioned above, quite high for this module. The risk levels shown by the figure reflect the relatively high failure rates associated with this Module and relatively low hazard ranges, as for Module 1.

4.3.8 Fatality Risk from the engineered system

With the aim of generating a general risk analysis for human life as endangered by CO_2 transportation, the study for CO_2 concentration plume footprints has been extended, considering the concentration of 100,000 ppm (10% by volume) as potentially fatal. The basic Risk Analysis approach is the same as that described in previous sections on 'impact' risks, with the hazard ranges based on the higher concentration level of 10% applied. Using this hazard range, and assuming that a concentration of 100,000 ppm results in a fatality probability of 1, the risk transects produced represent individual risk-of-fatality transects. These results are valid for a 30^{o} segment downwind the source.

In addition to the derivation of the individual risk of fatality associated with each release, societal risk results are derived in order to consider group risk. Societal risk is widely used in risk assessment to represent the overall risk associated with a plant, site or facility (Trbojevic, 2005). The risks to a population within hazard ranges are calculated in terms of Potential Loss of Life (PLL), which is effectively the number of fatalities per event.

4.3.8.1 Individual fatality risk criteria

Individual risk criteria are well established both within industry and by regulatory bodies. The criteria adopted by the UK HSE (HSE, 2001, HSE, 2005), which are widely used and considered most appropriate to this study are:

- Maximum tolerable risk for workers: 10^{-3} yr^{-1},
- Maximum tolerable risk for the public: 10^{-4} yr^{-1},
- Broadly acceptable risk: 10^{-6} yr^{-1}.

Between the maximum tolerable and broadly acceptable levels, risk must be reduced to a level which is as low as reasonably practicable (ALARP), taking account of the cost and benefits of any further risk reduction. Near to the broadly acceptable criterion, the risks are considered acceptable if the cost of risk reduction exceeds the improvement gained. Near to the maximum tolerable criterion, risks are only considered tolerable if risk reduction is impracticable or if its cost is grossly disproportionate to the improvement gained.

4.3.8.2 Societal risk criteria

Societal risk is defined as the relationship between the frequency of a specified hazard and the number of people suffering a given level of harm. It is usually taken to refer to the risk of death and expressed as a risk per year. As with individual risk, maximum tolerable and broadly acceptable criteria are set an upper and lower limit, where between these levels (termed the ALARP region) risk should be reduced wherever possible.

Societal risk criteria are more judgemental, and therefore less well established, than those for individual risk. The general aim of such criteria is to balance the risk from a facility to population groups with the benefits that groups, or society as a whole, receive.

Key assumptions made in estimating the societal risk for CO_2 transportation are:

- 100% of people within a cloud of 10% or greater concentration will be killed; outside the 10% concentration envelope no fatalities are assumed. This simple cut-off is appropriate for this analysis, although it should be noted that in reality the responses will not be a step function. There will not be 100% fatalities within the cloud, there may be fatalities at lower concentrations outside the 10% envelope, and the period of exposure has not been specified (see Table 4.2. Carbon dioxide is fatal after about 15 minutes of exposure, at this concentration). This assumption is similar to the one made by DNV in their study (Vendrig et al., 2003).
- The area covered by the concentration of interest is calculated differently for the two models used. The two-dimensional shape of the cloud, as modelled by PANACHE, can be approximated by an ellipse (see Figure 4.7) and the equation for calculating it is reported below [Equation (4.2)]. ALOHA gives a less precise shape for the generated clouds: the area covered by the specific concentration of carbon dioxide is based on a 30° downwind segment, as used for individual risk transects. The surface covered by the plume (S) is then calculated as:

$$S_{PANACHE} = \pi \, a \, b \qquad (4.2)$$

$$S_{ALOHA} = c^2 \sin\alpha \cdot \cos\alpha \qquad (4.3)$$

In the first equation, a and b represent the major and minor semi-axes of the ellipse; a equals half the downwind extent of the plume (including the upwind segment, characteristic of dense gas dispersion); b was found to be approximately equal to a/4 in F2 conditions and a/5 in D5 conditions. In the second equation, c is the maximum distance reached by the 100,000 ppm concentration and α is an angle of 7.5°.

- The number of fatalities N is calculated as:

$$N = \Phi * S \tag{4.4}$$

  where Φ is the population density within the area S for which the risk is being calculated (S). Representative values of Φ are given below.

- In the present study, the CO_2 stream has been taken as pure. Possible combustion contaminant such as NO_X and SO_X were not considered in the evaluation of societal risk.

- In order to provide a comparison of the societal risk impacts as would be calculated using different atmospheric dispersion models, uniform population estimates have been used as follows:
  - The 'average' population density is assumed to be $3 * 10^{-4}$ people per m^2. This is approximately mid-way between estimates of typical urban and rural populations in the UK (HSE, 2001, HSE, 2008)
  - An upper bound population of $3 * 10^{-3}$ people per m^2 is selected from the above sources. It should be noted that the typical urban population in the UK is around $2 * 10^{-3}$ people per m^2.

- To provide a further indication of the sensitivity of the societal risk to the assumed population density, a 'lower bound' population density of 10^{-4} people per m^2 is used. It should be noted that this is an indicative value: the population density can be zero and the typical rural population in the UK is around $5 \cdot 10^{-5}$ people per m^2.

4.3.8.3 Fatality Risk results

Risk of fatality is assessed in this section for the five modules considered. The hazard ranges for the 100,000 ppm concentration, derived in the same way as for the 2,000 and 15,000 ppm values in previous sections, are presented in Tables 4.7 to 4.9.

Transects in Figure 4.17 describe the individual risk for humans; the probability for a receptor to experience the fatal concentration of 100,000 ppm of CO_2 at distance from the Modules, for each of the five Modules. The downwind distances have been calculated with both the Gaussian ALOHA and the CFD PANACHE.

From Figure 4.17 it can be seen that predictions from the two models differ substantially. As for ALOHA, PANACHE considers 100,000 ppm concentration clouds to reach distances greater than 100 m with a maximum frequency of about 10^{-3} (once each 1,000 years). In any case, the transects in the figure show how the two models, considering the same release parameters, predict the formation of deadly concentration clouds posing risks of different magnitude.

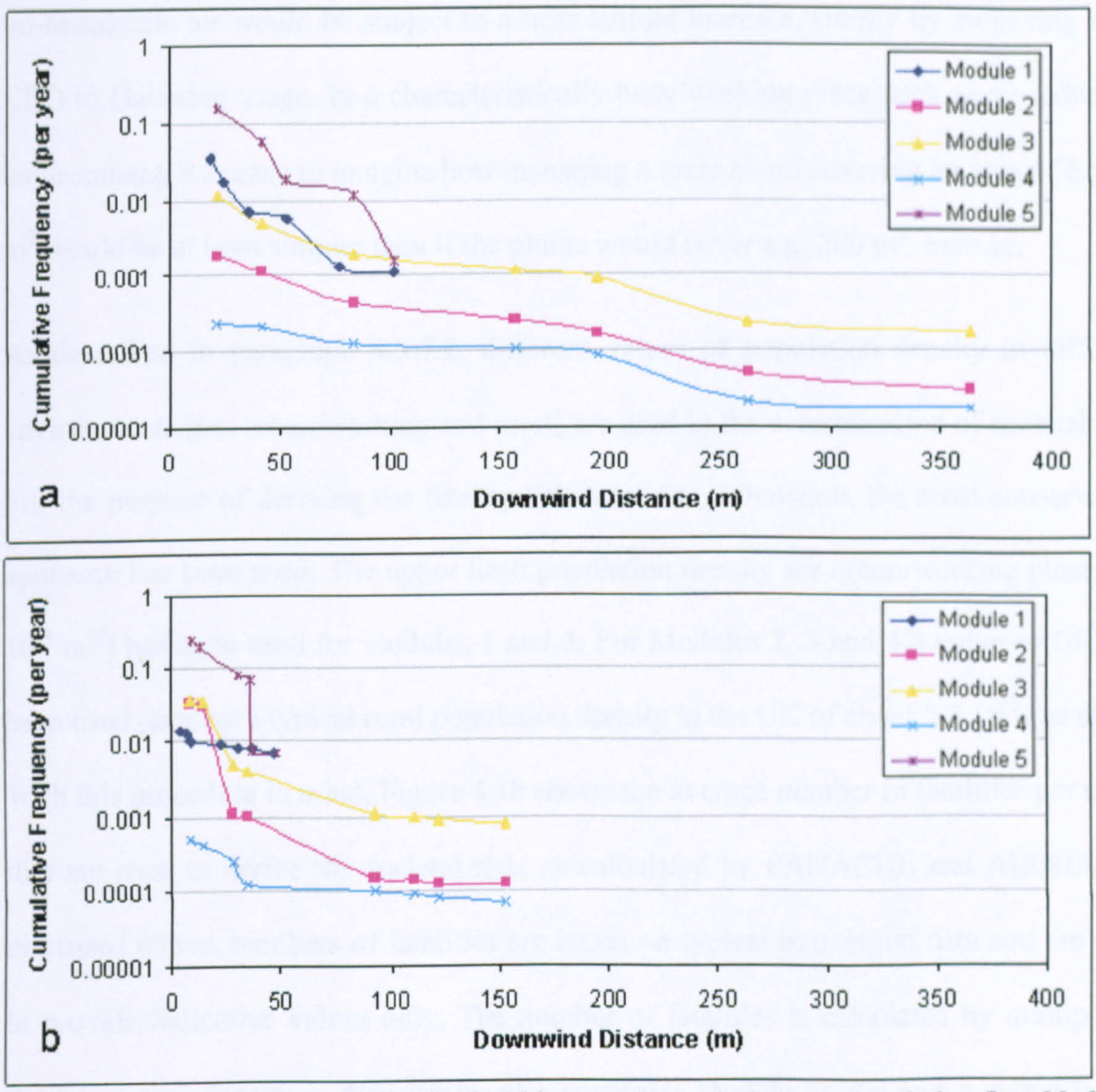

Figure 4.17 - Individual Risk of 100,000 ppm downwind to each of the five Modules. Downwind distance values calculated by a) ALOHA and b) PANACHE.

When dealing with dispersion of (dangerous) gases, although downwind distance is a linear measure, it is used in this context for representing the danger posed within a volume (by the mixture air/CO_2 with defined spatial dimensions – in this particular case, it embodies the 3D space filled by a toxic concentration of the gas). Transects of Modules 1 and 5 in the figure show how downwind distances reached by toxic clouds for PANACHE are doubled within ALOHA predictions. Assuming that, within identical dispersion scenarios, the width and height of the clouds would also double, the volume of

un-breathable air would be subject to a near tenfold increase, simply by switching from CFD to Gaussian usage. In a characteristically busy working place such as an industrial environment, it is easy to imagine how managing a toxic cloud covering an area of e.g. 50 m^2 would be at least simpler than if the plume would cover e.g. 200 m^2, instead.

As described in paragraph 4.3.7.2, different values of population density in different environments (i.e. urban/working and rural) are used in the determination of societal risk. For the purpose of deriving the fatality risk from CO_2 inhalation, the most conservative approach has been used. The upper limit population density for urban/working place ($3 \cdot 10^{-3}$ m^{-2}) has been used for modules 1 and 5. For Modules 2, 3 and 4 a value of 10^{-4} has been used (against a typical rural population density in the UK of about $5 * 10^{-5}$ per m^2). With this procedure in mind, Figure 4.18 shows the average number of fatalities per event that are used to derive the societal risk, as calculated by PANACHE and ALOHA. As discussed above, numbers of fatalities are based on typical population data and are used to provide indicative values only. The number of fatalities is calculated by multiplying the population density in the vicinity of a particular Module by the area covered by the deadly concentration. This surface is calculated using Equation (4.2) within PANACHE results and (4.3) for ALOHA'.

From Figure 4.18, the difference in forecasting, using results from the two models, is about one order of magnitude. In fact, while the CFD tool predicts a serious danger for human life with a frequency of about 10^{-2}, the Gaussian model forecast a potentially lethal accidental release of carbon dioxide with a frequency of about 10^{-1}. Both models predict a slightly higher probability of loss of life for Module 5, which is due to the frequency data used rather than to the use of a particular dispersion model.

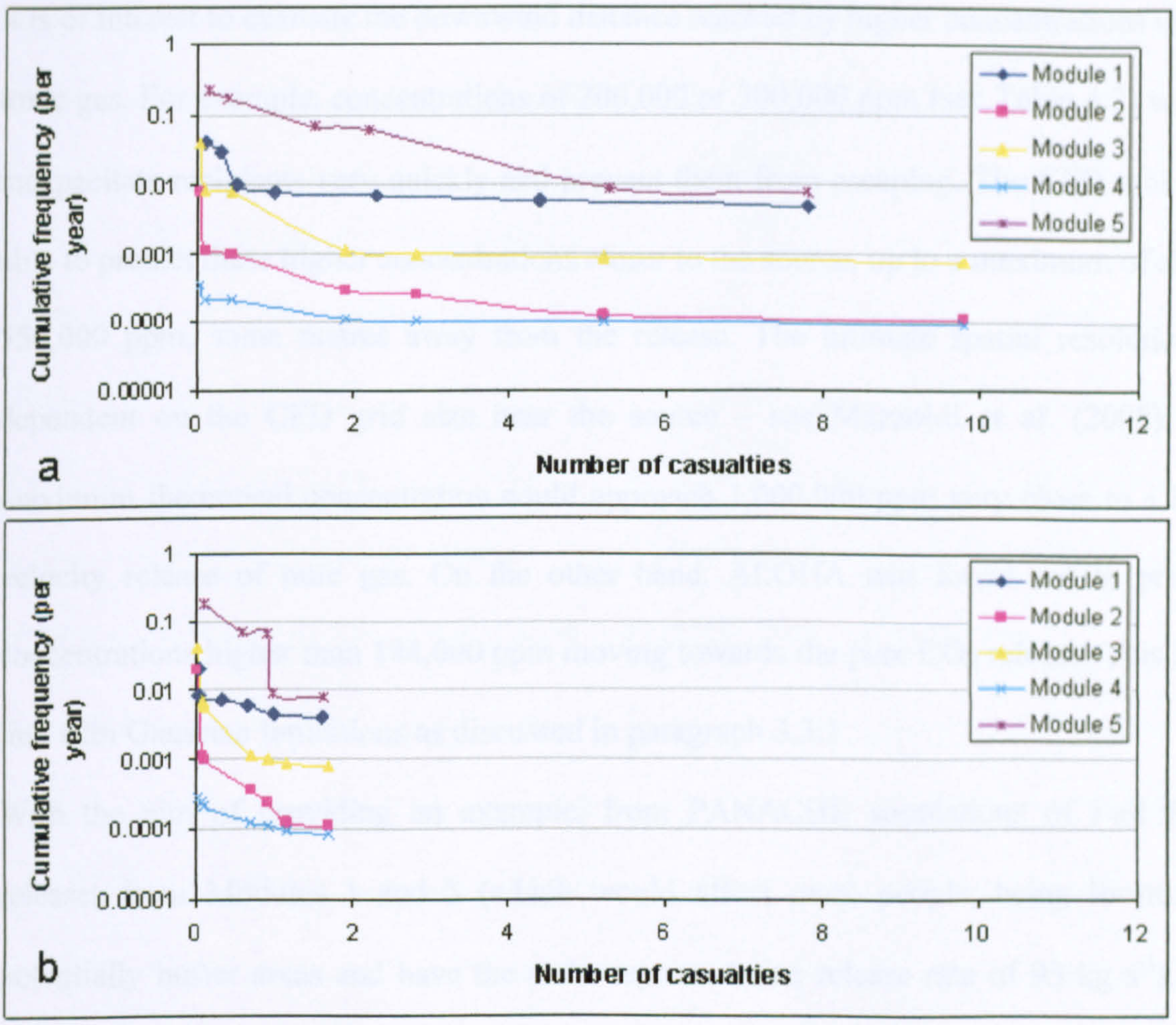

Figure 4.18 - Risk of fatality as modelled by a) ALOHA and b) PANACHE, using upper bound population data (par. 4.3.7.2).

4.3.8.4 Predicting concentrations near the source

The fatality risk analysis in this chapter assumed a simple step-function relationship between fatality and concentration (i.e. certain death for those exposed at concentrations of 100,000 ppm or higher and no risk of death at lower concentrations). This cut-off is appropriate for generic risk analyses when there is no specific site information (Vendrig et al., 2003). It should be noted that, in reality, the number of fatalities would vary with concentration: there will not be 100% fatalities within the cloud and there may be fatalities at lower concentrations outside the 100,000 ppm contour.

It is of interest to evaluate the downwind distance reached by higher concentrations of the toxic gas. For example, concentrations of 200,000 or 300,000 ppm (see Table 4.2) would incapacitate recipients very quickly and prevent them from escaping. The CFD tool was able to predict these higher concentrations closer to the source, up to a maximum of about 550,000 ppm, some metres away from the release. The ultimate spatial resolution is dependent on the CFD grid size near the source – see Mazzoldi et al. (2008): the maximum theoretical concentration could approach 1,000,000 ppm very close to a low-velocity release of pure gas. On the other hand, ALOHA was found not to predict concentrations higher than 144,000 ppm moving towards the pure CO_2 release. This is in line with Gaussian limitations as discussed in paragraph 3.3.1

With the aim of providing an example, from PANACHE simulations of Full Bore releases from Modules 1 and 5 (which would affect more people, being located in potentially busier areas and have the same representative release rate of 95 kg s^{-1}), the downwind lengths of plumes of 200,000 and 300,000 ppm concentration were considered. These lengths were respectively about 18 and 8 m in D5 atmospheric conditions, falling to about 14 and 5 m in F2 conditions. The presence of obstacles within these two modules and the jet flow release would both provide mechanisms for a more rapid dispersion of the cloud near the source (the former via the complexity induced in the wind field within a plant and the latter due to the jet mixing effect, as it will be seen in Chapter 6). Moreover these very highly concentrated plumes' downwind lengths do not seem to present an unmanageable hazard. Although simulating the dispersion of such plumes at low wind speeds and most frequent wind directions within specific built plant

environments would be of importance in minimizing the impact of a leak, in this chapter the main aim has been a straightforward comparison.

4.3.9 Risk of fatality: discussion

Due to the very generic nature of assigning population data, and to the fact that it is not appropriate to apply societal risk criteria to a generic study like this (where detailed facilities and population information that would be used in setting criteria for specific risk assessments are not available), results obtained by the application of the above criteria are given as examples and with the purpose of comparison between the models.

The difference in results is clear in Figure 4.18. As already stated, the Gaussian tool solves one single equation over the whole domain in order to calculate the distances covered by the different concentrations of carbon dioxide. Compared with predictions from a model that solves 5 main equations (conservation of mass, momentum and internal energy of the fluid, plus turbulence creation and dissipation) in up to about 100,000 Control Volumes in which scenarios are subdivided and up to 99,999 times (maximum cycles number for one simulation; in the simulations, a single cycle covered about 10^{-4}–10^{-2} s) per CV, Gaussian results can be thought as providing less precision in the outcomes.

Clearly, the validity of Risk Assessments results relies strongly on the frequency of different leaks and on the total amount of gas released per event. As discussed previously, these data were taken from the report of DNV and, although representing a detailed statistical analysis of hydrocarbon transportation incidents over the last 40 years (Vendrig et al., 2003), it is expected that new engineered systems will be constructed for CO_2

transportation, taking advantage of all the experience and expertise developed from hydrocarbon surface transport and from the early years of CCS introduction. Leakage frequencies of once per 1,000 years for particular-sized leaks need to be seen in the context that historic information on gas transportation, in general, only spans the last 100 years or so.

Also, it must be considered that ESD valves would be more frequent near populated areas, so that the inventory of releasable CO_2 would be lower than has been accounted for in this study. This is specifically valid for Modules 1 and 5, as will be seen in Chapter 6. In fact, whereas DNV assumed an ESD valve separation of 500 m for Modules 1 and 5, discussion with experts indicated that this value in a busy working place would be much lower, probably around 20 m.

The most recent risk assessment on CO_2 transportation within CCS projects is that drawn up by the Commission of the European Communities (EU, 2008a). In this, different estimations have been made based on the different Options dealt with (see paragraph 1.2.3.2). The European Commission did not use the same database applied within this chapter in evaluating the probability of unexpected CO_2 release (in their document the overall leakage probability seems to be lower than DNV's), but on the other hand, they used results of downwind plume extents from the work of DNV (Vendrig et al., 2003).

Within Option (d) [Making CCS mandatory for new coal- and gas-fired power station from 2020 onwards, together with retrofit of existing plants (built between 2015 and 2020) from 2020], which is the most ambitious, by 2030 the Commission forecast a total annual CO_2 capture rate of 517 Mt. Considering individual CO_2 pipeline systems' flow rate of 20 Mt yr^{-1} (see paragraph 4.3.6), it can be estimated, for this option, that between

40 and 60 CCS systems will be required by 2030. The European Commission's societal Risk Assessment estimated an average of around four fatalities per year, caused by accidental releases of CO_2. The simulations results in Vendrig et al. 2003 (where they used the Gaussian tool PHAST), are much closer to ALOHA's than to the CFD model's used here. This might imply that the usage of a CFD model for determining the areas covered by dangerous concentration of carbon dioxide in case of a leak event, would limit the expected number of fatalities, helping the technology to gain a stronger and earlier public acceptance.

However, it is worthwhile noting the limitations of the work described in this chapter. The very low release speed considered for comparing the two atmospheric dispersion models does not enable the jet mixing effect (the entrainment of large volumes of air by a high-speed concentrated flow, resulting in an early dispersion of the gas) to be allowed for. This is examined more closely in Chapter 6, where the capability of the CFD software will be studied in more depth.

Another factor that could alter the reliability of the results is, as stated above, the large spacing of the ESD valves. In their Risk Assessment, Kruse and Tekiela (1996) compared two values of ESD valve spacing, 5 km and 30 km, for a pipeline operating at 60 bar (6 MPa). The study showed that, with valves at 5 km intervals, a safe distance of 150 m was required but, at 30 km intervals, the safe distance increased to 600 m (due to greater quantity of gas available for release). With safety of the general public being paramount during the first decades after the introduction of the technology, it can be argued that, near densely populated areas, an ESD valves spacing of 50 km would not be sustainable.

The limitations described above do not allow the work presented in this chapter to be recognized as a full Risk Assessment, the comparison of the two models used being its main motive and outcome.

CHAPTER 5

SUBLIMATION OF CARBON DIOXIDE FROM A DRY-ICE BANK

Introduction

In the previous chapter, the risk of occurrence of specified leaks from CCS transportation facilities, posing a hazard to local populations, was introduced. The modules with the highest probability of failure are the ones associated with the capture of CO_2 at the plant site (Module 1), with the recompression of the CO_2 stream in the pipelines (Module 3) and with the final injection underground (Module 5). Although the natural gas/CO_2 transportation pipelines themselves are likely to be buried 1 m or more below the surface, Modules 1, 3 and 5 will be located above the surface, for ease of maintenance.

As seen in chapter 4, the Joule-Thomson effect freezes carbon dioxide as it passes from the high pressure environment within the transportation system to ambient pressure, after the occurrence of a leak within the system. At ambient pressure conditions (P = 1 atm = 0.1 MPa), solid carbon dioxide (also referred to as "dry ice") at the temperature of -78.8° C passes directly to its gaseous state, through the process of sublimation. The rate of sublimation is dependent on the energy balance of the dry ice bulk – including short- and long-wave radiation fluxes, latent and sensible heat fluxes and the heat flux from the ground. In the present chapter, the rate of sublimation of a dry ice bank formed as a

consequence of a downward leakage from a CCS transportation facility surface module will be considered, accounting for the different sources of environmental energy in particular periods of the year.

5.1 Leakage from a surface facility

As described in Chapter 4, carbon dioxide will be transported either in its supercritical phase ($P > P_c$ and $T > T_c$, where $P_c = 7.4$ MPa and $T_c = 31.1^{\circ}C$ – see Figure 4.1) or in the sub-cooled phase ($P > P_c$ and $T < T_c$), both of which are characterized by a high density of the fluid. In order to avoid pressure surges it is important to maintain stability of the single dense phase – supercritical or sub-cooled. The most widely used operating pressure is between 7.4 MPa (critical pressure) and 21 MPa, a range in which CO_2 exists as a dense single phase over a wide range of temperature (Barrie et al., 2004). Although the upper pressure limit for on-shore high-pressure transportation of gases in the U.K. is 105 atm (10.5 MPa) (Kaarstad and Hustad, 2003), for research purposes, in this chapter, values covering the whole of this range are considered, up to a limiting value of 20 MPa.

As can be seen from Table 4.3, the probability of a leak from one of the surface modules is 0.37 yr^{-1}, regardless of its dimension. A downward leak from one of these modules will have an occurrence frequency of the same order of magnitude. Hence, studying the formation of a solid carbon dioxide bulk and its resultant sublimation is of importance in the field of risk analysis.

5.1.1 Choked flow

In the previous chapter, the velocity of the flow leaking from a high-pressure transportation facility has not been considered. Having already specified values for leak rate and durations, attention is focused on the inventory released – assuming a near zero flow speed and that all leaks reach the atmosphere – and on the downwind length of plumes as modeled by Gaussian and CFD models. In the next chapter, the jet speed originated after a leak from a high pressure transportation facility is studied.

At high pressure differential a very high speed is expected for the leaking fluid flow. Choked flow is a limiting condition that occurs when a fluid at high pressure experiences a pressure jump through a restriction (Klapp et al., 2005). Choked flow occurs when the ratio of the absolute upstream pressure to the absolute downstream pressure is equal to or greater than $[(k + 1)/2]^{k/(k - 1)}$, where k is the specific heat ratio of the gas. For CO_2 k = 1.29 and choked flow occurs for $\Delta P \geq 0.18$ MPa. The mass flow rate for choked flow is given by (Perry and Green, 1997):

$$Q = C A \sqrt{k \rho P \left(\frac{2}{k+1}\right)^{(k+1)/(k-1)}} \qquad (5.1)$$

where: Q = mass flow rate, kg s^{-1}; C = discharge coefficient, dimensionless (usually 0.72); A = discharge orifice cross-sectional area, m^2; $k = c_p/c_v$ is the ratio of specific heats of the gas, $k_{CO2} = 1.29$; ρ = fluid density at T and P for supercritical CO_2, $\rho = 950$ kg m^{-3}; P = absolute upstream pressure (10-20 MPa) in Pa.

The above equation calculates the initial instantaneous mass flow rate for the pressure and temperature existing in the upstream pressure source when a discharge first occurs.

For a CO_2 pipeline, small and medium size releases (5 mm and 25 mm) can be considered not to result in depressurization of the pipeline (Turner et al., 2003). This is the range of leakage diameters considered here.

5.1.2 Formation of a dry ice bank

While an upward leakage would result in an instantaneous sublimation of the formed dry ice due to the resistance imposed by air to the high speed flow (Haines, 2006), a downward leakage from a CO_2 transportation system module would form a dry ice bank in the vicinity of the pipeline module. Equation 5.1 was used to evaluate the total mass of the forming bank within one hour, for two different leakage scenarios: (a) a leak of 10 mm diameter within a 10 MPa module and (b) a 20 mm (diameter) hole within a 20 MPa pressurized facility. For case (a), equation 5.1 gives a leakage rate of 3.7 kg s^{-1}, while for case (b) the rate would be of 20.7 kg s^{-1}.

Using these values, the total mass of the bank for case (a) would be more than 13 t, with a volume of about 8.4 m^3 (dry ice density is 1562 kg m^{-3}); case (b) would give corresponding values of 74.5 t and 47.7 m^3. Assuming an angle of repose for dry ice of 20°, the conical bank of 13 t will have a surface area of about 27 m^2 and a base area of 24.5 m^2, while the bank of 74 t will have corresponding values of 83.5 m^2 and 78.5 m^2. The values considered here should be regarded as extreme and would be attained only for perfectly vertical downward leaks, for which the majority of the leaked gas would impinge on the ground and remain there in its solid phase. In practice, there is likely to be some air entrainment and dilution of the high speed release, even if it points downward. For non-vertical leaks from surface modules, there will be an initial direct atmospheric

dispersion of part of the gas flow which potentially will subsequently be reduced by the rapidly-growing height of the bank (i.e. the leaking CO_2, at a certain point, would begin impinging on the bank itself).

5.1.2.1 Experimental trial

On 28 June 2007 on the Sutton-Bonington campus at the University of Nottingham, the potential of the Joule-Thomson effect to cool CO_2 sufficiently to reach the solid state was tested. From a liquid CO_2 supply tank (T = -15° C, P = 2.3 MPa), a downward pointing drain valve was opened and, irrespective of the flow velocity and mass rate, the formation of a dry ice bank was observed (Figure 5.1). The sharp vertex of the conical bank is due to the vertical orientation of the downward flow from which it was formed.

In this small scale trial, a pressure drop of about 2.3 MPa caused pure CO_2 to cool by more than 60° C; similar or greater cooling can be anticipated from a larger-scale event such as a leak from a CCS transportation facility at 10 MPa.

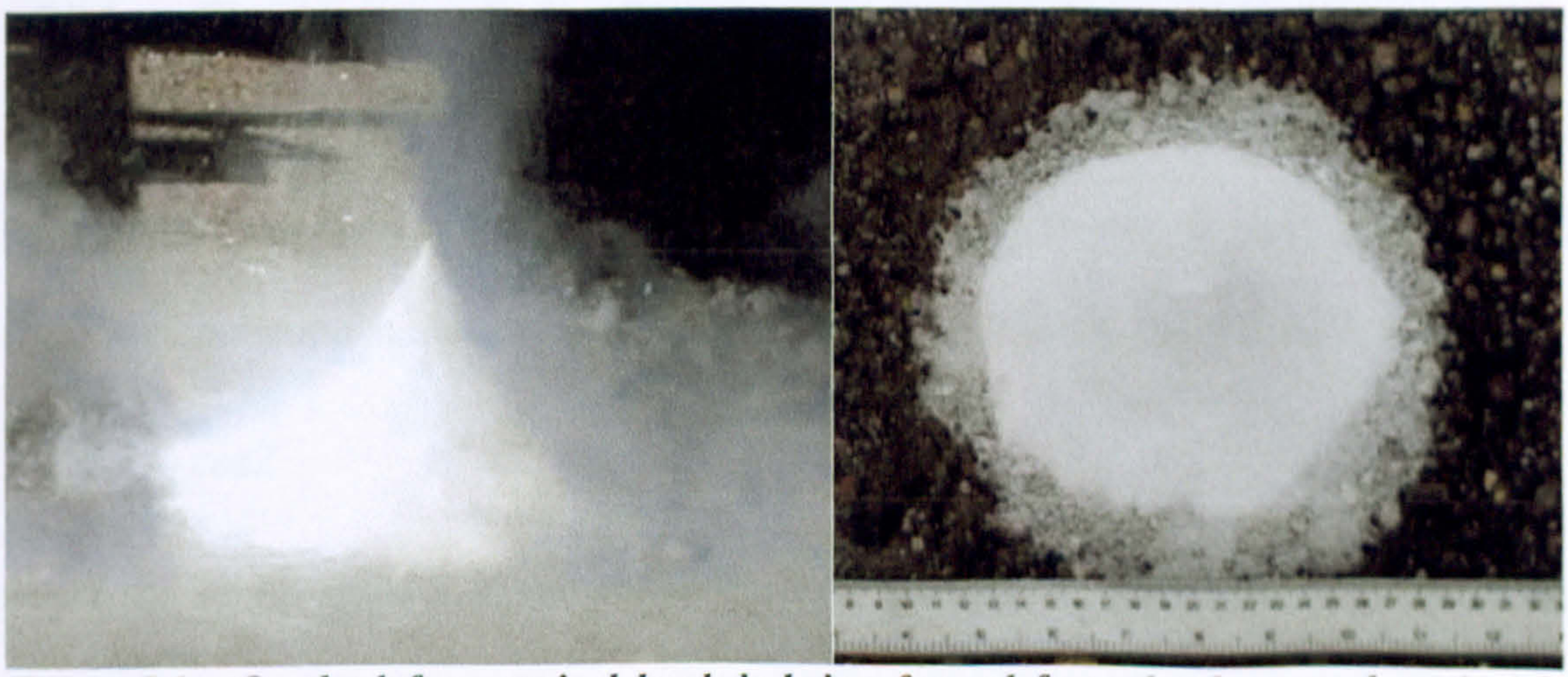

Figure 5.1 - On the left, a conical bank is being formed from the downward vertical jet of gaseous CO_2. On the right, a plan view of the solid bank. The plan view also shows a nimbus of condensed water vapour on the frozen soil around the bank, replacing sublimed carbon dioxide.

5.2 Energy balance of the bank

As with all natural substances, solid CO_2 needs a certain amount of energy per unit mass for changing its state (i.e. the Latent Heat of Sublimation, which value for CO_2 is 576.5 J g^{-1}), which is provided by direct solar radiation, heat transfer from the atmosphere and from the ground. The energy balance at the surface of the dry ice bank can be expressed as:

$$E = SW_d - SW_u + LW_d - LW_u + H + LE + G \tag{5.2}$$

where E is the energy available for the sublimation of CO_2 (W m^{-2}), SW_d is the downward short-wave radiation, SW_u is the reflected short-wave radiation, LW_d is the atmospheric long-wave radiation, LW_u is the upward long-wave radiation emitted by the bank, H is the sensible heat flux, LE is the latent heat flux and G is the heat flux from the ground under the bank (Koivusalo et al., 2001, Koivusalo and Kokkonen, 2002, Orsini et al., 2000).

5.2.1 Short wave radiation flux

The radiation striking the top of the atmosphere can be expressed as a fraction of the solar constant S, which has a value of approximately 1,367 W m^{-2}. The downward shortwave radiation at the top of the atmosphere normal to the Earth's surface is:

$$Q_t = S \cdot cosZ \tag{5.3}$$

where the zenith angle Z is calculated from the latitude Φ, solar declination δ and hour angle HA by: $cosZ = sin\Phi\ sin\delta + cos\Phi\ cos\delta\ cosHA$. The hour angle depends on solar time ht, $HA = 15^o \times (12 - ht)$ and declination depends on the Julian day J, $\delta = 23.45 \cdot sin(rad(360/365 \cdot (284+J)))$. 15° is the angle of rotation of the Earth in 1 hour and 23.45°

is the inclination angle between the Earth's rotational axis and its orbital plane (Lumb, 1964).

The reduction of this 'top of atmosphere' radiation on reaching the surface is parameterized by Bennett's correction (Bennett, 1982) that best fitted the observational data at Kew Observatory, England (Monteith and Unsworth, 1990):

$$Q_s = 0.72 \cdot Q_t \tag{5.4}$$

where Q_t is the short wave radiation flux at the top of the atmosphere and Q_s is the flux at the Earth's surface. When the sun is below the horizon the cosine will be negative - the equation does not account for the fact that the Earth is not transparent, and hence any negative values for Q_s are set to zero. For cloudy conditions Bennett's correction gives:

$$Q_s = (1-0.49 \cdot C) \cdot 0.57 \cdot \cos Z \tag{5.5}$$

where C is a coefficient representing the cloud amount (0-1).

5.2.2 Long wave radiation flux

The atmosphere emits radiation according to σT^4 (Idso and Jackson, 1969), where σ is the Stefan-Boltzmann constant (5.67×10^{-8} W m^{-2} K^{-4}) and T is the effective atmospheric temperature (K).

In practice, the irradiance on a horizontal surface under a clear sky can be estimated from the surface air temperature T_a with an empirical relation due to Idso and Jackson which fits experimental data and appears to be valid for all latitudes and seasons:

$$Q_l/\sigma T_a^4 = (1 - 0.261) \cdot \exp[-0.000777(273 - T_a)^2] \tag{5.6}$$

where Q_l is the downward atmospheric irradiance (for clear sky), σ is the Stefan-Boltzmann constant and T is the screen-level air temperature in Kelvin. The correction for cloudy sky has been taken from (Jacobs, 1978):

$$Q_l = Q_{l(clear)} \cdot (1 + 0.26C) \tag{5.7}$$

where C is a coefficient from 0 to 1 describing the average cloud cover.

Application of the Idso-Jacobs formula to the bank surface for evaluating the energy lost through long wave emission by the bank itself gives < 1 W m^{-2}, which may be neglected.

5.2.3 Sensible and latent heat flux

Sensible heat is the thermal energy of a body expressed as the product of the body's mass, specific heat and its temperature above a reference temperature. Latent heat is the amount of energy in the form of heat released or absorbed by a substance during a change of phase. In our case, sensible heat is transported by air via convective movements and the latent heat considered is the one released by water vapour condensing on the bank's surface. The fluxes of sensible and latent heat can be discussed together as they rely on the same basic theory and atmospheric conditions. Both are dependent on scalar transfer coefficients which in turn are derived from the parameterization of a number of surface-atmosphere interactions.

The transfer of sensible heat H between the air and the dry ice bank surface is dominated by the temperature difference between the air and the cold surface, $(T_a - T_s)$ (Launiainen and Cheng, 1998):

$$H = \rho_a \cdot c_a \cdot C_H \cdot (T_a - T_s) \cdot U \tag{5.8}$$

where U is the wind speed, ρ_a and c_a are respectively the density (1,205 kg m^{-3}) and specific heat capacity (1.005 kJ kg^{-1} K^{-1}) of air, and C_H is the bulk transfer coefficient for sensible heat (dimensionless and equal to $1.75 \cdot 10^{-3}$).

Similarly, the transfer of latent heat, *LE,* between the air and the dry ice bank is dominated by the water vapour content of the moist air, also referred to as specific humidity (q_a)

$$LE = \rho_a \cdot R_l \cdot C_E \cdot (q_a) \cdot U \qquad (5.9)$$

where C_E is the bulk transfer coefficient for latent heat and R_l is the enthalpy of fusion for water: $R_{l,0Cdeg} = 2.5$ kJ g^{-1} (Marsh, 1987).

Specific humidity is a function of saturated water vapour pressure (p_s), given by the following equation (Treier and Palge, 1985): $p_s = exp[(6.416 + 17.3 \cdot T_{Cdeg}/(238 + T_{Cdeg})]$, where T_C is the temperature in degrees Celsius and p_s is the saturation vapour pressure (in Pa) in the air at temperature T_C.

The diurnal variation in relative humidity was calculated from: $RH = 0.5+0.3 \cdot cos(rad(HA))$, ranging between 20 and 80%. The actual vapour pressure (p_w) is $p_s \cdot$ RH. The specific humidity or humidity ratio (kg_{water} / kg_{air}) is given by $q_a = 0.622\, p_w / (p_a - p_w)$, (Buck, 1981), where $p_w = RH \cdot p_s$, q_a is the partial pressure of water vapour in the moist air (Pa) and p_a = atmospheric pressure of the moist air (Pa).

The heat transfer coefficients are approximated by $C_H = C_E = 1.75 \cdot 10^{-3}$ (Parkinson and Washington, 1979).

5.2.4 Heat flux from the ground

The heat exchange with the ground, *G*, is an important contribution to the budget for cryogenic spills where temperature differences are large and the temperature in the spill material (the dry ice bank in this case) is constant at T_B (Reynolds, 1992). The ground is considered to be a semi-infinite solid with initially constant temperature T_G, whose surface is maintained at temperature T_B beginning at zero time. Because $T_B << T_G$ for any reasonable choice of initial ground temperature, errors in estimating T_G or due to initial bank non-uniformity are small. The solution to the initial boundary-value problem for *G* is provided by the work of (Carslaw and Jaeger, 1959).

$$G_{(t)} = \chi K_G * (\pi \Phi_G)^{-1/2} * (T_G - T_B)\, t^{-1/2} \qquad (5.10)$$

where T_G is the initial ground bulk temperature (K), χ is the ground roughness conversion factor (≈ 3), K_G is the ground thermal conductivity (W m^{-1} K^{-1}), Φ_G is the ground thermal diffusivity (m^2 s^{-1}, thermal diffusivity is the ratio of thermal conductivity to volumetric heat capacity of a material, volumetric heat capacity is defined as density times specific heat capacity), and *t* is the elapsed time of the spill, i.e. the time the pollutant has been on the ground (in seconds).

5.2.4.1 Heat transport in frozen soils

Convective water movement is one of the principal means for heat transportation in soil (Dos Santos and Mendes, 2003). These convective movements are responsible for 5% to 60% of the heat transport through the shallower part of the ground, for soil temperature ranging between 5° and 75° C (Hiraiwa and Kasabuchi, 2000). At lower temperatures most of the heat is transported through the soil matrix itself.

At a temperature of about -90° C, the dry ice bank would freeze the underlying soil, i.e. a permafrost layer of time-varying depth will develop under the subliming bank. Equation (5.10) is used with thermal properties of soils at 40° C for evaluating the heat flux from the ground (Reynolds, 1992). $G_{(t)}$ is compared using values calculated for frozen and unfrozen soils.

Different authors have studied the transport of heat in frozen soils (Grant, 2001, Hansson et al., 2004, Overduin et al., 2006, Peters-Lidard, 1997, Putkonen, 2003). Thermal conductivity for frozen ground is expected to be higher than for unfrozen ground (whatever the soil type and particle dimensions), at temperatures near 0° C. This is because the thermal conductivity of ice is about four times that of water and because at low temperature, above and below 0° C, the transportation of heat by water vapour can be neglected (Cahill and Parlange, 1998, Hiraiwa and Kasabuchi, 2000). Apparent soil heat capacity peaks at a temperature of ~0° C during soil thawing [up to 800 MJ m^{-3} K^{-1}, instead of the more normal 2-3 MJ m^{-3} K^{-1} (Overduin et al., 2006)] due to latent heat exchange. In order to compare soil thermal properties in frozen and unfrozen conditions the Johansen method (Peters-Lidard, 1997) was used to evaluate the soil thermal conductivity as a function of its saturation, porosity, dry density and phase of the water (frozen or unfrozen), for a sandy soil:

$$K = K_e \cdot (K_{sat} - K_{dry}) + K_{dry} \qquad (5.11)$$

where K_e is the Kersten number, a function of the degree of saturation S_r and phase of the water. For unfrozen soils $K_e = 0.7 \cdot \log S_r + 1.0$. For frozen soils $K_e = S_r$.

For estimating the volumetric heat capacity for unfrozen soils the de Vries method (1963) was used (Ochsner et al., 2001):

$$C = 837\rho_b + 4.19 \bullet 10^6 \theta_v \quad (5.12)$$

in J m^{-3} K^{-1}, where 837 is the average heat capacity of the solid constituents of the soil (J kg^{-1} K^{-1}), ρ_b is the dry density of the soil (kg m^{-3}), $4.19 \bullet 10^6$ is the volumetric heat capacity of the water component (J m^{-3} K^{-1}) and θ_v is the volumetric water content of the soil (m^3 m^{-3}). In the frozen soil case:

$$C = 837\rho_b + 0.9 \bullet 1.9 \bullet 10^6 \theta_v \quad (5.13)$$

in J m^{-3} K^{-1}, where 0.9 is the ice/water volumetric ratio and $1.9 \bullet 10^6$ is the volumetric heat capacity of ice (J m^{-3} K^{-1}).

The ground would not experience a significant decrease in thermal conductivity when passing from unfrozen to frozen conditions (see fig. 6 in the work of Overduin *et al.* 2006). From Equation (5.10) it can be seen that an increase in heat capacity would theoretically increase the heat flux from the soil; however, the process of interest in this study is the soil behaviour during the freezing period rather than during thawing. Figure 5.2 displays the differences in soil thermal properties for frozen and unfrozen conditions against S_r, calculated using Equations (5.11), (5.12) and (5.13).

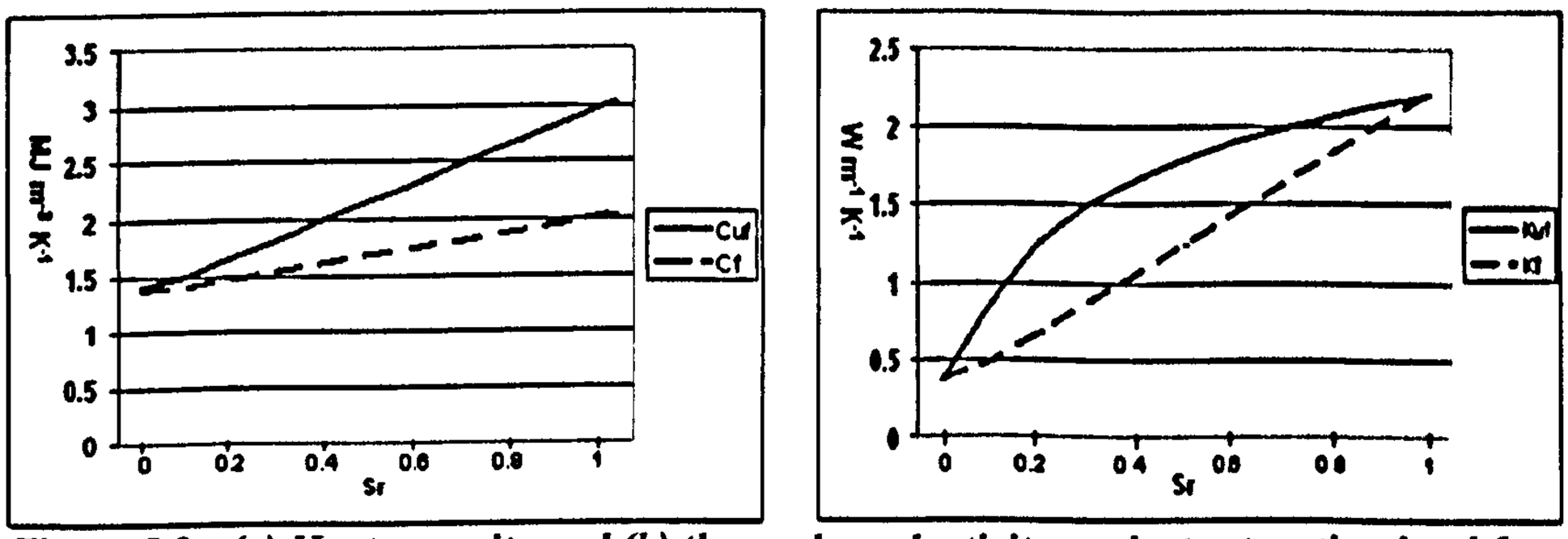

Figure 5.2 - (a) Heat capacity and (b) thermal conductivity against saturation level for sandy soil (40% pore space) in frozen (Cf, Kf) and unfrozen (Cuf, Kuf) conditions.

The contribution of the ground heat flux to the total energy balance of the dry ice bank was evaluated using Equation (5.10), with the values for frozen and unfrozen soil thermal conductivity and heat capacity for a sandy soil with θ_v = 0.3. Figure 5.3 quantifies the difference in heat flux from the ground using the above values for soil thermal conductivity.

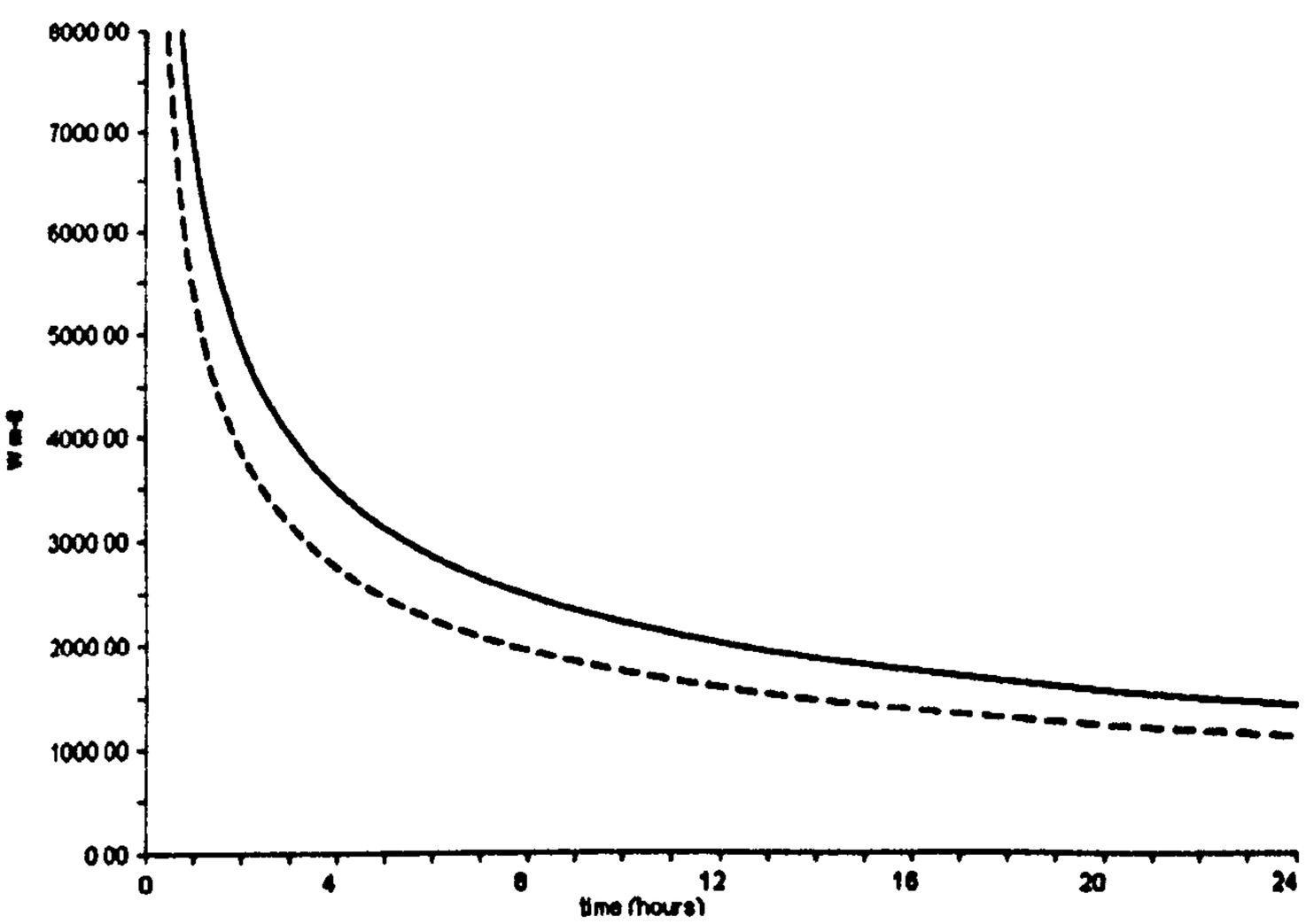

Figure 5.3 - Heat flux from the ground for a sandy soil (40% pore space, Ti = 15°C, Sr = 0.8) in frozen (dotted line) and unfrozen (solid line) conditions, during the first day after deposition of a bank.

From Figure 5.3 it can be seen that the difference between the values of $G_{(t)}$ calculated from the thermal properties of frozen and unfrozen soil amounts to 1000-1500 W m^{-2} during the first hours after the bank deposition, decreasing after some hours to 200-400 W m^{-2}. These differences are due to the presence or absence of water vapour as a heat transport medium.

5.2.5 Heat fluxes at the bank surface

In order to explore the risk from sublimation of CO_2 from a dry-ice bank, the energy balance at the bank surface has been evaluated for two weeks in June (10-24 June). Summer is the worst-case scenario, because the higher the average air temperature, the higher the potential sublimation rate. Characteristic winter values are discussed in paragraph 5.3.2.

Using Equations (5.3), (5.4) and (5.5) at latitude 52°, for a constant cloud cover of 0.3, the average maximum daytime surface short wave radiation flux is 582 W m^{-2} (varying slightly with date), decreasing to zero at night time. The data from the UK Meteorological Office indicate an average T_{max} in June of about 20° C and a T_{min} of 10° C. Using these values in Equations (5.6) and (5.7), the long wave radiation flux ranges between 298 and 365 W m^{-2}. Equations (5.8) and (5.9) gave sensible heat fluxes in the range 376-418 W m^{-2}, and latent heat fluxes in the range 18-140 W m^{-2}, for a relative humidity varying between 0.2 and 0.8 during the 24 hours.

For calculating the heat flux received by the bank from the ground, Equation (5.10) was used with the values of thermal properties for unfrozen (sandy) soil. Figure 5.3 represents the heat flux from the ground during the first day after the bank deposition. It can be seen that in the first hours there is a strong initial contribution by the ground to the bank's energy balance, which decreases subsequently, finally getting to 500–800 W m^{-2}, some days after its deposition (not shown in the figure).

5.3 Sublimation rate of carbon dioxide

An example calculation for the period 10-24 June (Julian days 161-175) is given. Equations (5.2) through (5.13) were used within ModelMaker 3 (Cherwell Scientific) to model the sublimation of the dry ice bank. The following assumptions have been made:

- The surface of the dry ice bank is at a constant temperature of -78.8° C (CO_2 sublimation T at P = 0.1 MPa).
- The bank has an initial albedo of 0.85, decreasing with time by 0.01 day^{-1}, due to the bank surface becoming contaminated with windblown material.
- All energy provided to the bank is used in the process of sublimation at the bank surfaces (lateral and base, i.e. no internal dissipation of energy).
- No precipitation.
- Latitude 52° N (Nottinghamshire, UK).
- Temperature ranges between 10° C and 20° C and relative humidity between 20% and 80% (0.2-0.8) on those days of the year.
- Constant cloud cover of 0.3 and wind speed of 2 m s^{-1}.
- For evaluating the heat flux from the ground, the thermal properties of unfrozen soil are used in Equation (5.10).

5.3.1 Results and discussion

Figure 5.4 gives the sublimation rate of solid carbon dioxide, due directly to the energy balance at the surface of the bank. There is a strong initial contribution by the heat flux from the ground which, together with the sensible heat flux, maintains the sublimation rate of the dry ice at considerable levels even during night time. The heat transfer from

the underlying surface gradually decreases with time due to the decrease of the temperature difference between the bank and the ground. On the other hand the energy contribution by solar radiation increases with time, due to the reduction of the bank albedo.

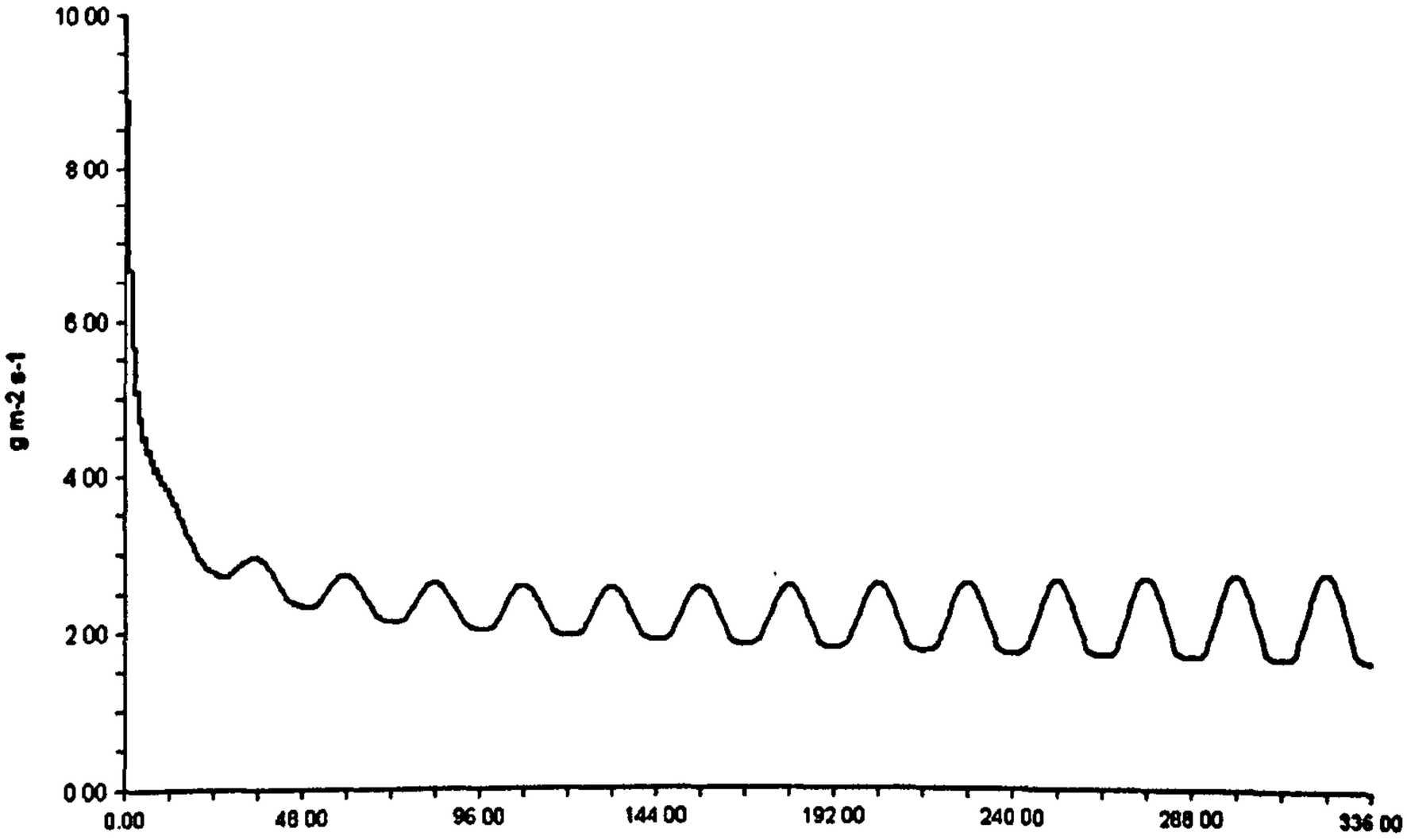

Figure 5.4 - Sublimation rate of the dry ice bank calculated during 14 days in June.

The subliming frozen CO_2 bank is a continuous source term for the subsequent dispersion of the dense gas in the atmosphere. Immediately after the sublimation takes place, gaseous carbon dioxide, at a temperature of -78.8° C, has a density of 2.8 kg m^{-3} (AIR-LIQUID, 2000), which is more than twice the density of air at ambient temperature (1.2 kg m^{-3} at 20° C). Hence, the dispersion will be analogous to that of gaseous methane at low temperature (Saraf and Melhem, 2005).

In steady atmospheric conditions, gas clouds are dispersed more rapidly by locally-generated turbulence than by unidirectional wind flow. For dense gas releases, the vertical density profile will be stably stratified, and turbulence and turbulent mixing may

be significantly reduced or entirely inhibited (Britter, 1979). The results in Chapter 4 are examples of this behaviour.

The density difference may be expressed as $g' = g \cdot [(\rho - \rho_a)/\rho_a]$, where g is the acceleration due to gravity, and ρ and ρ_a are the density of the gas and of the ambient fluid (air), respectively (Britter, 1979). This difference emphasizes the contrast between dense-gas dispersion and the dispersion of neutral-density, or "passive" pollutants.

However, the density difference is not the sole variable determining whether the release behaves as a dense gas. A very small release or release rate into a strong wind, or alternatively a release over a large source area, may be considered effectively passive (Britter, 1989). A continuous source of volume flow rate q_o, with source density difference characterized by g'_o may be considered effectively passive when:

$$(g'_o \cdot q_o/D)^{1/3}/U \leq 0.15 \qquad (5.14)$$

where D is the source dimension and U is the wind speed (Britter and McQuaid, 1988). In the present case $g' = \sim 13.1$, for $\rho_{CO2} = 2.8$ kg m^{-3} and $\rho_a = 1.2$ kg m^{-3}.

During daytime (some days after the bank formation and for the conditions imposed) the sublimation rate can reach 3 g m^{-2} s^{-1} (Figure 5.4). Using these values in Equation (5.14), with D = 1 m^2 and q_o given in kg m^{-2} s^{-1}, it is found that the sublimation of carbon dioxide from a dry ice bank can lead to the formation of a dense cloud for values of $U \leq 2.3$ m s^{-1}. For higher wind speeds, the dispersing carbon dioxide would behave as a passive pollutant, i.e. carried by the wind flow. In line with the approach typically used for generic assessment (e.g. by the UK Health & Safety Executive) where the site-specific wind information is not available, D5 conditions (Pasquill stability category D, neutral

stability, and 5 m s^{-1} wind speed) are assumed to occur for 80% of the time, with the remainder being F2 (Pasquill stability category F, very stable, and wind speed 2 m s^{-1} (Vendrig et al., 2003) – see previous chapter for in depth discussion). It can then be said that the conditions for which a subliming dry ice bank will be a health risk are very likely to occur over the UK.

5.3.2 CO_2 plume extent

The Gaussian dense gas dispersion modelling tool ALOHA 5.4 was used for evaluating the extent of the toxic cloud at different concentrations for the two cases studied (Figure 5.5) at the specified atmospheric conditions. With the bank acting as a continuous source, the gas cloud would be quasi-stationary, with the extent of the plume fluctuating only with diurnal changes in sublimation rate (see Figure 5.4).

Figure 5.5 shows the extent of the downwind plumes generated by the subliming dry ice banks at mid-day (i.e. maximum extent of the formed plume), 1 hour after the bank formation (Figure 5.5a) and some days after the bank formation (Figure 5.5b).

The concentration limits considered are:

- 2,000 ppm (Level Of Concern-1) – the limit below which no environmental detriment can be determined
- 15,000 ppm (LOC-2) – the limit below which no human detriment can be determined and also the occupational exposure limit in the UK.
- 70,000 ppm (LOC-3) – the lower limit above which human fatality is likely to occur.

For case (a) (13 t bank) it was found that in stable conditions (Pasquill atmospheric stability class F) the CO_2 concentration in the formed plume could exceed LOC-1 (2,000 ppm) up to a downwind distance of about 45 m, while for case (b) (74 t bank) the gaseous concentration of CO_2 could reach the IDLH (Immediately Dangerous to Life and Health) level of 70,000 ppm up to about 30 m and the 2,000 ppm concentration level would have a downwind extent of up to 130 m (Figure 5.5). On extremely warm days (T_{Max} = 30° C) the sublimation of carbon dioxide from the bank can reach 4 g m^{-2} s^{-1}, with a consequent downwind plume extent for case (a) of about 60 m (LOC-1) and the 70,000 ppm concentration isoline extending up to 10 m; for case (b) LOC-1 will be at more than 150 m, LOC-2 at about 80 m and IDLH concentration reaches 50 m downwind.

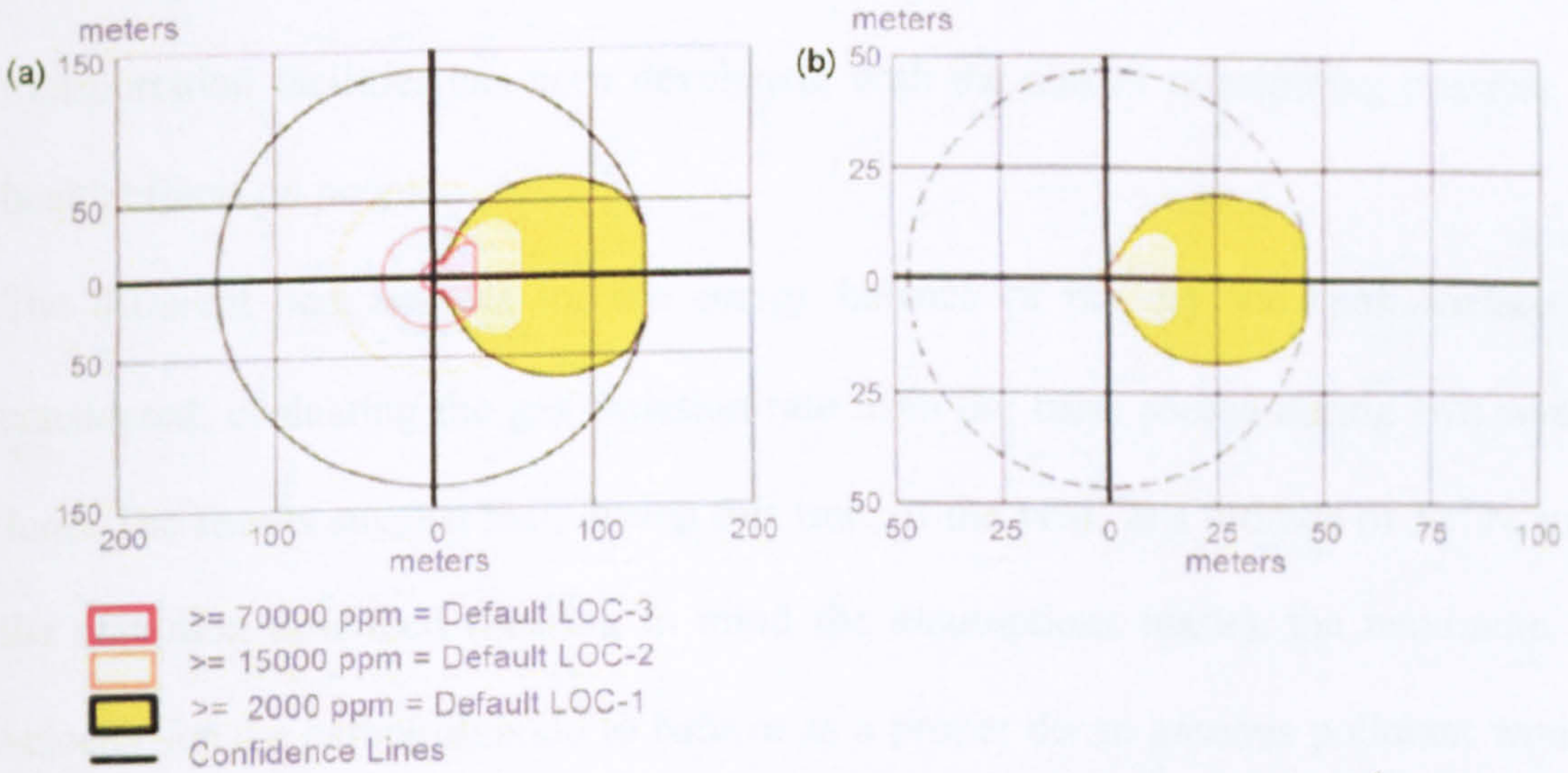

Figure 5.5 - Plume extent generated by a subliming dry ice bank for U = 2 m s^{-1} (ALOHA 5.4): (a) 1 h after bank formation and (b) some days after, during mid-day time.

The banks were assumed to have the shape of geometric cones, and the reduction of their surface area with time is proportional to the sublimation rate. Hence, for the cases considered and an average sublimation rate of ~2 g m^{-2} s^{-1} (during the time of year

considered here), bank (a) would naturally disappear between 3 and 6 days after its formation, and bank (b) would last for some weeks.

Considering the sublimation of the same banks (a) and (b) during a winter period (such as December, with air temperature ranging between -5° and 5° C, soil T = 5° C and the same wind and relative humidity range), the sublimation rate would have an average value of 1.8 g m^{-2} s^{-1}, reaching peaks at midday of 2.3 g m^{-2} s^{-1}. The durations of the two banks would not greatly exceed the corresponding summer values.

5.3.3 Risk posed by a subliming bank of solid CO_2 - summary

A model for evaluating the sublimation rate of a frozen CO_2 bank created after the occurrence of a downward leakage of the waste gas from high pressure CCS transportation facilities has been developed, with the aim of considering possible acute health effects on people.

The different heat sources for the energy balance of the dry ice bank surface were considered, evaluating the gas emission rate from the bank source during two weeks in June. The results suggest that, during this time of the year, at a latitude of 52° N and for the condition described (bearing in mind the assumptions made), the maximum wind velocity for the carbon dioxide to behave as a proper dense gaseous pollutant would be about 2.3 m s^{-1}.

The cloud extents calculated by ALOHA 5.4 for the two cases examined are to be taken as general results for the atmospheric conditions considered (F2, very stable with 2 m s^{-1} wind speed) and for a flat horizontal surface. The estimates relate to a bank created after a

leak of one hour duration: whenever the pipeline remains pressurized and the leak remains undetected, a larger bank may form, hence a bigger plume.

On the other hand, the CFD atmospheric dispersion model PANACHE predicts for the 70,000 ppm CO_2 cloud a downwind extent of about 8 m with no formation of the 100,000 ppm cloud, for the sublimation rate considered. These results have not been included here.

A very dense gas such as cold carbon dioxide would tend to remain close to the ground so that its dispersion would be strongly influenced by the specific topography of the area. Particularly, for near-zero wind conditions CO_2 would accumulate in topographic lows such as railway/road cuttings, posing a serious hazard for people and animals (e.g. the case of Lake Nyos). The time taken by the plume/cloud to disperse will be dependent on the atmospheric conditions during its occurrence and the complexity of the area of dispersion (i.e. topography and presence of obstructions).

Atmospheric dispersion of carbon dioxide after sublimation from a dry ice bank is of concern when dealing with safety criteria for the transportation of carbon dioxide in carbon sequestration projects. The outturn of this chapter confirms that cold gaseous CO_2 could result in human fatalities for particular conditions and situations, particularly in areas of complex topography. Caution is needed when dealing with a dry ice bank (e.g., during removal) after a downward leakage has occurred.

CHAPTER 6

FURTHER APPLICATIONS OF COMPUTATIONAL FLUID DYNAMICS FOR CO_2 DISPERSION

Introduction

In this chapter, some applications of the CFD tool are explored further. In the first part of the chapter, the process of CO_2 release from a high-pressure container (pipelines and other parts of the modularised transportation system considered) is investigated in more detail. In risk assessments drawn up in the past, the speed of the waste gas flow as it leaks out of a transportation facility has not always been considered, and when it has, only as an early dilution coefficient within the software used. Here, the implications of the high jet speed developed during a leakage from such high-pressure facilities are considered. PANACHE is used to model the initial dispersion of the gas due to the 'jet-mixing' effect: the strong resistance imposed by air to the high-speed flow and the consequent entrainment of large volumes of air by the flow itself. The failure parameters from Chapter 4 have been used for this analysis and the results compared with those for zero release speed.

In the second part of this chapter, PANACHE is used for modelling a release within the characteristic built environment of an industrial site (a 'capture ready' plant), focussing on the influence of obstacles such as buildings on the wind field and the consequent dispersion of the gas.

6.1 The jet release and its consequence for gas dispersion

As it leaks from a high pressure facility, a gas or supercritical fluid develops a velocity up to the speed of sound (Kuprewicz, 2007) and may entrain many times its own flow rate of ambient air (Wakes et al., 2002). The aim of the work described here is to explore the differences obtained in risk assessments if considering the jet release speed of a leak formed as a consequence of its high pressure, rather than assuming a negligible release speed. Figure 6.1 is a photograph of a leak from a surface high-pressure pipeline, which forms a jet perpendicular to the pipe.

Figure 6.1 – A jet-released leakage from a high-pressure gas pipeline (Townes et al., 2004).

A very dense fluid (in this case supercritical carbon dioxide) injected from a point source at a very high speed into a second relatively static fluid (air), has a strong impact on the concentration fields of both fluids around the leak. The jet effect, due to the difference in physical properties of the two substances (weight, density, temperature and, mainly, momentum), extends the region of very high concentrations into the ambient air. Later on, it will be seen how the above-mentioned jet can extend tens of meters away from the leaking point, at concentrations that can be considered dangerous, as predicted by PANACHE.

During this early motion into the atmosphere, carbon dioxide would intensively modify the wind field in the surrounding volume of air. Figure 6.2 shows the wind field during a jet-release simulation, before and after the beginning of the release.

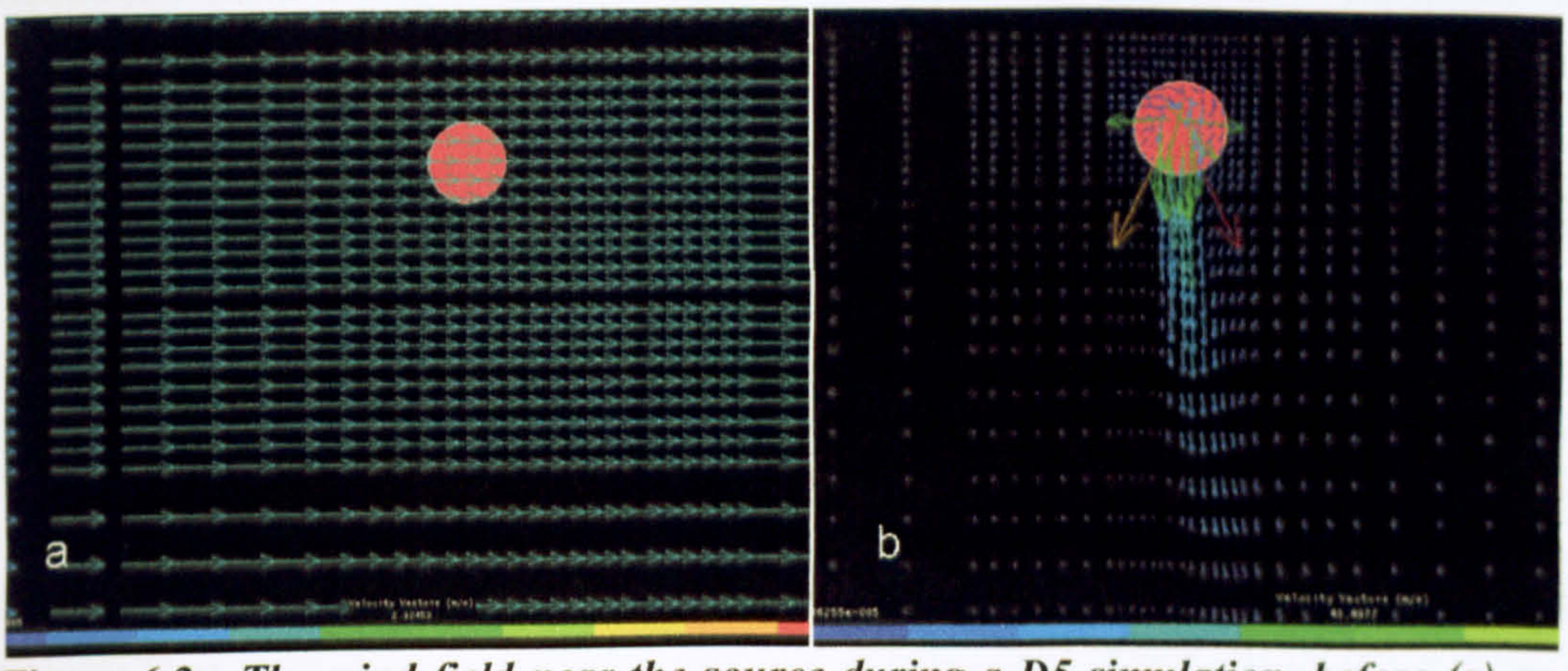

Figure 6.2 - The wind field near the source during a D5 simulation, before (a) and after (b) beginning of the jet release (xy plane).

In the image above, the arrows represent vectors characterizing the speed of the fluid at the particular point. Intensities of vectors are described by their length and colour and in fact, in Figures 6.2a and 6.2b, the difference in representing wind vectors not influenced by the jet release (e.g. behind the source, above the red dot in the figures) is not due to a divergence in the actual values of the vectors but to a matter of scale: in Figure 6.2b, PANACHE was scaled to distinguish the wind speed (3 m s^{-1}) from the jet speed of the release (up to about 50 m s^{-1}).

The effect of mixing between carbon dioxide and air is mainly governed by the difference in velocity between the two and the consequent strong initial resistance imposed by air to the flow of the jet. In any case, after travelling a relatively long distance, the jet would stop, enhancing its dilution with air.

6.1.1 Jet-release speed calculation

With the aim of calculating the release speed from high-pressure pipelines/transportation facilities, as a means of early dispersion of the gas, two different equations have been used: Bernoulli's principle (assuming the supercritical fluid as incompressible) and the equation for calculating the mass flow rate of a gas flowing through an orifice in choked conditions, which is the limiting case of the Venturi effect.

6.1.1.1 Bernoulli's principle

In fluid dynamics, Bernoulli's principle states that for an inviscid flow an increase in the speed of the fluid occurs simultaneously with a decrease in pressure or a decrease in the fluid's gravitational potential energy. Bernoulli's principle can be applied to various types of fluid flow, resulting in what is loosely denoted as Bernoulli's equation. In fact, there are different forms of the Bernoulli equation for different types of flow. The simple form of Bernoulli's principle is valid for incompressible flows (e.g. most liquid flows) and also for compressible flows (e.g. gases) moving at low Mach numbers, which is the case of interest for this study.

Bernoulli's principle is equivalent to the principle of conservation of energy. This states that in a steady flow the sum of all forms of mechanical energy in a fluid along a streamline is the same at all points on that streamline. This requires that the sum of kinetic energy and potential energy remain constant. If the fluid is flowing out of a reservoir the sum of all forms of energy is the same on all streamlines because in a reservoir the energy per unit mass (the sum of pressure and gravitational potential) is the same everywhere (Kundu and Cohen, 2004). Fluid particles are subject only to pressure and their own weight. If a fluid is flowing horizontally and along a section of a

streamline, where the speed increases it can only be because the fluid on that section has moved from a region of higher pressure to a region of lower pressure. The simple form of Bernoulli's equation is:

$$\frac{v^2}{2}+gh+\frac{P}{\rho}=constant \qquad (6.1)$$

Equation (6.1) can also be written as $\frac{v_i^2}{2}+gh+\frac{P_i}{\rho}=\frac{v_f^2}{2}+gh+\frac{P_f}{\rho}$, where v_i, v_f, P_i and P_f are respectively the initial and final flow velocities (inside the pipeline, taken as zero, and soon after the release, outside the pipeline) and the initial and final pressure (P_i = 10 MPa, P_f = 0.1 MPa – atmospheric pressure), ρ is the density of CO_2 (950 kg m^{-3}, supercritical density taken as constant before and soon after the leak), the term gh is equal to zero (h = 0). Applying this equation to our case and resolving for v_f gives for the leaking flow a velocity v = 145 m s^{-1}.

A particular application of Bernoulli's principle is the Venturi effect which governs the kinetic energy of particles in motion inside a tube, in response to the variation of the pipe section, via the determination of their potential energy (pressure).

6.1.1.2 Choked flow

The limiting case of the Venturi effect is choked flow, in which a constriction in a pipe or channel limits the total flow rate through the channel, because the pressure cannot drop below zero in the constriction. Choked flow is used to control the delivery rate of water and other fluids through spigots and other valves and can be also used to estimate the total mass of high pressure fluids leaked out of facilities when being transported (Mazzoldi et al., 2007). Equation (6.2) gives the leakage rate of a fluid through an orifice;

it has been used in Chapter 5 to calculate the weight of the dry ice bank formed when the leak points downward.

$$Q = CA\sqrt{k\rho P\left(\frac{2}{k+1}\right)^{(k+1)/(k-1)}} \qquad (6.2)$$

where Q is the mass flow rate (kg s^{-1}); C the discharge coefficient (usually 0.72); A the discharge orifice cross-sectional area (m^2); $k = c_p/c_v$ the ratio of specific heats of the gas ($k_{CO2} = 1.29$); ρ is the fluid density at T and P for supercritical CO_2 ($\rho = 950$ kg m^{-3}); P is the absolute upstream pressure (10 MPa) (Pa). The value obtained using this method is v = 49 m s^{-1}. It must be specified here that the values for c_p and c_v used are valid at STP conditions. Although these values are different for supercritical CO_2, their ratio is assumed not to vary significantly. The use of this formula is widespread in the literature for calculating the flow of liquids in pipes and the mass of leaked fluids (E.P.A., 1999, F.E.M.A., 1989, Perry et al., 1984). In this study, all releases were considered to be perpendicular to the wind direction, at ground level and with a 5° upward angle.

6.1.2 Jet-mixing effect and risk assessment

In Chapter 4 a potential Risk Assessment for CO_2 transportation was drawn up, taking release parameters from the literature (Vendrig et al., 2003). The release parameters (as in past risk assessments) did not account for high leaking flow speeds or for the resulting initial dispersion due to the jet-mixing effect.

In this section, PANACHE was given the same parameters as in Chapter 4 (release rates, durations, temperature of leaked gas, total amount of releasable CO_2 and atmospheric parameters) in order to consider leaks of the same dimensions as in Chapter 4, but

allowing for releases with an initial speed of 49 m s^{-1}. Results for jet-release simulations are also compared with 0 m s^{-1} simulation results, from Chapter 4.

6.1.2.1 Simulating a high-speed release

To simulate a jet leakage from a facility, with the aim of accounting for the CO_2/air mixing along the leak flow-line, PANACHE requires a very high density of Control Volumes (CV), in the area through which the jet passes. Figure 6.3 shows the fine mesh needed by PANACHE when accounting for high-speed releases.

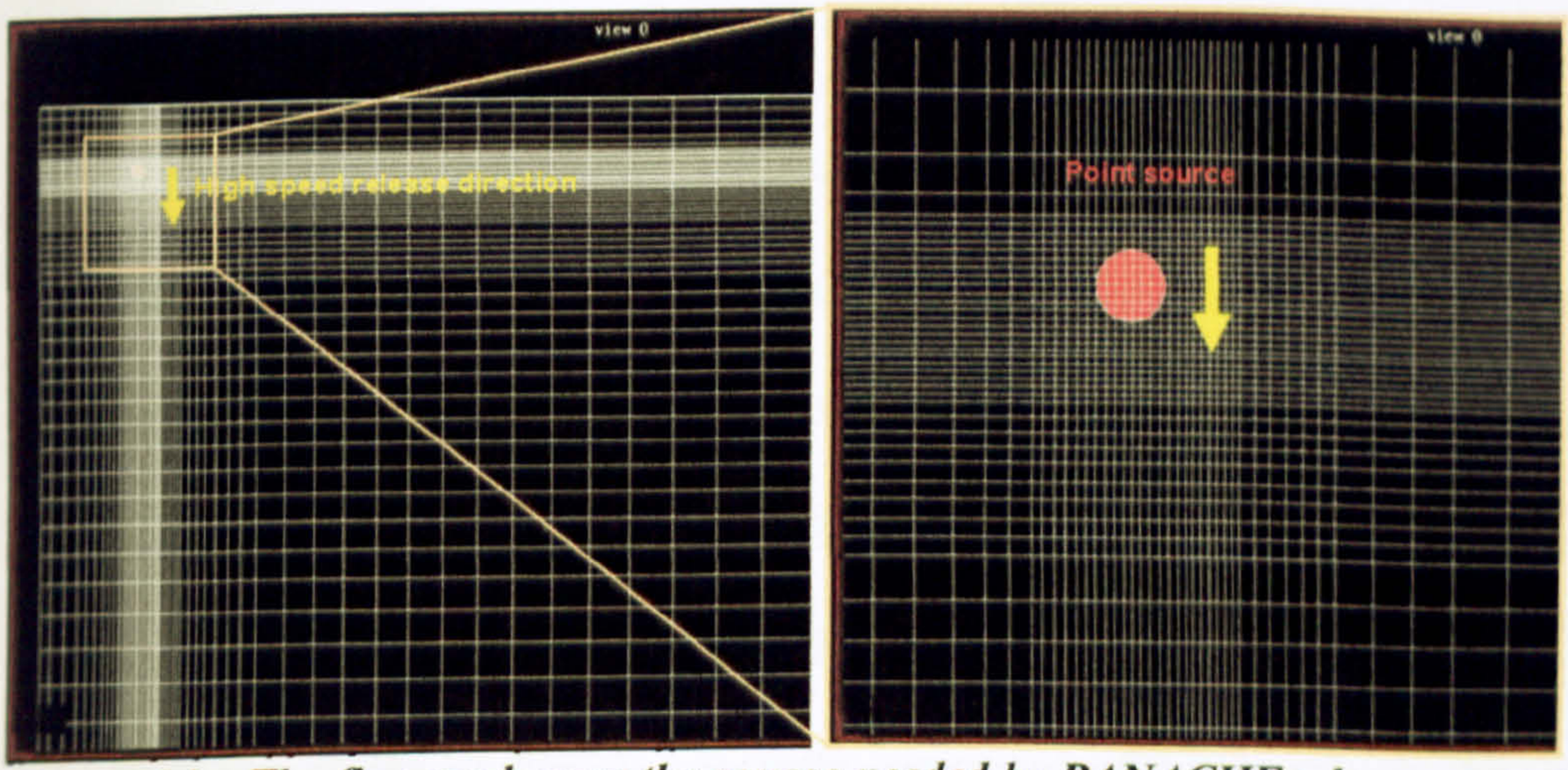

Figure 6.3 - The fine mesh near the source needed by PANACHE when accounting for the jet release, 2D views.

The interaction (mixing) between the jet and surrounding air is dominated by the difference in momentum, reaching a maximum hypothetical value once this difference has decreased (i.e. further away from the source). PANACHE can calculate this continuous process of jet-flow momentum loss in steps. The kinetic energy of the jet is accounted by the CFD tool solving the Navier-Stokes equations within the CVs affected by the high-speed flow. A very large number of CVs is needed, for when a very high speed is dealt with the model needs to evaluate its dissipation through a large number of

steps, calculating the effect of speed on gas concentrations and temperatures within the plume, at different distances from the source. The precision of PANACHE is enhanced at the cost of computational time.

Within every single CV, the gas enters with specified physical properties (speed, temperature, concentration, momentum), mixes with the air within the prescribed volume (changing its temperature and concentration, as estimated by the resolution of Navier-Stokes equations within each CV) and leaves the CV. When the jet momentum has decreased, further from the source, the gas flow is then controlled by the atmospheric wind speed and turbulence.

As demonstrated in paragraph 4.2 and in Chapter 5, as a consequence of adiabatic expansion after a leak from an e.g. 10 MPa facility, carbon dioxide gets frozen, at a temperature of the order of some degrees to some tens of degrees below its sublimation point (-78.8° C). Figure 6.4 has been taken from the TNO manual on calculating physical effects when modelling gas release (TNO, 1996). From the picture it can be seen how actually a two-phase jet flow is generally composed of three parts. In the specific case of carbon dioxide, the first part is the one in which the flow of CO_2 molecules would get frozen (partially or entirely) after expansion, under the Joule-Thomson effect. In the second part, molecules would sublime back to the gaseous state due to the heat provided by the resistance of air to the jet, while mixing with air takes place. Some of the dry ice droplets may not reconvert to the gaseous state, thus getting rained-out of the jet flow, falling on the ground in solid form. In the third phase, all the molecules composing the flow would be in the gaseous phase and the jet would continue its expansion with more air entrainment.

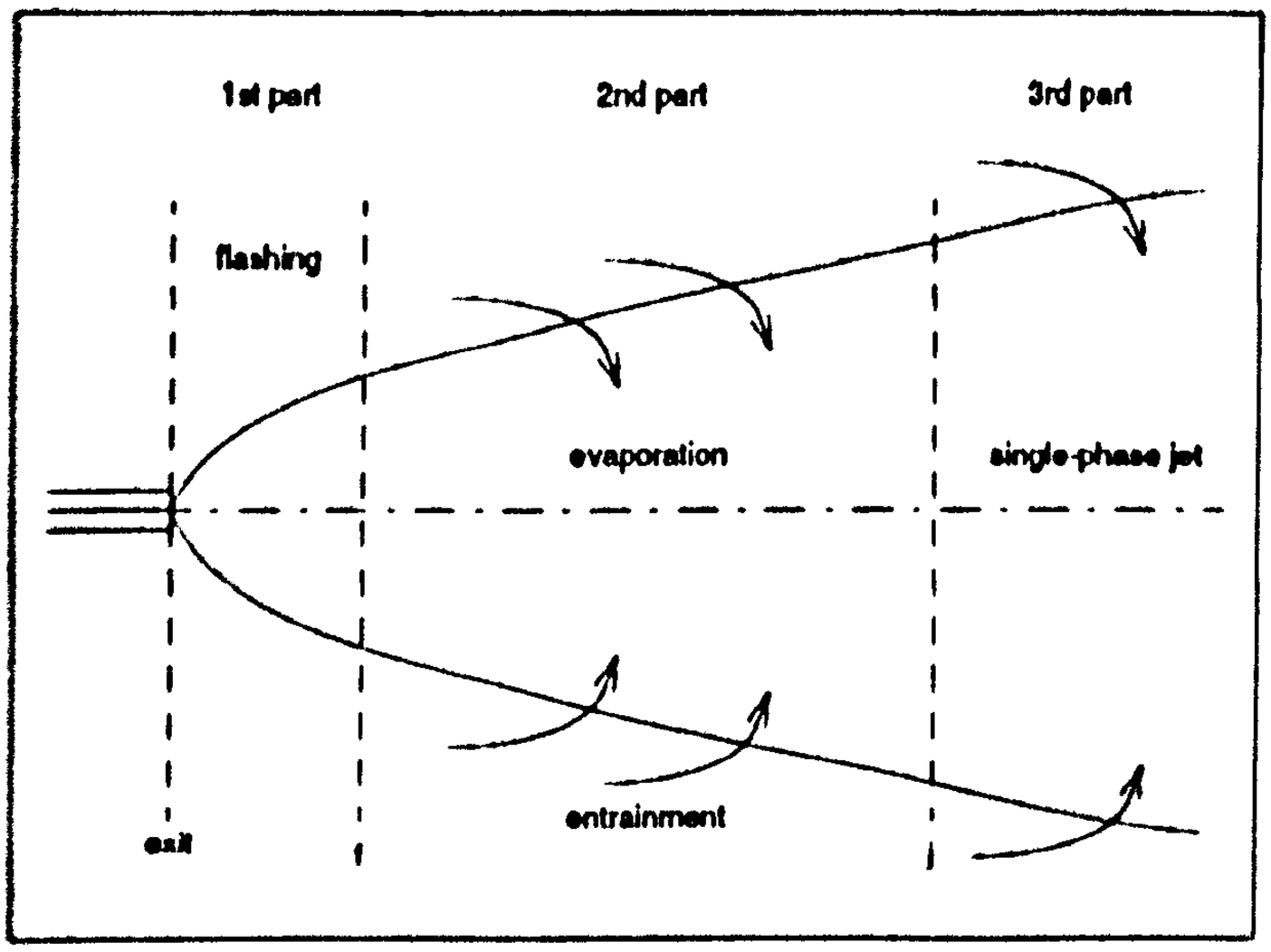

Figure 6.4 - Schematic view of two-phase jet release (TNO, 1996).

PANACHE cannot deal with a jet release of this kind. The software in fact does not consider the Joule-Thomson effect and the thermodynamic process of sublimation due to the heat provided by the air resistance. It is believed, however, that all, or a big part of, the molecules composing the flow would reconvert into gaseous phase, due to the high heat input from static air and to the fact that the Joule-Thomson effect is not likely to freeze CO_2 much below its freezing point, at -78.8° C.

6.1.2.2 Downwind extent of the plume

As described above, the release direction considered here is perpendicular to the wind direction, for every case studied. The goal of this chapter is not to make another Risk Assessment, and hence the consequences of the releases simulated here are not studied further and effects on humans and environment not considered. In fact, the only results contemplated are the downwind distances reached by plumes from leaks of different sizes from the different transportation Modules. In table 6.1 results are given for downwind

distances of the 15,000 and 100,000 ppm contours, for release velocities of 0 m s^{-1} and 49 m s^{-1}.

Table 6.1 - comparison of downwind distances between 0 m s^{-1} and 49 m s^{-1} release speed trials as simulated by PANACHE.

Leak case	Release parameters			MAX downwind distance (m) 0 m s^{-1}				MAX downwind distance (m) 49 m s^{-1}			
MOD 1	Duration (s)	Rate (kg/s)	Inventory (kg)	100,000 ppm		15,000 ppm		100,000 ppm		15,000 ppm	
				D5	F2	D5	F2	D5	F2	D5	F2
Full-bore	600	95	57000	47	36	149	127	12	10	193	98
Large	816	43	35329	29	21	125	111	11	8	104	88
Medium	3600	4	14040	7	6	38	33	3	2	35	28
Small	3600	2	7560	5	4	25	22	2	1 8	22	21
MOD 2,3,4	Duration (s)	Rate (kg/s)	Inventory (kg)	100,000 ppm		15,000 ppm		100,000 ppm		15,000 ppm	
				D5	F2	D5	F2	D5	F2	D5	F2
Full-bore	600	1800	1080000	152	125	440	339	52	33	374	263
Large	3600	633	2278800	112	94	340	292	31	18	158	239
Medium	3600	57	205200	35	28	169	148	12	9	92	87
Small	3600	3.1	11160	13	9	34	28	2.4	3	32	25
MOD 5	Duration (s)	Rate (kg/s)	Inventory (kg)	100,000 ppm		15,000 ppm		100,000 ppm		15,000 ppm	
				D5	F2	D5	F2	D5	F2	D5	F2
Full-bore	600	95	57000	47	36	149	127	12	10	190	88
Large	600	95	57000	47	36	149	127	12	10	190	88
Medium	3600	57	205200	35	28	129	108	11	8	102	68
Small	3600	3.1	11160	13	9	34	28	2.4	2	32	26

As for simulations with negligible release speed, for 49 m s^{-1} release speed simulations, downwind contour distances for D5 atmospheric conditions are greater than at F2 conditions. This is due to CO_2 being a dense gas, less affected by atmospheric turbulence than buoyant gases.

As it leaks from a high-pressure facility, a gas or supercritical fluid develops a high velocity, entraining many times its own flow rate of ambient air. The most important effect of the release speed is the high initial dispersion of the gas and the consequent shorter downwind distances reached by dangerous concentrations, if compared with zero release speed leaks.

Figure 6.5 displays an x-y (plan) view of the 100,000 ppm concentration envelope from two plumes from jet-releases, for different atmospheric conditions.

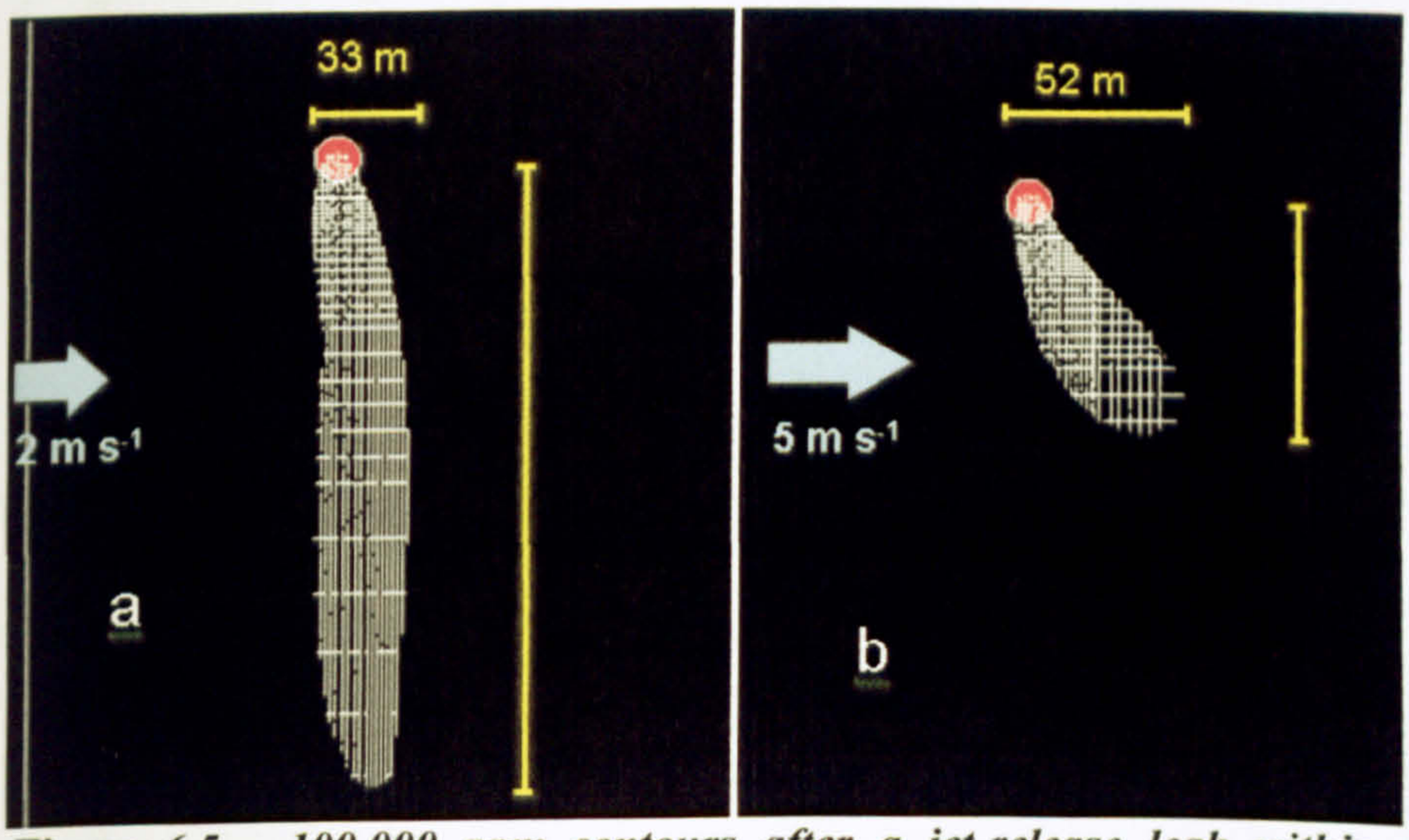

Figure 6.5 - 100,000 ppm contours after a jet-release leak within Module 2 in a CO_2 transportation system, for F2 (a) and D5 (b) atmospheric conditions.

The figure shows how downwind distances reached by dangerous concentrations of the gas, for jet release trials, are dependent on the direction of the leaking flow with respect to the wind direction, rather than on atmospheric conditions. In this particular case, for jet releases perpendicular to the wind direction, the development of the plume of the dangerous concentration of interest (100,000 ppm) is not much affected by the wind itself, for very low wind speed. The specified wind speeds are for a height of 10 m; PANACHE uses a logarithmic law to calculate speed at other heights. Figure 6.6 is the graphical representation of data in Table 6.1.

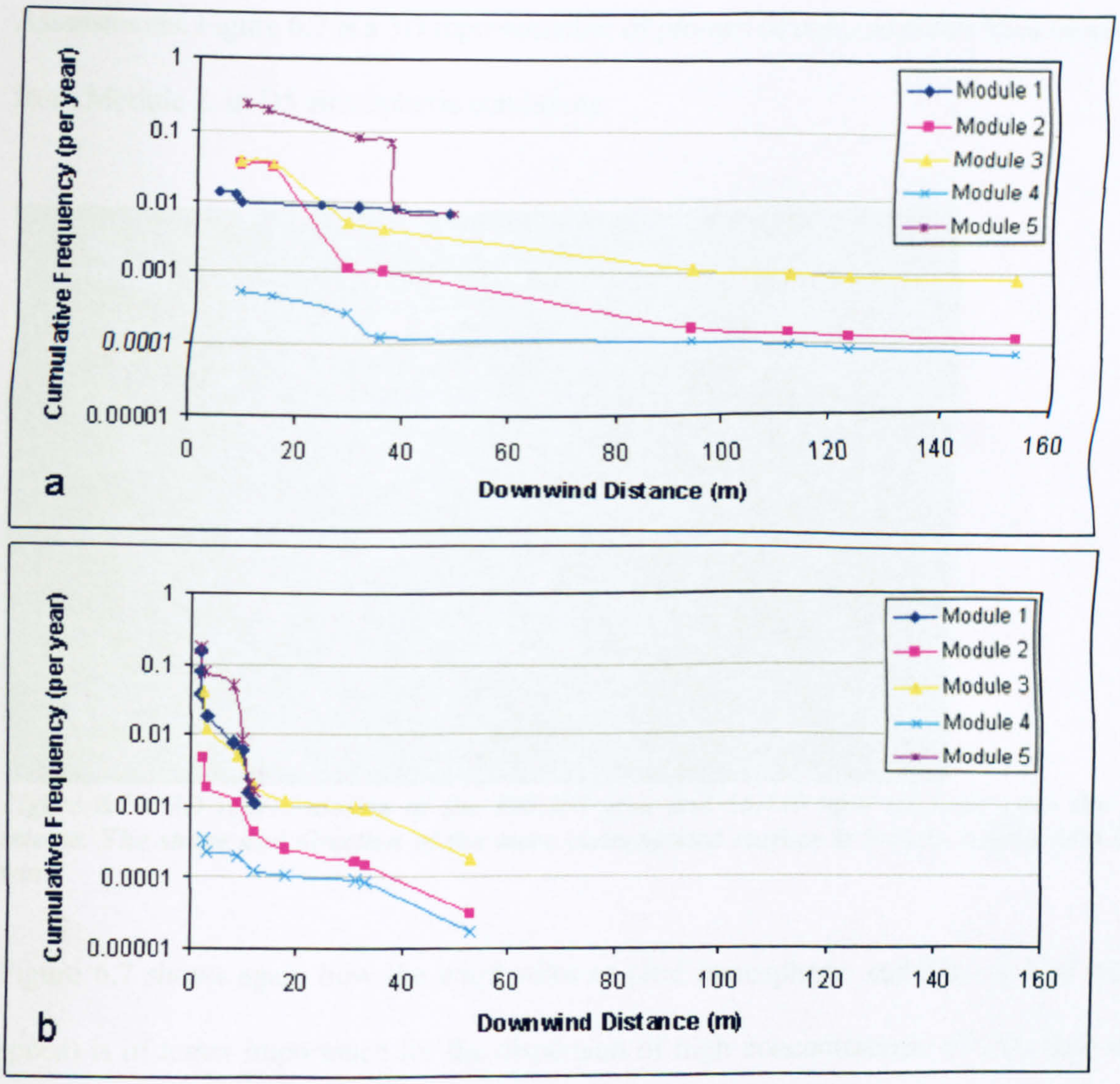

Figure 6.6 - comparison of downwind distances reached by 100,000 ppm concentrations for different Modules and for a) 0 m s^{-1} and b) 49 m s^{-1} release speeds.

From Table 6.1 and the graph above, the final effect of the initial mixing due to the jet-release can be appreciated: differences in downwind distances between plumes modelled with 0 m s^{-1} release speed and jet-releases are significant. For any particular Module, the former might extend up to three times further than plumes from jet releases.

The jet-mixing effect has a strong influence on the early dissipation of CO_2 leaked from CCS transportation facilities and should be accounted for when drawing up Risk

Assessments. Figure 6.7 is a 3D representation of plumes of concentration for a large leak from Module 2, in D5 atmospheric conditions.

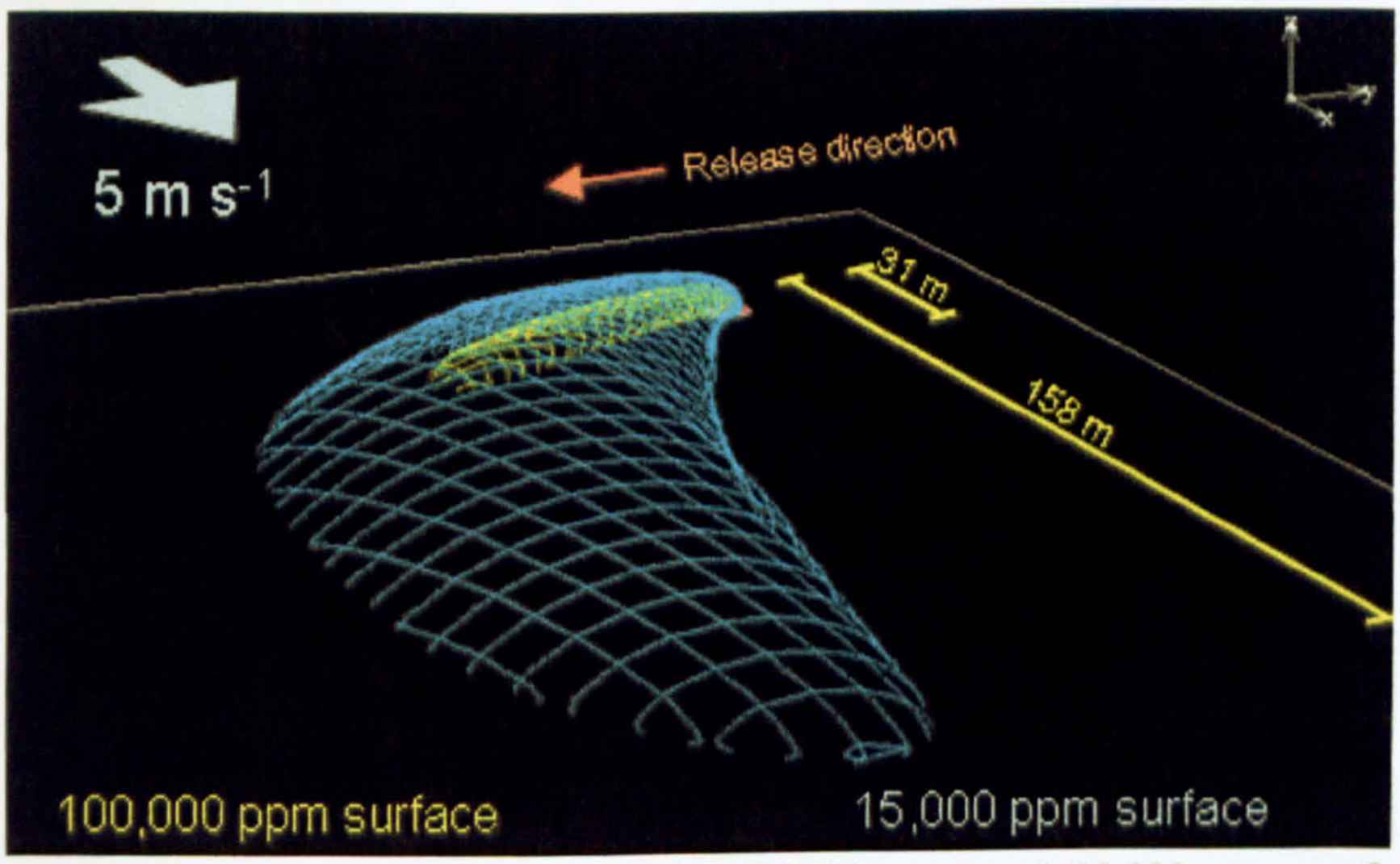

Figure 6.7 - 3D representation of the 100,000 ppm and 15,000 ppm surfaces after the jet release. The shape and direction of the more concentrated surface is loosely related with the wind.

Figure 6.7 shows again how the wind velocity (and atmospheric stability, at low wind speed) is of lesser importance for the dispersion of high concentrations of CO_2 than the angle between the wind direction and the leak. For lower concentrations of the gas, the wind speed assumes a major role in determining the shape and dimensions of the concentration distribution.

6.1.3 The CO_2 release experiment

Under the project 'CO_2 underground storage in Barendrecht', Netherlands, in December 2008 Shell carried out a field experiment (Kuijper, 2008) involving a vertical CO_2 release from a pressurized container. Figure 6.8 shows how the jet-release pushed the highly concentrated gas very high in the atmosphere.

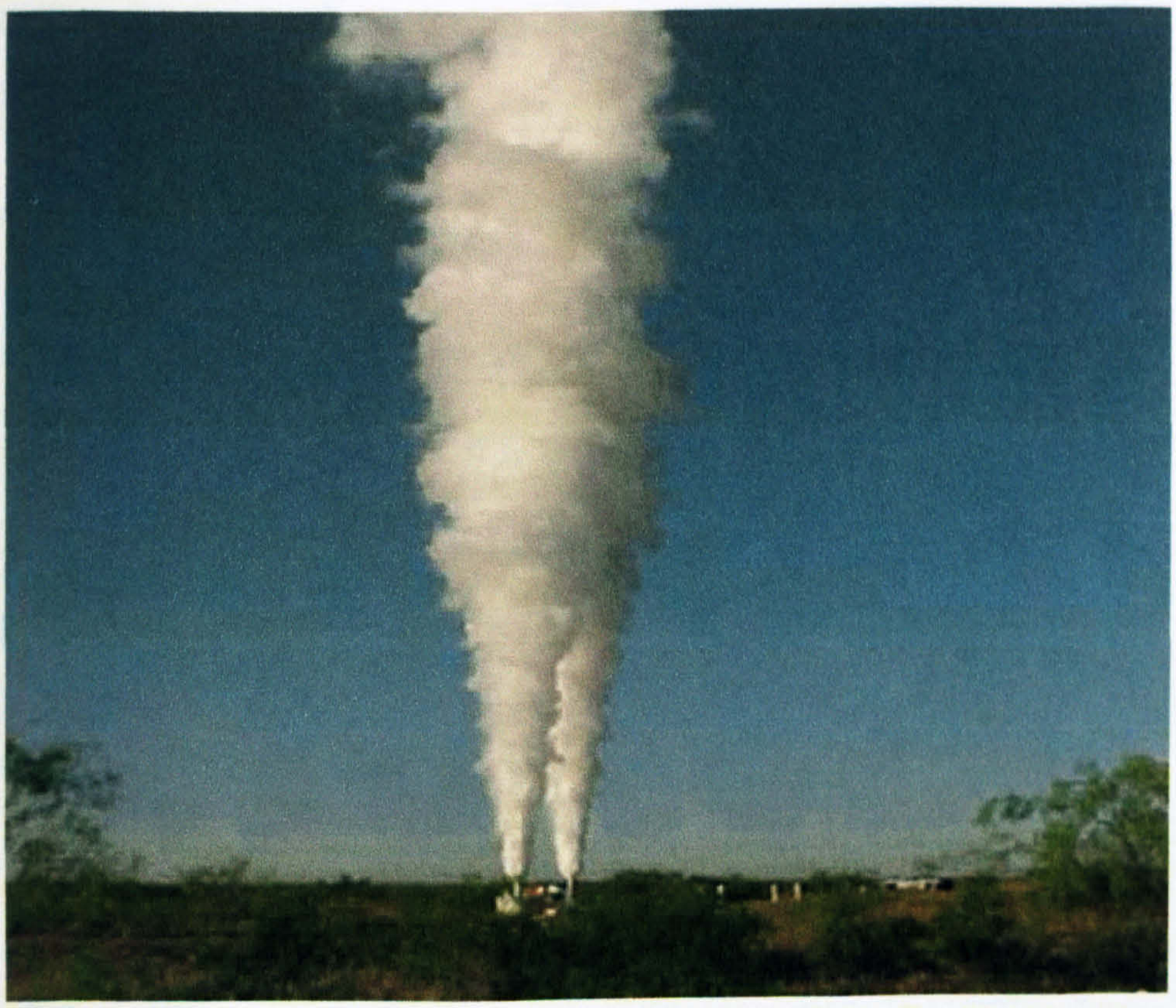

Figure 6.8 - CO_2 release experiment from Shell; release rate data unavailable (Kuijper, 2008).

Although carbon dioxide would experience a strong temperature drop after expansion, with a consequent increase of its density, it is clear that the gas is not much subjected to gravitational inputs but, due to its high momentum, after an upward vertical release, forms a plume that would not severely impact the surface environment with dangerous concentrations. Data about the rain-out of dry-ice from the plume are not available but, from the image, solid carbon dioxide seems to get reconverted into the gaseous phase almost entirely.

In this chapter, nearly-horizontal releases were considered because of the higher impacts they would have on nearby populations, although it must be emphasized that from buried pipeline, the most probable leak events will be vertical ones (caused by e.g. damage during excavation).

In Figure 6.9, a PANACHE simulation of a CO_2 vertical release is displayed. Particularly, the 100,000 (green surface), 15,000 (grey) and 2,000 (orchid) ppm concentration contours.

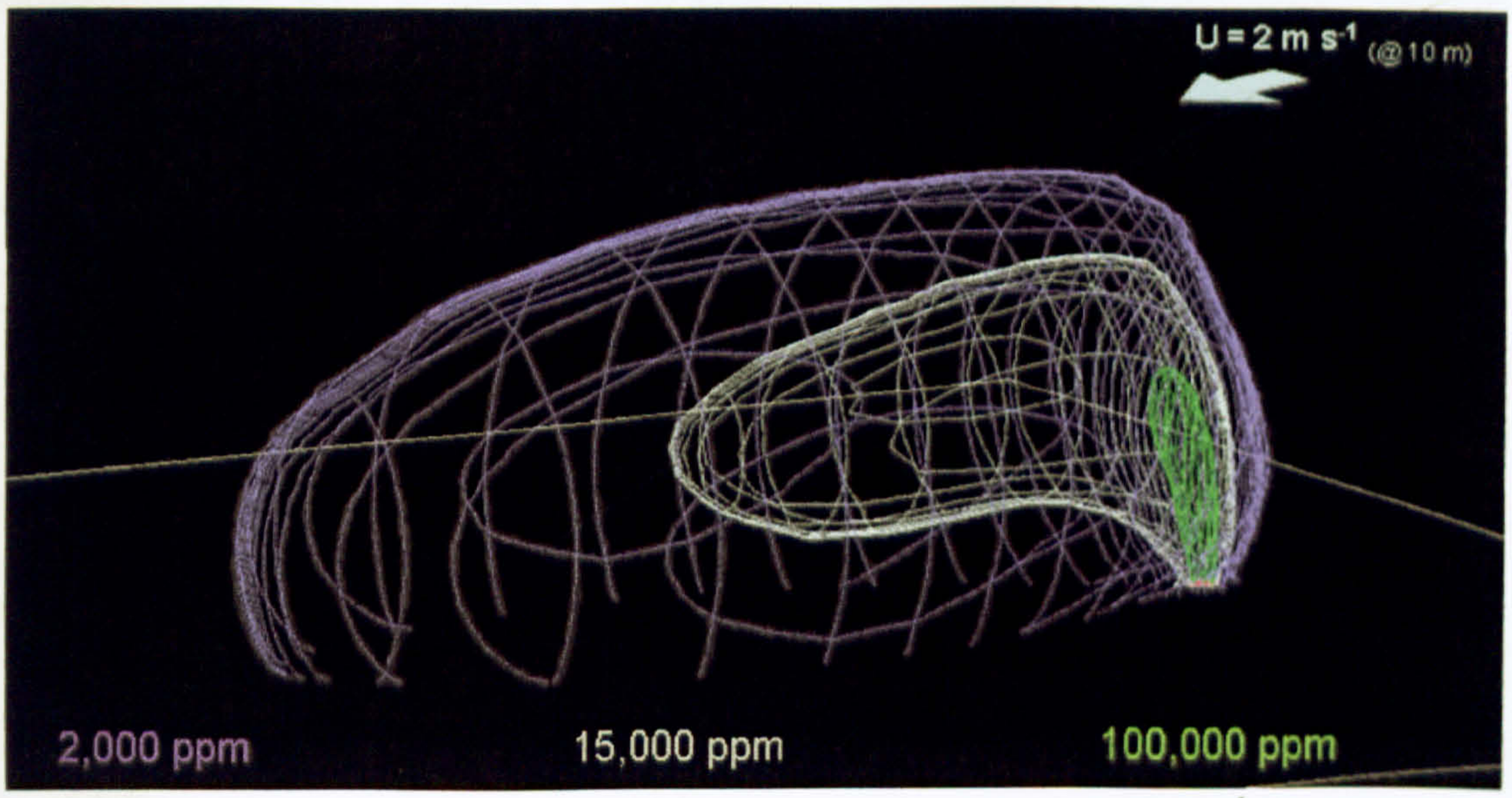

Figure 6.9 - Vertical release of concentrated CO_2 with a speed v = 49 m s^{-1}

Results from simulations of Large and Full-Bore vertical releases by PANACHE did not give a vertically-elongated plume for the 100,000 ppm concentration contours – as in the real case, Figure 6.8 and in the simulation in Figure 6.9 – when the release velocity chosen was 49 or 145 m s^{-1}, and for very low wind speeds. The shape of the cloud formed was more spherical at a certain height from the source. To reproduce this shape at a jet speed of 49 m s^{-1}, PANACHE required a much lower release rate of 4 kg s^{-1} (a Medium leak from Module 1, Figure 6.9). Given the precision of CFD, particularly when modelling a process such as a high speed flow, not influenced by variable entities like atmospheric stability, the velocity of the flow, in Figure 6.8, was probably much higher than the one used here.

6.2 CO_2 dispersion within the built environment of a plant

Wind flow and turbulence in the vicinity of groups of buildings have a significant effect on the dispersion of pollutant gases from nearby stacks or vents and from fugitive emissions, low level or dense gas discharges (Riddle et al., 2004). Although safety has always been a critical issue in the design and operation of chemical plants, the academic community overlooked this issue for a very long time (Jelemensky et al., 2003). The occurrence of catastrophic accidents such as Flixborough in 1974, Seveso in 1976, Bhopal in 1984, Piper Alpha in 1988, Longford in 1998 (Greenpeace, 2006) resulted in lower public acceptance of chemical/process industry and led to the development of new safety standards and regulations, such as the European directive SEVESO II.

A realistic understanding of hazards associated with identification of initiating events would be based on all known information on the process, including quantitative data – i.e. leakage rates. In practice, there is a lack of realistic information on the probable leak strength in a Capture Plant (Module 1 for DNV, Vendrig et al., 2003); hence, the aim here is to study the effects of buildings and facilities in a plant environment on the dispersion of CO_2, leaked from its high-pressure containment, soon after being captured.

6.2.1 Total inventory of releasable CO_2 and leakage rate

Inventory data used in Chapter 4, describing a potential leak within a plant environment, are derived from DNV's work. As can be seen from Table 4.3, they assume a total pipeline-system length inside a plant of 500 m, with an ESD-block valve at the end of the assumed connections. After a discussion with experts at E.ON-UK, this value seems too high and not representative of the real situation. A capture-ready installation

will probably follow the very latest directives for workers' safety, in order to minimize the potential harm to employees. It is thought that a more probable value representing a maximum bond for block-valve distance would be some tens of metres.

Also, Vendrig et al. allowed for a detection and isolation time, after the occurrence of a leak within a typical industrial environment, of 10 minutes. It is thought that, in a busy working place such as a modern power plant, with safety of people working in such areas being paramount, computerized shut-off systems would be used for ensuring minimization of detection and isolation times after the occurrence of a serious leakage. Therefore, it is believed that a more representative maximum-time value for blocking the flow of carbon dioxide within a plant piping system would be of 2-3 minutes, at worst.

DNV studied the leakage of carbon dioxide from a CO_2-recovery installation facility, upstream of the compressor. In this chapter, simulations concerned a potential leak in a plant site downstream of the compression stage and an inlet pressure of 100 atm has been considered. Then, the exaggeration in representative values for length of isolatable pipeline sections and response times of the emergency shut-down system are counterbalanced, in the work of Vendrig *et al.*, by the consideration of a piped CO_2 pressure of 20 atm, in the plant environment. The authors accounted for a worst-case scenario leaking rate of 95 kg s^{-1} after a full-bore rupture, based on the pressure of 20 atm. Here, this leaking rate value seemed correct also for a leak of some centimetres diameter, based on an inlet pressure of 100 atm.

To summarize: a leaking rate of 95 kg s^{-1} lasting for 2 minutes and with a constant gas exit velocity of 49 m s^{-1} was accounted for.

6.2.2 Plant layout and the wind field within

Figure 6.10 shows a plant layout for a representative capture plant, scaled in 2D with dimensions of buildings and distances. This layout has been considered for simulating potential releases in plant environments.

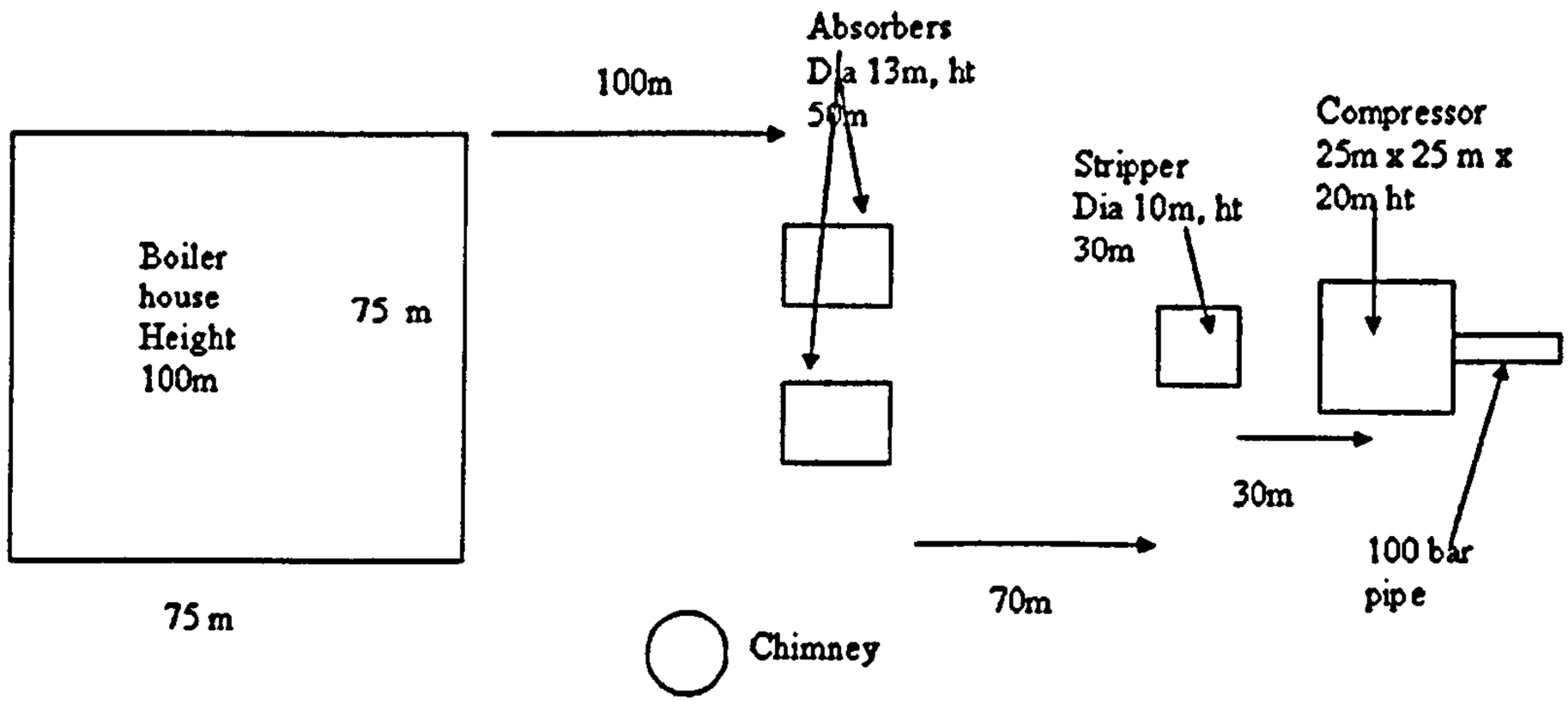

Figure 6.10 - A representative capture plant layout in two dimensions. Data from E.ON-UK.

The total length of the plant environment (on the x dimension, left to right) considered is about 300 m, including some tens of meters at the left of the boiler house and at the right of the compressor. The position of the leak was thought most likely to be along the pipeline after leaving the compressor, at the right of Figure 6.10.

The atmospheric conditions considered in these simulations are quite distinctive. The wind direction was taken as the one that, for the particular leak direction specified, would divert the escaped gas toward the middle of the built environment. The wind speeds considered were all between 4 and 8 m s^{-1} and the atmospheric stability class always taken as F (which, although not reflecting the most likely condition in the UK, confines the gas near the ground most effectively and hence represents the worst-case scenario).

Figure 6.11 shows the wind field within the plant environment in a normal situation (without any leakage taking place) and for the conditions considered.

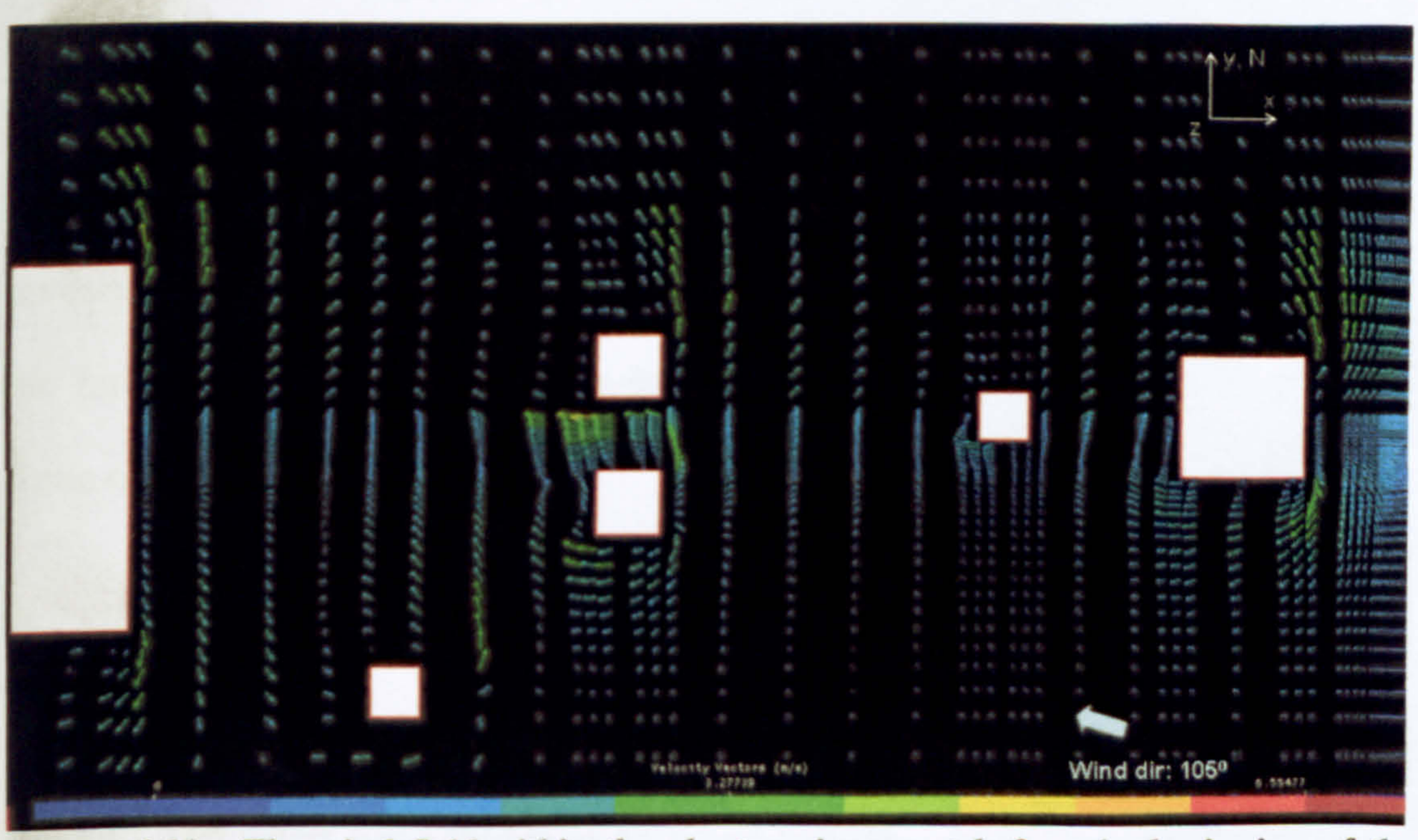

Figure 6.11 - The wind field within the plant environment before the beginning of the leak. The wind flows from 105° at a speed of 8 m s^{-1} (at 10 m height). In the figure, the North coincides with the y direction.

From the flow vectors it can be seen how a constant, unidirectional wind is complicated by the presence of buildings. CFD simulations can provide detailed output of flow fields (describing eddies, dead zones, accelerated flows), turbulence levels and concentration fields generated around the buildings. In the figure, the reason for the non-homogeneity of the wind vector density is the need to have a very fine grid near the source of the outflow (not yet present in Figure 6.11) and near buildings – every Control Volume generates a wind vector, with wind vectors' length and colour representing their intensity (the wind velocity at the point).

Looking again at Figure 6.11, a consequence of the presence of buildings is the channelling of the wind between the two absorber towers (see Figure 6.10), accelerating

the air inside the 'channel' and downwind of the absorbers themselves. This effect can be quantified with Bernoulli's principle, where a narrowing of the section of the path in which a flow is taking place generates a pressure drop, causing the flow to accelerate when passing through the restriction, in response to the law of mass conservation.

The effects of gas discharge from a number of simulations on this site have been investigated in order to assess the on-site pollutant concentrations in the areas between the buildings and the potential for drawing gases into the air conditioning systems of some of the buildings.

6.2.3 The dispersion of concentrated CO_2 in a plant environment

For the purpose of simulating a potential leakage within a CO_2 capture plant, source strength parameters were chosen as introduced above. Figure 6.12 displays the dispersion of the 2,000 ppm CO_2 cloud after about 2 minutes of 95 kg s^{-1} leakage (note that Figure 6.12, and 6.13 are inverted with respect to Figure 6.10, 6.11 and 6.14: the point of view in the former 3D images is different from the latter). As can be seen from the picture, this non-hazardous concentration would, for a medium/large release in a plant environment such as the one considered, cover a big part of the plant itself within a few minutes from the start of the leakage – it has been found that the 2,000 ppm cloud reached its steady state in approximately 1 min 45 sec, in the simulations described here.

Figure 6.12 - Dispersion of 2,000 ppm CO_2 surface within a hypothetical plant environment and for the conditions described. The purple ground is the surface roughness z_0 = 1.5 m, used in order to consider small obstacles.

Comparing Figure 6.11 (which represents the initial wind field) with Figure 6.12 it can be seen how the large building at the right side of the picture (the Boiler House at the left end of Figures 6.10 and 6.11) diverts the wind vectors and creates a barrier to the propagation of the concentrated gas surface.

Another effect of buildings on the configuration of the wind field is the irregularity of the 2,000 ppm concentrated cloud surface, parallel to the Boiler House wall (y axes direction on the image). This is due to the channelling of the wind between the two towers (as seen in the previous paragraph), causing the acceleration of the wind vectors, resulting in the cloud having this particular shape. When the channelling is caused by long lines of packed tall buildings (as in streets within cities) the effect is more marked than in this case and referred to as an 'urban canyon' (Pavageau and Schatzmann, 1999, Yamada, 2004).

In Figure 6.13, the distribution of the 15,000 ppm contour from the same simulation is displayed.

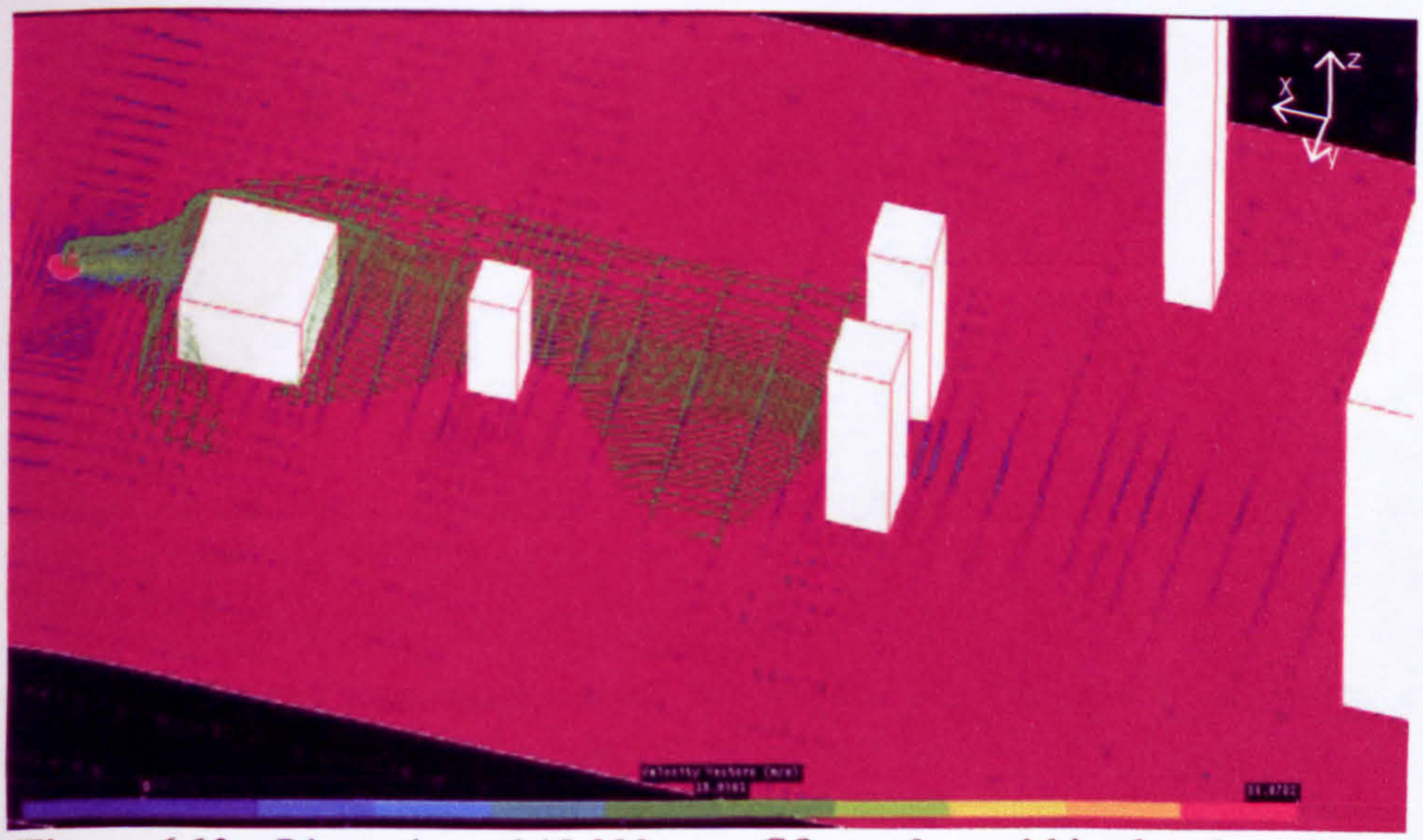

Figure 6.13 - Dispersion of 15,000 ppm CO_2 surface within the plant. The line representation of the cloud surface highlights the wind vectors of the jet release on the ground.

This picture does not provide further information about the dispersion of the gas as a direct consequence of the distortion of the wind field by the buildings. In the simulation considered, the 15,000 ppm cloud extended to a length of about 150 m although, as seen above, these values are only representative of potential occurrences. In any case, it is worth remembering that this concentration (15,000 ppm) has minor effects on people.

Also, the image illustrates how the concentration of interest follows the high speed flow soon after escaping the pipeline, broadening after encountering the upwind wall of the nearest building. This can be better understood by looking at Figure 6.14, where the dispersion of the concentration of 100,000 ppm within the simulation of interest is displayed. From the image, it can be judged how the surface considered is linked to the

wind field in the sector near the source, as it has been modelled by the CFD tool after the jet-release.

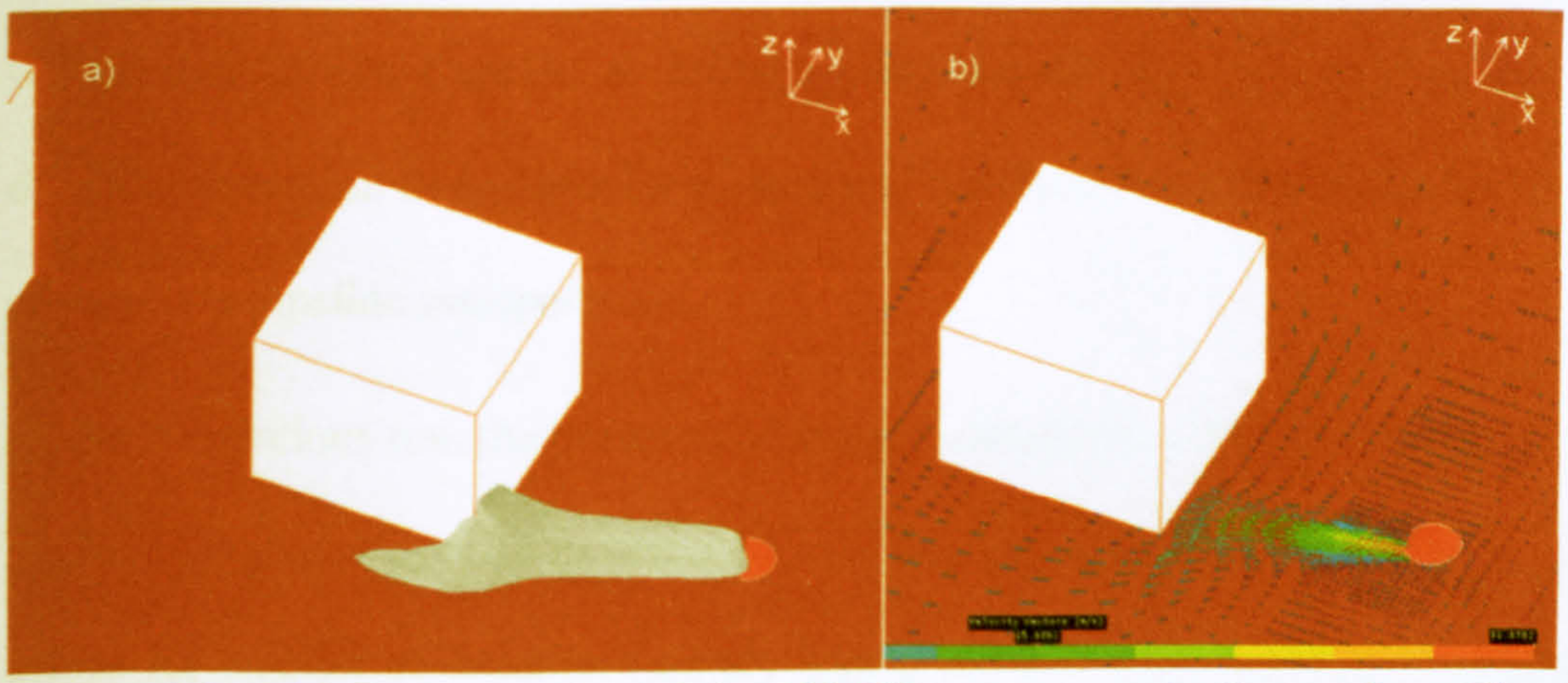

Figure 6.14 - (a) Representation of the 100,000 ppm concentration surface. The shape of the cloud is strictly dependent on the wind vectors (b) carrying the flow in the proximity of the source.

As explained in paragraph 6.2, the jet-mixing effect is more effective once the flow speed has decreased. In Figure 6.14, the building has little effect on the dispersion of the 100,000 ppm concentration, although it might have had if it had been closer to the source. The extent of this high concentration is about 30 m: thus, it may be of concern for the high speed created, the toxicity of the 100,000 ppm CO_2 cloud and the very cold temperature on the surrounding of the flow. Although these issues are with the remit of this study, where the principal goal has been the evaluation of the plume geometry in the built environment within a power plant, they would be of relevance when risk assessments are drawn up for particular cases, describing hazard situations that could directly involve employees.

6.2.4 Concluding remarks

The CFD tool for atmospheric dispersion modelling has been used to simulate the release of CO_2 within the characteristic environment of a hypothetical capture plant, where the Carbon Capture & Storage chain would start with the process of carbon dioxide separation from other by-products of combustion, before being sent to geological storage via pipeline transportation.

In the simulations run, the presence of major buildings has been directly accounted for. A surface roughness $z_0 = 1.5$ m was used over the remainder of the plant grounds in order to allow for smaller obstruction (mainly pipes, but also vehicles, containers, persons and other small obstacles).

Secondary exposures, such as carbon dioxide being drawn in by the ventilation system of offices, within the plant, have not been considered. In fact:

(a) The total amount of releasable gas and the leaking rate of CO_2 used in these simulations represent two reasonable values, not necessarily worst-case scenarios: the leak might be greater or less. Moreover, the actual dimensions of failures could be influenced by unpredictable outcomes such as the propagation of fractures on the surface of the facility due to the Joule-Thomson effect, during the leak.

(b) The jet-release flow speed, used in order to account for the jet-mixing effect, has not been validated experimentally: a higher speed would enhance the early dispersion of the gas (mainly for small leaks) while a near zero release speed would make concentration clouds longer by up to a factor of ten (see previous paragraphs).

(c) There is no definite plan of office locations in the plant layout presented in this section (Figure 6.8). However, even if there were offices in the Boiler House building the simulation results in this study would not predict a high level of risk.

The exercise conducted in this chapter has shown the reliability of CFD atmospheric dispersion models and the possibility of their application to specific cases where conditions (topographical, at least) are known and can be used as input parameters for simulating potential leak events.

CHAPTER 7

CONCLUSIONS

Carbon capture and storage (CCS) is often considered in the literature as one of the short-term technological solutions to control carbon dioxide emissions from large point sources. The European perspective on CCS seems favourable for the beginning of a large scale implementation of the technology, during the next decade. The build up of an extensive CO_2 transport infrastructure is foreseeable, including a large network of CO_2 pipelines over European on-shore territory. Part of this infrastructure is expected to be located near densely populated areas. Safety issues surrounding the operation of pipelines in these areas are expected to be more complex compared to current practice.

A review of Risk Assessments drawn up for the transportation of CO_2, in the literature, identifies important knowledge gaps regarding for instance the dispersion behaviour and modelling of supercritical CO_2 released into the atmosphere. Risk-related uncertainties pertain specifically to assumptions made by modellers before attempting to simulate potential releases (e.g. leaking rates, dispersion models used, distribution of populations surrounding a facility, pipeline diameter, pressure, temperature, pipeline material and thickness, CO_2 thermodynamic behaviour, etc.). In this work, most of these atmospheric modelling input data and population distribution approximations were taken from the Risk Assessment for CO_2 transportation, by DNV (Vendrig et al., 2003).

The main goal of this study has been the validation of Computational Fluid Dynamics modelling in assessing the dispersion of carbon dioxide, within transportation in CCS

projects. Fluidyn PANACHE is a Computational Fluid Dynamics software, developed solely for the purpose of atmospheric dispersion modelling. Its relative ease of use makes it a good choice for future CO_2 dispersion modelling. PANACHE has been validated against the Prairie Grass and Kit Fox field experiments, involving a total of about 100 trials. The statistical model performance evaluation method suggested by Hanna and Chang (2001) for the evaluation of atmospheric modelling software has been applied to the results: outcomes put the model performances well within the limits of acceptability for atmospheric dispersion software.

In the evaluation exercise, the average under-prediction of results within the simulations of most field dispersion trials was due to the natural extreme short-term variation in wind speed and direction during the field experiments. Maximum values represent short term peaks caused by the random accumulation of the gas, due to this natural variability, and do not influence much the total amount of toxic gas intake by a potential bystander (Figure 3.7). CO_2 is toxic above a certain threshold-concentration and during a prolonged exposure-time. It is evident that Computational Fluid Dynamics models may only under-predict results. Not accounting for processes leading to the generation of highly differentiated gas concentration in plumes over time and space, CFD tools give an accurate description of average gas concentration, omitting the naturally occurring short-term concentration peaks.

The model performances have been compared with the results of a Gaussian plume dispersion model (ALOHA 5.4). The latter also gave fairly good overall results. The basic knowledge needed for setting up model runs and the short computational times give these models priority over all other dispersion tools in accident situations, when

rapid responses are required for starting emergency procedures or alerting rescue teams. In any case, still from Figure 3.7, predictions by ALOHA for the trials KF0404 reflects the general tendency of this class of models towards an over-estimation of the total amount of gas in the atmosphere near an unintended release, when results are considered during a continuative period. In order to account for this, it has been suggested that the boundary values of performance ranges be lowered for two of the statistical measures (Fractional Bias, FB, and Geometric Mean Bias, MG) as defined by Hanna et. al. (1993, 2001, 2003 and 2004) for model acceptability measures, within the gas dispersion risk assessment context.

With the aim of providing an example of CFD application in the evaluation of the risk connected with the transportation of carbon dioxide, PANACHE has been used for calculating the distance covered by given concentrations of the gas after leaks from a hypothetical transportation system within the carbon capture and storage chain. Modular system technical characteristics, release parameters, assumptions and frequencies of leakages have been taken from the literature (DNV), with atmospheric conditions reflecting the most likely meteorological *situation over* the UK. CFD results were compared with Gaussian. Predictions from the two models have been found comparable and in line with the ones from the work of DNV. It must be pointed out, however, that in fact the CFD software gave for certain simulations downwind distances of up to one order of magnitude lower than the Gaussian tool. This is in line with what was discussed above about Gaussian over-estimations of gas concentration in the air at a distance from a source and overall amount of dispersing gas.

For the sake of completeness, a Fatality Risk evaluation for singular transportation systems has been drawn up. The severe restrictions and limitations described for this method of conducting Risk Assessments do not enable its validation and wider application. This limits the use of the results from Chapter 4 of this thesis for comparison purposes. A discussion about the EU choice to use results from DNV (Vendrig et al., 2003) for drawing a preliminary Impact Assessment is made below.

The potentials of a dry ice bank, created as a consequence of a downward leakage from a CCS transportation facility, in posing a risk to workers and the general public were considered. The energy balance at the surface of the bank, on a characteristic English summer day, gave different results for the subliming bank, dependent on the model used to evaluate the formation of a toxic CO_2 cloud. Although results from the CFD model being more reliable, the possibility of the formation of, and the risks posed by, a solid carbon dioxide deposit, should not be ignored.

In the near future, Risk Assessments in the establishing sector of CCS are expected to be made with the usage of advanced software, for evaluating potential events in complex environments. One of the crucial issues will be a clear understanding of the physical and physico-chemical behaviour of CO_2 after leaking in the atmosphere from a high pressure facility – i.e. there is a need to quantify the effects of the jet release on (a) the initial dilution of the waste gas once in the atmosphere, (b) conditions for its total or partial re-conversion to gas phase after the Joule-Thomson effect made a solid out of a leaked critical-state substance, and (c) the velocity and average temperature of the leaking flow. All this, in order to give atmospheric dispersion models valid input parameters for

estimating potential size of toxic concentrations within plumes created after an accidental leak from a CCS transportation facility.

The high speed release has been accounted for in Chapter 6. The assumptions made in choosing leakage parameters (such as the flow velocity soon after leaving the pipe) were reasonable. Downwind distances of toxic concentrations of CO_2 have been found to be up to three times lower when accounting for the high velocity of the release, and this is valid for a relatively low speed value (i.e. 49 m s^{-1}). However, results of this exercise suffer from the limitations affecting PANACHE when simulating the physico-chemical processes characteristic of CO_2 after a pressure drop, and should be considered as an attempt to compare two different methods of drawing up a Risk Assessment. The release velocity parameter represents one of the knowledge gaps cited above. The field experiment conducted in December 2008 in Barendrecht, Netherlands, presents strong qualitative similarities with releases modelled using the CFD tool.

The dispersion of gases in complex situations such as the case of buildings in close proximity is a difficult problem, but important for the safety of people living and working in such areas. This thesis has also dealt with a potential large CO_2 release within a capture-plant environment. It has been seen how the CFD model can predict the effect of the built environment on the wind field, and how this latter clearly affect the dispersion of the leaked gas.

7.1 European CCS deployment

Recognizing that human activities contribute significantly to climate change, the EU has adopted ambitious targets for reducing the emissions of greenhouse gases in the coming decades. These targets will not be achieved without significant reduction of CO_2 emissions from the energy sector, where the use of fossil fuels in power generation leads to approximately 40% of all CO_2 emissions in the EU. The WWF Living Planet 2008 report points out how a 20% carbon emission reduction by 2020 will not be sufficient for meeting the 2° C target for temperature stabilization, the threshold level for unacceptable risks, during this century (WWF, 2008).

To reclaim the reputation of leader in the fight against climate change, Europe needs to reduce emissions by 30% below 1990 levels by 2020 and by up to 70-90% by 2050. Funds will also need to be provided to developing nations for them to achieve emissions reductions equivalent to a further 15 per cent of Europe's level of emissions. Deployment of CCS for hydrocarbon power generation, in parallel with the production of renewable energies, is the only way to meet the target for temperature stabilization.

Clearly, public opinion is of paramount importance in the development and deployment of a technology that would help to stabilize climate change, offer thousands of high-skilled job opportunities but that, at the same time, would pose a certain risk for the general public. The Commission of the European Communities edited in the recent past a compilation of documents describing the climate policing situation in the EU, the efforts Europe is intended to observe in the battle against climate change and the urgent need for an early deployment of carbon capture and storage. Aiming at an introduction of the technology to members of the general public, regional scale administrators and policy

makers, the Commission compiled an Impact Assessment on CCS (EU, 2008a), particularly focussing on the transportation of carbon dioxide. For this work, the CEC also used the results from the risk analysis report by DNV (Vendrig et al., 2003). For the post-2020 scenario, each of the four options studied (described in paragraph 1.2.3.2) gave by 2030 an accidental release rate of CO_2 of up to 0.83 Mt yr^{-1}, with the consequent fatality risk of up to 4.4 persons per year, based on Gaussian modelling. Among other things, this Ph.D. thesis has demonstrated how a Risk Assessment drawn following results from Gaussian models can over-estimate the risk in a way not favourable when furthering the widespread introduction of the technology. The over-simplification induced by not accounting for the high speed of a leaked-gas flow, and the consequent analysis of the risks posed by consideration of the downwind distance covered by high concentration of the gas, is an over-conservative methodology. A more reliable Risk Analysis for CCS over European territories, and that could be generally applicable, is hoped within the next years.

7.2 Suggestions for future work

In this thesis, different issues have been examined from a generic point of view. Due to the lack of site-specific cases, the research was aimed to clarify the differences in expected risks using diverse methodologies and assumptions. Once CCS is introduced on a wider scale, the transportation of carbon dioxide will be of primary concern and pipeline routes will be decided, based on balanced estimations of costs and risks for populations. Based on available data of failure frequencies, also presented in this work, a matter of concern will be the location of surface modules of transportation systems (i.e.

booster stations), accounting for the topography of areas examined for this purpose. The CFD model is capable of considering topographical effects of specific areas on the dispersion of dense gases such as CO_2.

The Kyoto Protocol mechanism of carbon trading allows operators that have not used up their quotas to sell their unused allowances as carbon credits. Under this trading scheme, industries with potentially large environmental impacts in terms of greenhouse gas emissions (e.g. energy providers) will find early application of CCS to be more profitable, since this will allow more carbon credits to be accrued. In this way, a number of capture-ready power plants can be expected to start separating CO_2 and sending it to storage in a relatively short time. Risk assessments within the built environment of industries will be of importance, as stated in Chapter 6 of this thesis. With the safety of employees in mind, the application of CFD atmospheric dispersion modelling to specific plant sites can provide important help in the planning of ad hoc emergency routes, in case of large releases from installations.

Alberto Mazzoldi

10.03.2009, University of Nottingham

References

ACKERMAN, F. & STANTON, E. (2006) Climate Change – the Costs of Inaction. Tufts, Global Development and Environment Institute, Tufts University, http://ase.tufts.edu/gdae/Pubs/rp/Climate-CostsofInaction.pdf.

AIR-LIQUID (2000) CO2 ; Carbon dioxide CAS Number : 124-38-9; Physico-chemical properties Group, AIR LIQUID (Ed.) *WEB page: http://encyclopedia.airliquide.com/encyclopedia.asp?GasID=26*. Paris.

ALDHOUS, P. (2004) Land remediation: Borneo is burning. *Nature,* 432, http://www.nature.com/nature/journal/v432/n7014/full/432144a.html, doi:10.1038/432144a, 144-146.

AMORINO, C., BENCINI, R., CARA, R., CINTI, D., DERIU, G., FANDINÒ, V., GIANNELLI, A., MAZZOTTI, M., OTTIGER, S., PIZZINO, L., PINI, R., QUATTROCCHI, F., SARDU, R. G., STORTI, G. & VOLTATTORNI, N. (2005) CO2 geological storage by ECBM techniques ; the Sulcis area. *Second International Conference on Clean Coal Technologies for our Future.* Castiadas (Cagliari), Sardinia, Italy; http://www.iea-coal.org.uk/publishor/system/component_view.asp?LogDocId=81308&PhyDocId=5697.

ASTM (2000) Standard guide for statistical evaluation of atmospheric dispersion model performance. West Conshohocken, PA, American Society for Testing and Materials, Designation: D 6589-00

ATKINS, P. W. (1981) *Chimica Fisica,* Bologna. ISBN: 0 306 40800 7, Zanichelli.

BARAD, M. L. (1958) Project Prairie Grass, a field program ; diffusion. *Geophys. Res.*. Vol. I and II, Air Force Cambridge Research Center, AFCRC-TR-58-235.

BARRIE, J., BROWN, K., HATCHER, P. R. & SCHELLHASE (2004) Carbon dioxide pipelines: a preliminary review of design and risks. Fluor (Ed.) Calgary.

BELL, R. (1978) Isopleth Calculations for Ruptures in Sour Gas Pipelines. *Energy/Processing/Canada,* 71, 36-39.

BENNETT, T. J. (1982) A coupled atmosphere-sea-ice model study of the role of sea ice ; climatic predictability. *Journal of Atmospheric Science,* 39, 1456-1465.

BIRD LIFE INTERNATIONAL (2006) Bio-energy: dream or nightmare for biodiversity? *World Birdwatch* http://www.birdlife.org/news/features/2006/06/biofuels.html.

BLUETT, J., GIMSON, N., FISHER, G., HEYDENRYCH, C., FREEMAN, T. & GODFREY, J. (2004) Good Practice Guide for Atmospheric Dispersion Modelling. Environment, New Zeland Ministry (Ed.) Wellington, National Institute of Water and Atmospheric Research, Aurora Pacific Limited and Earth Tech Incorporated ISBN: 0-478-18941-9.

BRIGGS, G. A. (1982) Similarity forms for ground-source surface-layer diffusion. *Bound. Layer Meteorol.*, 23, 489-502. ISSN: 0006-8314

BRIGGS, G. A. (1988) Analysis of diffusion field experiments. Venkatram, A. & Wyngaard, J.C. (Eds.) *Lectures on Air Pollution Modelling.* Boston, Amer. Meteor. Soc.

BRITTER, R. E. (1979) The spread of a negatively buoyant plume ; a calm environment. *Atmospheric Environment* 13, 1241-47.

BRITTER, R. E. (1989) Atmospheric dispersion of dense gases. *Annual Review Fluid Mechanics,* 21, 317-344.

BRITTER, R. E. & MCQUAID, J. (1988) Workbook on the dispersion of dense gases. *Health & Safety Executive contract research.* Sheffield, UK., Health & Safety Report no. 17/1988.

BUCK, A. L. (1981) New equations for computing vapor pressure and enhancement factor. *J. Appl. Meteorol.*, 20, 1527-1532.

BURGHERR, P. & HIRSCHBERG, S. (2005) Comparative Assessment of Natural Gas Accident Risks. Institut, Paul Scherrer (Ed.) *http://www.dgc.dk/nyhedsservice/pdf/accident_risks.pdf.*

BURMAN, J. (1998) An evaluation of topographical effects on neutral and heavy-gas dispersion with a CFD model. *Wind Engineering and Industrial Aerodynamics,* 74-76, 315-325.

CAHILL, A. & PARLANGE, M. (1998) On water vapor transport ; field soils. *Water Resources Research,* 34, 731-739.

CANADELL, J. G., LE QUERE, C., RAUPACH, M. R., FIELD, C. B., BUITENHUIS, E. T., CIAIS, P., CONWAY, T. J., GILLETT, N. P., HOUGHTON, R. A. & MARLAND, G. (2007) Contributions to accelerating atmospheric CO2 growth from economic activity, carbon intensity, and efficiency of natural sinks. William C. Clark, Harvard University (Ed.) *Sustainability Science.* Cambridge, Global Carbon Project, Australia; School of Environment Sciences, University of East Anglia, Norwich UK; British Antarctic Survey, Cambridge, UK; Department of Global Ecology, Washington; International Institute for Applied Systems Analysis, Laxenburg, Austria. 0702737104/DC1.

CAPP (2002) Recommended Practice for Mitigation of Internal Corrosion ; Sweet Gas Gathering Systems. Calgary, Canadian Association of Petroleum Producers. 2002-0013.

CARSLAW, H. S. & JAEGER, J. C. (1959) *Conduction of Heat ; Solids,* London. ISBN 0198533683.

CAVALIERI, D. J., PARKINSON, C. L. & VINNIKOV, K. Y. (2003) 30-year satellite record reveals contrasting Arctic and Antarctic decadal sea ice variability. *Geophysical Research Letters,* doi:10; GL018031.

CHANG, J. C. (1998) Evaluation of VLSTRACK with the Prairie Grass Field Data. University, George Mason (Ed.) Fairfax, Institute of Computational Science and Informatics.

CHANG, J. C. & HANNA, S. R. (2004) Air quality model performance evaluation. *Meteorology and Atmospheric Physics,* 87, 167-196. DOI: 10.1007/s00703-003-0070-7.

COLENBRANDER, G. W. (1980) A Mathematical Model for the Transient Behaviour of Dense Vapour Clouds. *3rd International Symposium on Loss Prevention and Safety Promotion ; the Process Industry.* Basel, Switzerland.

CROWLEY, T. J. (2000) Causes of Climate Change Over the Past 1000 Years. *Science,* 289, 270-277 DOI: 10.1126/science.289.5477.270.

DAI, A., FUNG, I. Y. & GENIO, A. D. D. (1997) Surface observed global land precipitation variations during 1900-1988. *J. Climate* 10 2943-2962. doi:10.1175/1520-0442(1997)010<2943.

DEVAULL, G. E., KING, J. A., LANTZY, R. J. & FONTAINE, D. J. (1995) *Understanding atmospheric dispersion of accidental releases,* New York. ISBN: 0816906815.

DHARMAVARAM, S., HANNA, S. R. & HANSENC, O. R. (2005) Consequence Analysis—Using a CFD Model for Industrial Sites. *Process Safety Progress,* 24, 316-327.

DOS SANTOS, G. H. & MENDES, N. (2003) Unsteady combined heat and moisture transfer ; unsaturated porous soils. Pontificial Catholic University of Parana', R. Inculada Conceição (Ed.) Curitiba, Brazil. 80.215-901.

E.P.A. (1999) Risk Management Program Guidance For Offsite Consequence Analysis. Washington DC, U.S. Environmental Protection Agency; EPA-550-B-99-009.

ENGEBØ, A., NILSEN, S., KIRCHSTEIGER, C., PERRETTE, L., MERAD, M. & ANDERSEN, H. B. (2007) Bienal report on Hydrogen Safety. Det Norske Veritas, Hydro, JRC, INERIS, Risoe; http://www.hysafe.org/download/1199/BRHS_Chap4_V1p2.pdf.

EPSTEIN, P. R. & MILLS, E. (2005) Climate Change Futures: Health, Ecological and Economic Dimensions. Mills, Paul R. Epstein and Evan (Ed.) United Nationa Development Program, The Center for Health and the Global Environment. Harvard Medical School, http://chge.med.harvard.edu/programs/ccf/documents/ccf_report_oct_06.pdf.

ERNSTING, A. (2007) Agrofuels in Asia: Fuelling poverty, conflict, deforestation and climate change. *Seedling,* http://www.grain.org/seedling_files/seed-07-07-4-en.pdf, 25-33.

EU (2007) Presidency Conclusions – Brussels, 8/9 March 2007. Brussels, European Council, 7224/1/07 REV 1.

EU (2008a) Accompanying document to the proposal for the "Directive of the European Parliament and of the Council on the geological storage of carbon dioxide - Impact Assessment". Brussels, Commission of the European Communities. http://ec.europa.eu/environment/climat/ccs/pdf/ccs_ia_jan2008.pdf.

EU (2008b) Communication from the Commission to the European Parliament, the Council the European Economic and Social Committee and the Committee of the Regions. Supporting early demonstration of Sustainable Power Generation from Fossil Fuels. Brussels, Commission of the European Communities, http://ec.europa.eu/energy/climate_actions/doc/2008_co2_comm_en.pdf.

F.E.M.A. (1989) Handbook of Chemical Hazard Analysis Procedures, Appendix B. Federal Emergency Management Agency. Washington DC, U.S. Dept. of Transportation, and U.S. Environmental Protection Agency; (312) 972-3275

GALE, J. (2001) Transmission of CO2: Experience to be Gained from CO2/EOR Projects. *CO2 NET Meeting.* Copenhagen, 6-7 June 2001, IEA Greenhouse Gas R&D Programme.

GALE, J. & DAVISON, J. (2004) Transmission of CO2--safety and economic considerations. *Energy,* 29, 1319-1328.

GIFFORD, F. A., JR. (1976) Turbulent diffusion – typing schemes: a review. *Nuclear Safety,* 17, 68-86.

GRANT, S. A. (2001) Expected Cost Effect of Increasing the Size of a Frozen-Ground Waste Containment Project at Ft. Detrick, Maryland. *Cold Regions Research and Engineering Laboratory,* ERDC/CRREL TN-01-1 US Army Corps of Engineers.

GREENPEACE (2006) The Seveso disaster 30 years on: lessons learned for EU policy. Media Briefing, 6 July; http://www.greenpeace.org/raw/content/eu-unit/press-centre/policy-papers-briefings/the-seveso-disaster-30-years-o.pdf.

GRIFFITHS, R. F. (1991) Research Requirements ; Major Hazards Risk Analysis. *Risk Analysis,* 11, 399-494.

GRONKVIST, S., MOLLERSTEN, K. & PINGOUD, K. (2006) Equal opportunity for Biomass ; Greenhouse gas accounting for CO2 Capture and Storage: a step towards more cost-effective climate change mitigation regimes. *Mitigation and Adaptation Strategies for Global Change,* 11, 1083–1096, DOI: 10.1007/s11027-006-9034-9.

HAINES, M. (2006) Supercritical $_{CO2}$ atmospheric dispersion modelling. mike@ieaghg.org. Personal communication. Cheltenham.

HANNA, S., BRIGGS, G. & RAYFORD, H. (1982) Handbook on Atmospheric Diffusion. D.O.E. (Ed.), U.S. Dept of Energy, Technical Information Centre. DE82002045(DOE/TIC-11223).

HANNA, S. R. (2003) Overview of atmospheric transport and dispersion modelling. *Tracking and predicting the atmospheric dispersion of hazardous material releases: implication of homeland security.* Harvard School of public Health, Boston. http://books.nap.edu/openbook.php?record_id=10716&page=69.

HANNA, S. R. & CHANG, J. C. (2001) Use of the Kit Fox field data to analyze dense gas dispersion modelling issues. *Atmospheric Environment,* 35, 2231-2242, PII: S1352-2310(00)00481-7.

HANNA, S. R., CHANG, J. C. & STRIMAITIS, D. G. (1993) Hazardous gas model evaluation with field observations. *Atmos. Environ.,* 27, 2265-2285. ISSN: 1352-2310

HANNA, S. R., HANSEN, O. R. & DHARMAVARAM, S. (2004) FLACS CFD air quality model performance evaluation with Kit Fox, MUST, Prairie Grass and EMU observations. *Atmospheric Environment,* 38, 4675-4687, doi:10.1016/j.atmosenv.2004.05.041.

HANSSON, K., SIMUNEK, J., MIZOGUCHI, M., LUNDIN, L. & VAN GENUCHTEN, M. T. (2004) Water Flow and Heat Transport ; Frozen Soil: Numerical Solution and Freeze–Thaw Applications. *Vadose Zone Journal,* 3, 693-704.

HEAVNER, B., ZUGEL, M. & JACOBSON, D. (2001) Affordable, reliable, renewables. The pathway to california's sustainable energy future. Trust, CALPIRG Charitable (Ed.) Sacramento,

http://www.environmentcalifornia.org/uploads/Lr/O9/LrO9hHsD_ya-QPvwbLjnrw/Affordable_Reliable_Renewables.pdf.

HIRAIWA, Y. & KASABUCHI, T. (2000) Temperature dependence of thermal conductivity of soil over a wide range of temperature (5°-75°C). *European Journal of Soil Science,* 51, 211-218.

HIRSCHBERG, S., BURGHERR, P., SPIEKERMAN, G. & DONES, R. (2004) Severe accidents in the energy sector: comparative perspective. *Journal of Hazardous Materials,* 111, 57-65.

HOLLOWAY, S. (2001) Storage of fossil fuel-derived carbon dioxide beneath the surface of the Earth. *Annu. Rev. Energy Environment,* 26, 145-166.

HORST, T. W. (1979) Lagrangian similarity modeling of vertical diffusion from a ground-level release. *J. Applied Meteorol.,* 18, 733-740.

HOUGHTON, J. T., DING, Y., GRIGGS, D. J., NOGUER, M., VAN DER LINDEN, P. J., DAI, X., MASKELL, K. & JOHNSON, C. A. (2001) Climate Change 2001: the scientific basis. *IPCC Report 2001.* Cambridge, UK, and N.Y., USA., Cambridge University Press.

HSE (2001) *Reducing risk, protecting people*, Health and Safety Executive ISBN 0 7176 2151 0.

HSE (2005) List of approved Workplace exposure limits (as consolidated with amendements October 2007) - EH40/2005. HSE, Health and Safety Commission.

HSE (2008) PADHI (Planning Advice for Developments near Hazardous Installations). *HSE's Land Use Planning Methodology.* http://www.hse.gov.uk/landuseplanning/padhi.pdf.

IDSO, S. B. & JACKSON, R. D. (1969) Thermal radiation from the atmosphere. *J. Geophys. Res.*, 5397-5403.

IEA (2001) IEA World Energy Outlook, 2001 Insights. IEA/OECD (Ed.) Paris; http://www.iea.org/textbase/nppdf/free/2000/weo2001.pdf.

IEA (2003) Barriers to overcome in implementation of CCS: Rules and standards for the transmission and storage of CO_2. Iinternational Energy Agency Greenhouse Gas R&D Programme. PH4/23.

IPCC (1995) Second Assessment Synthesis of Scientific-Technical Information relevant to interpreting Article 2 of the UN Framework Convention on Climate Change. Intergovernmental Panel on Climate Change, http://www.ipcc.ch/pdf/climate-changes-1995/2nd-assessment-synthesis.pdf.

IPCC (2001) Climate Change 2001: the scientific basis. Press, Cambridge University (Ed.) *IPCC Technical Papers.* Cambridge, Intergovernmental Panel on Climate Change ISBN: 92-9169-104-7.

IPCC (2005) *Special Report on Carbon dioxide Capture and Storage,* New York, Cambridge University Press. ISBN: 92-9169-119-4.

IPCC (2007a) Climate Change 2007: Mitigation. Contribution of Working Group III to the Fourth Assessment Report of the Intergovernmental Panel on Climate Change. B. Metz, O.R. Davidson, P.R. Bosch, R. Dave, L.A. Meyer University Press (Ed.) *IPCC Assessment Reports.* Cambridge, UK and New York, NY, USA, Itergovernmental Panel on Climate Change. ISBN 978-0-521-88011-4; http://www.ipcc.ch/pdf/assessment-report/ar4/wg3/ar4-wg3-frontmatter.pdf.

IPCC (2007b) Climate Change 2007: Synthesis Report. Summary for Policymakers. *IPCC Assessment Reports.* Valencia, Spain, Intergovernmental Panel on Climate Change, http://www.ipcc.ch/pdf/assessment-report/ar4/syr/ar4_syr_spm.pdf.

JACOBS, J. D. (1978) Radiation climate of Broughton Island: Energy budget studies ; relation to fast-ice breakup processes ; Davis Strait: occasional paper. Jacobs, Eds. (Ed.) Boulder, Colorado, University of Colorado, U.S.A.

JELEMENSKY, L., HARISOVA, J., MOLNAR, A. & MARKOS, J. (2003) Reliable risk estimation ; the Risk Analysis of chemical industry; Case study: Ammonia storage pressurized spherical tank. *Chem. Papers* 58, 48-54; http://www.sappress.sk/chempapers/58-01-08.pdf.

KAARSTAD, O. & HUSTAD, C. W. (2003) Delivery of carbon dioxide to Gullfaks. Fredericia, Denmark., Kinder Morgan CO_2 Company L.P., Elsam A/S, New Energy Statoil - http://www.co2.no/download.asp?DAFID=17&DAAID=6.

KARL, T. R., CHRISTY, J., SANTER, B., WENTZ, F., SEIDEL, D., LANZANTE, J., TRENBERTH, K., EASTERLING, D., GOLDBERG, M., BATES, J. & MEARS, C. (2002) Understanding recent atmospheric temperature trends and reducing uncertainties. ISeries Program, US Climate Change Science (Ed.) *Strategic Plan for the Climate Change Science Program.* Washington, DC, http://www.climatescience.gov/Library/stratplan2003/temptrends-wp-26nov2002.pdf.

KEELING, C. D., CHIN, J. F. S. & WHORF, T. P. (1996) Increased activity of northern vegetation inferred from atmospheric CO2 measurements. *Nature,* 382, 146–149.

KELLY, A. & GOULDEN, M. (2008) Climate Change Caused Widespread Tree Death ; California Mountain Range, Study Confirms. *ScienceDaily,* http://www.sciencedaily.com/releases/2008/08/080811195317.htm.

KLAPP, J., SIGALOTTI, G., GALINDO, S. & SIRA, E. (2005) Two-dimensional treesph simulations of choked flow systems. *Revista Mexicana de fisica* 51 563–573.

KOIVUSALO, H., HEIKINHEIMO, M. & KARVONEN, T. (2001) Test of a simple two-layer parameterisation to simulate the energy balance and temperature of a snow pack. *Theoretical Applied Climatology,* 70, 65-79.

KOIVUSALO, H. & KOKKONEN, T. (2002) Snow processes ; a forest clearing and ; a coniferous forest. *Journal of Hydrology,* 262, 145-164. PII: S0022-1694(02)00031-8.

KOORNNEEF, J., SPRUIJT, M., MOLAG, M., RAMIREZ, A., FAAIJ, A. & TURKENBURG, W. (2008) Uncertainties ; risk assessment of CO2 pipelines. *9th International Conference on Greenhouse Gas Control Technologies, 16-20 November 2008.* Washington D.C., Elsevier.

KOUTSOURAKIS, N., VLACHOGIANNIS, D., SFETSOS, A. & BARTZIS, J. G. (2003) CFD in atmospheric dispersion problems - state of the art. *A Thematic Network For Quality and Trust in the Industrial Application of CFD,* 2, 10-13.

KRUSE, H. & TEKIELA, M. (1996) Calculating the consequences of a CO2-pipeline rupture. *Energy Conversion,* 37, 1013-1018.

KUIJPER, M. (2008) MER Ondergrondse opslag van CO_2 in Barendrecht. Den Haag, Shell CO_2 Storage B.V. EP200809225671; http://www-static.shell.com/static/nld/downloads/co2/mer_rapport_2.pdf.

KUNDU, P. K. & COHEN, I. M. (2004) *Fluid Mechanics; Third Edn.*, New York, Elsevier Academic Press. ISBN: 9780121782535.

KUPREWICZ, R. (2007) Observation on practical: Leak Detection for Transmission Pipelines - an experienced perspective. *Pipeline Safety Trust.* Alaska state, Accufacts Inc. http://pstrust.org/library/docs/leak_detection_paper.pdf.

LAMBECK, K. & CHAPPELL, J. (2001) Sea level change through the last glacial cycle. *Sciance,* 292, 679-686.

LANGFORD, N. J. (2005) Carbon Dioxide Poisoning. *Toxicological Reviews,* 24, 229-235. url = "http://www.ingentaconnect.com/content/adis/txr/2005/00000024/00000004/art00003".

LAUNIAINEN, J. & CHENG, B. (1998) Modelling of ice thermodynamics ; natural water bodies. *Cold Regions Science and Technology* 27, 153-178; PII S0165-232X(98)00009-3.

LEGGETT, J. (2000) *The Carbon War: Dispatches from the End of the Oil Century*, London, Penguin Books, ISBN: 071399360X.

LI, Z., DONG, M., LI, S. & HUANG, S. (2006) CO2 sequestration ; depleted oil and gas reservoirs—caprock characterization and storage capacity. *Energy Conversion Management,* 47 1372–1382, doi:10.1016/j.enconman.2005.08.023.

LORENZONI, I. & PIDGEON, N. F. (2006) Public views on climate change: European and U.S.A. perspectives. *Climatic Change,* 77; DOI: 10.1007/s10584-006-9072-z, pp 73-95

LUMB, F. E. (1964) The influence of cloud on hourly amounts of total radiation on the sea surface. *Quarterly Journal of the Royal Meteorological Society,* 90, 43-56.

LUND, J. W. & FREESTON, D. H. (2000) World-wide direct uses of geothermal energy, 2000. *Geothermics,* 30, 29-68, doi:10.1016/S0375-6505(00)00044-4

MACDONALD, M., JONES, J. A., GRIFFITHS, R. F. & NELSON, N. (2004) Guidelines for the Preparation of Dispersion Modelling Assessments for Compliance with Regulatory Requirements – an Update to the 1995 Royal Meteorological Society Guidance. Committee, UK Atmospheric Dispersion Modelling Liaison (Ed.) *Contract reports for ADMLC.* Reading, ADMLC, DMUG, University of Manchester ADMLC. http://www.admlc.org.uk/model_guidelines/documents/ADMLC-2004-3.pdf.

MARSH, K. N. (1987) Enthalpy of vaporization of water. Recommended Reference Materials for the Realization of Physicochemical Properties,. Editions, Martull (Ed.) Blackwell, Oxford. http://www2.bren.ucsb.edu/~dturney/WebResources 13/WaterSteamIceProperties/EnthalpyOfVaporizationH2O.pdf.

MAZZOLDI, A., HILL, T. & COLLS, J. J. (2007) CO2 transportation for carbon capture and storage: Sublimation of carbon dioxide from a dry ice bank. *International journal of greenhouse gas control,* 2, 210-218.

MAZZOLDI, A., HILL, T. & COLLS, J. J. (2008) CFD and Gaussian atmospheric dispersion models: a comparison for leakages within carbon dioxide transportation and storage facilities. *Int. J. Atmospheric Environment,* 42, DOI: 10.1016/j.atmosenv.2008.06.038.

MINTZER, I. M. (1990) Energy, Greenhouse gases and climate change. *Annual Reviews, Energy 1990,* 15, 513-550,

http://arjournals.annualreviews.org/doi/pdf/10.1146/annurev.eg.15.110190.002501.

MONTEITH, J. L. & UNSWORTH, M. H. (1990) Radiation Environment. . ISeries Arnold., E. (Ed.) *Principles of Environmental Physics.* London, Hodder and Stoughton Limited; ISBN-13: 9780713129311

MPS (2008) The Environmental Audit Committee appointed by the House of Commons: Reaching an international agreement on climate change. *Reports of Session 2007–08.* London, House of Commons. Report number: HC 355.

MUELLER, M. & WALLACE, R. (2008) Enabling science and technology for marine renewable energy. *Energy Policy,* 36, 4376-4382, DOI: 10.1016/j.enpol.2008.09.035

NASA (2002) Global Warming. *The Earth Science Enterprise Series.* Greenbelt, Maryland 20771 Goddard Space Flight Center, NF-222 http://www.gsfc.nasa.gov.

OCHSNER, T., HORTON, R. & REN, T. (2001) A New Perspective on Soil Thermal Properties. *Soil Science American Society Journal* 65, 1641-1647.

OLDENBURG, C. M. & UNGER, A. J. A. (2004) Coupled Vadose Zone and Atmospheric Surface-Layer Transport of Carbon Dioxide from Geologic Carbon Sequestration Sites. *Vadose Zone Journal,* 3, 848-857. ISSN: 1539-1663.

OPPENHEIMER, M. & TODOROV, A. (2006) Global Warming: the psychology of long term. *Climate Change,* 77, 1-6; DOI: 10.1007/s10584-006-9086-6.

ORSINI, A., CALZOLARI, F., GEORGIADIS, T., LEVIZZANI, V., NARDINO, M., PIRAZZINI, R., RIZZI, R., SOZZI, R. & TOMASI, C. (2000) Parameterisation of surface radiation flux at an Antarctic site. *Atmospheric Research,* 54, 245-261. PII: S0169- 8095(00)00047-8.

OVERDUIN, P. P., KANE, D. L. & VAN LOON, W. K. P. (2006) Measuring thermal conductivity ; freezing and thawing soil using the soil temperature response to heating. *Cold Regions Science and Technology,* 45, 8-22.

PARKINSON, C. L. & WASHINGTON, W. M. (1979) A large-scale numerical model of sea ice. *Journal of Geophysical Research,* 84, 311-337.

PASQUETTO, S. & PATRONE, L. (1994) Comportamento della materia allo stato gassoso. ISeries S.p.A., Masson (Ed.) *Chimica Fisica 2.* Milano.

PASQUILL, F. (1961) The estimation of the dispersion of windborne material. *Meteorology,* 90, 33-49.

PAVAGEAU, M. & SCHATZMANN, M. (1999) Wind tunnel measurements of concentration fluctuations ; an urban street canyon. *Atmospheric Environment,* 33, 3961-3970; PII:S1352-2310(99)00138-7.

PEARSON, P. N. & PALMER, M. R. (2000) Atmospheric carbon dioxide concentrations over the past 60 million years. *Nature,* 406, 695–699.

PERRY, R. H. & GREEN, D. W. (1997) *Perry's Chemical Engineers' Handbook,* McGraw-Hill.

PERRY, R. H., GREEN, D. W. & MALONEY, J. O. (1984) *Perry's chemical engineers' handbook,* London, McGraw-Hill.

PETERS-LIDARD, C. D. (1997) The Effect of Soil Thermal Conductivity Parameterization on Surface Energy Fluxes and Temperatures. *Journal of the Atmospheric Sciences:,* 55, 1209–1224.

PINE, J., SAJO, E. & EAST, R. (1998) An Assessment of the Transportation of Extremely Hazardous Substances for the Calcasieu and Southern Mississippi River Corridors. *Technical report for the Louisiana State Police* LSU Institute for Environmental Studies, LSU Nuclear Science Center, UII: 431-9537-g.

PLASYNSKI, S. I. & BECKERT, H. (2008) Lake Nyos and Mammoth Mountain: What Do They Tell Us about the Security of Engineered Storage of CO_2 Underground? Pittsburgh, Morgantown, U.S. Department Of Energy, Office of fossil energy. http://www.netl.doe.gov/publications/factsheets/program/Prog064.pdf.

PULLENA, J., BORIS, J. P., YOUNG, T., PATNAIK, G. & ISELIN, J. (2005) A comparison of contaminant plume statistics from a Gaussian puff and urban CFD model for two large cities. *Atmospheric environment,* 39, 1049-1068.

PUTKONEN, J. (2003) Determination of Frozen Soil Thermal Properties by Heated Needle Probe. *Permafrost and periglacial processes,* 14, 343-347.

QUAAS, J., BOUCHER, O., DUFRESNE, J.-L. & TREUT, H. L. (2004) Impacts of greenhouse gases and aerosol direct and indirect effects on clouds and radiation ; atmospheric GCM simulations of the 1930–1989 period. *Climate Dynamics,* 10; 10.1007/s00382-004-0475-0.

RAUPACH, M. R., MARLAND, G., CIAIS, P., QUERE, C. L., CANADELL, J. G., KLEPPER, G. & FIELD, C. B. (2007) Global and regional drivers of accelerating CO2 emissions. *Proceedings of the National Academy of Science,* 104, 10288–10293. doi:10.1073pnas.0700609104: http://www.pnas.org/content/104/24/10288.full.pdf+html.

REYNOLDS, R. M. (1992) ALOHA™ 5.0, Theoretical description. Seattle, Washington, National Oceanic and Atmospheric Administration. NOS ORCA-65; http://orise.orau.gov/emi/emisec/hazard-assess/files/resources/ALOHA-Theoretical-Description.pdf.

RIDDLE, A., CARRUTHERS, D., SHARPE, A., MCHUGH, C. & STOCKER, J. (2004) Comparison between FLUENT and ADMS for atmospheric dispersion modelling. *Atmospheric Environment,* 38, 1029-1038. doi: 10.10.1016/j.atmosenv.2003.10.052.

ROBYE, T., NICHOLAS, H. & BARRY, H. (2002) Quantifying the risks associated with a CO_2 sequestration pipeline. Australia - http://64.233.183.104/search?q=cache:d2OGjOPoR2YJ:https://extra.co2crc.com.au/modules/pts2/download.php%3Ffile_id%3D950%26rec_id%3D368+Quantifying+the+risks+associated+with+a+CO2+sequestration+pipeline.+Australia.&hl=en&ct=clnk&cd=1&gl=uk.

ROGERS, G. F. C. & MAYHEW, Y. R. (1980) *Engineering thermodynamics work and heat transfer,* Essex, UK ISBN-10: 0582305004 Logman Group Ltd.

ROGIE, J. D., KERRICK, D. M., SOREY, M. L., CHIODINI, G. & GALLOWAY, D. L. (2001) Dynamics of carbon dioxide emission at Mammoth Mountain, California. *Earth and Planetary Science Letters,* 188, 535-541; doi:10.1016/S0012-821X(01)00344-2

ROTHROCK, D. A., YU, Y. & MAYKUT, G. A. (1999) Thinning of the Arctic Sea-Ice Cover. *Geophysical Research Letters* 26 (23), 3469-3472; 00948276/99/199GL900000.

SARAF, S. R. & MELHEM, G. A. (2005) Modeling LNG pool spreading and vaporization. *AIChE Spring Meeting.* Mosaic Corporation, Atlanta, GA. http://archives1.iomosaic.com/whitepapers/LNG%20-%20Pool%20Spreading%20and%20Vap.pdf

SCARGIALI, F., DI RIENZO, E., CIOFALO, M., GRISAFI, F. & BRUCATO, A. (2005) Heavy gas dispersion modelling over a topographically complex mesoscale - a CFD based approch. *Trans IChemE - Process Safety and Environmental Protection,* 83, 242-256.

SCHWARTZ, P. & RANDALL, D. (2003) An Abrupt Climate Change Scenario and Its Implications for United States National Security GBN (Ed.) U.S., Global Business Network, DOI:10.1111/j.1749-8198.2007.00066.

SCRIPPS (2009) Keeling curve lessons: lessons for long-term earth observations. *Scripps CO_2 program,* http://scrippsco2.ucsd.edu/program_history/keeling_curve_lessons.html.

SEIERSTEN, M. (2001) Material selection for separation, transportation and disposal of CO_2. *Proceedings Corrosion 2001.* paper 01042., National Association of Corrosion Engineers.

SIEGENTHALER, U., STOCKER, T. F., MONNIN, E., LUTHI, D., SCHWANDER, J., STAUFFER, B., RAYNAUD, D., BARNOLA, J. M., FISCHE, H. & MASSON-DELMOTTE, V. (2005) Stable Carbon Cycle–Climate Relationship During the Late Pleistocene. *Science,* 310, 1313–1317; DOI: 10.1126/science.1120130.

SKLAVOUNOS, S. & RIGAS, F. (2004) Validation of turbulence models ; heavy gas dispersion over obstacles. *Hazardous Materials,* A108 (2004), 9-20. doi:10.1016/j.jhazmat.2004.01.005.

SKOVHOLT, O. (1993) CO2 transportation System, Proceedings of the International Energy Agency Carbon Dioxide Disposal Symposium. *Energy Conversion,* 34, 1095-1103.

SMITH, J. C. (1999) Atmospheric Dispersion Modelling. *Annual Report 1996/1997.* Chilton. Didcot, Oxfordshire,, National Radiological Protection Board.

SMITH, T. A. & WARWICK, R. G. (1981) A survey of defects ; Pressure Vessels ; the UK for the period 1962-1978 and its relevance to Nuclear Primary Circuits. *Safety and Reliability Directorate.* AKAEA SRD R203.

STEFFEN, W. (2006) Stronger Evidence but New Challenges: Climate Change Science 2001-2005. Government, Australian (Ed.) Canberra, Department of the Environment and Heritage. Australian Greenhouse Office http://www.greenhouse.gov.au/science/publications/science2001-05.html.

STODDARD, L., ABIECUNAS, J. & O'CONNELL, R. (2006) Economic, Energy, and Environmental Benefits of Concentrating Solar Power ; California. DOE, U.S. (Ed.) Golden, Colorado, National Renewable Energy Laboratory, http://www.nrel.gov/csp/pdfs/39291.pdf, NREL/SR-550-39291.

SVENSSON, R., ODENBERGER, M., JOHNSSON, F. & STROMBERG, L. (2004) Transportation systems for CO2 - application to carbon capture and storage. *Energy Conversion and Management,* 45, 2343-2353; doi:10.1016/j.enconman.2003.11.022.

TANG, W., HUBER, A., BELL, B. & SCHWARZ, W. (2006) Application of CFD simulations for atmosheric dispersion over open fields and within arrays of

buildings. Inc, US EPA & Fluent (Ed.) *14th Joint Conference on the Applications of Air Pollution Meteorology with the A&WMA.* Atlanta, GA.

TEGEN, S. (2006) Comparing Statewide Economic Impacts of New Generation from Wind, Coal, and Natural Gas ; Arizona, Colorado, and Michigan. Information, U.S. Department of Energy Office of Scientific and Technical (Ed.), National Renewable Energy Laboratory, Technical Report NREL/TP-500-37720.

TNO (1996) Yellow Book: Methods for the calculation of physical effects due to the releases of hazardous material (licuids and gases). Van den Bosch, C.J.H. & Weterings, R.A.P.M. (Eds.) *Committee for the Prevension of disasters.* The Hague, TNO; CPR 14E.

TOWNES, M. S., BOARDMAN, J. H. & SKINNER, R. E. (2004) Pipelines and land use - a risk informed approach. Board, Transportation Research (Ed.) Washington D.C., the National Academies. Special Report 281; http://onlinepubs.trb.org/Onlinepubs/sr/sr281.pdf.

TRANSOFT (2006) Transoft International, User's Manual of Fluidyn - PANACHE. Paris.

TRBOJEVIC, V. M. (2005) Risk creteria ; the EU. *Project "Safety and Reliability of Industrial Products, Systems and Structure" Risk Support Limited.* London, U.K., SAFERELNET, European Commission. B26P2.

TREIER, V. & PALGE, V. (1985) Comparison of Formulas for Calculating Water Vapour Saturation Pressure. Tartu, Estonia, Estonian Agricultural University.

TURNER, R., HARDY, N. & HOOPER, B. (2003) Quantifying the Risks associated with a CO2 sequestration pipeline: a methodology and case study. Camberra, Cooperative Research Centre for Greenhouse Gas Techonlogies (CO_2CRC).

USA (2004) Code of Federal Regulations. Goverment, United States of America (Ed.).

VAN ULDEN, A. P. (1978) Simple estimates for vertical diffusion from sources near the ground. *Atmos. Environ.,* 12, 2125-2129.

VENDRIG, M., SPOUGE, J., BIRD, A., DAYCOCK, J. & JOHNSEN, O. (2003) Risk Analysis of the Geological Sequestration of Carbon Dioxide. . Crown (Ed.), Department of Trade and Industry's Cleaner Coal Technology Transfer Programme. R246 DTI/Pub URN 03/1320.

WAKES, S. J., HOLDØ, A. E. & MEARES, A. J. (2002) Experimental investigation of the effect orifice shape and fluid pressure has on high aspect ratio cross-sectional jet behaviour. *Hazardous Materials,* 1-27, PII: S0304-3894(01)00307-7.

WEIL, J. C., SYKES, R. I. & VENKATRAM, A. (1992) Evaluating air-quality models: review and outlook. *J. Appl. Meteor.*, 31, 1121–1145.

WILSON, D. (1979) The Release and Dispersion of Gas from Pipeline Ruptures Calgary, Alberta Environment. Research Report: Contract 790686, 91pp.

WOLFE, P. (2008) The future for renewable energy. http://www.smallcapnews.co.uk/article/The_future_for_renewable_energy/6384.aspx, SmallCapNews. Philip Wolfe, Director General of the Renewable Energy Association.

WOODHILL (2003) Barriers to overcome ; the implementation of CO2 Capture and Storage: Rules and Standards for the Transmission and Storage. Areport prepared byWoodhill Engineering Consultant for International Energy Agency. IEA (Ed.) Cheltenham, Report number: PH4/23

WRI, W. R. I. (1998) Final report on the 1995 Kit Fox project, Vol 1 - Experiment Description and Data Processing. Laramie, WRI.

WWF (2005) 2° is too much! Rosentrater, Lynn (Ed.) LDR Consulting, Oslo Norway, WWF International Arctic Programme. http://assets.panda.org/downloads/050129evidenceandimplicationshires.pdf.

WWF (2008) Living Planet Report, 2008. Hails, Chris (Ed.) *Living Planet Reports.* Gland, Switzerland, WWF, http://www.wwf.org.uk/news_feed.cfm?uNewsID=2294.

YAMADA, T. (2004) Merging CFD and atmospheric modelling capabilities to simulate airflows and dispersion ; urban areas. *Computational Fluid Dynamics,* 13, 329-341.

ZEP (2008) EU Demonstration Programme for CO2 Capture and Storage (CCS) - ZEP's Proposal. Brussels, European Technology Platform for Zero Emission Fossil Fuel Power Plants (ZEP); http://www.zero-emissionplatform.eu/website/docs/ETP%20ZEP/EU%20Demonstration%20Programme%20for%20CCS%20-%20ZEP's%20Proposal.pdf.

ZHANG, Z. X., WANG, G. X., MASSAROTTO, P. & RUDOLPH, V. (2006) Optimization of pipeline transport for CO2 sequestration. *Energy Conversion and Management,* 47, 702-715; doi:10.1016/j.enconman.2005.06.001.